



## Continuous on-line non-invasive cortisol measurement in aquaculture

D'Costa, Claudy

*Publication date:*  
2021

*Document Version*  
Publisher's PDF, also known as Version of record

[Link back to DTU Orbit](#)

*Citation (APA):*  
D'Costa, C. (2021). *Continuous on-line non-invasive cortisol measurement in aquaculture*. DTU Bioengineering.

---

### General rights

Copyright and moral rights for the publications made accessible in the public portal are retained by the authors and/or other copyright owners and it is a condition of accessing publications that users recognise and abide by the legal requirements associated with these rights.

- Users may download and print one copy of any publication from the public portal for the purpose of private study or research.
- You may not further distribute the material or use it for any profit-making activity or commercial gain
- You may freely distribute the URL identifying the publication in the public portal

If you believe that this document breaches copyright please contact us providing details, and we will remove access to the work immediately and investigate your claim.

# Continuous on-line non-invasive cortisol measurement in aquaculture



Claudy D'Costa

Department of Bioengineering

Technical University of Denmark

This dissertation is submitted for the degree of

*Doctor of Philosophy*

I would like to dedicate this thesis to my mom...

## Declaration

I hereby declare that except where specific reference is made to the work of others, the contents of this dissertation are original and have not been submitted in whole or in part for consideration for any other degree or qualification in this, or any other University. This dissertation results from my own work from February 2018 to August 2018 and includes nothing which is the outcome of work done in collaboration, except where specifically indicated in the text. This dissertation contains less than 65,000 words, including appendices, bibliography, footnotes, tables and equations, and has less than 150 figures.

Claudy D'Costa

2021



## Acknowledgements

I would like to thank Jenny Emnéus for being my scientific godmother and giving me all the freedom to do research better than the way I envisaged. Thank you for remoulding my scientific temperament.

Thanks to Anders Wolff for providing me with so many inspirational ideas at the start of my PhD and M.-Pilar Marco for hosting me at your excellent lab in Barcelona.

A heartfelt thanks to Arto Heiskanen, the electrochemistry wizard and a very gentle human being. I have always admired your ultra-precision while executing even a simple experiment. As a researcher, I have set you as the gold standard and will always be my inspiration.

A special thanks to Lotte Nielsen and Ole Kristoffersen. I have never seen someone more selfless than you two. I would have lost the PhD battle without you.

I am immensely grateful to J.-Pablo Salvador, who took me under his wings and patiently taught me immunoassay. From you, I learnt how to balance research and have fun at the same time!

A very short and memorable encounter at DTU Aqua, I would like to thank Manuel Gesto, who helped me get the first breakthrough with cortisol detection.

My brothers in arms Suman Basak and Zoltan Andras Guller, I would have been **'chemistry' less without your company. I could not have wished for better buddies.** I am grateful for the friendly neighbour Van Ngoc Huynh who was always so generous with electronic components and a good friend. Thanks to my ikka, Firoze Babu, for being the big brother. A highly caffeinated thanks to Toppi for riding along the treacherous PhD path!

I want to thank all the staff at Nanolab, especially Thomas Aarøe Anhøj and Karen Birkelund. Dear Thomas and Karen, you would never know how much I am grateful for all the help you gave me.

And thanks to all the musicians of the world! Who kept me company all these years.

## Abstract

The work described in this thesis is derived from the need to establish good welfare for fish in aquafarms. Sea food has become an integral part of the quest to meet the protein demands of an ever-growing world. When the world scrambles towards higher production rates, both sustainability and the welfare of the farmed animals are jeopardised. The work presented in this thesis focuses on a particular type of high-density fish farming called the recirculating aquaculture system (RAS), posed to have the potential for meeting the increasing demands for fish and allied products.

The stress hormone cortisol is an apt indicator of non-optimal conditions in (RAS). Nevertheless, it is not straightforward to measure the cortisol level of fish without going for invasive procedures. However, a breakthrough was made by researchers in the Centre for Environment Fisheries and Aquaculture Science (CEFAS), UK, when they establish beyond doubt that fish release cortisol into the surrounding water and can be measured by collecting that water sample. The drawback of the method was that it was laborious and not suitable for continuous measurement.

It was clear that cortisol had to be continuously monitored to use the data for welfare assessment since variation from circadian rhythm needs to be established to determine the change in cortisol level. The way ahead was to develop a system that could measure cortisol (i) non-invasively, (ii) continuously, (iii) in the pM range and (iv) automatically. The solution was to create a flow injection analysis system that could take samples from the fish tank without disturbing the fish, measure the cortisol level and keep repeating the same every day. This thesis presents how such an automated non-invasive flow system for cortisol measurement was developed.

The system comprised multiple peristaltic pumps and injection valves controlled through a custom-made LabView operated automation circuit. Two different

immunoreaction chamber (IRC) formats were tested, where cortisol antibody was bound to Protein G on either a gold surface or superparamagnetic beads. They provided an IC<sub>50</sub> and LOD of 0.91 nM and 0.6 pM (gold), 7.8 nM and 1.3 pM (beads), respectively.

Actual water samples were tested from a model RAS at DTU Aqua. The IRC with magnetic beads was modified to incorporate an immuno-supported liquid membrane (ISLM) unit for sample cleaning and enrichment. Despite the higher IC<sub>50</sub> and LOD, the loaded Protein G modified magnetic beads render the system highly versatile for use. After 900 s of sample flow through the ISLM donor phase, the antibody binding sites in the acceptor phase were fully occupied by cortisol, showing that continuous cortisol detection in water is feasible. The automation system has been designed to accommodate more pumps and valves if the need arises. Also, the design and fabrication methods have been adapted for industrial manufacturing practices.

The signal output from the system can be integrated into the central control system of the aquafarm to facilitate a better idea regarding the welfare situation in the aquafarm. Corrective actions can then be initiated to maintain a good level of welfare. The developed system shows excellent promise in the aquafarming sector.

## Abstrakt

Det arbejde, der er beskrevet i denne afhandling, stammer fra behovet for at etablere god velfærd for fisk i vandbrug. Havfødevarer er blevet en integreret del af søgen efter at imødekomme proteinkravene i en stadig voksende verden. Når verden kæmper mod højere produktionshastigheder, bringes både bæredygtighed og husdyrenes velfærd i fare. Arbejdet, der præsenteres i arbejdet, fokuserer på en særlig type indramning af høj densitet fisk kaldet det recirkulerende akvakultursystem (RAS), der kunne have potentiale til at imødekomme de stigende krav til fisk og allierede produkter.

Stresshormonet cortisol er en passende indikator for ikke-optimale forhold i (RAS). Ikke desto mindre er det ikke ligetil at måle cortisolniveauet af fisk uden at gå til invasive procedurer. Men et gennembrud fik forskere i Center for Miljøfiskeri og Akvakulturvidenskab (CEFAS), Storbritannien, da de uden tvivl fastslår, at fisk frigiver cortisol i det omgivende vand og kan måles ved at indsamle denne vandprøve. Ulempen ved metoden var, at den var besværlig og ikke egnet til kontinuerlig måling.

Det var klart, at cortisol løbende skulle overvåges for at bruge dataene til velfærdsvurdering, da variation fra døgnrytme skal etableres for at bestemme ændringen i cortisolniveau. Vejen frem var at udvikle et system, der kunne måle cortisol (i) ikke-invasivt, (ii) kontinuerligt, (iii) i pM-området og (iv) automatisk. Løsningen var at oprette et flowinjektionsanalyzesystem, der kunne tage prøver fra akvariet uden at forstyrre fisken, måle cortisolniveauet og blive ved med at gentage det samme hver dag. Denne afhandling præsenterer, hvordan et sådant automatiseret ikke-invasivt flowsystem til cortisolmåling blev udviklet.

Systemet omfattede flere peristaltiske pumper og indsprøjtningstilstyring gennem et specialfremstillet LabView-betjent automatiseringskredsløb. To

forskellige formater for immunreaktionskammer (IRK) blev testet, hvor cortisolantistof blev bundet til protein G på enten en guldoverflade eller superparamagnetiske partikler. De leverede en IC50 og LOD på henholdsvis 0,91 nM og 0,6 pM (guld), 7,8 nM og 1,3 pM (partikler) Faktiske vandprøver blev testet fra en model RAS på DTU Aqua. IRC med magnetiske perler blev modificeret til at inkorporere en immun-understøttet flydende membran (ISLM) enhed til prøverensning og berigelse. På trods af den højere IC50 og LOD gør de indlæste Protein G -modificerede magnetiske perler systemet meget alsidigt til brug. Efter 900 sek. Prøveflow gennem ISLM -donorfasen blev antistofbindingsstederne i acceptorfasen fuldt ud optaget af cortisol, hvilket viser, at kontinuerlig kortisoldetektion i vand er mulig. Automatiseringssystemet er designet til at rumme flere pumper og ventiler, hvis behovet opstår. Desuden er design- og fremstillingsmetoderne blevet tilpasset til industriel fremstillingspraksis.

Signaludgangen fra systemet kan integreres i akvafarmens centrale kontrolsystem for at lette en bedre ide om velfærdssituationen i akvagården. Korrigerende handlinger kan derefter initieres for at opretholde et godt velfærdsniveau. Det udviklede system viser fremragende løfter i akvafarmsektoren.

# Contents

Contents.....	ix
List of Figures.....	xiii
List of Tables.....	xix
List of publications and submitted papers.....	xx
Publications not included in this thesis.....	xxi
My contributions to the paper.....	xxii
Chapter 1 Background.....	1
1.1 SUREAQUA.....	2
Chapter 2 Thesis, Hypothesis and objectives.....	5
2.1 Hypothesis.....	5
2.2 Objectives.....	5
2.3 Thesis overview.....	7
Chapter 3 Aquaculture.....	9
3.1 Significance of aquaculture.....	9
3.2 Aquaculture systems.....	10
3.2.1 RAS control system and welfare.....	12
3.3 Factors influencing the productivity of aquaculture.....	13
3.3.1 Fish welfare.....	13
3.3.2 Stress and welfare of fish.....	14
3.3.3 Economics of fish farming and its relationship to stress.....	17
3.4 Measurement of cortisol.....	18
3.4.1 Cortisol measurements in aquaculture systems.....	18
3.4.2 Strategies for cortisol measurement.....	20
Chapter 4 Immunoaffinity-based assays.....	23
4.1 The Antibody.....	23
4.2 Immunoassays.....	25
4.2.1 Immobilisation of antibody.....	27
4.2.2 Labels for immunoassays.....	30

4.2.3	Immunoassays for cortisol .....	31
4.3	Immunosensors.....	33
4.3.1	Surface plasmon resonance (SPR) immunosensor .....	34
4.3.2	Quartz crystal microbalance (QCM) immunosensor .....	35
4.3.3	Electrochemical immunosensors .....	36
4.3.4	Surface fouling .....	38
4.3.5	Matrix effects .....	38
4.3.6	Immuno supported liquid membrane (ISLM) extraction .....	39
Chapter 5	Analytical techniques employed .....	43
5.1	Flow Injection Analysis (FIA) .....	43
5.2	Electrochemical techniques .....	47
5.2.1	Cyclic voltammetry .....	50
5.2.2	Amperometry .....	51
5.2.3	Electrochemical Impedance Spectroscopy (EIS) .....	52
Chapter 6	Fabrication and Characterization .....	55
6.1	Polymer fabrication of flow cells, Immunoreaction chambers (IRC) and test setups .....	57
6.1.1	Test setups.....	59
6.1.2	Immunoreaction chamber (IRC).....	63
6.1.3	Injection moulded IRC.....	72
6.1.4	Injection moulded polymer substrates.....	76
6.2	Electrodes.....	82
6.2.1	A pilot study with commercial electrodes.....	83
6.2.2	Cleanroom fabrication of electrodes .....	91
Chapter 7	Immunoassay development .....	103
7.1	Competitive cortisol assay using labelled Ab.....	103
7.2	Competitive cortisol assay using labelled antigen .....	108
7.2.1	Optimisation of Protein G immobilisation .....	109
7.2.2	Regeneration of the antibody surface .....	112
7.2.3	Electrochemical substrate for the HRP enzyme.....	114
7.2.4	Optimisation of Protein G based ELISA.....	115
7.2.5	Immobilisation of Protein G in IRC .....	116
Chapter 8	Automation of the FIA system.....	121
8.1	<b>The 'brain' of the system</b> .....	123
8.1.1	Interface to the outside world - NI6009 .....	125
8.2	Circuit board for the actuators.....	128

8.3	Process flow algorithm.....	132
Chapter 9	Conclusion and prospects.....	135
9.1	Conclusion.....	135
9.2	Challenges addressed.....	138
9.3	Challenges not addressed.....	138
9.4	Recommendations for Future Work.....	139
References	.....	A-1
Appendix A	Protocols.....	A-1
A.1	DTU Aqua experiments.....	A-1
A.2	Detector electrode on Si substrate.....	A-3
A.3	Single TOPAS substrate processing.....	A-7
A.4	Creating the BSA-cortisol hapten.....	A-12
A.5	Functionalization of glass surface using GTPMS - Electrode preparation...A-15	
A.6	Competitive assay with new BSA Cortisol hapten.....	A-17
A.7	ELISA for cortisol analyte.....	A-19





# List of Figures

Figure 1.1- Themes of SUREAQUA.....	2
Figure 3.1- Data from FAO Fisheries Division ( <a href="http://www.fao.org/fishery/statistics/">http://www.fao.org/fishery/statistics/</a> ) .....	10
Figure 3.2- Recirculating aquaculture system developed by AKVA group, Norway. ...	12
Figure 3.3- Stressors and the primary, secondary, and tertiary response.....	15
Figure 3.4- Mean food consumption of fish and specific growth rate (SGR). Fish with cortisol shows lower SGR. Reused with permission from [44] .....	17
Figure 3.5- Chemical structure of cortisol. (Attribution: Calvero. derivative work: Anasagora, Public domain, via Wikimedia Commons).....	20
Figure 4.1- An immunoglobulin - IgG (~150 kDa). Fab denotes the antigen-binding fragment, and Fc denotes the constant region. The heavy chains are ~50-70 kDa, and light chains are ~23 kDa .....	24
Figure 4.2- Various immunoassay formats .....	26
Figure 4.3- Various immobilisation methods. (A) Direct physisorption on a surface (B) Physisorption of an Fc binding protein and further binding with an Ab (C) Covalent bonding of the Ab to the surface using a linker (D) Covalent bonding of the Fc binding protein to a linker and Ab binding after that (E) Same technique as C but using a superparamagnetic bead (F) Same technique as D but using a superparamagnetic bead.....	28
Figure 4.4 - (A) Physisorption of the cortisol Ab on the well plate (B) Physisorption of the Fc binding protein (Protein-G) and subsequent Ab binding (C) Covalent bonding of the Fc binding protein to a linker (MPA) and Ab binding after that.....	32
Figure 4.5 - General principle of an immunosensor. ....	34
Figure 4.6 - (A) Biocore T200 system (B) basic principle of SPR is depicted (C) typical response curve showing association and dissociation of the target analyte. Adapted from [99] with permission from © Portland Press .....	34
Figure 4.7 - (A) A quartz crystal microbalance system with its accompanying crystal element. (B) Antibodies are immobilised on the gold surface, and (C) the change in frequency is detected when the antibody captures the target. Figure adapted from [108] .....	36
Figure 4.8 -(A) An electrochemical system with an electrode chip comprising a WE, RE, and CE connected to a potentiostat. (B) The WE is modified with an antibody to	

amperometrically detect the formed oxidised product or the impedance change when the tracer binds to the antibody.....	37
Figure 4.9 - SLM systems for extraction of acids (A) and bases (B) with the difference in pH used to entrap analytes. (C) An immuno-extraction based SLM (ISLM) system with antibodies placed in the acceptor to entrap and enrich the analyte.....	40
Figure 5.1- (A) FIA concept diagram. Adapted from [129] Copyright © 2014 Elsevier (B) A commercial FIA system from FIALab Instruments, Inc.....	43
Figure 5.2- Various analyte plugs and their corresponding peaks. Adapted from <a href="https://www.flowinjectiontutorial.com/~">https://www.flowinjectiontutorial.com/~</a> .....	44
Figure 5.3- Poiseuille Flow profile inside a tube. (B) The profile of the signal is obtained at the electrode.....	45
Figure 5.4- A schematic showing the difference between a good and bad connection. ....	47
Figure 5.5- Circuit for performing voltammetry (adapted from Tektronix [130]).....	48
Figure 5.6- Schematic diagram of a potentiostat connected to a three-electrode system. Adapted from the Gamry instrument manual. ....	50
Figure 5.7- (A) A sample cyclic voltammogram (B) CV of the substrate TMB and (C) <b>Samples CV's depicting different scenarios. Adapted from [132].</b> ....	51
Figure 5.8- An amperometric signal (reduction current) generated in a FIA system...	52
Figure 5.9- (A) A Nyquist plot in the complex impedance plane (B) Equivalent Randles circuit model (C) Bode plot showing the log magnitude and phase angle vs log frequency.....	53
Figure 6.1 - The schematic representation of the final FIA system with the major hardware components such as pumps (1,2,3), a two-position injection valve (2PV, 9) and a multi-position valve (MPV) (10), Immunoreaction chamber (IRC) (here ISLM extraction unit is shown) (17), a control circuit (14), a PalmSense4 potentiostat (13), and detector electrode (12).....	55
Figure 6.2 - (A) Schematic showing a micromilling process and different profiles of material removal. (B) Schematic showing LASER ablation of polymer and the subsequent profiles of the formed channels formed. Adapted from [133].....	58
Figure 6.3 - (A) Micromilled channel on a PMMA substrate. (B) CO <sub>2</sub> Laser ablated groove on PMMA. Adapted from [134,135]. Figures are reused with permission.....	59
Figure 6.4 - (A) CAD model of a required test setup (B) A milling tool in action (representative) (C) The finished test setup after assembling the different micro-milled parts.....	60
Figure 6.5 - Different test setups that were fabricated for various electrode designs. ....	60
Figure 6.6 - The PTFE tube snug fitting. An extra layer of silicone paste (red circle) to prevent air bubbles.....	61
Figure 6.7 - The flow simulation inside the wall-jet configuration. The velocity is shown in m/s (A) Front view of the chamber (B) Top view of the chamber (C) Two-point perspective of the chamber. The lines with arrow represent velocity. ....	62

Figure 6.8 - Schematic of a simple IRC with a gold layer in the channel to immobilise the antibody.....	64
Figure 6.9 - The different configurations of IRC. (A), (B) and (C) represent IRCs assembled using screws, whereas (D), (E) and (F) are bonded together using UV assisted thermal bonding. ....	65
Figure 6.10 - Schematic of an IRC with the location of alignment holes and an actual micromilled PMMA based IRC after UV assisted thermal bonding .....	67
Figure 6.11 - (A) Hydrophobic nature of Celgard® 2500 (B) SEM images of Celgard® 2500 the 'support' at two different magnifications. Adapted from [138] [Creative Commons Attribution by NC ND] .....	69
Figure 6.12 - SLM based IRCs (A) with screws used for assembly and (B) with UV assisted thermal bonding used for assembly.....	70
Figure 6.13- Testing the IRC.....	71
Figure 6.14- Different steps in an injection moulding process. ....	73
Figure 6.15 - The entire mould where the inserts are marked with a solid red line ( <a href="http://tsquality.ch/">http://tsquality.ch/</a> -).....	74
Figure 6.16- (A) Micromilled and polished aluminium insert with a central channel, (B) the mould insert of the injection moulding machine, and (C) two injection moulded COC parts bonded together. The dotted red square indicates the efficiency of bonding after trying to pull the pieces apart. (D) Gold layer deposited on an injection moulded part. The holes were micromilled later. ....	75
Figure 6.17- Surface roughness comparison of (A) Si wafer and (B) commercial injection moulded COC .....	77
Figure 6.18- Surface roughness comparison of (A) ID-1 (B) ID-3 .....	81
Figure 6.19- Dropsense gold IDEs and a micromilled test setup. The gold fingers are 10 µm wide separated by a 10 µm gap and with an overall length of 6760 µm .....	85
Figure 6.20 (A) Impedance spectra (Nyquist plots) acquired on: (a) bare gold IDE, (b) the same IDE after GTPMS and hBST-BSA modification, (c) As147 Ab affinity reaction, and (d) regeneration using NaOH. 10 mM ferri/ferrocyanide redox probe was used, and 1 Hz to 100 kHz was scanned. B) Stepwise modification of the electrode surface with the hbSt-BSA conjugate. (C) Impedance spectra from the surface modification of gold digits (D) Stepwise modification of electrode with MUA, Protein-G and As87.I..	87
Figure 6.21 - (A) A test setup with four commercial screen-printed planar electrodes in a batch type test setup (B) A schematic figure representing the gold working electrode modification.....	88
Figure 6.22 - (A) Impedance spectra for the gold surface using MUA as SAM (B) Stepwise modification of electrode with MUA, Protein-G, As87 and 4d-HRP. (C) Impedance spectra for the gold surface using 4ATP as SAM (D) Stepwise modification of electrode with 4ATP, GA, Protein-G, As87 and 4d-HRP .....	90
Figure 6.23 - Three parallel linear electrode chips in a batch setup (A) and in a fluidic thin-film electrochemical cell (B). (C) Electrode configuration fabricated on a Si wafer and the design showing CE, WE and RE. (D) The surface modification of the WE electrode.....	92

Figure 6.24 - (A) Impedance spectra after each modification (B) Multiple regeneration runs showing poor inter-assay stability (C) Electrode instability over repeated injections of the substrate . . . . .	93
Figure 6.25 - (A) Different electrode designs fabricated on a silicon substrate with varying working electrode areas. (B) Test setup for the electrodes (C) Flow set up where the fluid impinges on the working electrode. . . . .	95
Figure 6.26 - (A) Electrodes fabricated on a PMMA substrate (COC substrate not shown). Insets: electrode test setup and microscopic image. (B) CVs acquired in 10 mM ferri/ferrocyanide for electrodes on both PMMA and COC polymer substrates. ....	98
Figure 6.27- (A) An injection moulded 50 mm disc. (B) Micromilled disc to remove burred edges with fabricated IDE (Inset shows the microscopic images of the digits). . . . .	99
Figure 6.28 - UV exposure dose testing from 75 mJ/cm <sup>2</sup> to 95 mJ/cm <sup>2</sup> to ensure that <b>the gold 'lift off' was functioning properly</b> . . . . .	100
Figure 6.29 - (A) Testing of the electrode using Ag/AgCl as a pseudo-RE. (B) Cyclic voltammograms for polymer substrate-based IDE with 10 mM ferri/ferrocyanide. .	100
Figure 6.30- Gold surface on COC showing bubbles and cracks on the surface. The scale bar is 50 μm. . . . .	101
Figure 6.31 - Except for the first design, an IDE on a polymer substrate, the rest are all three-electrode configurations on a silicon substrate. (The contact pads are 1 mm in diameter). . . . .	102
Figure 7.1 - Active Ester method for the conjugation of cortisol to BSA. . . . .	104
Figure 7.2- Results from MALDI TOF MS for BSA and cortisol conjugated with BSA indicating (A) CH19-BSA (B) CH8-BSA (C) CH4-BSA and (D) CH2-BSA. . . . .	106
Figure 7.3 - ELISA results (A) 1D assay - indirect format. (B) Competitive assay with CH8-BSA . . . . .	107
Figure 7.4- Structural homology of cortisol and various steroid molecules. . . . .	108
Figure 7.5 - Absorbance measurements for (A) varying Protein G concentrations while maintaining a fixed antibody and tracer concentration; and (B) varying Protein-G concentrations at three different antibody concentrations and fixed tracer concentration at 2 μg/L (C) A competitive assay performed with and without Protein-G with 2.5 μg/mL of Irgarol antibody As87 and 2 μg/mL of tracer 4d-HRP. . . . .	111
Figure 7.6 - (A) Schematic of biosensor regeneration showing relevant forces in binding and de-binding. Adapted from [151] (B) Improper regeneration leads to erratic signals in each complete run. . . . .	113
Figure 7.7 - Comparison of substrate stability at HRP concentration of 1 μg/mL. (A) The in-house substrate precipitated (B) The commercial substrate proved to be stable. . . . .	115
Figure 7.8 - ELISA results for assays at three different HRP tracer dilutions: (A) Absorbance at varying concentrations of cortisol antibody and (B) calibration curves for cortisol. . . . .	116
Figure 7.9 - Immobilisation strategies: (A) An MPA SAM on the gold surface with antibodies immobilised after intermediate activation of the carboxylic groups; (B) an	

MPA SAM with covalently immobilised Protein-G and antibodies bound to the Protein-G; (C) Superparamagnetic beads with covalently immobilised Protein-G and bound antibodies (zoom-in of the details in the inset). .....	117
Figure 7.10 - Protein immobilisation strategies where a SAM of 3-Mercaptopropionic acid and 11-Mercaptoundecanoic acid is used in combination with zero-length crosslinkers to bind the protein. Adapted with permission from [165] Copyright 1997 American Chemical Society. ....	118
Figure 8.1- Control system block diagram.....	122
Figure 8.2- Schematic of the automation system. ....	123
Figure 8.3 - A sample graphical program written in LabVIEW, and the entire program with almost 30 of such sequences is shown on the right. ....	124
Figure 8.4- (A) Front panel of the LabVIEW program (B) Flowchart to run the assay. ....	125
Figure 8.5 - (A) The USB NI6009 DAQ unit from National instruments and (B) the corresponding pinout diagram.....	126
Figure 8.6- The working of a transistor configured as a switch (A) Circuit for NPN transistor along with a relay and motor (B) NPN transistor depicted as a switch. (C) The closed switch powers the relay (SPDT) (D). The closed relay switches the motor ON.....	128
Figure 8.7- (A) Layer1 (top) of the PCB (B) Layer0 (bottom) of the PCB (C) 3D rendering of the final circuit with components and (D) The actual circuit being used in the control system.....	129
Figure 8.8- Circuit diagram for the control board. ....	130
Figure 8.9- Flowchart for the entire assay and the potentiostat measurement. The time required for one assay is fed into the PSTrace script. ....	131
Figure 8.10- Photographs of the actual setup. (A) Shows the various pumps and valves used. (B) The circuit board with all the connections made (C) Close up of the IRC and detector electrode inside the flow cell.....	132



## List of Tables

Table 4.1 - Various labels or label products and their possible detection strategies..	30
Table 6.1 - Optical profilometry results for a commercial injection moulded COC compared with a silicon wafer.....	78
Table 6.2 - Different parameters tested for injection moulding.....	80
Table 6.3 - Optical profilometry results for a commercial injection moulded COC .....	81
Table 6.4 - Cyclic voltammetry results. ....	97
Table 7.1 - Number of hapten per BSA molecule obtained from MALDI TOF MS analysis.....	105
Table 7.2 - Performance of the IRC based assay using the three different immobilization strategies.....	119
Table 8.1 - Logic for the digital output from Ni6009 and the corresponding decimal code used in the program.....	127



# List of publications and submitted papers

*To be submitted*

(Paper I)

Flow injection immunoassay for continuous monitoring of cortisol.

**Claudy D'Costa**, Arto Heiskanen, Zoltán Guller, Manuel Gesto, J.-Pablo Salvador, M.-Pilar Marco, Anders Wolff, and Jenny Emneus.

## Publications not included in this thesis

### *Submitted*

Impedance-based E-screen assay for real-time screening of xenoestrogenic compounds.

Naricha Pupinyo, **Claudy D'Costa**, Arto Heiskanen, Wanida Laiwattanapaisal, Jenny Emnéus

## My contributions to the paper

Paper I      I designed and planned all the experiments. I performed the fabrication of polymer parts and electrodes. I performed most of the electrochemical measurements, evaluated the result and took part in writing the manuscript.

# Chapter 1 Background

*"Everything that has a beginning has an ending. Make your peace with that and all will be well".*

*-Buddha*

---

The Blue Economy has gained focus after the United Nations 17 Sustainable Development Goals (SDG). One of the critical aspects is the development of a sustainable marine environment. Marine fisheries contribute \$270 billion annually to global GDP. A subdivision of that is aquaculture or fish farming. Humans have come a long way in fish farming from the traditional open sea trawling to a controlled environment closed recirculating aquaculture and inland fish farming system. Such technology has increased production as well as challenges. Aquaculture has become the fastest-growing food source, and fish is an easy source of protein for developing nations [1]. **Fisheries and aquaculture form one of the world's most prominent protein sources, thereby a crucial element in ensuring global food security [2].**

Ensuring sustainable development calls for comprehensive monitoring of fish welfare. Modern control systems used in technologically advanced fish farms help the farmers increase their yield and ensure sustainable development. Finding this right balance would help nations build upon their existing capacity without risking adverse environmental consequences. SDG Indicators 14.4.1 and 14.7.1 emphasise minimising the detrimental effects of aquaculture on ecosystems and sustainable aquaculture management [2].

Multiple agencies around the world are striving towards ensuring the SDGs. Norway is the second-largest exporter of fish and allied products, and hence the Nordic Council has initiated many projects to meet these SDGs.

## 1.1 SUREAQUA

My PhD project has been an integral part of the Nordic Centre of Excellence for Sustainable and Resilient Aquatic Production (SUREAQUA), funded by NordForsk. SUREAQUA has been formed to address current challenges and devise practical and deployable solutions. The goal is to ensure the resilience and sustainability of aquafarming in the Nordic region and provide competence, innovation, and technology in aquatic production chains in the Nordic region through an integrated multidisciplinary toolbox of assessment methods

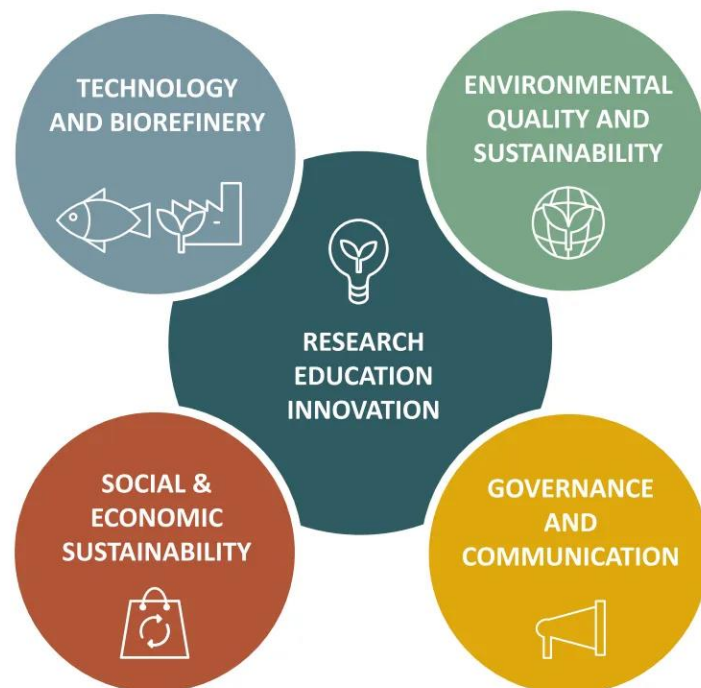


Figure 1.1- Themes of SUREAQUA

Figure 1.1 depicts the four major themes involved in SUREAQUA. Theme 1, Technology and Biorefinery, focus on innovative solutions to enhance production and profitability while preserving aquatic integrity. Theme 2, Environmental Quality and Sustainability, and theme 3 Social and Economic Sustainability, address finding sustainable solutions to large-scale societal challenges and maintaining a

---

competitive industry while maintaining a healthy environment. Theme 4, Governance and Communication, deals with policymaking, communicating various research findings to the public, and providing data to help policymakers. The idea was to facilitate (1) cost-effective use of resources and research infrastructures, (2) develop multidisciplinary research networks in the Nordic region, as well as (3) train and educate future stakeholders in the blue bioeconomy. To meet these goals, the centre is creating novel technologies to enhance the sustainability and resilience of aquatic production while increasing yields and profitability for industries. Various projects have been implemented to achieve the set goals.

A sub-theme of theme 1 specifically focuses on the environmental factors that affect the welfare of aquatic creatures and, simultaneously, determine those elements that adversely affect the optimal growth of fish, leading to an economic disadvantage. Therefore, the framework of this PhD work has been to develop a microfluidic sensor platform that acts as an early warning system indicating any deterioration or deviation from the optimal growth conditions. The output can be qualitative, quantitative or both, based on the parameters being measured. With this information, necessary corrective actions could be taken to avert possible stressors (undesirable stimuli).

The development of a biosensing unit for continuous monitoring of cortisol from the aquatic environment to assess the welfare state of the fish forms the basis of this PhD work.



# Chapter 2 Thesis, Hypothesis and objectives

*"Our plans miscarry because they have no aim.  
When a man does not know what harbour he is making for, no wind is the right wind".*

*-Seneca the Younger*

---

## 2.1 Hypothesis

I hypothesise that - developing a system capable of non-intrusive continuous monitoring of cortisol by sampling water from the fish tank instead of sampling fish's blood can provide data for a better aquafarm control system, thereby improving the fish's welfare, farm productivity and overall sustainability.

## 2.2 Objectives

The objectives, as set by the consortium to achieve the goals of theme 1, are as follows.

1. Identify a critical parameter that can help improve the welfare of the fish, assist in the sustainable development of fish farms, and provide some economic advantage to the farmers.
2. Develop strategies to measure/detect the identified parameter.
3. Design, develop and optimise a system capable of non-invasive and continuous monitoring of the said parameter.
4. Test the system with actual samples and ensure that the system is industrially scalable.



The initial hurdle was to find the critical element that would enable us to formulate better welfare for the farmed fish—this required knowledge in sociological and physiological aspects of high-density fish farming. After a thorough literature survey, the stress hormone cortisol was chosen as the ideal candidate to assess the fish's welfare indirectly. Since elevated cortisol levels have been shown to lower the growth rate and increase fish mortality, measuring cortisol becomes relevant to the farmer. One of the biggest challenges in measuring cortisol is the requirement of a system capable of measuring cortisol in the pM range. An immunoassay is capable of sensing cortisol at such low levels. Since the need was for an electrical signal as the output, the straightforward choice was to use an electrochemical detector.

Moreover, there was the requirement to maintain a non-invasive system, which called for the development of an automated remote controlled flow system with on-line sampling and analysis. Altogether, this required a truly multidisciplinary approach, which necessitated combining microfabrication of a fluidic handling system (preferably using industrial fabrication techniques), electrochemical sensors fabrication, immunoassay development, and electronic design circuits and control systems. The PhD project was therefore divided into the following tasks and subtasks.

1. Development and testing of an apt immuno-sensing format to measure cortisol at pM levels
2. Design and fabricate electrodes for electrochemical detection of the formed substrate product from the immunoassay.
3. Fabrication of polymer parts for handling fluid, provide mechanical support for the immunoassay and testing of electrodes:
  - a. Implement industrial manufacturing techniques for ways of scaling up the production of the said polymer parts.
4. Implementation of a flow injection (FI) system:
  - a. Automation of the entire assay

---

Hence to materialise this project, aspects from mechanical (pumping, dosing, fluidics), electrical (circuits, power, and control system), chemical (surface modification, conjugation), biochemical (immunoassay and proteins), and microfabrication techniques had to be incorporated to achieve the goals of this project.

## 2.3 Thesis overview

The chapters have been arranged to follow a logical order to help the reader understand the building blocks of the final system.

Chapter 1 provides a bigger perspective on how and why such research was undertaken and its relevance in the real world.

Chapter 2 sets the objectives and tasks required to fulfil the project hypothesis.

Chapter 3 introduces the world of aquaculture, challenges faced, fish welfare and the proposed solution.

Chapter 4 is about immunoassay, the different aspects of immunoassay and the different detection strategies.

Chapter 5 deals with the techniques used to run the main experiment, which is a flow injection system with electrochemical detection methods.

Chapter 6 describes all the fabrication methods and protocols followed in this thesis.

Chapter 7 is about the actual development of the immunoassay, the challenges faced and solutions.

Chapter 8 demonstrates how the automation of the entire flow injection analysis system was achieved.

Chapter 9 gives a glimpse into the future of the technology presented in this thesis.



# Chapter 3 Aquaculture

*"It is impossible for a man to learn what he thinks he already knows."  
— Epictetus*

---

## 3.1 Significance of aquaculture

A good starting point in understanding the importance of aquaculture is from the biennial report - The State of World Fisheries and Aquaculture (SOFIA) from the Food and Agricultural Organisation (FAO) of the United Nations.

Fish derived from aquaculture has since 2016 surpassed wild-caught fish, and the trend is expected to continue (Figure 3.1). In 2018, except for China, the biggest producer and exporter of fish, every other nation has seen an upward trend in the production of farmed aquatic animals. On a global scale, the growth rate was 5.3% for the period 2001 - 2018. In 2018 the aquaculture production peaked at 114.5 million tonnes and accounted for almost \$263.6 billion in sale value. Particularly interesting is the contribution of inland fish farming to the global food fish production at 62.5% [2].

All these indicators are good except when it comes to the biologically sustainable levels of fish stocks. The level decreased from 90% in 1974 to 65.8% in 2017. Here the UN SDG 14 (Life below water) becomes relevant. Although the SDG focuses on the entire marine ecosystem (both open sea and inland farms), our primary focus is on sustainable development and operation of recirculating aquaculture systems (RAS) - a method for high-density inland fish farming in an environmentally controlled closed-loop system.

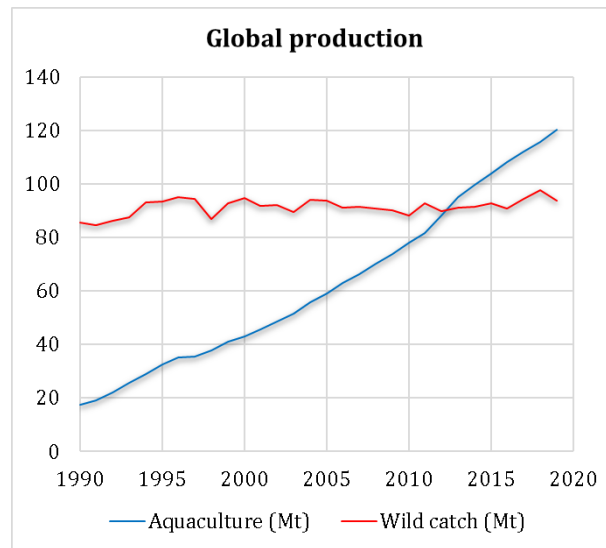


Figure 3.1- Data from FAO Fisheries Division (<http://www.fao.org/fishery/statistics/>)

However, it is to be noted that not everyone thinks that high-intensity farming, although made sustainable, is the solution for sustainability in marine and inland fish farming on a global scale. Researchers point out that the specialised feed provided for fish in such an intense farming system is derived from smaller fishes that can be consumed as it is. Moreover, fish produced from such farms are expensive, which only rich countries can afford [3,4].

## 3.2 Aquaculture systems

Farming of fish can be done through naturally occurring systems like ponds to intensive farming in recirculating systems. The function of a farm is to manage the environment and provide the maximum growth rate at the highest efficiency and lowest wastage of resources [5]. The most common formats of aquaculture are described below.

Ponds are inland water bodies either naturally occurring or artificially created near a water body. Oxygen, temperature, waste removal and feed are all naturally controlled. It is a simple system and hence less control of various parameters like algae bloom or infections.

Flowthrough raceways are large artificial troughs that use water from a river, stream or a well diverted into a specific structure where fish can be grown. It is like a pond, but water continuously flows through the channels. Like ponds, the raceways are also naturally controlled. These are used for rainbow trout farming.

Net Pens or cages are special enclosures in the open water body in freshwater lakes, and open sea made with mesh or net screens. Here also, the environment is not controlled.

Bottom Culture is mainly for oysters, mussels, scallops, clams, and seaweed. It is located on the seabed; hence environmental parameters are naturally controlled.

Off-bottom Culture system is used for culturing shellfish. Long ropes suspended from buoys are used to culture shellfish by growing on them. Here also the system is naturally controlled.

Recirculating Tanks are artificial concrete tanks with a controlled environment. They have a continuous in and out flow of water. They have many advantages like preventing fish from escaping, lesser pollution, higher density, prevention of potential disease and parasite transfer into the wild.

A RAS (Figure 3.2) is the technologically advanced version of recirculating tanks. The concept of RAS was established during the early 1900s. Arisune Saeki described how various parameters could be controlled for farming fish [6]. Later, multiple publications have described different approaches adopted for water filtration [7,8] and the design of RAS [9].

In a RAS, huge concrete tanks are used for farming fish, and the water is recirculated. There is better control of feed, nutrients, temperature, pH, salinity, dissolved oxygen, carbon dioxide and nitrogen levels, ammonia and organic matter, particles, and even infections [10-12]. Since only a single species is cultivated in a very controlled environment, higher stocking densities are also achieved. The primary design focus of a RAS is based on energy consumption and environmental impact. Various

measures are taken to reduce energy consumption and protect the environment from **the aquaculture system's effluents** [13-15]. It is assumed that the fish are provided with optimal conditions for growth. All appear to function well until the welfare of the fish is taken into consideration.

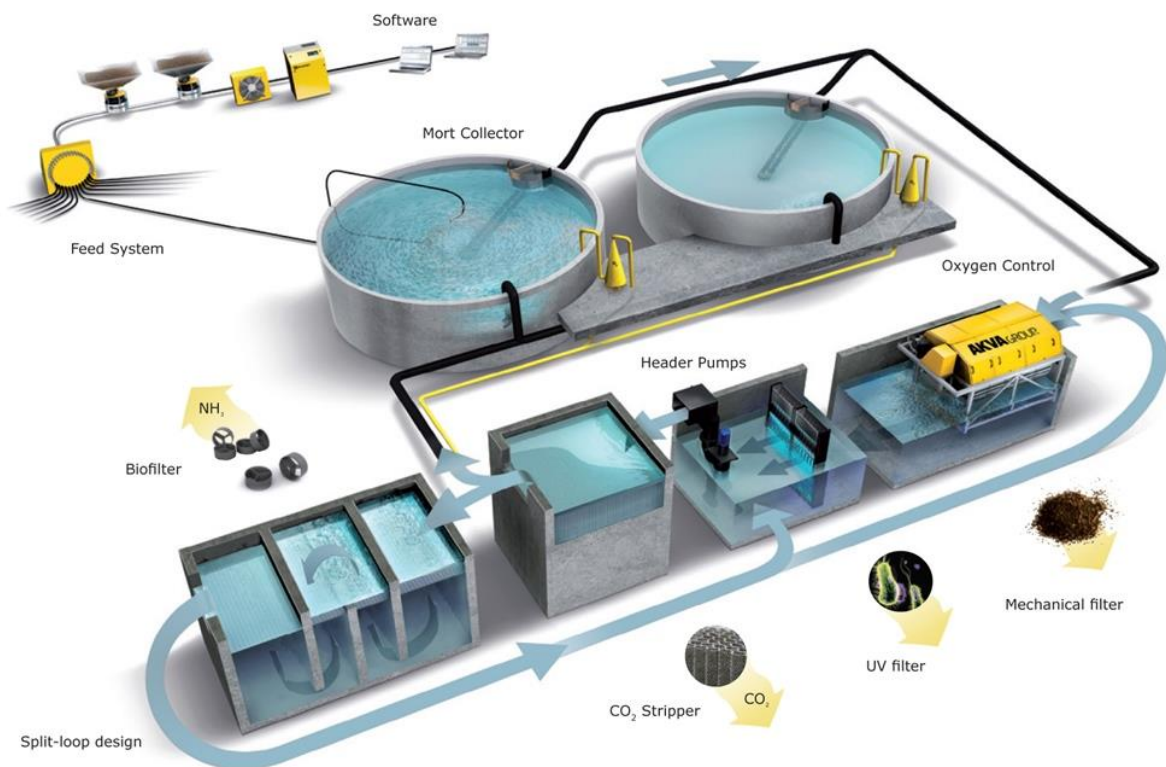


Figure 3.2- Recirculating aquaculture system developed by AKVA group, Norway.

### 3.2.1 RAS control system and welfare

Management of a sizeable indoor aquafarm requires monitoring and controlling of multiple pumps, filters, sensor arrays, power supply, lighting, temperature, pressure regulators and many similar parameters. Automation of such aquafarms has been reported long back [16-19]. Modern RAS have built-in supervisory control and data acquisition (SCADA) system as part of the overall aquafarm control. The SCADA system [20] monitors all the critical and non-critical parameters of the fish farm and performs necessary corrective or maintenance actions for the day-to-day functions of

the farm. It is a data logging unit that keeps track of the farm through various instruments and at the same time controls various aspects like water temperature, water inflow, and feed delivery [18]. SCADA is a very complex system such that it can initiate preventive actions when it detects the onset of a deteriorating trend. In short, the SCADA system can monitor and log data, automatically control the farm, perform trend analysis, initiate preventive action, give warnings and alarms, and even send regular reports. Incorporating the measured cortisol level into such a control system facilitates easy data integration to determine or isolate the potential stressor or stressor source.

### 3.3 Factors influencing the productivity of aquaculture

#### 3.3.1 Fish welfare

The topics discussed so far in this thesis are generic data or technical descriptions of various systems. The issue I am about to explain is beyond my expertise as an electronics and biomedical engineer. Nonetheless, efforts have been made to ensure that accurate information is presented.

**Jeremy Bentham, a famous advocate for animals' moral status, asked, 'The question is not Can they reason? or Can they talk? but Can they suffer?'** [21]. Fast forward many years, the outcome of a meeting held in Edinburgh in November 2004 was to establish beyond doubt that animal welfare, and fish welfare, in particular, needs to **be addressed for the 'blue revolution' to be genuinely sustainable** [22]. The book by Edwards Branson is a good starting point to understand fish welfare, the need for welfare, and the mechanism of stress. It was long considered that since fish do not have a well-developed pain perceiving system, such welfare aspects need not be considered. However, according to Guidelines for the treatment of animals in behavioural research and teaching [23], every animal including fish needs to be treated in a way that involves minimum stress, pain or discomfort. It is also pertinent



---

to mention the five freedoms proposed by the Farm Animal Welfare Committee [24] as welfare indicators. These guidelines emphasise the importance of welfare in aquaculture. It is essential to understand that there is always an ulterior motive from the side of humans when they want to farm animals for their needs. Providing a system as close to its natural habitat, feed, and a pathogen-reduced environment may seem like a solution for better welfare. However, this is an ethical debate beyond the scope of the present study.

There are three significant ideals regarding welfare: function-based, feelings-based, and nature-based [25]. A proper understanding of all these three approaches and their interplay is essential for developing better welfare strategies. Weiss and others have demonstrated the impact of stress on growth, normal immune response, and behaviour [26]. Some fish species indicate their distress through increased activity and reduced food intake [11,27], which an experienced farmer uses to evaluate welfare. However, since it is challenging to use such markers to quantify an animal's stress level, it becomes our duty as researchers to help all concerned animals represent their perspective or feelings towards external stressors. It is pertinent to note that some researchers suggest that fish lack the cognitive ability to experience suffering [28]. At the same time, there are enough indicators to show that they do respond to stressful situations. Understanding how stress relates to fish and the welfare thereof is needed.

### 3.3.2 Stress and welfare of fish

Hans Selye extensively studied stress and came up with his notable work regarding stress and its effects on any organism [29]. He defined stress as the total psychological response of an organism towards an external chemical or physical **'force' to re-establish** its normal metabolism. Pickering, in his book, describes stress as the external disturbance that brings discomfort to the fish [30]. Presently, stress is defined as a psychological, physiological, and behavioural response to a stressor - a change in the environment, physical or chemical conditions or stimuli that can evoke

the said response [31]. Many researchers who have studied stress have pointed out that the elevated corticosteroid levels like cortisol (stress hormone) are to protect the animal from autoimmune complications [32], and to allow the central nervous system to organise a biological defence to handle the stress stimuli [33].

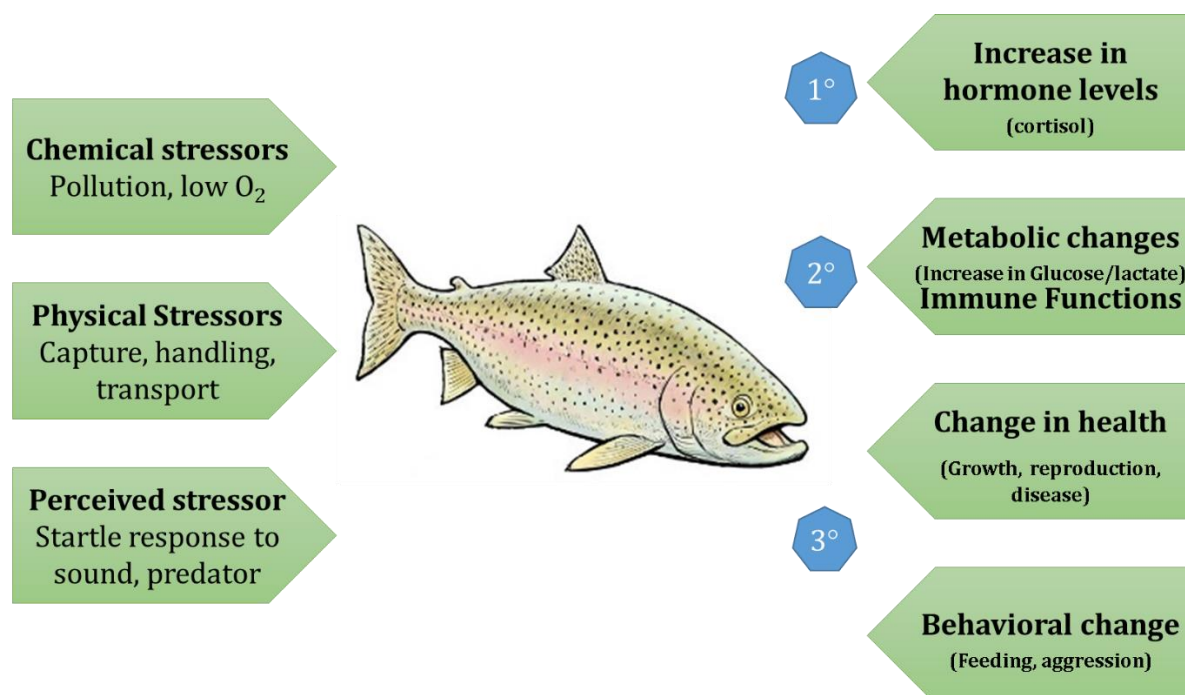


Figure 3.3- Stressors and the primary, secondary, and tertiary response.

Many factors can lead to stress in a farming situation (Figure 3.3). Most of the stressors are artificial, such as high-density farming, artificial lighting, noises from machinery, and fish feed, to name a few. Physical conditions, physiological status, and behavioural patterns could be used separately or together to assess the welfare of fish [22]. The feelings of an animal may be difficult to measure, but the changes in different functions of an animal in response to an external stressor can be measured. Although the physical conditions of the fish are an excellent indicator of welfare, they are not easy to quantify. The physiological status indicated by stress markers like hormonal changes in the blood can be invasively measured.

---

There are well established and studied physiological pathways, such as the hypothalamic-pituitary-adrenal axis, which respond to stressors [34]. The presence of cortisol, the steroid hormone released in response to stress, was established in fish already in 1957 [35]. The stress response triggered by a threat and the subsequent release of cortisol is a coping mechanism of most animals for a fight-or-flight situation. It helps for a short-term reallocation of energy to cope with the external stressor and regain homeostasis [30,36,37]. Such a response helps the individual to survive an adverse condition or a threat in its natural environment for a short duration. However, for a farmed species, the stressor might be chronic or present due to the very design of intensive farming environments (e.g. artificial lighting, confined tanks, stocking density, lack of natural shelters) [38,39].

A chronic elevation of cortisol level may inhibit the fish from responding to immediate threats or changes in the environment [36]. Measuring elevated plasma cortisol levels is an apt indicator of a stressful encounter and sensitive enough that it can be triggered even when there is a larger fish (aggression) in the surrounding [40]. Therefore, cortisol is one of the most commonly measured indicators of stress [41]. With its slower response to stressors than catecholamines, it is easier to take blood samples before and after inducing a stressor [42]. Most of the research related to fish stress or cortisol studies is performed on rainbow trout (*Oncorhynchus mykiss*), Nile tilapia (*Oreochromis niloticus*) and Atlantic salmon (*Salmo salar*) since **they are considered to be 'domesticated' fish species** [43].

Cortisol mediates water and salt balance in marine fish, helps some fish species complete their parr-smolt transformation and could also be elevated during mating contests. However, none of these conditions are related to poor welfare. Even age has been shown to affect the release of cortisol [44]. So, due diligence should be given not to associate every increase in blood plasma cortisol level with a negative or stressful situation. Also, the circadian cortisol cycle should be taken into account [45]. Environmental and behavioural parameter indices should also be considered to assess welfare [22,25]. Another significant parameter is elevated chronic stress and

coping mechanisms of different species to such non-adaptable stressors; in such cases, some researchers have pointed out that a correlation between stress and poor growth could not be established [46]. Hence, multiple entities like physical and chemical environmental parameters, crowding density, the types of fish in a single tank (sex, age, size), fish movement, and other tertiary stress indicators must be monitored to avoid misinterpretation of bad welfare.

### 3.3.3 Economics of fish farming and its relationship to stress

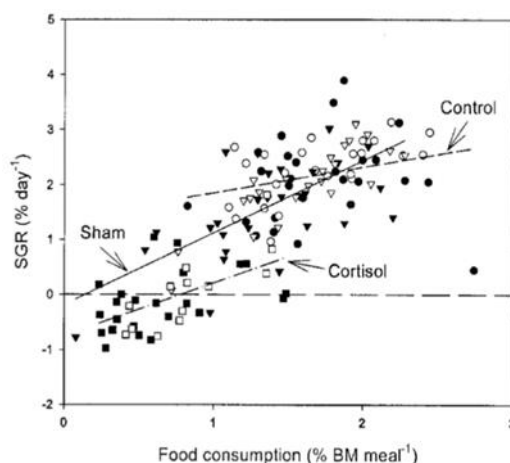


Figure 3.4- Mean food consumption of fish and specific growth rate (SGR). Fish with cortisol shows lower SGR. Reused with permission from [47]

The fish farmer's primary concern is the fish's health, growth, and mortality, and they form the driving force for better welfare. Fish health (lower infection), growth rate (size), and mortality (loss of stock) impact the farmer financially. Stress affecting the metabolism, reproduction and immune systems forms the critical point of concern in fish farming since it directly affects the health of the fish as well as lowers their specific growth rate (Figure 3.4), leads to population decline, and increases mortality [34,47]. This tertiary response to stress causes long-term problems, such as increased susceptibility to viral, bacterial, and fungal infections, immunosuppression, reduction in feed uptake, reduced protein synthesis, and lower reproductive

---

performance [34,48-50]. Studies have shown that elevated stress can even lead to deterioration of meat quality [47].

## 3.4 Measurement of cortisol

### 3.4.1 Cortisol measurements in aquaculture systems

The discussion above has outlined how stress affects fish welfare and the importance of cortisol. The stress hormone cortisol acts as an apt indicator for the presence of a stressor. The source of the stressor could be deduced by detecting the deviation in cortisol level by continuous monitoring and incorporating data analysed from all related parameters. Cortisol can be measured from blood plasma, mucus, scales, urine, faeces, or release via gills. Routine cortisol measurement is done by sampling blood from the tail portion of the fish and analysing the sample using radioimmunoassay (RIA) or enzyme-linked immunoassay (ELISA). The sampling procedure involves taking the fish out from the water, anaesthetising it and drawing blood from the tail region before releasing it back into the tank. The entire process is stressful for the individual fish and the remaining fish in the water [51,52] but is, nevertheless, the widely used standard method in the absence of a better solution.

There was a paradigm shift in cortisol measurement of fish when Alexander P Scott at the Centre for Environment, Fisheries and Aquaculture Science (CEFAS), U.K., came up with the idea of measuring cortisol directly from the water in the fish tank rather than taking blood samples. The idea was supported by the fact that fish passively released almost 40% of free steroids into the water [53]. It was later experimentally proven that the release took place via the gills [54]. Further detailed experiments have demonstrated the feasibility of the idea [52,55,56]. The apparent advantage is that the method is non-intrusive. Cortisol collected from water over a period gives an integrated picture of the mounting stress response from the fish. The cortisol freely passes through the gills unconjugated, which is the physiologically active form. It also

provides a snapshot of the stress level of the population, which might be more beneficial from a farming perspective.

A review by Tim Ellis et al. [57] gives detailed information regarding the advantages and critical pointers for non-invasive cortisol measurement. The essential parameters to be considered for the measurement are the gill surface area, the permeability of the gill, blood flow via the gills, properties of the surrounding water and temperature [56]. Since the measurement is performed in a recirculating system, cortisol concentration will depend on the biomass of fish in the tank, release duration, and dilution due to the recirculating water flow. So instead of concentration, the unit of measurement is cortisol release rate.

$$H_t = \frac{Vkt(C_t - C_0 e^{-kt})}{(1 - e^{-kt})} \quad \text{Eq (1)}$$

$H_t$  is the amount of cortisol released in ng,  $V$  is the volume of water in the tank,  $k$  is the instantaneous rate of decrease in concentration due to water inflow,  $C_0$  and  $C_t$  are cortisol concentrations at times '0' and 't', respectively.

The  $V$  in the tank is related to the in-flow of water,  $R$ , which in a well-mixed tank is given by

$$R = -\ln(1 - F) \left( \frac{V}{t} \right) \quad \text{Eq (2)}$$

Where  $F$  is the fraction of water replaced.

Eq (2) can be rearranged as;

$$1 - F = e^{-\left(\frac{R}{V}\right)t} \quad \text{Eq (3)}$$

Here the fraction  $R/V$  represents  $k$

Using Eq (1), the fish biomass and time, it is possible to calculate the cortisol release rate (ng/g/h). These equations are valid for a RAS system.

$H_t$  indicates a trend in the cortisol release and provides data regarding the deviation from the established baseline. Therefore, the dynamic behaviour of the system can be understood. However, the fish biomass cannot be accurately measured, and it is impossible to guarantee a homogenous solution while sampling with a single input line.

Again, it is emphasised here that mere cortisol detection cannot provide any valuable information to the farmer. However, it acts as an indicator for suboptimal growth conditions or the presence of a stressor. A detailed analysis of all the measurable physical and chemical parameters in the RAS combined with behavioural cues will lead us to the source of the stressor. Hereon necessary actions can be taken to eliminate or mitigate the problem. In this regard, the advanced process control system built for RAS is beneficial.

### 3.4.2 Strategies for cortisol measurement

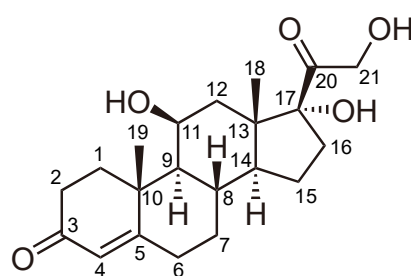


Figure 3.5- Chemical structure of cortisol. (Attribution: Calvero. derivative work: Anassagora, Public domain, via Wikimedia Commons)

Ideally, a cortisol sensor system required for aquaculture should (a) detect cortisol concentrations below 100 pM, (b) be non-invasive, (c) perform sample clean-up and enrichment, (d) have good stability, (e) provide an electrical output that can be fed into the control system, (f) be capable of automated sampling, and (g) run the entire

---

assay automatically with minimal user participation. The need to measure concentrations below 100 pM comes from the fact that cortisol gets highly diluted once released into the vast volume of water surrounding the fish [52]. Non-invasiveness is to make sure the fish is not disturbed and helps establish the baseline for the measurements. Since the water sample is not clean and contains a low level of cortisol, the sample should be cleaned up to reduce the matrix effect and be enriched to facilitate measurements despite a cortisol concentration below the limit of detection (LOD) of the sensor. To have a fit-and-forget sensor system, the critical aspect is to have proper system stability. When it comes to signal-conditioning, the most straightforward signal to manipulate is an electrical signal; hence it is preferred to have an electrical signal as the output of a sensor. The need for automation is dictated by incorporating the sensor into a more extensive automated control system like the supervisory control and data acquisition system (SCADA). It is always efficient to automate complex procedures; therefore, both the sampling procedure and the assay should be automated. This is not an exhaustive list, but it is expected for the sensor to have all the standard static (sensitivity, readability, repeatability, reproducibility, resolution, precision, accuracy, linearity, drift, and hysteresis) and dynamic (response time, lag, step response, ramp response, overshoot, dynamic error, and fidelity) characteristics of an excellent sensor system.

Recently challenges in designing non-invasive cortisol sensors for aquaculture and their potential for continuous monitoring were discussed by Sadoul [58]. Most of the literature available on the measurement of cortisol is for samples of human origin. There is much more research done on stress in humans than in animals. The central focus is to detect stress in similar ways as glucose measurement or incorporate it into wearable technology [59-61]<sup>1</sup>. Nevertheless, the detection strategies can be extended to other animals with minor or some modifications.

---

<sup>1</sup> On a lighter note, the spike in reviews on cortisol might be an effect of the ongoing pandemic



Some of the techniques to measure cortisol are listed below [62-64]:

### 1. Chromatographic Techniques

- Liquid chromatography-tandem mass spectrometry (LC-MS)
- Thin-layer chromatography
- High-performance liquid chromatography (HPLC)

### 2. Immunoaffinity based methods

- RIA
- Luminescent immunoassay
  - Chemiluminescent Immunoassays*
  - Fluorescence Immunoassay*
- ELISA
- Immunosensors
  - Optical - Surface Plasmon resonance (SPR)*
  - Mass - Quartz Crystal Microbalance (QCM)*
  - Electrochemical - amperometric, impedimetric, voltametric, field effect transistors*

The methods used to quantify cortisol in a laboratory setting and the techniques being developed for point-of-care testing have different approaches. Instruments such as LC-MS and HPLC are used for analytical procedures to assess cortisol levels in samples in a laboratory. These instruments have high sensitivity and specificity, but are generic, bulky, expensive, require extensive sample pre-treatment, and are not designed for a point-of-care application.

The main theme of my thesis is the development of immunoaffinity based methods and more specifically an immunoaffinity based biosensing platform for the detection of cortisol as will be described in Chapter 4

## Chapter 4 Immunoaffinity-based assays

*We are at the beginning of a new era of immunochemistry,  
namely the production of "antibody based" molecules.  
— César Milstein - Nobel Lecture (8 Dec 1984)*

---

In 1956, R. S. Yalow and S.A. Berson demonstrated the basic concept of a RIA for detecting insulin [65], and in 1959 their short communication regarding RIA was published [66]. After that, in 1960, the complete paper on RIA was published [67]. 1975. G. Köhler and C. Milstein developed a hybridoma technique to produce monoclonal antibodies [68]. In the same year, Jiri Janata reported a new technique called **"Immuno-electrode"**, paving the way for electrochemical immunoassays [69]. R. S. Yalow (in 1977), G. Köhler and C. Milstein (in 1984) received the Nobel prize for their respective research and laid the foundation upon which the central theme of this thesis is based.

This chapter covers general aspects and requirements of immunoassays, which is then followed by the description of the special case of immunoaffinity biosensors, more commonly referred to as immunosensors.

### 4.1 The Antibody

An essential component of any immunoassay is the antibody (Ab). Antibodies are glycoproteins produced in response to a foreign antigen entering the body. The versatility of an Ab lies in its high specificity towards the antigen. The immunoassays use this inherent property of the antibody to capture various analytes for further measurement.

Figure 4.1 shows the various components of an Ab. It has a heavy chain and a light chain, and the molecular weight is typically in the range of 150 kDa. Antibodies or immunoglobulins are depicted as a linear Y structure, although the 3D structure indicates globular domains [70]. The Ab has two antigen-binding regions, and the part within the antibody which interacts with the antigen is called paratopes. In contrast, a complementary surface configuration on an antigen is called an epitope. Antigens can have multiple epitopes, and sometimes this leads to cross-reactivity [71].

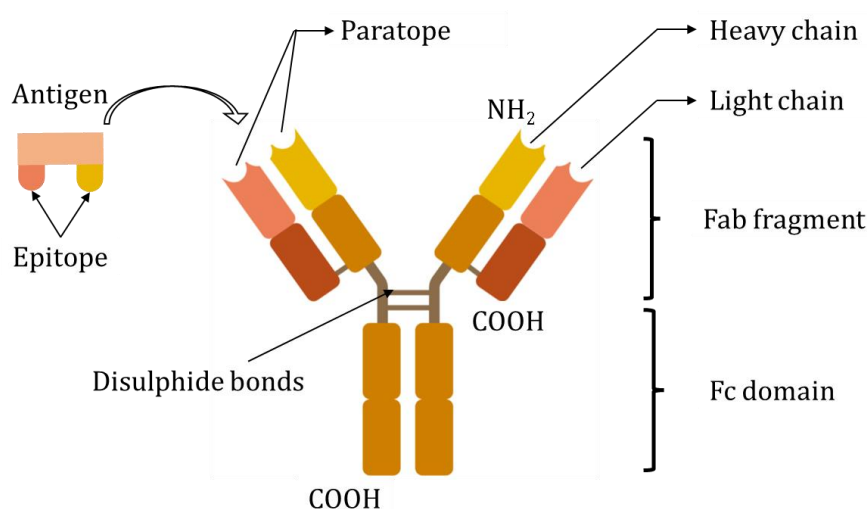


Figure 4.1- An immunoglobulin - IgG (~150 kDa). Fab denotes the antigen-binding fragment, and Fc denotes the constant region. The heavy chains are ~50-70 kDa, and light chains are ~23 kDa

Depending on the constant region of the heavy chain, the antibodies are classified into five different classes, IgG, IgA, IgD, IgE and IgM. IgG is the most abundant (Elgert 2009), and in this thesis, a subclass of IgG called the IgG2a is the primary biorecognition element.

The traditional method to obtain antibodies for research is through immunisation of small animals and collecting their serum. The immune response is elicited in the animal by injecting the antigen. However, in some cases, when the antigen is very small, like cortisol (< 1000 kDa), a macromolecule needs to be covalently attached to it to elicit an immune response. The antibodies produced by this method are

---

polyclonal, constituting a mixture of various antibodies. To obtain highly specific antibodies, i.e., monoclonal antibodies, the hybridoma technique can be used. Here, a single clone of antibody-producing hybridoma cells is used as the factory to produce monoclonal antibodies.

Both polyclonal and monoclonal antibodies can be used to create an immunoassay, as described by Jiri Janata [72]. Although cross-reactivity is considerably less pronounced in monoclonal antibodies, it should still be tested for different assays to ensure specificity. There are instances where non-specific binding might masquerade as specificity or selective cross-reactivity [73].

## 4.2 Immunoassays

Immunoassays encompass the detection techniques where the recognition or biorecognition element is an antibody. There is a trove of literature regarding immunoassay and its different formats [73,74]. Some of the major classifications and practical aspects of the immunoassays used in this thesis are discussed here.

Immunoassays can be classified into either indirect and direct, competitive- and non-competitive, as well as homogenous and heterogeneous assays [75]. Homogeneous assays require no separation step between the bound and unbound fraction before detection, whereas heterogeneous assays require a separation step.

This thesis focuses on the heterogeneous type of immunoassay, which requires an immobilisation step for the antibody or the antigen. In simple terms, the antibody or the antigen is attached to a solid surface and remove unbound fractions with a simple washing step. Although the complexity increases for heterogeneous immunoassays, these have certain advantages, such as better sensitivity and specificity since the washing step removes other interfering substances from the samples [76,77]. Figure 4.2 depicts various possible combinations of heterogenous immunoassay, performed on a solid support, using an enzyme labelled antibody or

antigen. In the case of an ELISA on a 96-well microtiter plate, the polymer plate forms the solid support.

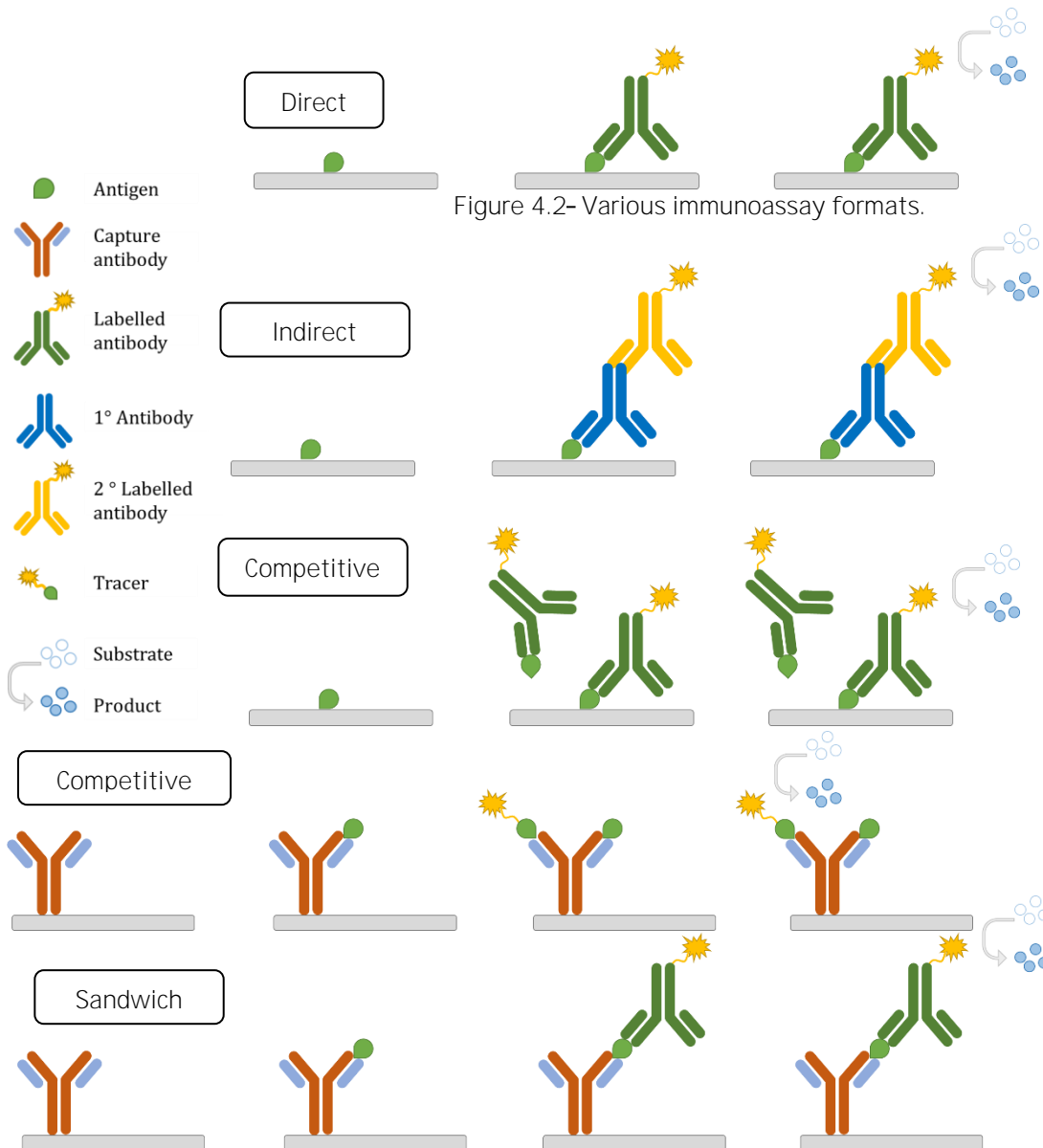


Figure 4.2- Various immunoassay formats.

Direct assay is the most straightforward format, where the antigen is coated on the surface, and a labelled antibody is allowed to bind. The excess antibody is washed away, and a suitable substrate is added. Depending on the amount of labelled

antibody present, the reaction on the substrate leads to the formation of a detectable signal like colour or fluorescence.

Indirect assay is an extension of the direct assay. Instead of preparing a label conjugated antibody for each analyte, a universal labelled antibody raised explicitly against the primary antibody is used. For example, if the primary detecting antibody was raised in rabbits, a labelled antibody raised against rabbit in goat (Goat against rabbit - GAR) is to be used. Now, this labelled GAR antibody can be used for any primary antibody raised in rabbits.

Competitive assay with a labelled Ab is based on that antibody in solution competes with a labelled antibody for binding to an immobilised antigen. Here, we use the term competitive to indicate how the labelled and unlabelled entities occupy the binding sites. This format is not very popular since we need a lot of antibodies for each assay.

Competitive assay with a labelled Ag is based on that the antigen in solution has to 'compete' with a labelled antigen (tracer) for the limited binding sites on an immobilised antibody. The distribution is again dependent on the ratio between the labelled and unlabelled entities. This assay format was chosen for the present thesis.

Sandwich assay is based on immobilised capture antibodies, to which the labelled secondary antibodies bind to a different site (epitope) on the antigen. This approach increases the specificity and is a non-competitive assay format.

In this thesis, the competitive heterogeneous assay format that relies on immobilising the antibody on different surfaces is used in most of the experiments.

#### 4.2.1 Immobilisation of antibody

The antibody needs to be immobilised to a solid surface for heterogeneous immunoassays; As depicted in Figure 4.3, different strategies are used to bind the antibody to a solid surface [78-82].

Physisorption is a weak physical interaction between two objects with no apparent chemical bonds [83]. It is the most straightforward technique to attach a molecule to a surface. ELISA plates made of polystyrene are treated with a corona discharge to make the surface hydrophilic. Manufacturers claim such plates to have a high protein binding capacity of around 600-650 ng IgG/cm<sup>2</sup>. MaxiSorp<sup>®</sup> from Nunc is an example of such pre-treated plates. In this thesis, the IgG was prepared in a buffer adjusted to a pH of around 9.6 to make it negatively charged. The hydrophilic/hydrophobic nature of the antibody makes it ideal for adsorption on a similar hydrophilic/hydrophobic surface through ionic and hydrophilic interactions.

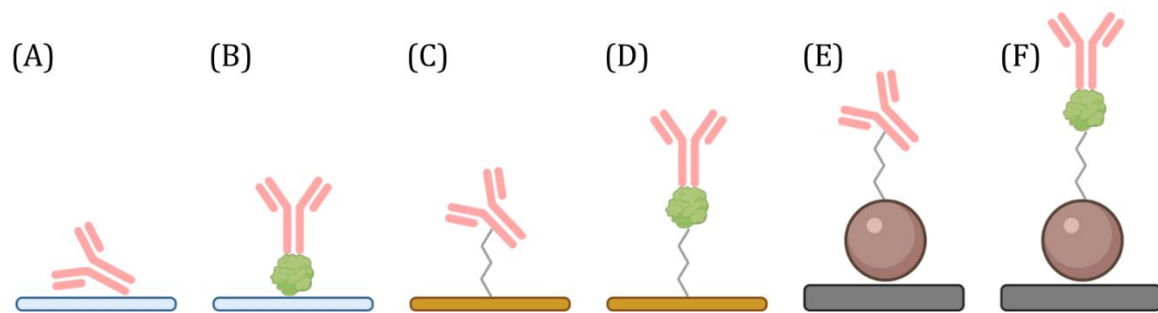


Figure 4.3- Various immobilisation methods. (A) Direct physisorption on a surface (B) Physisorption of an Fc binding protein and further binding with an Ab (C) Covalent bonding of the Ab to the surface using a linker (D) Covalent bonding of the Fc binding protein to a linker and Ab binding after that (E) Same technique as C but using a superparamagnetic bead (F) Same technique as D but using a superparamagnetic bead.

Covalent coupling: For surfaces made of gold, as is the case with a gold electrode system, physisorption might not be the best choice for adsorbing or binding the antibody. The usual approach is to use covalent binding. The gold surface is usually modified with a self-assembled monolayer of a suitable thiolated compound like 3-mercaptopropionic acid (MPA) or 11-Mercaptoundecanoic acid (MUA). The carboxylic ending can bind to the amine groups available on the antibody surface using zero-length crosslinkers, i.e. the crosslinking compounds mediate the conjugation in such a way that while forming the bonds, no new chemical structure is added between the conjugating molecules. One of the most popular zero-length crosslinkers used is 1-

---

ethyl-3-(3-dimethyl aminopropyl)carbodiimide (EDC), carbodiimides that can help in the formation of amide linkages between a carboxylate and amine group.

Fc binding proteins: Certain proteins are found on the surfaces of numerous cells and viruses that bind to the Fc part of immunoglobulins. Protein-A and Protein-G derived from *Staphylococcus aureus* and *Streptococcus* spp. bacteria are the best-studied examples of such proteins. These proteins have been used as ligands in affinity applications, mainly protein-A-affinity chromatography for antibody purification [84]. However, many immunosensor applications have used these proteins for immobilising the antibody onto a solid support. The protein, in turn, can be either physisorbed or covalently bound to the surface. Such a method would ensure that the orientation of the antibody is upright with the antigen-binding sites exposed. In this thesis, a genetically modified variant of Protein-G denoted by Protein-G', where the albumin binding sites have been removed, was used [85]. The recombinant Protein-G' is stable up to a temperature of 100°C and in the pH range of 1.5 - 11.0 [86]. This stability will be instrumental during the regeneration of the antibody surface (section 7.2.2)

Magnetic beads: A convenient strategy for attaching any protein on a surface is to bind the protein to superparamagnetic beads and then use magnets to keep them on any surface. The surface of the beads can be modified to bind the antibody or Protein-G covalently. In this approach, all the binding reactions can be performed in suspension, and the final mixture can be flown through a channel where permanent magnets can be used to attach the magnetic beads. There are many advantages of using a particle-based assay as it can (i) drastically increase the surface area being a 3D structure compared to a planar 2D surface, (ii) reduce diffusion distance since it is suspended in solution and not fixed on the surface and (iii) be easily removed and introduced.

Other strategies include attaching the antibody to nanoparticles made of gold, polymer beads, or carbon nanoparticles. Only relevant strategies used in this work



has been discussed. More details about the chemistry and protocols will be discussed in the coming chapters.

In this thesis work, the competitive assay format as shown in Figure 4.2 as well as several of the immobilisation strategies in Figure 4.3 have been used.

#### 4.2.2 Labels for immunoassays

As indicated in Figure 4.2, immunoassays usually need a label (but not always) to enable the detection of the antibody-antigen reaction. Numerous labels have been employed, such as radioisotopes, fluorophores, chemical probes, nucleic acids, and nanoparticles. [87], however, the most common labels are enzyme labels [88-90]. The most common enzyme labels are horseradish peroxidase (HRP),  $\beta$ -galactosidase, alkaline phosphatase (AP), and glucose oxidase (GOX). The antigen-antibody interactions are quantified by assaying the label conjugated to either the antigen or antibody. These enzymes then react with suitable substrates to form a product that is detected.

Table 4.1 show different possible options for the detection of different labels, where the label itself is directly detected, or the label is detected indirectly as for an enzyme label where the product of the enzymatic reaction is detected.

Table 4.1 - Various labels or label products and their possible detection strategies.

Label/label product	Detection method
Radioactive isotope	Gamma counter [91]
Chemiluminescent/Fluorescent	Photomultiplier tube or CMOS sensor [92]
Electroactive	Electrochemical

---

Chromogenic	Spectrophotometer, CMOS-sensor
None or some mass*	Quartz Crystal Microbalance (QCM) - change in frequency [93]
None or some mass*	Surface Plasmon resonance (SPR) - incident beam detection using charge- coupled device (CCD) [94]

---

\*For QCM and SPR, in certain cases, a nano or micro mass is added as a label to enhance sensitivity.

In this thesis, the enzyme label HRP had been employed along with electrochemical detection of the formed product from the enzyme-substrate reaction.

### 4.2.3 Immunoassays for cortisol

Historically RIA, and presently ELISA, are used for cortisol measurement [95]. Due to the risk of radioactivity and requirements of special permission, to work with radioisotopes, RIA is less prevalent. Researchers working with fish use ELISA as the standard method to determine the plasma cortisol level of fish [96]. Commercial kits for determining cortisol in humans are used to determine cortisol levels in fish [97].

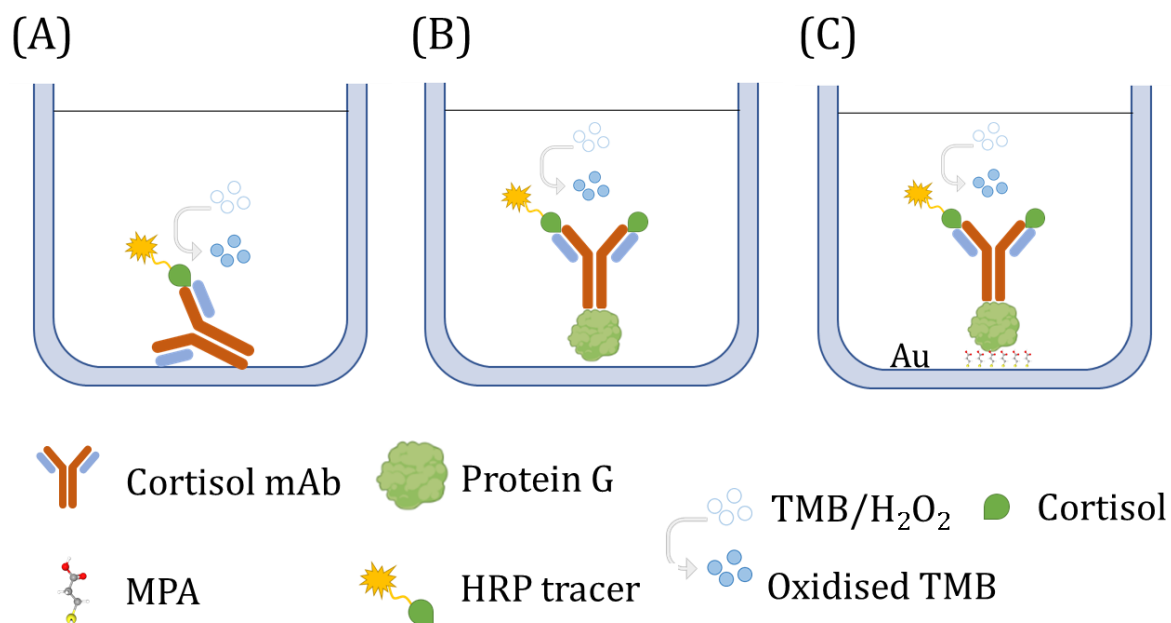


Figure 4.4 - (A) Physisorption of the cortisol Ab on the well plate (B) Physisorption of the Fc binding protein (Protein-G) and subsequent Ab binding (C) Covalent bonding of the Fc binding protein to a linker (MPA) and Ab binding after that.

Figure 4.4 shows the heterogeneous competitive assay strategy generally used to capture a small target analyte like cortisol with antibodies using an enzyme labelled competitor (tracer) to assess the analyte's concentration indirectly. In the standard ELISA set-up, based on a 96-well microtiter plate, the antibody is commonly physisorbed to the plate surface; however, specific binding proteins such as protein G can favourably be used to orient the antibody upright [98], as depicted in the schematic of Figure 4.4. The strategies in Figure 4.4 A and B were compared in this thesis for cortisol detection using the standard 96-well microtiter plate ELISA set-up. In a standard, ELISA set up the colour change due to the formation of the enzymatically oxidised product is usually measured at a suitable wavelength by a spectrophotometer. Here, **HRP is used as the label and 3,3',5,5'-tetramethylbenzidine (TMB) and hydrogen peroxide (H<sub>2</sub>O<sub>2</sub>) as the substrate, measuring the blue product's**

colourimetrically at 630 nm<sup>2</sup>, alternatively at 450 nm after adding the stop solution (4N sulphuric acid).

Figure 4.4C depicts another immobilisation strategy used in this thesis, using anti-cortisol antibodies immobilised on a gold surface with Protein-G as the protein to orient the antibody [99,100]. The protein G was immobilised via MPA. The tracer used for the competitive assay was a cortisol hapten conjugated to HRP. Similar to the above, the tracer competes with cortisol to bind to the antibody, and the generated signal is inversely proportional to the bound cortisol molecules, i.e., cortisol concentration. The HRP substrate used in this assay was 3,3',5,5'-tetramethylbenzidine (TMB) mixed with hydrogen peroxide, where the product was electrochemically detected at an electrode.

### 4.3 Immunosensors

From an instrumentation engineers perspective, a general principle of any measurement instrument is to have an input, a signal transduction and an output [20]. **A word of caution; the term 'signal transduction' is not to be confused with the intracellular information transfer in a biological context. It is similar to the classical case of how a 'cell' is different from the perspective of a physicist, chemist and biologist [101]. Many parts of this thesis will have similar words used purely from an instrumentation engineer's point of view than, say, a chemist or a biologist.**

Extending the idea of an instrumentation system from a regular plate immunoassay to an immunoaffinity biosensor - an immunosensor - the principle is that the biorecognition element (the antibody in this case) must be immobilised in close proximity to the physical transducer. We have the analyte that we need to measure, an antibody as a biorecognition element to capture the analyte, immobilised directly on the transducer, a transduction method to convert a chemical or physical change to

---

<sup>2</sup> 650 nm filter was not available in our instrument.

a detectable signal, and finally, a device to convert that signal to information, as shown in Figure 4.5.



Figure 4.5 - General principle of an immunosensor.

There are numerous examples of different immunosensor formats using different transducers and detection principles. Below some of those that have been used for cortisol detection are described.

#### 4.3.1 Surface plasmon resonance (SPR) immunosensor

In 1983 Bo Liedberg showed how the reflectivity of a thin layer of metal could be affected by the optical variations on one side of it [102]. Here surface plasmons act as very sensitive probes for the boundary layer condition of the metal film.

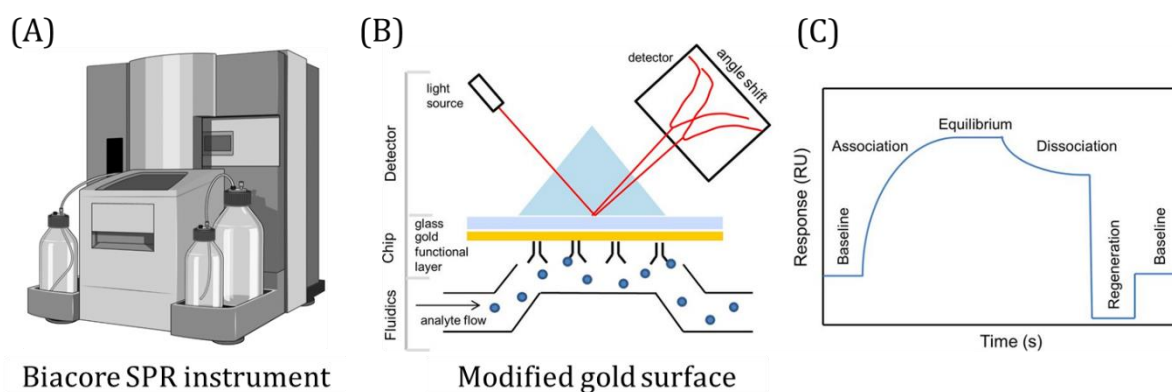


Figure 4.6 - (A) Biacore T200 system (B) basic principle of SPR is depicted (C) typical response curve showing association and dissociation of the target analyte. Adapted from [103] with permission from © Portland Press

The change in resonance angle indicates some change in the refractive index of the medium above, which can be exploited to detect the changes when an antigen-

---

antibody interaction occurs. Gold can be used to form very thin metal films, and then suitable surface modifications can be performed to immobilize the biorecognition element and subsequently the target analyte. Figure 4.6 shows a system where a microfluidic channel is used to deliver the target to the surface and an optical system to detect the subsequent shift when the target is captured. **Richard Schasfoort's** monograph, *Handbook of SPR*, gives in-depth details regarding SPR [104].

SPR based immunoassay is a label-free technique since no tracer, or a labelled element is necessary for detection, only the surface interaction is utilized. However, there have been many attempts at enhancing the signal using nanoparticles [105], gold nanoparticles [106,107] and magnetic beads [108]. The SPR technique has matured into a formidable technology for studying molecular interactions and bound complexes at the boundary layer (e.g., the Biacore system by G.E. Healthcare). The SPR technique can be adapted to be used in a flow system and hence automated. However, it necessitates sample pre-treatment to reduce the matrix effect caused by non-specific binding to the thin layer. A system for cortisol measurement which utilised a flow system and incorporated a simple sample pre-treatment technique (hollow fibre membrane extraction) was described by Stevens et al. [94]. However, the detection limit for this hollow fibre membrane integrated SPR sensor was only 3.6 nM even after membrane extraction. Although SPR is a robust technique for few measurements, repeated use of the same sensor surface for both immobilisation and measurement cause considerable baseline drift.

#### 4.3.2 Quartz crystal microbalance (QCM) immunosensor

Quartz crystals have a property called the piezoelectric effect, which is a reversible effect. An applied electrical potential on a quartz crystal makes it vibrate (resonate) in a plane perpendicular to the applied voltage. Also, if mechanical stress is applied, the crystal, in turn, generates a small voltage. This property was exploited by Gunter Sauerbrey, who coined the name quartz crystal microbalance (QCM) in 1959 [109], but unfortunately (for me), the paper is in German. However, the paper gives the

equation, known as the Sauerbrey equation, that is generally used today to relate the oscillation frequency with the mass deposited on a piezoelectric crystal. A QCM system detects the frequency shift observed on the resonator due to the change in mass when a target attaches to the surface [110]. A typical QCM (Figure 4.7) has a specific cut quartz crystal (AT plane) coated with a layer of conductive material like gold. This gold layer acts both as an electrical connector and a surface where antibodies or similar biorecognition elements can be immobilised [111,112]. QCM sensors have been used to detect cortisol [93].

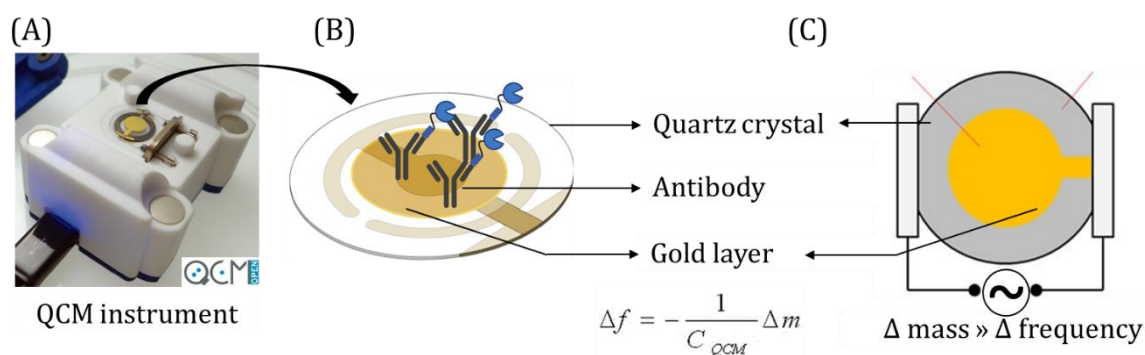


Figure 4.7 - (A) A quartz crystal microbalance system with its accompanying crystal element. (B) Antibodies are immobilised on the gold surface, and (C) the change in frequency is detected when the antibody captures the target. Figure adapted from [113]

Multiple analytes have been detected using QCM sensors, and with many companies manufacturing instruments for QCM, it is an up-and-coming platform. Some significant concerns include the high cost of the quartz crystal electrodes, limiting continuous monitoring and point-of-care applications. QCM sensors suffer from the disadvantage of matrix effect, non-specific binding, and baseline drift since the same sensor surface is used for immobilisation and sensing.

### 4.3.3 Electrochemical immunosensors

In electrochemical immunosensors, the antibody or the antigen are immobilised on an electrode surface. A simple three-electrode system, comprising a working electrode

(WE), reference electrode (RE), and counter electrode (CE), is utilised to detect the change in current or impedance between a working electrode and a counter electrode. There are several examples of electrochemical immunosensors for the detection of cortisol in the literature [114-122]. Figure 4.8A shows a schematic view of the electrochemical immunosensor system developed in this thesis using a gold electrode, and Figure 4.8B shows capture antibodies immobilised on the working electrode, and HRP is used as the label. The enzymatic reaction with the TMB/H<sub>2</sub>O<sub>2</sub> substrate produces a detectable electroactive molecule.

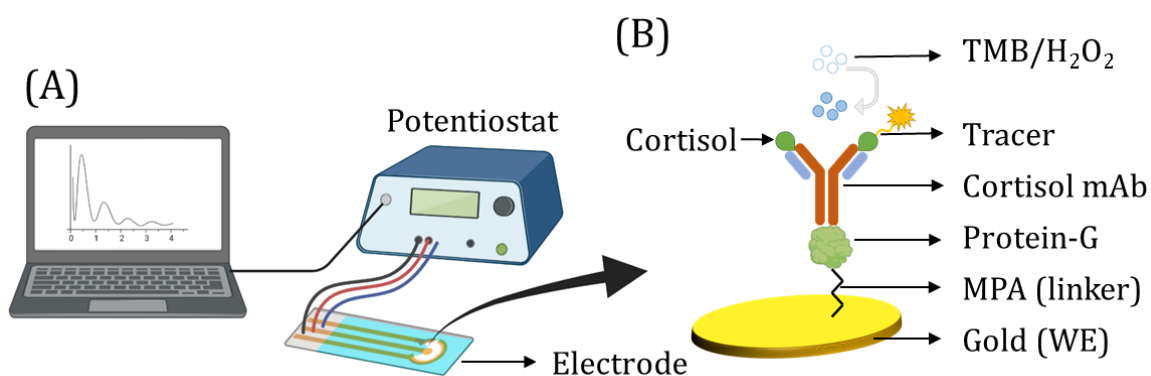


Figure 4.8 -(A) An electrochemical system with an electrode chip comprising a WE, RE, and CE connected to a potentiostat. (B) The WE is modified with an antibody to amperometrically detect the formed oxidised product or the impedance change when the tracer binds to the antibody.

Note that all the techniques discussed so far have a layer made of gold or a polymer, where the antibodies are immobilised with or without a spacer and with and without an Fc binding protein (Figure 4.3). Gold is commonly used as the base layer material for electrochemical analysis, quartz crystal microbalance, and surface plasmon resonance sensors. By chemisorption of thiol molecules on the gold layer, antibodies can be linked to the gold layer. The linker or spacer provide suitable functionalities for immobilization of biorecognition elements and reduces steric hindrance. Adding a protein like Protein G can provide a better orientation to the immobilised antibodies [98]. Aptamers [123] and molecular imprinted molecules (MIPs) [118] are sometimes used instead of antibodies for the detection of cortisol.



#### 4.3.4 Surface fouling

Proteins have amino acid residues with side chains exhibiting amino, carboxylic and methyl groups, the former two are hydrophilic and the latter hydrophobic hence they have the property of adsorbing to surfaces. Proteins can adsorb on gold also via various surface interactions like van der Waals forces or hydrogen bonding since an untreated gold surface is hydrophobic and a clean gold surface being hydrophilic. Depending on the final application, this surface adsorption of protein on a polymer or gold surface can be advantageous and disadvantageous. During an antibody-antigen assay, if the target analyte (antigen) or the tracer attaches to any other surface other than the binding site on the antibody, it is called non-specific binding. Suppose some other molecule other than the target analyte attaches to the specific binding site; it is called cross-reactivity. Any other molecule from the matrix attaching to the detection surface is interference. Non-specific binding and cross-reactivity lead to erroneous quantification of the analyte, and interference leads to lower sensitivity by preventing reactive species from reaching the electrode in the case of electrochemistry or increasing the background noise in the case of SPR and QCM.

The different strategies to eliminate non-specific binding are blocking the surface or using non-ionic surfactants to reduce surface or interfacial tension. BSA and caseins are used to coat surfaces to prevent the target analyte from attaching non-specifically to the surface. Dextran and polyethyleneglycol (PEG) are also used to coat the surface to prevent cell adhesion. However, it is pertinent to mention that protein adsorption onto polymer surfaces is precisely utilised while performing ELISA on a standard 96-well plate.

#### 4.3.5 Matrix effects

A significant concern in immunoassays, in general, is the effect of the sample matrix on the antibody-antigen binding and measurements. The matrix is the combined effect of all the sample components, excluding the analyte of interest [124]. The

---

matrix could be water, blood, urine, milk, or juice, to name a few. A sound measurement system should resolve all the components and give a very high signal only for the analyte of interest. Matrix effect is any deviation in the measured signal due to factors other than the analyte of interest. It occurs mainly due to non-specific binding or adsorption of unwanted proteins, debris, or elements on the antibody or the support surface. One needs to ensure that any interfering or cross-reacting components are removed before measurement. Such processes used to reduce or remove the matrix effect can be called sample pre-treatment or sample conditioning. Sample pre-treatment forms the most time-consuming part of any analytical method.

Depending on the measurement technique or the instrument, the sample pre-treatment steps may vary. Many methods have been developed for sample pre-treatment and, in some cases, even sample enrichment, where the target analyte is selectively enriched to improve its detectability. In immunoassays, the standard methods for sample pre-treatment are based on liquid-liquid extraction (LLE), solid-phase extraction (SPE), affinity separation, affinity filtration, and membrane extraction [125-128]. In this thesis, membrane extraction and specifically immune supported liquid membrane (ISLM) extraction for sample clean-up and enrichment has been employed, as will be described below.

#### 4.3.6 Immuno supported liquid membrane (ISLM) extraction

Supported liquid membrane (SLM) extraction is an advanced form of liquid-liquid extraction. In LLE, two immiscible liquid phases extract small analytes based on their partition coefficient and concentration gradient between the two phases. The famous octanol-water interface system is a good example. An SLM is formed by impregnating a nanoporous support membrane with an organic liquid phase, which is sandwiched between two aqueous phases, forming three distinctive layers (Figure 4.9), a donor phase, the SLM, and an acceptor phase. The organic SLM only allows extraction of non-ionic analytes, which means that depending on whether the analyte is an acid or a base, it can be rendered non-ionic or ionic by adapting the pH

in the donor and acceptor phase, respectively. In other words, the analyte should be made non-ionic on the donor side and reinstated in its ionic form on the acceptor side. A concentration gradient is created between the donor and acceptor by virtue of the change from non-ionic to ionic form, allowing extraction and enrichment of the analyte in the acceptor, as schematically illustrated for acids and bases in Figure 4.9A and B. In a typical flow based SLM extraction system (as developed in this thesis), during the extraction step, the sample with the analyte is continuously perfused through the donor channel, whereas the volume of the acceptor channel is kept small and stagnant, thus enabling very efficient enrichment of the analyte in the acceptor.

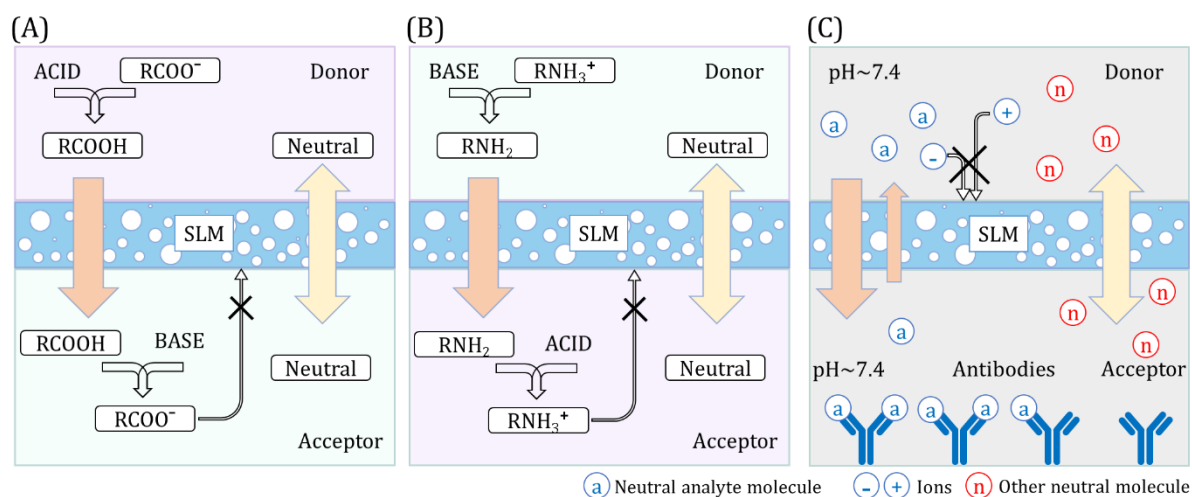


Figure 4.9 - SLM systems for extraction of acids (A) and bases (B) with the difference in pH used to entrap analytes. (C) An immuno-extraction based SLM (ISLM) system with antibodies placed in the acceptor to entrap and enrich the analyte.

The nanoporous support membrane is usually made of polypropylene or polytetrafluoroethylene. The choice of organic liquid depends on the partition coefficient of the target analyte, where common organic liquids used are Dihexyl ether and undecane. It was reported that for analytes with a log  $K_{ow}$  value less than 3, dihexyl ether is preferred over n-undecane [129]. Cortisol has a log  $K_{ow}$  value of 1.61; hence dihexyl ether was used.

---

Immuno-supported liquid membrane (ISLM) extraction (Figure 4.9C) is a variant of the SLM extraction method, in which antibodies are present on the acceptor side [130-132]. The mass transport and enrichment of the analyte is, in this case, driven by the concentration gradient created by the antibody-antigen interaction since the analyte is trapped by the antibody in the acceptor. For the antibody-antigen reaction to occur at optimal conditions, the donor pH has to be adjusted to be around pH 7.4. The advantage of ISLM extraction compared to normal SLM is on the one hand that permanently neutral compounds in principle can be extracted if the corresponding antibody exists, and on the other hand that the specificity and sensitivity can be improved. Cortisol is essentially a non-ionic species at neutral pH and can thus be extracted from the donor at the same pH as in the acceptor, where the antibody-antigen interaction is optimal. In the present study, a preliminary ISLM extraction system was developed and tested for clean-up and enrichment cortisol from fish tank samples where the fish had been exposed to different stressors. The result of these experiments will be described in more detail in Chapter 6 and Paper I.

If immobilized antibodies are exposed to a continuous flow like in a typical flow based immunosensor, they may eventually get detached due to shear from the flow [133]. In ISLM, this is prevented by separating the flowing inlet donor channel from the stagnant acceptor channel containing the antibodies



## Chapter 5 Analytical techniques employed

*Because a thing seems difficult for you, do not think it impossible for anyone to accomplish.*

*-Marcus Aurelius, Roman Emperor*

### 5.1 Flow Injection Analysis (FIA)

The different methods used in analytical chemistry employ routine laboratory procedures. There is much liquid handling involved, and repeatability can become a problem with manual handling. Automated solution handling seems to be a viable solution to reduce labour-intensiveness and errors. A flow injection (FI) system can replace all the mixing, addition, removal or separation of samples or reagents using standard glassware in a laboratory with a flow system that automatically performs the same operations (Figure 5.1).

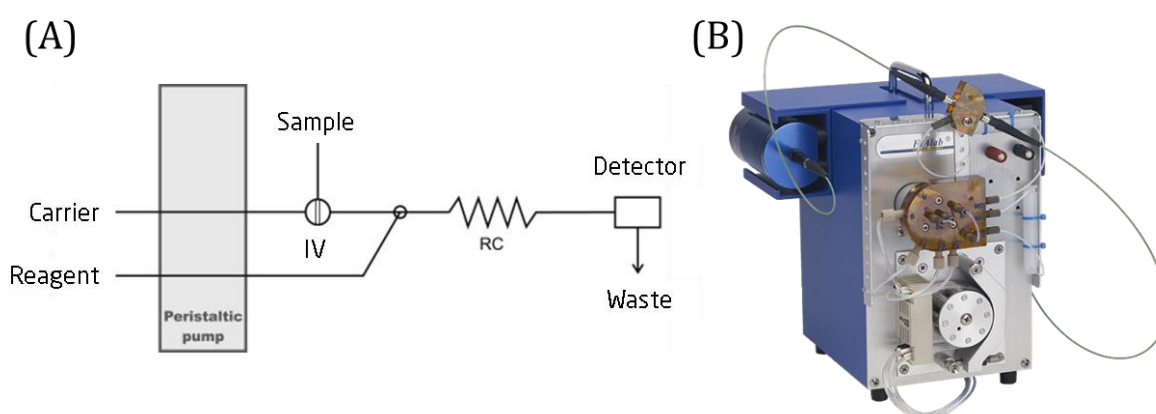


Figure 5.1- (A) FIA concept diagram. Adapted from [134] Copyright © 2014 Elsevier (B) A commercial FIA system from FIALab Instruments, Inc.

The history of FIA dates back to 1974 when Jaromir Ruzicka and Elo Hansen of DTU Chemistry developed a simple method of injecting a sample plug into a carrier flow to

transport it in a reproducible manner into a flow-through detection chamber. Monographs authored by the inventors Jaromir Ruzicka and Elo Hansen in 1988 and Bo Karlberg and Gil E Pacey in 1989 give a good idea of FIA systems and their applications. Jaromir Ruzicka also maintains a website describing the historical development from FIA to the newer SIA (sequential injection analysis) technique. It is an excellent read to understand how something gets invented and propagated.

A simple FIA system can be constructed from a peristaltic pump, low-pressure injection valve, a reaction coil, and a flow-through detector, all interconnected via Teflon tubing (Figure 5.1A). It works according to a straightforward principle: A defined analyte sample volume is injected via the injection port into the continuously flowing carrier stream, pumped by the peristaltic pump. The analyte plug is then transported and dispersed by the carrier flow in a controlled manner. When the analyte plug reaches the detector, it is detected (Figure 5.1C), which results in the typical FIA peaks shown in Figure 5.2.

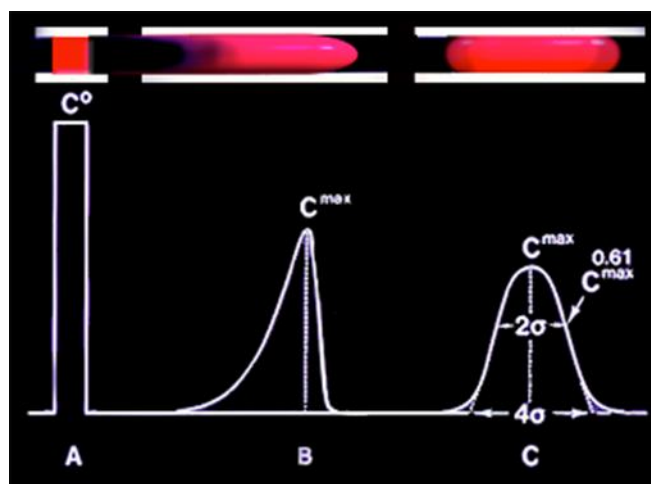


Figure 5.2- Various analyte plugs and their corresponding peaks. Adapted from <https://www.flowinjectiontutorial.com/~>

The flow profile of an incompressible liquid inside a tube with no-slip boundary condition is given by the Poiseuille flow profile, which is parabolic.

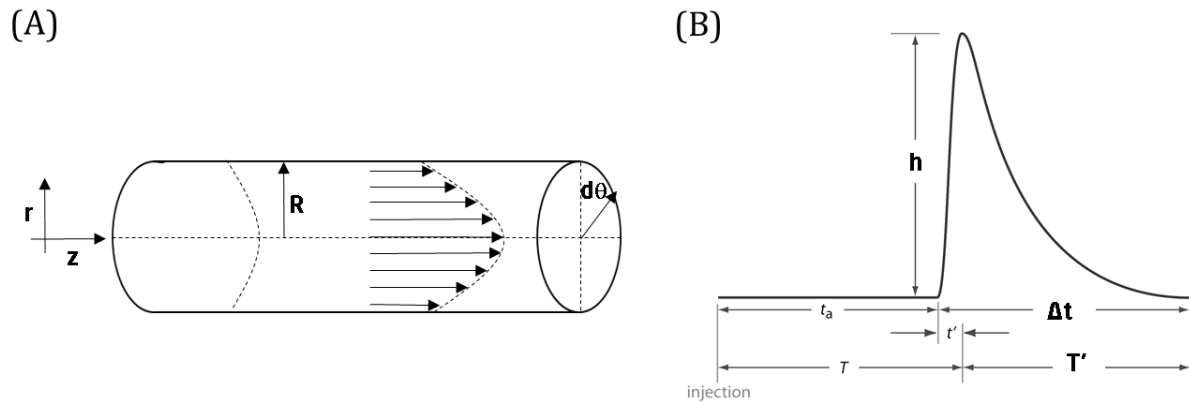


Figure 5.3- Poiseuille Flow profile inside a tube. (B) The profile of the signal is obtained at the electrode.

The flow velocity is given by

$$V_r(r) = V_{z0} \left( 1 - \frac{r^2}{R^2} \right)$$

where  $V_{z0}$  is the maximal axial velocity and 'R' the radius of the tube and 'r' is the radial distance of a volume element from the centre of the tube. If pressure and viscosity is included then,

$$V_r(r) = \frac{1}{4\eta} \frac{dP}{dz} (R^2 - r^2)$$

When 'r' reaches 'R' near the wall, the velocity becomes zero. When such a plug hits the electrode, the detector peak profile is given in Figure 5.3 B. Here the peak height 'h' is the most crucial parameter as it corresponds to the concentration of the analyte.

However, in a rectangular channel, the cylindrical polar coordinate must be changed to cartesian geometry. Let the channel have a height 'h'. The boundary conditions are midplane symmetry and no-slip at the walls.

$$V_x = \frac{1}{8\eta} \frac{dP}{dz} \left( z^2 - \left( \frac{h}{2} \right)^2 \right)$$



Another consideration is when a tube enters and leaves a rectangular channel in the z-axis, which causes a change in flow direction increasing the dispersion of the analyte plug. The curved tubes used in the injection loop can cause Dean flow attributed to the secondary rotational flow in the tube due to the centrifugal force created by the circular geometry.

**By Fick's second law of diffusion,**

$$\frac{\partial c}{\partial t} = D \nabla^2 c$$

where  $c$  is concentration,  $t$  is time and  $D$  is the diffusion coefficient of the species. For flow in one dimension, the equation can be written as

$$\frac{\partial c}{\partial t} = D \frac{\partial^2 c}{\partial x^2}$$

where ' $x$ ' is the distance. Hence, the concentration decreases with distance and time.

It has been shown that the dispersion in a FIA system increases with the square root of residence time  $T'$  given by

$$T' = \pi \left( \frac{d}{2} \right)^2 \frac{L}{Q}$$

where  $L$  is the tube length,  $d$  is the tube diameter, and  $Q$  is the volumetric flow rate. These are the factors that affect dispersion. However, it is to be noted that if the tube diameter is drastically reduced then, the fluidic resistance will be too high for the low-pressure pumping system to handle. So there needs to be a trade-off between the tube length, diameter, and pumping rate.

Another issue in a FIA system is caused by air bubbles. In my work, the primary cause of bubbles was due to bad fitting connectors (Figure 5.4).

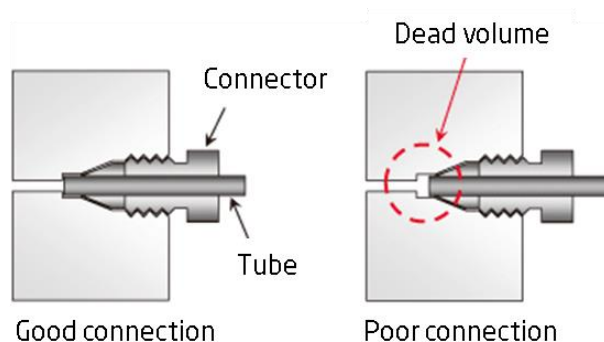


Figure 5.4- A schematic showing the difference between a good and bad connection.

Although there are proprietary instruments available for FIA, a FIA system was developed in-house to increase the design and automation flexibility. Chapter 8 is dedicated to discussing and developing a fully automated online FIA system for cortisol detection.

## 5.2 Electrochemical techniques

In a standard ELISA, the development of a coloured product that results from a reaction catalysed by the enzyme label and its subsequent absorbance measurement is used as the quantifier. In some cases, the coloured product is also electroactive. When a compound is electroactive, an electrochemical cell, as shown in Figure 5.5, can be used to investigate the compound further since it can fully or partially participate in a redox reaction. The electroactive product can be quantified using appropriate electrodes and electrochemical techniques (amperometry and voltammetry). The final signal in such a measurement system is electrical. Amperometry and voltammetry as electrochemical techniques can be used to quantify the analyte concentration in the bulk solution based on electron transfer (oxidation or reduction) at the interface between the electrode and electrolyte. Impedance spectroscopy is another technique that is used in electrochemical sensing. However, it is used to study changes at the electrode/electrolyte interface (e.g. affinity interaction between molecules on the electrode surface), not to quantify a

product resulting from enzyme catalysis. This thesis deals with electrochemical detection. The relevant electrochemical techniques used in this thesis are namely cyclic voltammetry, amperometry and impedance spectroscopy. Amperometry was used to quantify the enzyme product, while cyclic voltammetry was used to study the electrochemical behaviour of the enzyme substrate and product as well as to characterise electrodes. Impedance spectroscopy was primarily used to characterize electrode behaviour and the progress of electrode modifications.

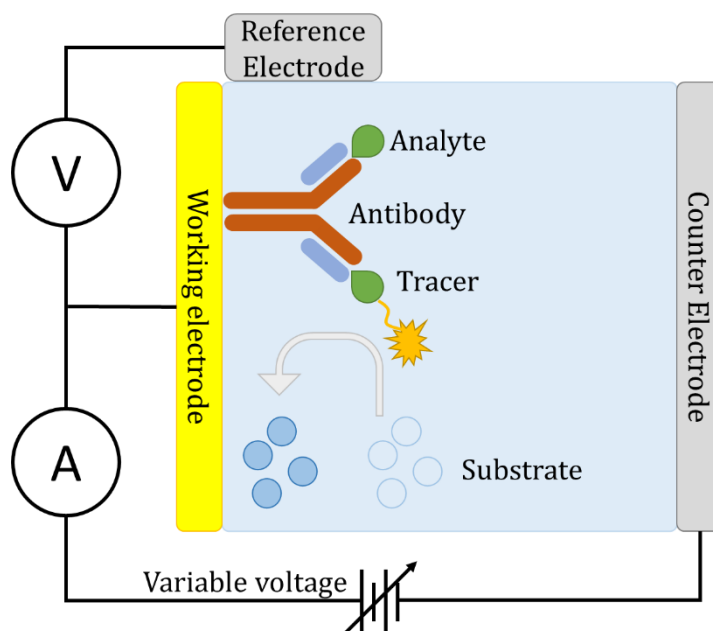


Figure 5.5- Circuit for performing voltammetry (adapted from Tektronix [135])

Electrolytic electrochemical cells have an electrode system where the applied potential is held constant or varied with time, and the current is measured. The minimum requirement for such a system is two electrodes for completing the current circuit - a working electrode (WE) and a counter electrode (CE). However, most often, a three-electrode system is used, as shown in Figure 5.5. The voltage at the WE is adjusted with respect to the RE. The resulting current passes between the WE and CE. The WE is the electrode under study where the reaction of interest happens. The typical material of choice for a WE are carbon or noble metals, such as gold or

---

platinum. For the CE, an inert material such as platinum is chosen, and the area should be large enough not to limit the overall current. The third electrode, the RE, is used as a reference point for poisoning the WE at the desired potential. The RE consists of well-defined materials capable of ensuring a steady potential. The stability of the reference electrode is crucial for measurement repeatability. The silver/silver chloride (Ag|AgCl) electrode is a widely used reference electrode (half-cell potential +0.197 V (saturated KCl) vs SHE). Due to its extremely fast electrode reaction, the potential of the RE does not change from its equilibrium potential. One virtue of the high-impedance circuitry of a potentiostat, at ideal conditions, zero current is expected to pass through the RE.

Figure 5.6 shows a simplified schematic diagram of a three-electrode system and an ideal potentiostat. It clearly shows that no current can pass between the RE and WE since it is connected to the input of an ideal operational amplifier configured as a unity gain differential amplifier or a voltage follower (buffer), which has infinite input impedance. The standard input to the electrode system is in the form of a triangular wave. However, the resolution of the digital to analogue converter will introduce small voltage steps, sometimes visible in cyclic voltammograms. The range for current measurement is decided by the resistor  $R_m$ . The lower the current, the higher the resistance value of  $R_m$ . The control amplifier with negative feedback from the RE will adjust the current at the CE to compensate for any apparent changes, thus maintaining a constant current or voltage [136].

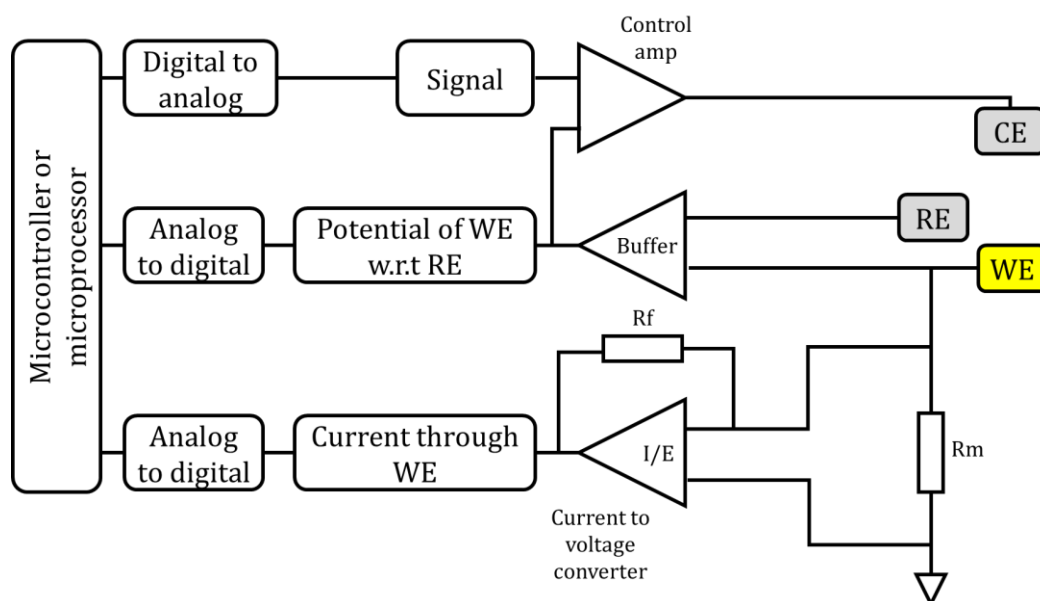


Figure 5.6- Schematic diagram of a potentiostat connected to a three-electrode system. Adapted from the Gamry instrument manual.

### 5.2.1 Cyclic voltammetry

Oxidation or reduction of an electroactive chemical species can be achieved by applying a potential at the electrode-electrolyte interface in cyclic voltammetry (Figure 5.7). A linearly varying voltage in the form of a triangular wave is used to scan the potential of an electrode. When the voltage is varied from a negative potential to a positive one, it is called the anodic scan where oxidation happens, and when the voltage is varied from a positive potential to a negative one, it is called a cathodic scan, and here reduction happens. The current is measured as a function of the changing potential. As the name suggests, the voltage is cycled between two values to elicit oxidation and reduction (redox) reactions of an electroactive chemical species (e.g. hexacyanoferrate(III/II), also known as ferri/ferrocyanide). An overpotential is applied to change the equilibrium state. A cyclic voltammogram (CV) gives essential information on the quality of electrodes when checked with standard redox probes by looking at the ratio of reduction and oxidation peak current, the peak potential difference, and hysteresis. In this thesis, cyclic voltammetry has been used

to characterise the behaviour of the different electrodes as well as to determine the optimal constant potential to apply for amperometric measurements (see next section and Figure 5.7B)

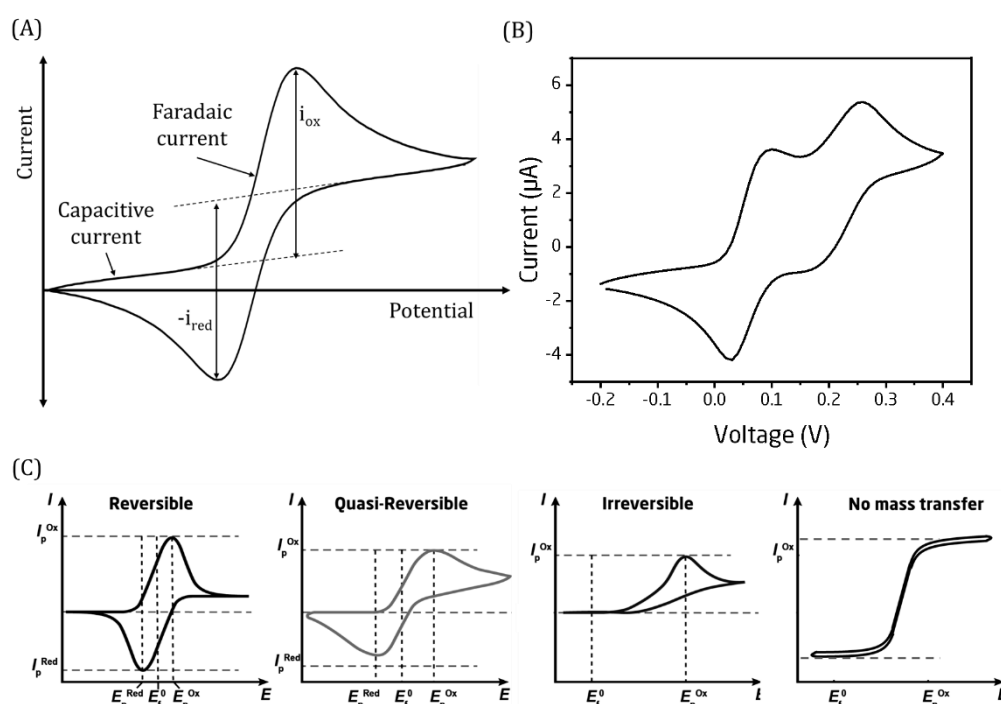


Figure 5.7- (A) A sample cyclic voltammogram (B) CV of the substrate TMB and (C) Samples CV's depicting different scenarios. Adapted from [137].

### 5.2.2 Amperometry

Amperometry is a voltammetric technique where a constant potential (overpotential) is applied to force the system to either favour reduction of oxidised species or vice versa. In an enzyme labelled assay, if the product formed in the enzyme-substrate reaction is electroactive, as in the case of HRP and TMB/H<sub>2</sub>O<sub>2</sub>, the product can be injected in a FIA system onto an electrode poised at a particular potential (overpotential for the reactive species) to measure the current response. In the case of HRP - TMB reaction, the formed product is oxidised TMB (TMB<sub>ox</sub>). The potential is set to force the reduction of TMB<sub>ox</sub>. Due to the flow, the electroactive product stays at the electrode interface only momentarily, and the current signal appears as a peak.

The amplitude of the current thus measured is proportional to the concentration of  $\text{TMB}_{\text{ox}}$  (Figure 5.8). Amperometry is useful when used for downstream detection where the immunoreaction takes place elsewhere.

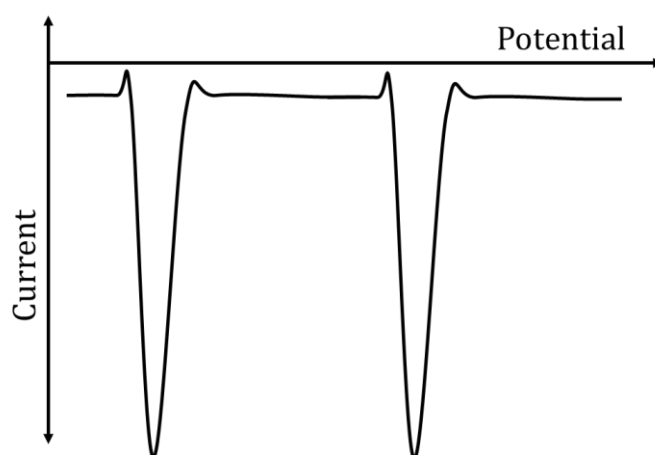


Figure 5.8- An amperometric signal (reduction current) generated in a FIA system.

### 5.2.3 Electrochemical Impedance Spectroscopy (EIS)

In EIS, the impedance of the electrochemical cell is measured over a range of varying sinusoidal frequencies and used to investigate the electrical properties of material and interfaces. It gives valuable information regarding the solution or system resistance ( $R_{\text{tot}}$ ), the charge transfer resistance ( $R_{\text{ct}}$ ), the double-layer capacitance ( $C_{\text{dl}}$ ), which all contribute to the overall impedance at various frequencies. EIS is used in corrosion studies, electric double layer formations, interfacial electron transfer, and charge transport kinetics. Figure 5.9A shows an obtained ideal impedance spectrum obtained. EIS is frequency-dependent due to the capacitive element. Therefore, the plot has both real and imaginary values and is called a Nyquist plot. The same plot can be represented as two separate plots of logarithmic magnitude and phase versus the logarithm of frequency called the Bode plot (Figure 5.9 C). The Randles equivalent circuit (Figure 5.9 B) is used to fit the experimental data to model the behaviour of the electrochemical cell.

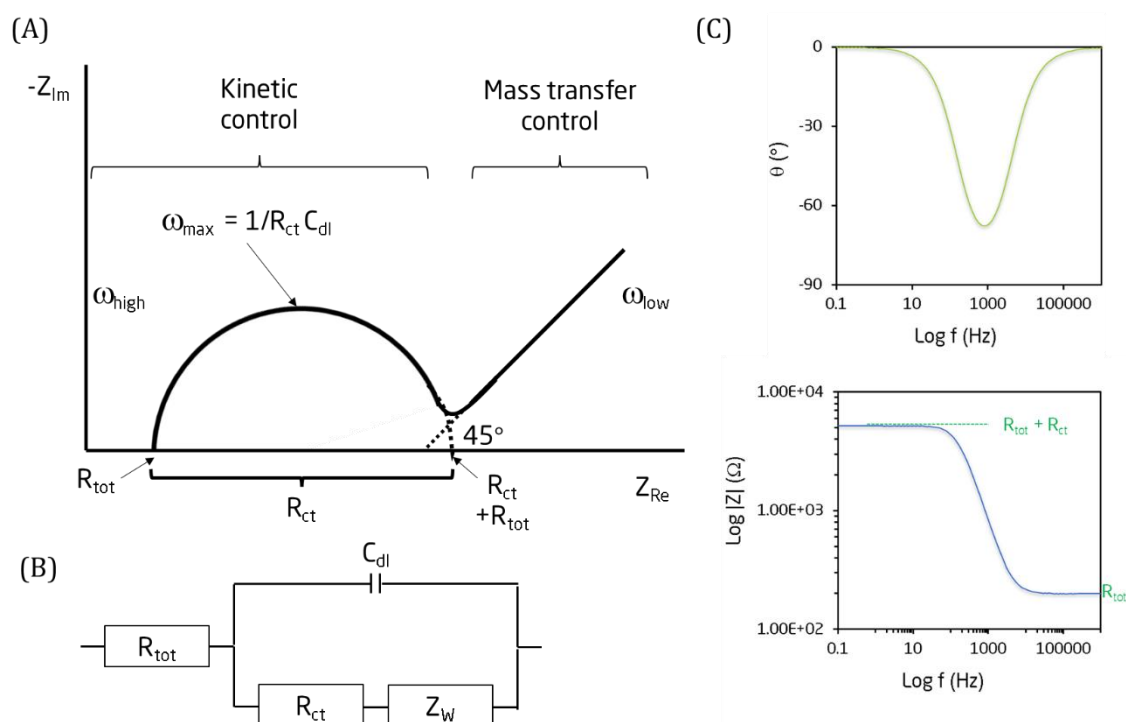


Figure 5.9- (A) A Nyquist plot in the complex impedance plane (B) Equivalent Randles circuit model (C) Bode plot showing the log magnitude and phase angle vs log frequency.

The total resistance ( $R_{\text{tot}}$ ) shown in the Randles equivalent circuit caters to solution resistance and all the other uncompensated resistances like connector resistance and wire resistance.  $C_{dl}$  indicates the double layer capacitance at the interface,  $R_{ct}$  is the charge transfer resistance, i.e., impediment of redox processes at the electrode interface, and  $Z_w$  the Warburg impedance representing the impedance contribution of diffusion. In an actual situation, the  $C_{dl}$  is represented by a constant phase element (CPE), which is a semiempirical component, accounting for deviations from pure resistance and capacitance.

The impedance of CPE is given by

$$Z_{CPE} = \frac{1}{Q(j\omega)^\alpha}$$

Where  $\alpha$  varies from 0 - 1. The condition  $\alpha = 0$  represents a pure resistor, whereas  $\alpha = 1$  corresponds to a pure capacitor.



Mathematically, the Warburg impedance can be represented by the same equation as is used for the CPE. In this case, the  $\alpha$  is 0.5.

In this thesis, EIS has been used to characterise the different immobilisation layers on the electrode and label-free detection using mainly interdigitated electrodes (IDEs).

## Chapter 6 Fabrication and Characterization

*"Failure is central to engineering. Every single calculation that an engineer makes is a failure calculation. Successful engineering is all about understanding how things break or fail."*

- Henry Petroski

The construction of an automated flow-based immuno-biosensing system for cortisol detection requires multiple components to be designed, fabricated and optimised. The essential components are the electrode and its flow cell for electrochemical detection, the immunoreaction chamber in which an ISLM step can be integrated, and the fully integrated FIA system, including pumps, valves, control circuitry and software, as depicted in Figure 6.1. There were two distinct levels of fabrication, at the component level and at the integrated system level.

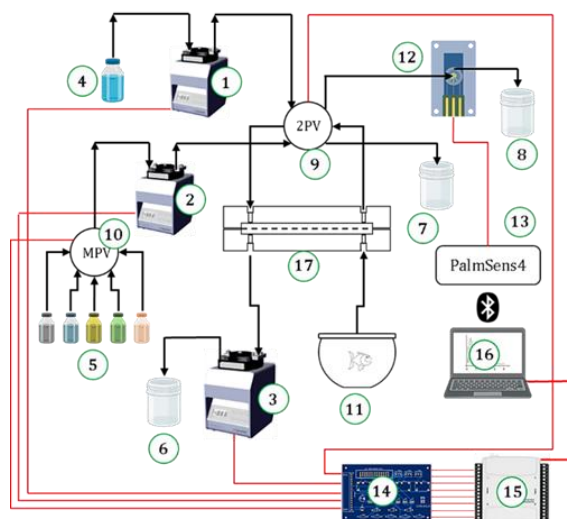


Figure 6.1 - The schematic representation of the final FIA system with the major hardware components such as pumps (1,2,3), a two-position injection valve (2PV, 9) and a multi-position valve (MPV) (10), Immunoreaction chamber (IRC) (here ISLM extraction unit is shown) (17), a control circuit (14), a PalmSense4 potentiostat (13), and detector electrode (12).

The project goal was to construct a system that not only functions well under laboratory conditions but should also be scalable and field-deployable in fish farms. This ambition was demanding considering the duration of a PhD project. Nevertheless, efforts were made to ensure this aspect during both design and fabrication. The fabrication ideology involved specific efforts to use industrial-scale manufacturing processes with polymer substrates and conscious efforts not to use polydimethylsiloxane (PDMS). On the integrated system level, it involved avoiding unstable chemicals and the elimination of manual intervention during the assay. Other factors explicitly used to enhance system versatility will be discussed when such topics are deliberated. This chapter deals with the fabrication and characterization of electrodes and polymer-based electrochemical flow cells and immunoreaction chambers. Their integration into the fully automated immunobiosensing system will be described in Chapter 7 and Chapter 8.

The good thing about being at DTU is the access to the state-of-the-art class 10-100 cleanroom nano- and microfabrication facility called DTU Nanolab (earlier DTU Danchip). Most of the electrode fabrication was done inside the cleanroom using highly specialised tools. The tools in the cleanroom are periodically decommissioned and upgraded, so one may find some tools missing but replaced by a piece of better equipment. Therefore, occasionally some of the processes may have to be re-optimised with different parameters before implementation. The detailed process flow for various processes is available in Appendix A.2. The other major pieces of equipment used outside the cleanroom were a micro-milling machine (CNC Mini-Mill/3 Pro from Minitech Machinery Corp, Georgia, USA), a LASER micromachining tool (microSTRUCT vario from 3D-Micromac AG, Germany), an injection moulding machine (Engel Victory 80/45 Tech from Engel GmbH, Austria), a benchtop CO<sub>2</sub> LASER (Epilog Mini 18 from EpilogLaser, Golden, CO, USA), and a soldering station (Weller-tools, USA). Multiple software packages for computer-aided design (CAD) (AutoCAD, SolidWorks, Fusion360 and Inventor), photolithography mask design (CleWin5) and G

Code generation (EZ-Cam17 and Cimatron 12) were also used. The electrochemical equipment was a Palmsens4 potentiostat (PalmSens BV, Netherlands).

## 6.1 Polymer fabrication of flow cells, Immunoreaction chambers (IRC) and test setups

The major polymer parts are the IRC, the flow cells and test setups for the electrodes. The chosen materials were polymethyl methacrylate (PMMA), polycarbonate (PC) and cyclic olefin copolymer (COC). PMMA has the advantage of optical transparency (92% transmission of visible light) and machinability. PC was sometimes replacing PMMA for setups where ethanol was used since PMMA cannot withstand ethanol. Finally, COC has the advantage of superior optical quality and chemical resistance. While it was relatively easy to acquire PMMA and PC sheets or plates of thickness ranging from 0.5 mm to 15 mm, it was almost impossible to get similar COC sheets or plates. In the case of COC, the parts were either injection moulded in-house or procured from the few companies providing sheets typically having a thickness range from 1 mm to 1.5 mm. The primary method for machining the parts was to use micromilling. Micromilling is a mechanical method where a sharp rotary tool removes material from a solid workpiece. The rotary tool is called an endmill. The process is as depicted in Figure 6.2 A.

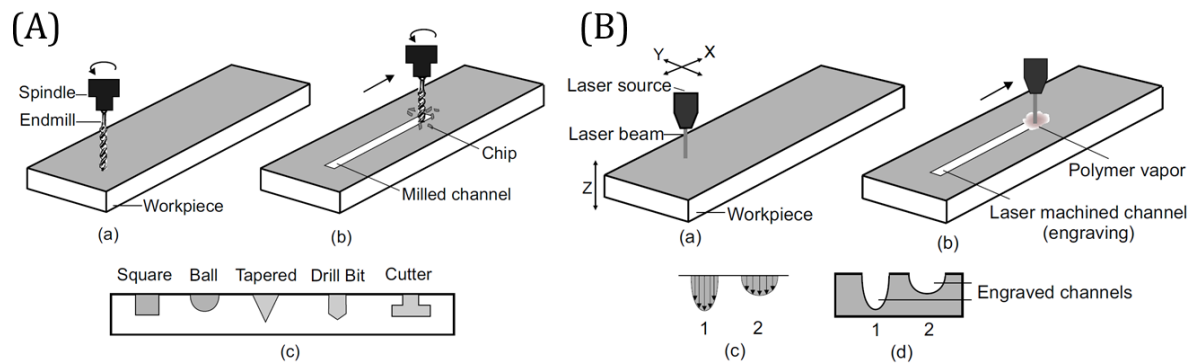


Figure 6.2 - (A) Schematic showing a micromilling process and different profiles of material removal. (B) Schematic showing LASER ablation of polymer and the subsequent profiles of the formed channels formed. Adapted from [138]

The second method reported in many papers deals with Laser ablation. Here a powerful pulse train of LASER beam is focussed on the surface of a material to ablate it in small increments (Figure 6.2B). LASER ablation has a better resolution than micromilling. However, both micromachining processes have some drawbacks. If the micromilling tool is not very sharp or a wrong machining parameter is set, the milled surface will have uneven or protruding edges (burr) due to incomplete material removal (Figure 6.3A). This edge effect mainly causes problems during the bonding of two surfaces; hence, a deburring step is required for better bonding. Laser ablation inadvertently causes redeposition of some material on the surface when channels are created, or structures are cut out (Figure 6.3B). This material deposition also hampers bonding.

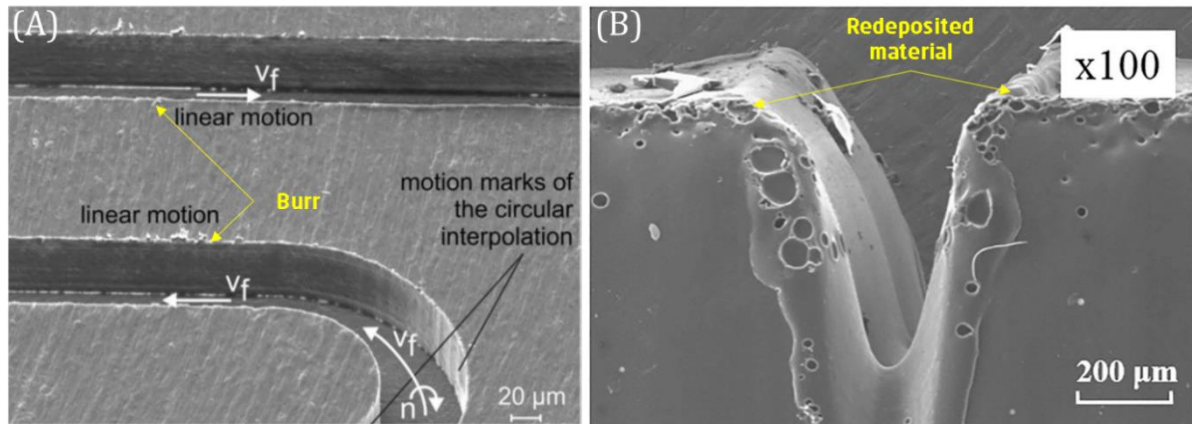


Figure 6.3 - (A) Micromilled channel on a PMMA substrate. (B) CO<sub>2</sub> Laser ablated groove on PMMA. Adapted from [139,140]. Figures are reused with permission.

### 6.1.1 Test setups

Test setups are components created to test the fabricated electrodes, providing the required liquid-tight sealing and electrical and fluidic connections to the electrodes. The materials of choice were PMMA and PC. Both batch and flow systems were fabricated. The required CAD models (Figure 6.4A) were created using AutoCAD or SolidWorks and converted to G Code using EZ-Cam or Cimatron. The G Code is a computer numerical control (CNC) programming language used to control micromilling machines. They contain the data required for motor movement, feed rate and tool change. The spindle rotation speed and feed rate were optimised based on the tip size of the end mill or drill bit being used (Figure 6.4B). A test setup entirely milled from PMMA with slots for four electrodes in an open well (batch) format is shown in Figure 6.4C.

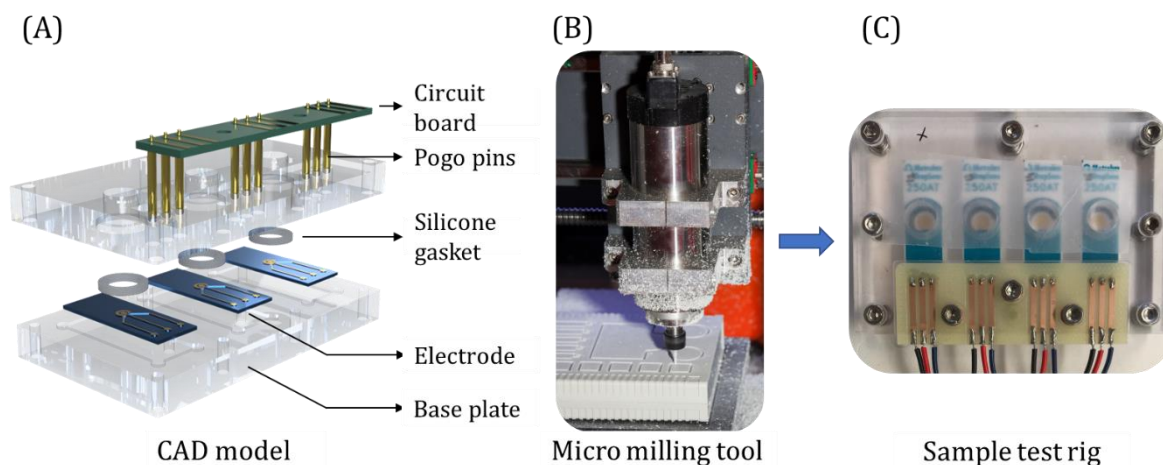


Figure 6.4 - (A) CAD model of a required test setup (B) A milling tool in action (representative) (C) The finished test setup after assembling the different micro-milled parts.

The parts created using micromilling are limited only by the workpiece dimension the tool can handle and by the 2.5D axis. The machine can only move in two directions at a given time. Such micromilling machines convert a 2D image into 3D with an additional depth input. Hence, overhanging, or sloped structures cannot be fabricated. Nevertheless, with some improvisation or adding sloped base support, even these restrictions can be overcome. So, the realisable designs are only limited by our imagination and the tool restrictions mentioned above. Figure 6.5 shows the different test setups fabricated during the project to cater for different commercial and cleanroom fabricated electrodes. Some of the designs can cater up to eight electrodes at a time.

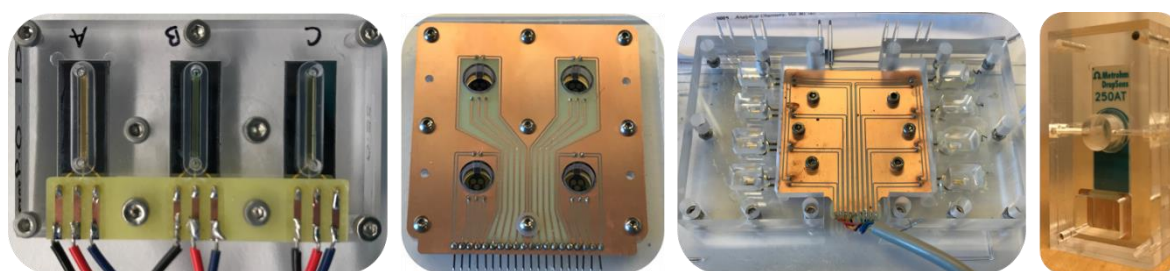


Figure 6.5 - Different test setups that were fabricated for various electrode designs.

Circuit boards fitted with spring-loaded pins (pogo pins) were fabricated to create electrical contact with each electrode. The soft loading of the pogo pins ensured that the delicate gold layer was not destroyed with repeated use while ensuring good electrical contact. A FR4<sup>3</sup> circuit board was also micromilled to create the required circuit. The silicone gasket used to ensure liquid-tight fitting was laser cut using a benchtop CO<sub>2</sub> Laser. A 0.1 mm radial and 0.2 mm axial tolerance were given to the gasket design to ensure slight pressure when assembled. High-grade silicone rubber was chosen for its outstanding elastic properties, chemical resistance, and temperature tolerance. However, there is a possibility of limited swelling with mineral oils or solvents. The assemblies in (Figure 6.5) are held together using either M2 or M3 screws and nuts.

Batch systems were designed to have an open well type of configuration, and the flow cells had either wall-jet or thin-film configuration. Polytetrafluoroethylene (PTFE) tubing (with 1/16" outer diameter) was interfaced to the flow cells, and the design was made to create a snug fit between the tubing and the fabricated part (Figure 6.6). An inlet/outlet hole of 1.575 mm in diameter gave the required snug fit

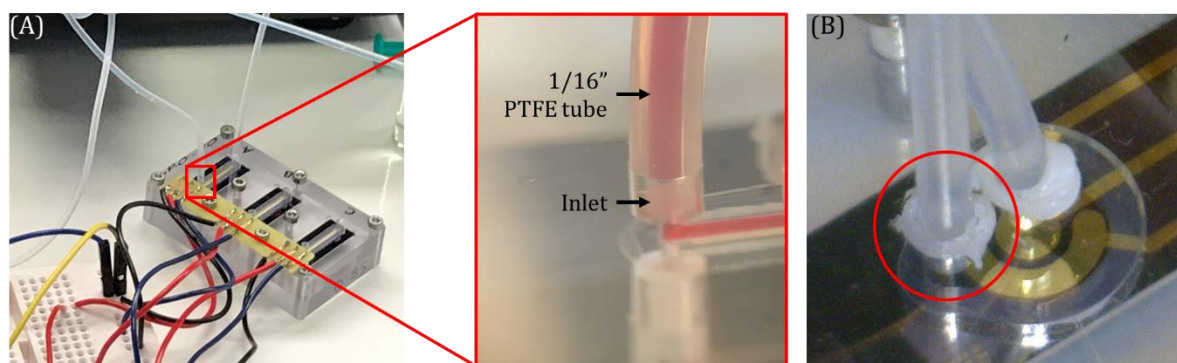


Figure 6.6 - The PTFE tube snug fitting. An extra layer of silicone paste (red circle) to prevent air bubbles.

<sup>3</sup> fiberglass-reinforced epoxy-laminated sheets (FR4 is the classification of the flame retardant board)



for the PTFE tubing. The inlet hole size needs to be reoptimized depending on the used material

The flow profile of a wall jet configuration using COMSOL simulation is given in Figure 6.7.

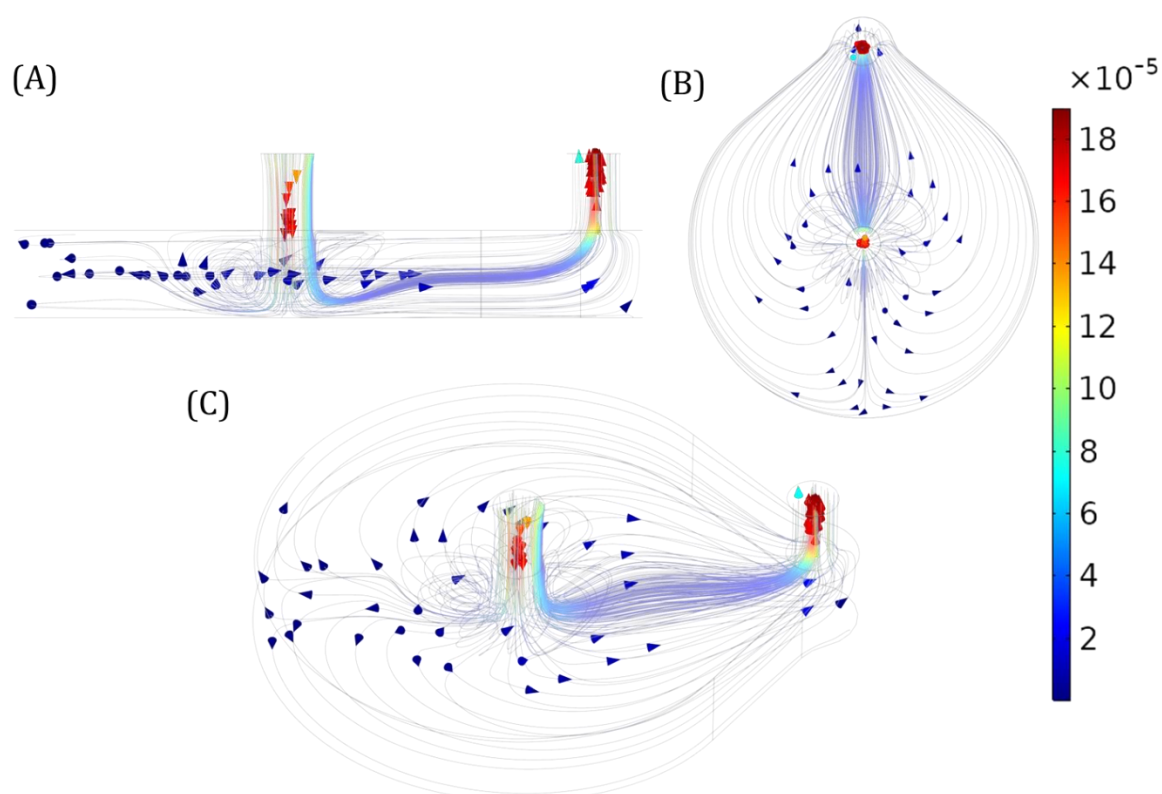


Figure 6.7 - The flow simulation inside the wall-jet configuration. The velocity is shown in m/s (A) Front view of the chamber (B) Top view of the chamber (C) Two-point perspective of the chamber. The lines with arrow represent velocity.

As it can be seen, in the wall jet configuration the fluid through the inlet directly impinges on the working electrode and spreads radially. In an ideal situation, there should be multiple radial outlets to have a uniform distribution of flow. However, for practical reasons only one outlet has been designed.

The following section describes the design and fabrication of the IRC and the faced challenges.

### 6.1.2 Immunoreaction chamber (IRC)

The function of an IRC is similar to an ELISA well plate. It provides the solid support required for an immunoassay but is performed in a flow channel (Figure 6.8). The IRC houses the immobilised capture antibody, allows the flow of multiple buffers and reagents, and performs an assay including substrate conversion and regeneration.

**The system is designed such that the IRC forms the 'injection loop' of the FIA system,** which means that the product formed in the IRC can be injected into the detection chamber.

The machining of the IRC polymer parts was mainly done using micromilling, but towards the end, the injection moulding technique was utilised to demonstrate such capabilities. The easiest option to assemble the parts to form leak-proof channels is to use a silicone gasket and screws to fasten the parts during assembly. However, industrial manufacturing techniques, such as UV assisted thermal bonding and ultrasonic welding to join the parts together, were also tested. Other possible bonding methods, such as solvent assisted bonding, pressure-sensitive double-sided adhesive bonding, and thermal fusion bonding, were not considered [141]. The final aim was to create injection moulded parts that could be bonded using UV assisted thermal bonding. Figure 6.8 presents the general IRC design; the purpose, design logic and function are described below.

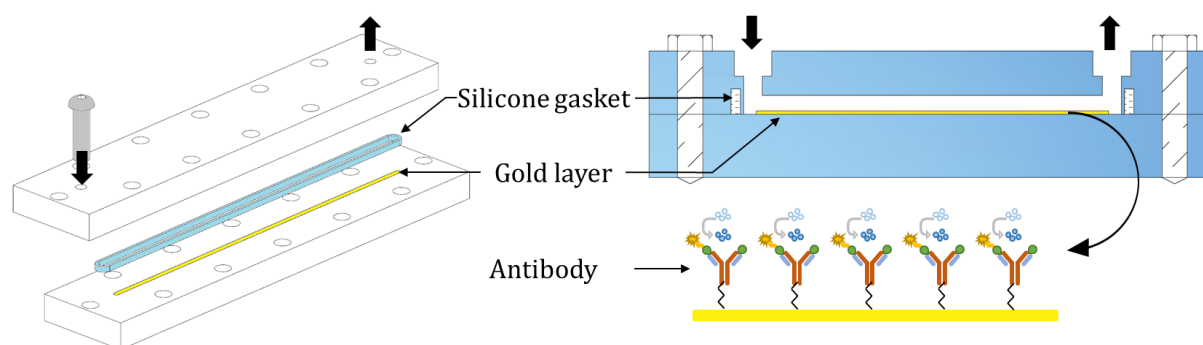


Figure 6.8 - Schematic of a simple IRC with a gold layer in the channel to immobilise the antibody.

Figure 6.9 shows different designs using the two different assembly methods (blue designs using screws (A-C)) and green designs using UV assisted thermal bonding (D-F)).

The 1<sup>st</sup> design (Figure 6.9A and D) had the aim to be used with antibodies immobilised on magnetic beads. It was fabricated using 5 mm thick PMMA sheets and had two 88 mm x 18 mm parts. The lower part formed the base plate with a 66 mm long, 2 mm wide, and 3 mm deep slot for housing a permanent rare earth magnet, and the upper part had a rectangular 68 mm long, 0.5 mm wide, and 0.4 mm deep channel. The choice of the rectangular channel was for ease of machining (flat end mill) and provided no advantage for the assay. The inlet and outlet to the channel **were designed to allow a snug fit of 1/16" PTFE tubes with an inner diameter (ID) of 0.5 mm.** The cross-sectional area of the rectangular channel was designed to match that of the tubing. A slot was milled around the channel to house a silicone gasket. The silicone gasket was 1 mm thick and was cut out from a silicone sheet using a CO<sub>2</sub> laser. M3 screws were used to fasten the two parts together. The device was leak-proof and could be used to perform assays with magnetic beads. The design in Figure 6.9 (D) is like in (A), except that UV-assisted thermal bonding was used instead of screws for assembling the parts.

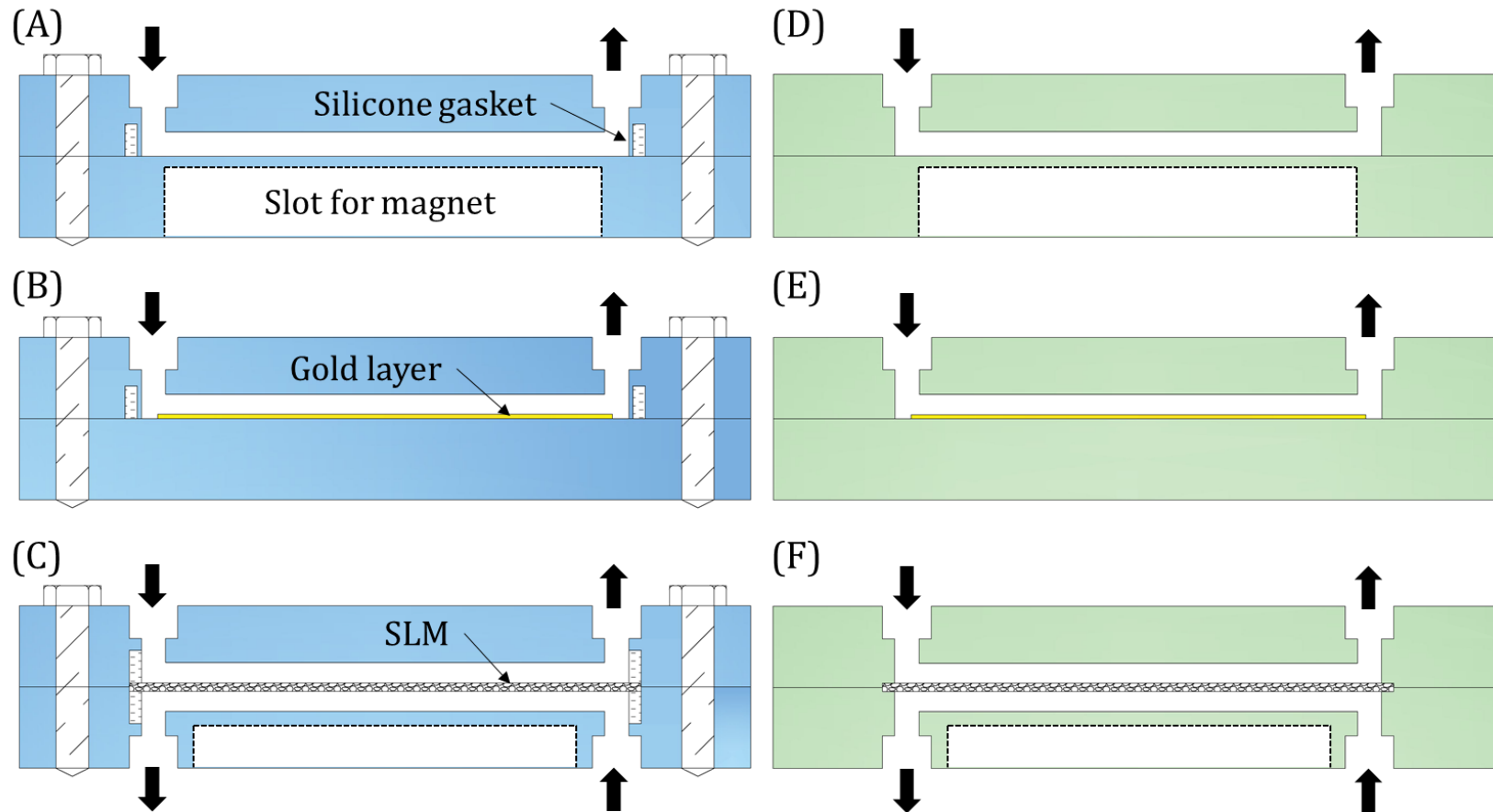


Figure 6.9 - The different configurations of IRC. (A), (B) and (C) represent IRCs assembled using screws, whereas (D), (E) and (F) are bonded together using UV assisted thermal bonding.



UV assisted thermal bonding represents a solid-state welding process, where components fabricated of a thermoplastic material like PMMA are briefly exposed to deep UV and then pressed between two temperature-controlled plates. Upon UV irradiation, the PMMA surface undergoes photolytic degradation by which the polymer chains on the surface (a few micrometres deep) are cleaved, thereby lowering the glass transition temperature of the polymer [142]. The advantage is that bonding can be achieved without reaching the glass transition temperature of the bulk polymer. Hence, the integrity of the micromilled structures is maintained.

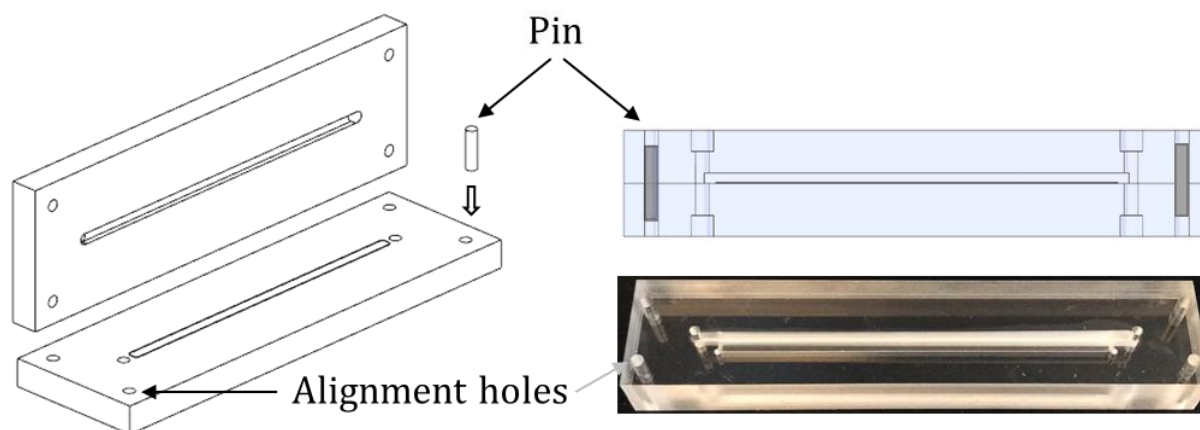


Figure 6.10 - Schematic of an IRC with the location of alignment holes and an actual micromilled PMMA based IRC after UV assisted thermal bonding

The polymer parts to be welded together were wiped with isopropanol (IPA) before placing them in the UV chamber equipped with a 380 W UVB mercury lamp (DYMAX, 5000 EC with bulb 36970, CT, USA). The exposure time was optimised to be 45 - 50 s since anything above 60 s would start to heat the polymer parts. The heating is due to infrared emitted by the mercury lamps. Although there are setups where the **infrared is filtered out to get a 'cold' UV** [142], it was unavailable in our instrument. Immediately after exposure to UV, the polymer parts were aligned and placed between preheated (85 °C) thermal bonding press plates. The alignment was done using stainless steel pins ( $\varnothing$  2 mm; length 4 mm) inserted into the alignment holes of each part (Figure 6.10). The plates were pressed together at  $\sim$ 6.3 MPa for 5 min. The heating was turned off, and the pressure kept on for another 45 mins or till the setup had cooled down to 50°C. The passive cooling step was implemented to relieve the

thermal strain. The pressure was optimised for 5 mm thick polymer parts. Lower pressure could be used for thinner polymer parts to prevent deformation. A significant consideration during thermal bonding was to ensure equal force distribution on the polymer parts. The bonding press could only ensure the bonding of parallel surfaces. However, if the parts have non-contacting surfaces like a slot or hole, the bonding around such places would be improper. Therefore, the magnetic slots and inlet holes were machined after the bonding. The alignment holes were used to realign the part on the stage of the milling machine.

The 2<sup>nd</sup> design (Figure 6.9B and E) uses a gold layer as the antibody immobilisation support. The previous design using magnetic beads provided versatility but less stability than the gold support. The base plate in this design was COC, and an e-beam evaporator in the cleanroom was used to deposit a 50 nm titanium adhesion layer and 200 nm of gold onto the COC substrate. A PMMA shadow mask was used to define the pattern. The structure of the upper plate and the assembly technique were the same as in the design of Figure 6.9A and D. Many initial trials of the immunoassay and FIA system were tested using this configuration. Design (E) is like the one in (B), except that the assembly was done through UV assisted thermal bonding.

The two designs discussed so far were fabricated and tested to be integrated into the FIA system (Chapter 7). Although these designs could measure cortisol in a lab setting, we needed to consider the matrix effect caused by the actual water samples and methods to reduce or eliminate the same, as well as the potential need of an enrichment step. The SLM extraction described in section 4.3.6 was utilised for sample clean-up and enrichment.

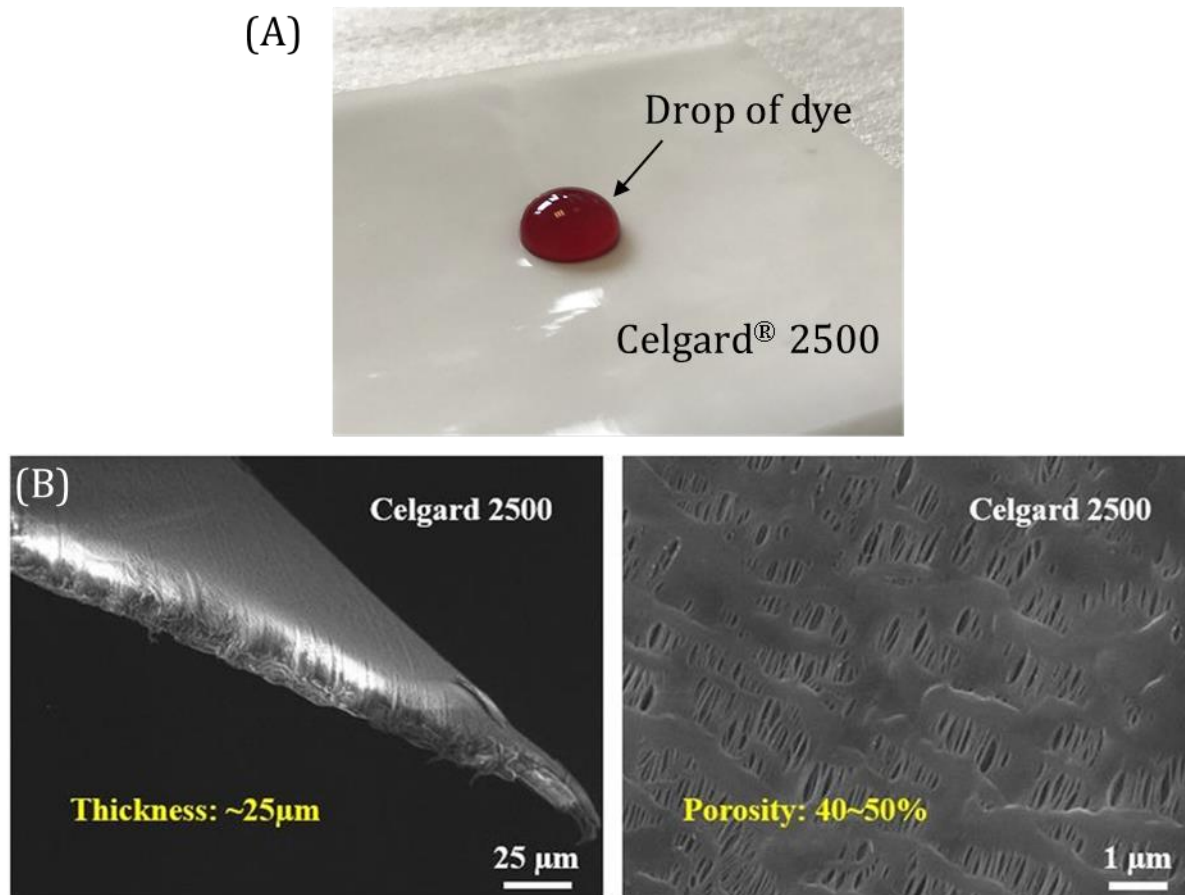


Figure 6.11 - (A) Hydrophobic nature of Celgard® 2500 (B) SEM images of Celgard® 2500 the 'support' at two different magnifications. Adapted from [143] [Creative Commons Attribution by NC ND]

The 3<sup>rd</sup> design in Figure 6.9C and F has an SLM integrated into the IRC. The SLM consists of an organic liquid impregnated on a thin (25 μm) porous sheet of polypropylene PP (Celgard® 2500) with a nominal pore size of 200 nm (Figure 6.11). The membrane is the 'support' for the impregnated 'liquid'; hence, the name supported liquid membrane. The PMMA parts were designed to have a channel on each side; one called the 'donor', where the sample is flown, and the other called 'acceptor', where the antibodies are immobilised (see Figure 4.9C). Slots were milled for the silicone gasket around each channel. Another 3 mm wide, 3 mm deep, and 66 mm long slot for the permanent magnet was made under the acceptor channel.



The design in Figure 6.9F is the UV assisted thermally bonded version of the design in (C). However, it was much more challenging to include such a thin membrane between the PMMA parts. Each membrane was manually cut into 72 mm long and 2 mm wide strips. The membrane was carefully placed on the PMMA part immediately after the UV exposure and carefully aligned to the channel. This time the bonding press heater was kept on for 10 min instead of the usual 5 min. The design in (F) was chosen to be integrated into the final FIA system.

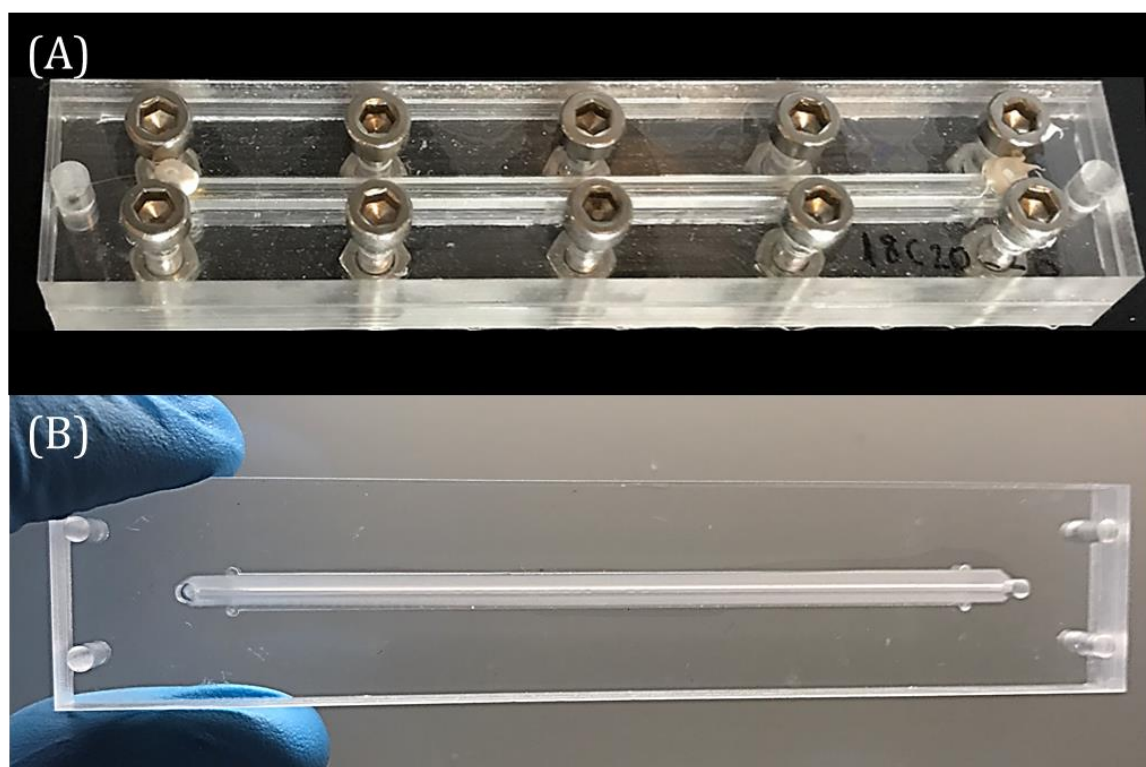


Figure 6.12 - SLM based IRCs (A) with screws used for assembly and (B) with UV assisted thermal bonding used for assembly.

Figure 6.12A shows the SLM-IRC version with screws as fasteners. The advantage of designs with screws is that they can be dismantled if needed. The image in Figure 6.12B is the SLM- IRC that has been bonded using UV assisted thermal bonding. The thermal bonding forms a permanent assembly as the material of the components fuses together, which is impossible to dismantle. However, it is better to have a permanently bonded structure in a FIA system since it is much more robust than an

IRC with screws as fasteners, hence the thermally assisted UV bonded design was chosen to be integrated into the final FIA system.

### 6.1.2.1 Leak test of IRC

The IRC designs without the membrane were leak tested by pumping MilliQ through one inlet and gently closing the outlet. The flow rate was set a bit higher than the usual working condition to ensure a robust system. However, for the designs with SLM, the leak test was done before and after impregnating the membrane with Dihexyl ether or n-undecane. Before adding the solvent, instead of MilliQ water, nitrogen was flown into the donor side inlet with the donor outlet closed. Since it is a porous membrane, nitrogen should exit through the acceptor opening. After impregnating the membrane, the same test was repeated, and in a leak-proof setting, there would be no nitrogen coming out through the acceptor outlets.

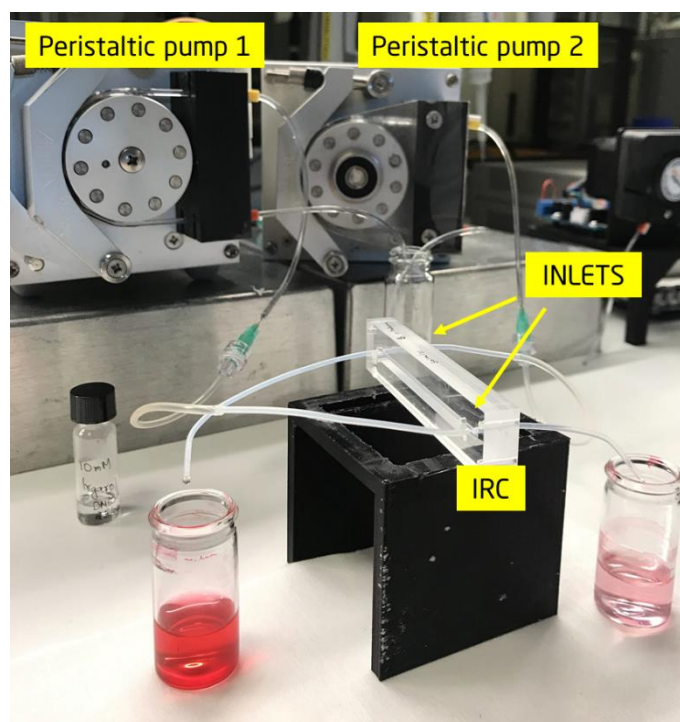


Figure 6.13- Testing the IRC.

### 6.1.3 Injection moulded IRC

The importance of design for manufacturability has long been established (Bralla 1999) and forms the central theme of this thesis: to design a system that could be smoothly transferred to an industrial setting. In industry, micromilling is suitable for prototyping, die designing, producing a limited number of samples, or manufacturing customized individual components. Although micromilling can produce precise geometrical features, the operation time and cost is not suitable for mass production. To realise polymer parts using an industrially relevant technique requires adherence to the standard large-scale industrial manufacturing practices. One of the most versatile and popular choices for mass production is injection moulding [144].

In simple terms, the injection-moulding process involves the melting and injection of plastic into a specific cavity (mould), followed by cooling, solidification, and release [145]. Figure 6.14 depicts a simple schematic of an injection moulding process. Injection moulding is a discreet process, and the process is highly repeatable. Almost all the thermosetting polymers can be injection moulded. All the three materials, PMMA, PC and COC, can be injection moulded.

The critical mechanical system of an injection moulding machine is the mould. The mould is the cavity where the molten plastic is filled and is composed of movable parts to form a closed cavity that can be moved apart to release the finished product. The mould is a complex system built to withstand high pressure, heat, and usually with an inbuilt heating or cooling unit. For design versatility, the mould has a part called the mould insert (Figure 6.15). By simply changing the mould insert, the mould can be used to manufacture a different part. The design and dimension of the final product are decided by the mould size and insert design.

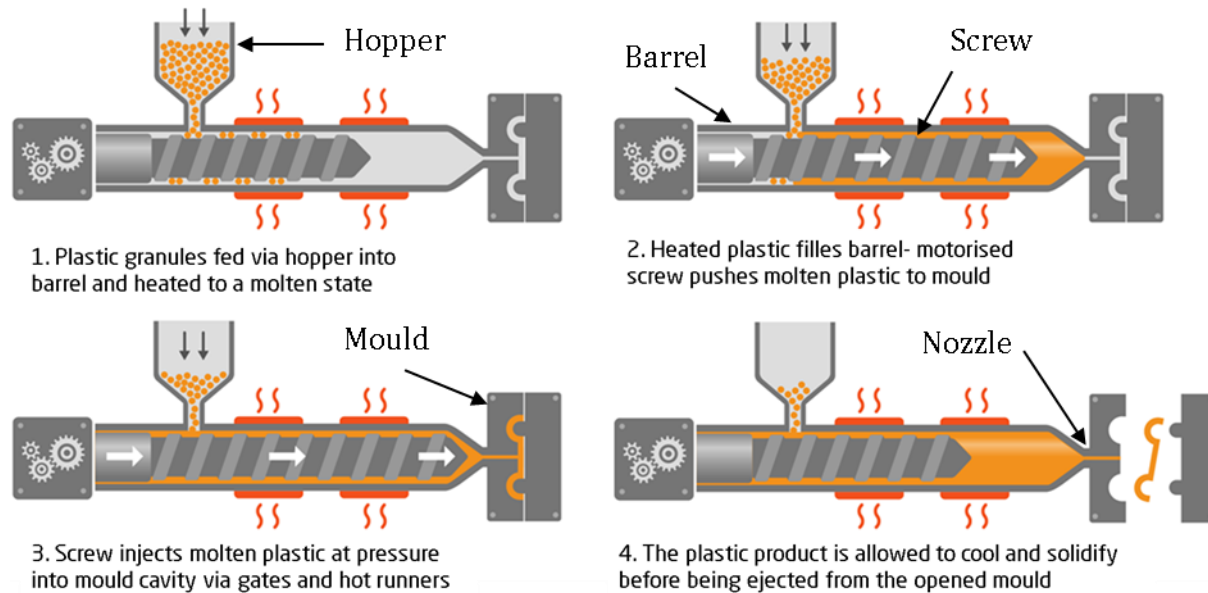


Figure 6.14- Different steps in an injection moulding process.

The IRC can also be manufactured through injection moulding. However, at DTU Nanolab, where the fabrication was carried out, only three moulds were available with standard inserts: A  $\varnothing$  50 mm disc with Luer connectors, a flat  $\varnothing$  50 mm disc with 1.5 mm thickness (used in section 6.2.2.2), and a design similar to a microscope slide (76 mm x 26 mm with 1 mm thickness). Another limitation with the inserts was that only a single surface could be modified. Hence, only simple channels and patterns could be realised. Nevertheless, in most microfluidic applications, the single surface design is sufficient. For this project, the chosen design was the microscope slide, and the material was COC. The injection moulding machine was a hydraulic (Engel Victory 80/45 Tech) with a 450 kN clamp force and a maximum tool temperature of 150°C.



Figure 6.15 – The entire mould where the inserts are marked with a solid red line ([http://tsquality.ch/-](http://tsquality.ch/))

Depending on the feature size, the insert could be fabricated in two ways. For designs with features in the range of few tens of nanometres to around 50 micrometres, cleanroom fabrication must be used, whereas micromachining can be used for features above 50 micrometres. A significant trade-off between the cleanroom process and micromachining is the final surface finish. Nickel-based inserts produced in the cleanroom have a surface finish close to the silicon wafer (tens of nanometres). However, for micromachined parts, the surface roughness is in the order of hundreds of nanometres. An additional polishing step was involved in micromilling to improve surface finish since the surface roughness played a crucial role in bonding effectiveness.

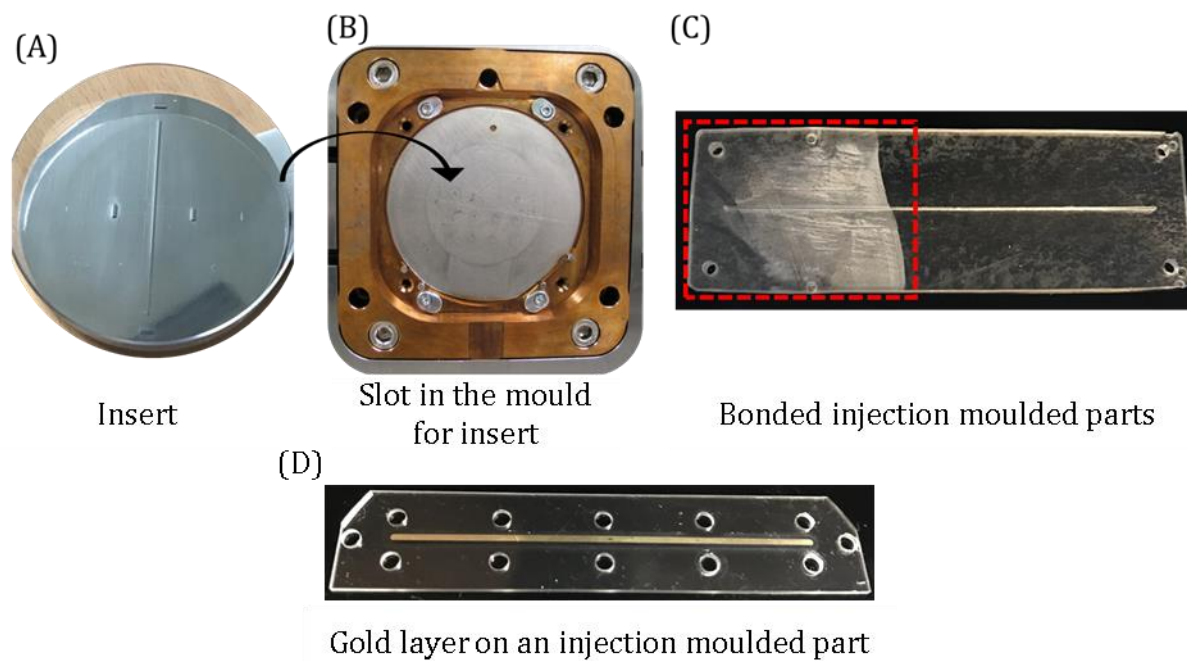


Figure 6.16- (A) Micomilled and polished aluminium insert with a central channel, (B) the mould insert of the injection moulding machine, and (C) two injection moulded COC parts bonded together. The dotted red square indicates the efficiency of bonding after trying to pull the pieces apart. (D) Gold layer deposited on an injection moulded part. The holes were micromilled later.

The IRC chambers were designed with 0.5 mm wide and 0.4 mm deep channels. Hence the insert was fabricated by micromilling in an aluminium alloy (Aluminium 2017) plate. The micromilling parameters were carefully chosen to reduce surface roughness. The final chosen tool was a 300  $\mu\text{m}$  end mill, and the feed rate was set so low that it took almost 25 h to complete the milling process. Subsequently, the surface was polished with aluminium polish. The machining and polishing processes have been explained in detail elsewhere [146]. Figure 6.16A shows the finished aluminium insert and the injection moulded part. The injection moulded parts had a channel in the middle with the exact same dimensions as the PMMA based IRC in Figure 6.12. After injection moulding, the inlet holes were drilled, and parts were bonded together using UV assisted thermal bonding with similar procedures as for PMMA except that the plate temperature was kept at 125°C for COC. After bonding,

the parts were pulled apart to test the bonding strength. As expected, the surface material was getting removed from the bonding interface, indicating proper bonding (area marked by the broken red square in Figure 6.16C).

Since UV assisted thermal bonding requires a certain level of surface smoothness for successful bonding, only Nickel inserts, fabricated in the cleanroom, were used [147,148]. It was shown that by choosing the correct machining parameter and a thorough polishing process, a smooth enough surface for good bonding could be achieved with the aluminium insert. This is the first documented demonstration of UV assisted thermal bonding of an injection moulded COC part made using a micro-milled metal insert.

#### 6.1.4 Injection moulded polymer substrates

To have a complete polymer-based system, the electrode used for electrochemical detection was also made on polymer substrates. One major issue with the fabrication of gold electrodes with small features on injection moulded substrates is the surface roughness. For electrode fabrication, the deposited gold layer is usually 200 nm thick deposited on a titanium adhesion layer of 50 nm. To obtain good electrodes, very smooth surfaces with  $S_z^4$  values around 50 nm are required. However, the value for injection moulded parts made in-house is more than 150 nm, while a Si wafer has an  $S_z$  value around 10 nm. Figure 6.17 shows the topography of a Si wafer and injection moulded COC substrate.

The limitation regarding surface smoothness, dimension and thickness of the injection moulded part is mainly due to the non-availability of professionally polished mould inserts, larger mould and required tonnage (clamping force), respectively, for the injection moulding machine at DTU. Nevertheless, by careful selection of moulding parameters, Macro Matteucci *et al.*, successfully injection moulded polymer

---

<sup>4</sup>  $S_z$  is the sum of the highest peak and the lowest pit in a surface of a given area.



parts with smooth surfaces and fabricated electrodes on them [149]. Initially, commercial injection moulded TOPAS® COCO 100mm disc with 1 mm thickness were procured from microfluidic ChipShop GmbH, Germany but proved to be of poor surface quality; hence no further experiments were carried out on these substrates. By chance, there was an old batch of high quality injection moulded COC discs of Ø85 mm and ~1.5 mm thickness procured from Terma A/S, Denmark. The disc shape was preferred for ease of adaptation in cleanroom instruments. The surface profile of the polymer along with a silicon wafer is shown in Figure 6.17.

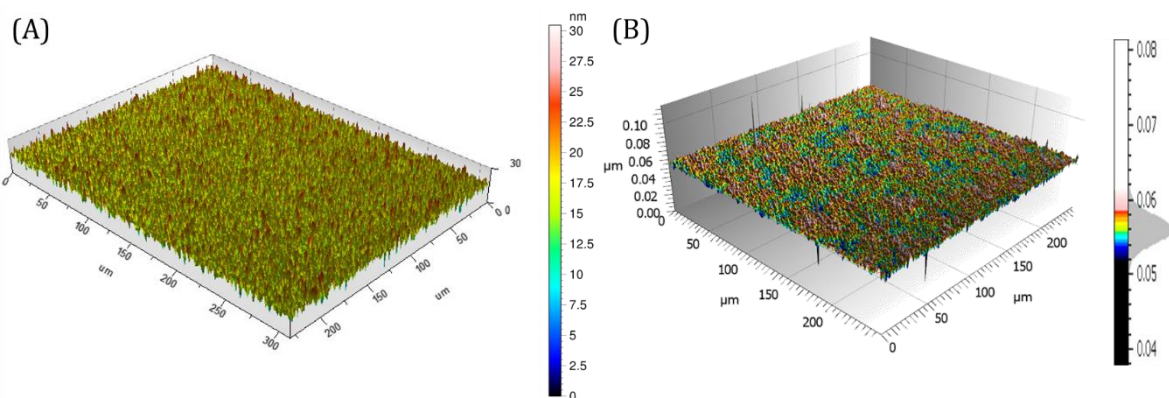


Figure 6.17- Surface roughness comparison of (A) Si wafer and (B) commercial injection moulded COC

An optical profilometer, S Neox 3D Optical Profiler (Sensofar, Spain), was used for the surface analysis. The results are tabulated below. Note that the standard values, such as arithmetical mean height ( $S_a$ ), given in the table do not directly reflect the actual situation since it is the mean of the absolute ordinate values of peak height and pit [150]. These values should be compared with the topography or colour map to understand how the surface exactly behaves. The Si wafer clearly shows a colour corresponding to around 15 nm, and COC shows around 55 nm. I consider  $S_z/2$  as an indicative value to compare surfaces as it forms a value closer to the observed topography and compensates for the modulus function.



Table 6.1 - Optical profilometry results for a commercial injection moulded COC compared with a silicon wafer.

Parameter (ISO 25178)	Si wafer	Commercial COC
RMS of height ( $S_q$ )	2.87 nm	10.4684
Maximum peak height ( $S_p$ )	14.28 nm	58.1686
Maximum pit height ( $S_v$ )	16.19 nm	44.6374
Sum of $S_p$ and $S_v$ ( $S_z$ )	30.47 nm	102.806
Arithmetical mean height ( $S_a$ )	2.24 nm	8.70348

Electrodes were fabricated on the commercial COC substrates and characterised. (Section 6.2.2.2). The challenge was to injection mould similar COC substrates in-house with similar surface quality.

The COC polymer used for injection moulding is TOPAS® 5013L-10 with a glass transition temperature of 130°C. The major parameters that can be adjusted in an injection moulding machine (see Figure 6.14 and Table 6.2) and their relevance are listed below.

Mould temperature (MT) is the temperature to which the mould is heated. It should be less than the glass transition temperature of the polymer being moulded, else the polymer will not solidify. For TOPAS® 5013L-10, the MT is kept below 100°C. At too low a temperature, small features are not be replicated properly due to rapid cooling.

If the MT is set too high, the part will not demould from the mould and might cause diesel effect<sup>5</sup>.

Melt temperature (MLT) and Nozzle temperature is the temperature at which the barrel to the nozzle is kept to ensure that the polymer has melted properly and can flow smoothly. For TOPAS® 5013L-10 the MLT at the nozzle is in the range from 240-300 °C. Setting a lower MLT will cause the viscosity of the polymer to go up and it can no longer flow into the mould properly and might damage the machine.

Injection velocity (IV) determines the time taken to fill the mould cavity. Lower velocity can cause shear thinning. There is an optimum time required to let the air inside the cavity to escape and influences how the structures are filled inside. If it is a plain cavity with no structure, then the IV can be increased.

Switch over pressure (SOP) determines the end point of filling the cavity and switches to the next step in the process. The SOP is set so that the machine will wait till the pressure is reached before moving to the next step. Lower than optimal SOP will lead to incomplete filling of the cavity and higher SOP will make it difficult to demould.

Holding pressure (HP) is necessary to maintain the pressure inside the cavity till the mould completely solidifies. The HP time is usually set to 5 s. A shorter HP will cause the polymer to flow back or out of the cavity and causes surface waviness. A longer HP leads to denser packing of polymer and induces stress.

Cooling time (CT) is the time in seconds given for the part to cool to make demoulding easy.

For the injection moulding process, a Nickel insert had to be fabricated from the clean room. 350 µm of Nickel is electrodeposited on a silicon wafer coated with Nickel-

---

<sup>5</sup> Spontaneous combustion of polymer vapour at high pressure and temperature.

Vanadium seed layer. The Nickel deposition is a long process (18 h). Slower deposition increases density of the Nickel insert. The required thickness for the mould insert is 1.32 - 1.35 mm. Hence, a 1 mm thick circular stainless-steel plate (back plate) is kept behind the Nickel insert to make the final thickness of 1.35.

Table 6.2 - Different parameters tested for injection moulding.

ID	MT (°C)	MLT(°C)	IV (cm <sup>3</sup> /s)	SOP (bar)	HP (s)	CT (s)
1	65	280-250	40	1000	900	15
2	70	290-260	45	812	850	20
3	75	300-270	52	396	850	20
4	80	270-250	54	510	750	15
5	90	270-250	58	596	700	30

The surface profiles were tested, and the worst (marked red) and best (marked green) samples in Table 6.2 have been shown in Figure 6.18 and the results tabulated in Table 6.3

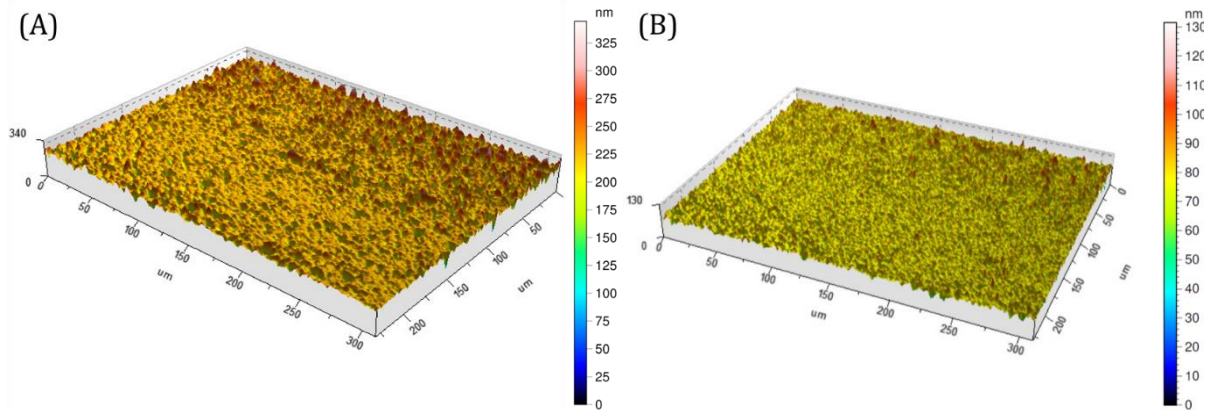


Figure 6.18- Surface roughness comparison of (A) ID-1 (B) ID-3

The poor performance of ID-1 could be attributed to the high SOP combined with the low MT which resulted in poor filling of the cavity and higher holding pressure. However, ID-3 seems to be working well but repeated use of the Nickel insert caused surface waviness. It is relevant to note that any roughness of the back plate can get transferred onto the Nickel insert if the HP is too high. Further electrode fabrication on these substrates are described in section 6.2.2.2

Table 6.3 - Optical profilometry results for a commercial injection moulded COC

Parameter (ISO 25178)	ID - 1	ID - 3
RMS of height ( $S_q$ )	22.58 nm	6.69
Maximum peak height ( $S_p$ )	123.70 nm	54.14
Maximum pit height ( $S_v$ )	220.70 nm	77.42
Sum of $S_p$ and $S_v$ ( $S_z$ )	344.41 nm	131.57

---

Arithmetical mean height ( $S_a$ )	14.19 nm	4.81
------------------------------------	----------	------

---

## 6.2 Electrodes

In an electrochemical measurement system, electrodes can be used to perform voltammetry, amperometry or impedance spectroscopy. All three techniques were described in Chapter 5 and used at various stages of the electrode system development. Impedance and voltammetric measurements were performed during the characterisation phase, and amperometric measurements were used during the detection phase.

Since the plan was to develop an immunobiosensing system, there were multiple design possibilities for the sensing electrodes. The 1<sup>st</sup> approach was to use electrodes appropriately modified to covalently bind the antibody to perform a label-free assay by detecting a change in impedance when the antibody binds to the target antigen. The 2<sup>nd</sup> approach was the attachment of the antibody to the electrode surface with a subsequent competitive assay using an enzyme labelled tracer in combination with *in situ* detection of the formed enzyme product. The 3<sup>rd</sup> approach was to use a separate immunoreaction chamber where a competitive assay or an ISLM step could be performed. The electrode was then merely used to quantify the formed product downstream upon conversion of the substrate by the enzyme tracer in the immunoreaction chamber.

To understand various surface modifications, run pilot studies on the different assays and select the best possible electrode configurations, different electrodes, such as screen-printed gold electrodes (SPGE), and physical vapour deposited gold interdigitated electrodes (IDE), were tested. Trial experiments were also performed using commercially available electrodes from Metrohm DropSens (a subsidiary of

---

Metrohm AG, Herisau, Switzerland). Then depending on the electrode configuration, specific designs were fabricated in the cleanroom on silicon wafers using standard photolithography. Some of the limitations of the different commercial electrodes were considered while designing the process flow for the cleanroom fabrication. The final step was to adapt the fabrication techniques, designed initially for silicon substrates, to polymer substrates such as PMMA or COC. This adaptation helps to bridge the gap between laboratory techniques and industrial-scale manufacturing processes.

### 6.2.1 A pilot study with commercial electrodes

Gold interdigitated electrodes (IDE) for impedance studies, and SPGEs for amperometric and voltammetric experiments were purchased from Metrohm DropSens. For the WE, the choice of metal was gold for the relative ease of thiol modifications. We selected thiol compounds with a carboxylic terminal group to further conjugate with proteins and antibodies.

Individual test setups for electrodes were micromilled in either PMMA or PC. PC was explicitly used for experiments that involved ethanol, as it is resistant to ethanol, unlike PMMA. Liquid-tight sealing was ensured using laser-cut silicone gaskets (Silicone sheet, Reichelt Chemietechnik GmbH + Co., Germany) and fastened together using metal screws.

#### 6.2.1.1 Interdigitated electrodes (IDE)

Ab initio training in the development of immunosensors was carried out during the external research stay at the Institute for Advanced Chemistry of Catalonia (IQAC), Spain, the Nanobiotechnology for Diagnostics (Nb4D) group led by Professor Pilar Marco, who kindly provided all reagents and equipment. At Nb4D, the immunosensor research spanned from synthesising haptens and immunogens to induction of immunoresponse in small animals, collection, purification and characterisation of the

antibody; and developing SPR and electrochemical based sensors. The model analytes that were used for my training were Stanazolol and Irgarol. Stanazolol is an artificial steroid, similar to testosterone and Irgarol is an algaecide used in antifoulant paint for fishing vessels.

My first immunosensor design was based on work previously conducted in Nb4D where they had immobilised an atrazine hapten conjugated to BSA onto the glass substrate between the digits of IDEs, previously activated with (3-glycidoxypropyl)trimethoxysilane, followed by impedance measurements for detection of atrazine by flowing both the atrazine antibody and atrazine onto the electrode [151]. Functionalising the empty spaces between the digits of IDEs, i.e., not on the electrode surface, is more common in label-free capacitive type biosensors [152].

The initial experiments were performed with commercial Dropsense gold IDEs (DRP-G-IDEAU10) with 10  $\mu\text{m}$  wide fingers separated by a 10  $\mu\text{m}$  gap (Figure 6.19). The IDEs were tested for the development of a label-free impedance-based detection of the immuno-affinity interaction where a hapten conjugate was immobilised on the glass surface between the IDE digits. Gold IDEs on glass substrate have the advantage that, for surface functionalisation, both the gold and glass surface can be modified using thiol compounds and 3-glycidoxypropyltrimethoxysilane (GPTMS), respectively.

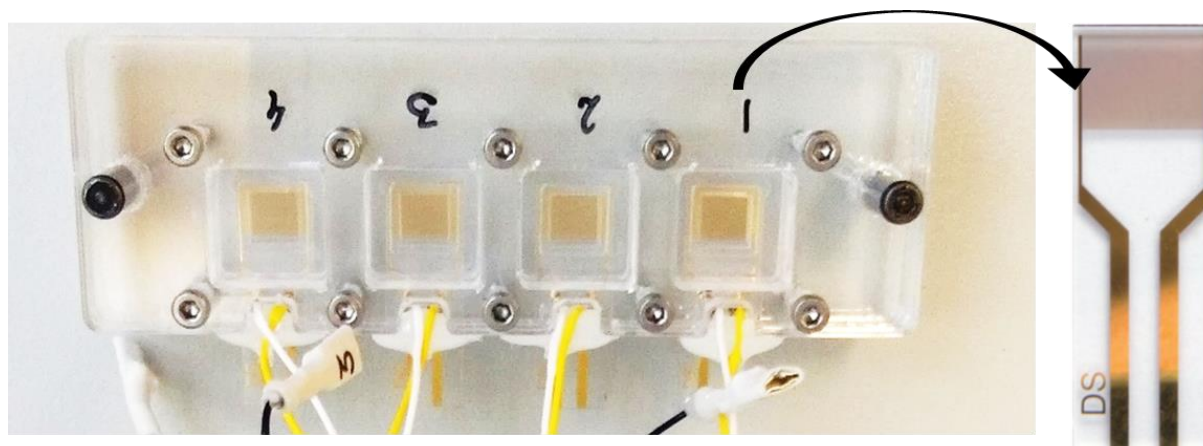


Figure 6.19- Dropsense gold IDEs and a micromilled test setup. The gold fingers are 10  $\mu\text{m}$  wide separated by a 10  $\mu\text{m}$  gap and with an overall length of 6760  $\mu\text{m}$

The glass surface was modified so that with each additional layer, the electrode impedance would change (Figure 6.20A and B). In this instance, a competitive assay format for the model analyte Stanozolol was pursued. Stanozolol was conjugated with BSA (hb\_ST-BSA) and immobilised on the glass surface. After cleaning the IDE in an Ozone/UV chamber for five minutes, GTPMS was introduced, and hb\_ST-BSA was added [153]. A stanozolol antibody (As147) was then added to perform the biorecognition. Regeneration was performed by removing the antibody with NaOH. The impedance spectra acquired during each step are depicted in Figure 6.20A. Even after multiple experiments and optimisation, the regeneration of the surface was not complete, i.e., the charge transfer resistance seen in Figure 6.20A c could not be decreased to that in Figure 6.20A b. There could be many reasons for improper regeneration, including the application of a batch system (Figure 6.19) instead of a flow system, physisorption on the gold surface, or failure in the integrity of the gold IDEs.

Subsequently modification was tried on the gold layer instead by immobilising an antibody on the surface. 2.5 mM of a carboxylated thiol, 11-Mercaptoundecanoic (MUA) was added to the electrode and kept for 7 h to form a SAM. Using 200 mM of EDC and 50 mM NHS in MES buffer (pH 6), the carboxylic group was activated, and 2  $\mu\text{g}/\text{mL}$  Protein-G was added. After that 2  $\mu\text{g}/\text{mL}$  of Irgarol antibody (As84) was added.



Impedance spectra were taken during each modification step, but the results (Figure 6.20 C) show some anomalies during the modification. The  $R_{ct}$  of the Protein-G and As87 step was lower than the bare electrode, indicating an anomaly. Usually, after the thiol modification, especially with a long chain molecule like MUA, the  $R_{ct}$  value should be substantially increased compared to that of the bare electrode in an IDE, i.e., the electron density formed at the carboxylic terminal usually increases the impedance. Nevertheless, once the Protein-G is added, along with the effect of the negative charge being reduced due to the formation of the amide bond (lowers  $R_{ct}$ ), the presence of Protein-G introduces more steric hindrance (increases  $R_{ct}$ ). However, it should still be more than the  $R_{ct}$  of the bare electrode.

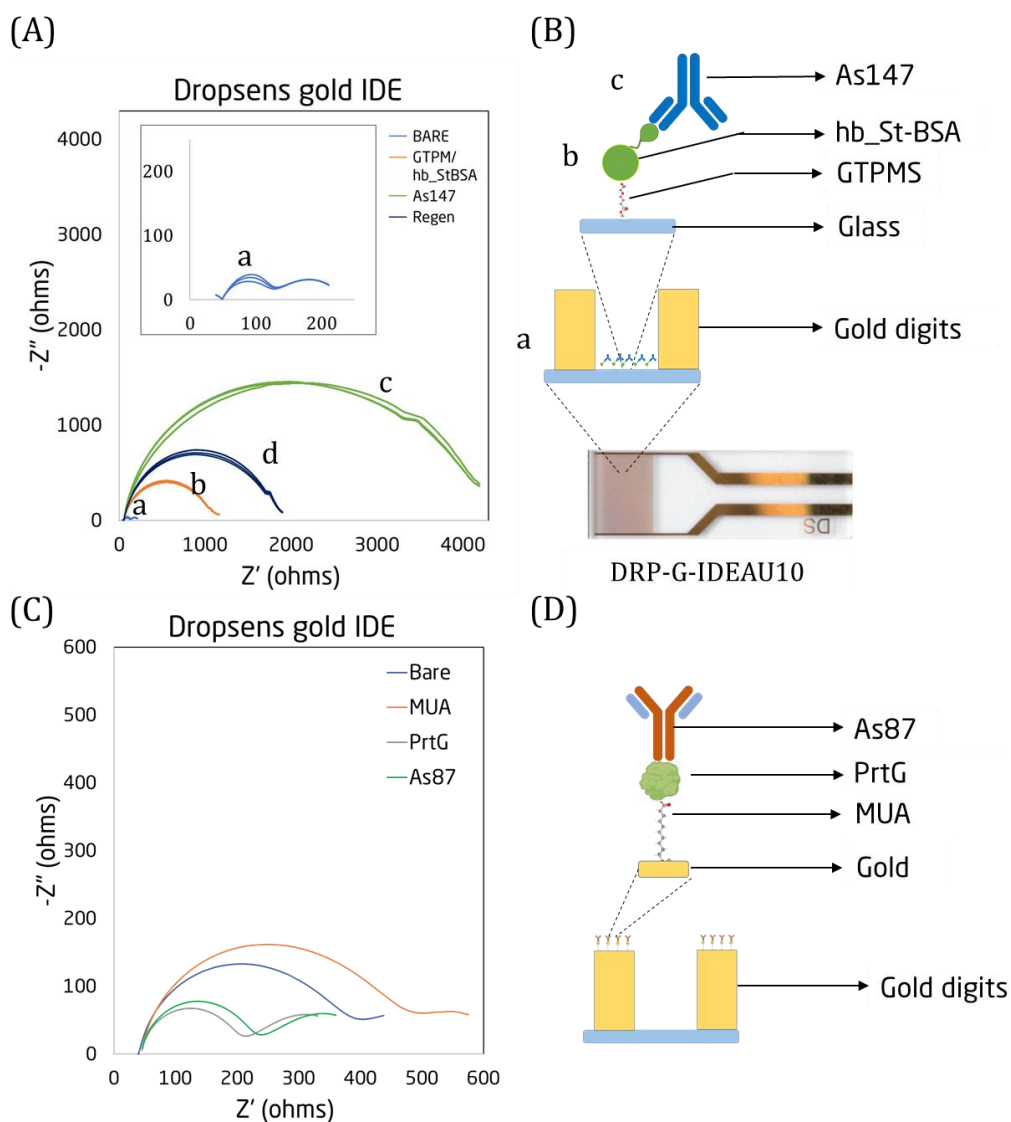


Figure 6.20 (A) Impedance spectra (Nyquist plots) acquired on: (a) bare gold IDE, (b) the same IDE after GTPMS and hbSt-BSA modification, (c) As147 Ab affinity reaction, and (d) regeneration using NaOH. 10 mM ferri/ferrocyanide redox probe was used, and 1 Hz to 100 kHz was scanned. B) Stepwise modification of the electrode surface with the hbSt-BSA conjugate. (C) Impedance spectra from the surface modification of gold digits (D) Stepwise modification of electrode with MUA, Protein-G and As87.I

Considering all the factors, the work on IDEs was terminated, and the focus was shifted to planar three-electrode systems.

### 6.2.1.2 Screen-printed electrodes

Commercial gold-based screen-printed electrodes (SPE) from Dropsense (DRP250AT) were used to test surface modification and went from immobilising a hapten-conjugate to instead immobilising a capture antibody (Irgarol Ab As87) via protein G directly on the electrode surface, as well as using a labelled HRP tracer for detection. The test setup and immobilisation strategy are depicted in Figure 6.21.

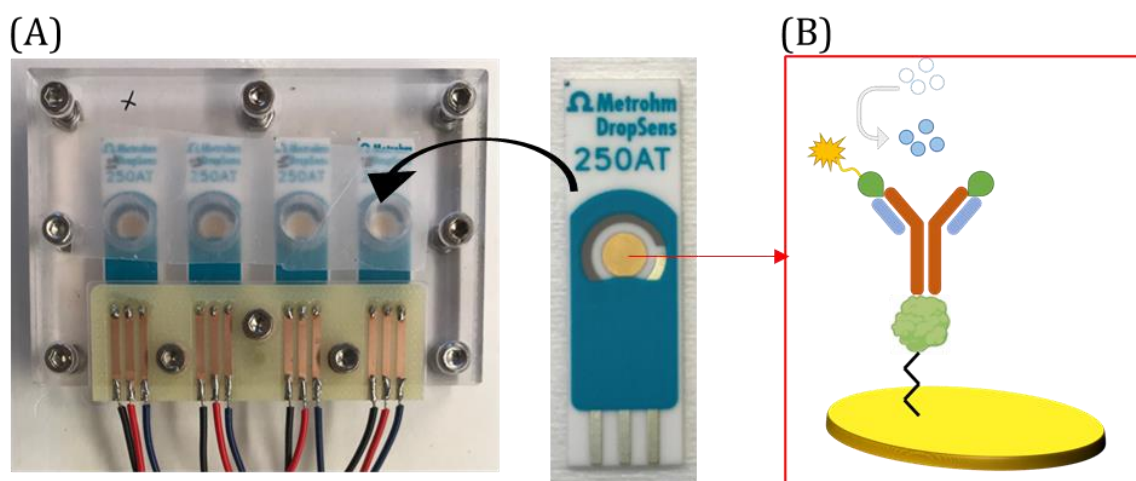


Figure 6.21 - (A) A test setup with four commercial screen-printed planar electrodes in a batch type test setup (B) A schematic figure representing the gold working electrode modification.

It was first confirmed through cyclic voltammetry that the electrode could detect the HRP label catalysed TMB substrate conversion. The next step was thiol modification of the surface using a suitable thiol. The thiol would form a SAM on the gold layer allowing further modifications of the gold.

Initially, MUA was tested, and the surface modification seemed to work, as shown in Figure 6.22 A. However, when the substrate TMB/H<sub>2</sub>O<sub>2</sub> was added, there was no change in colour, indicating the absence of HRP. To check each step, many different thiol modifications were tried, such as MUA, MUA and 6-Mercaptohexanol (MH), 3-Mercaptopropionic acid (MPA), 4-Aminothiophenol (4ATP) in 3-mercaptopropionic acid (MPA). MUA, MUA: MH, 4ATP and MPA modification were done using ethanol as solvent, and it was observed that the passivation layer on the electrode was slightly

---

removed. Hence MPA in an aqueous buffer was tested but failed. The modification using 4ATP and Glutaraldehyde (GA) is shown in Figure 6.22C. None of these assays worked at the final substrate stage. This was strange considering that thiol modification of gold is very straightforward. The impedance spectra seemed like something was getting attached to the electrode, but the modification was not functioning correctly. The surface modification was changed to check the physisorption of Protein-G directly on the gold surface, but it did not work. Later, we realised that screen-printing of gold involves the mixing of gold nanoparticles with a polymeric binder that hinders proper thiol modification of the surface. Therefore, a sulphuric acid cleaning of the surface was tested, but the thiol layer could not be realised. While looking in the literature, only a single paper was found describing such a modification being done on a similar SPE [154]. This lack of publications indicated that it might not be the best immobilisation approach for SPEs.

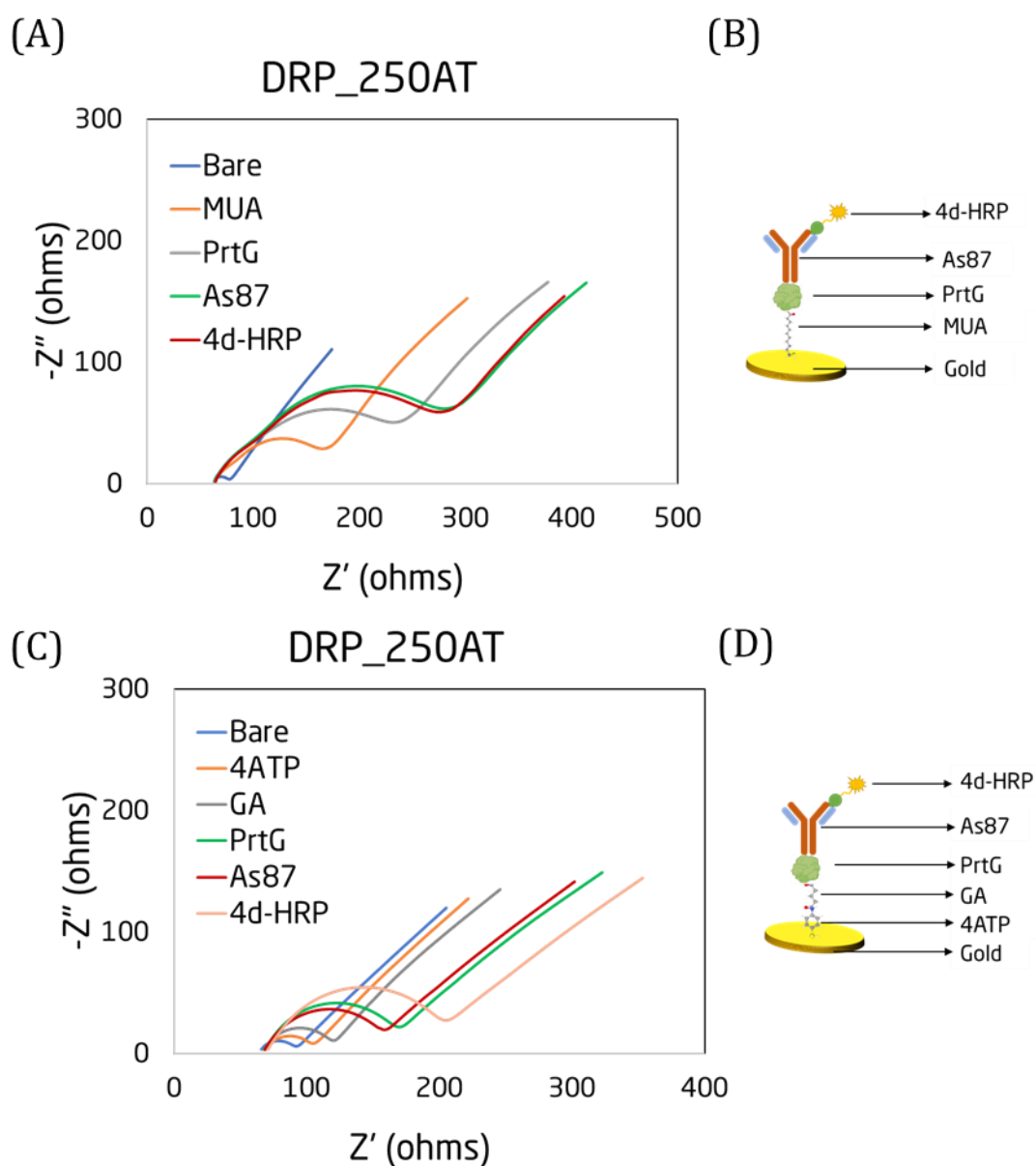


Figure 6.22 - (A) Impedance spectra for the gold surface using MUA as SAM (B) Stepwise modification of electrode with MUA, Protein-G, As87 and 4d-HRP. (C) Impedance spectra for the gold surface using 4ATP as SAM (D) Stepwise modification of electrode with 4ATP, GA, Protein-G, As87 and 4d-HRP

The next option was to fabricate planar electrodes in the cleanroom.

## 6.2.2 Cleanroom fabrication of electrodes

### 6.2.2.1 Detector electrodes on silicon substrate

For the fabrication of electrodes on a silicon wafer a process flow was adapted from a similar fabrication process established in our lab for another project [155] (Appendix A.2). In brief, silicon wafers were cleaned and kept in a furnace to grow a 1  $\mu\text{m}$  silicon oxide layer as insulation for the upcoming gold layer. Then, using a standard UV photolithographic process, various electrode patterns were realised. 50 nm titanium adhesion layer and 200 nm of gold were deposited using e-beam evaporation of the metals. Through a process called lift-off, the underlying resist was removed, thereby leaving only the desired metal pattern. A passivation layer was applied to define the electrode area and contact pads. Silicon nitride, as well as photoresists SU8 and AZ5214E, were tested as a passivation layer.

The initial idea was to create a system with a long linear working electrode that could be housed at the bottom of the acceptor channel of an ISLM system, as illustrated in Chapter 4, Figure 4.9C. The capture antibody could then be immobilised directly on the gold surface, and the formed oxidised HRP product could be detected *in situ* on the electrode surface. In this way, the immobilised antibody layer would serve both for immuno-extraction and for *in situ* immuno-sensing.

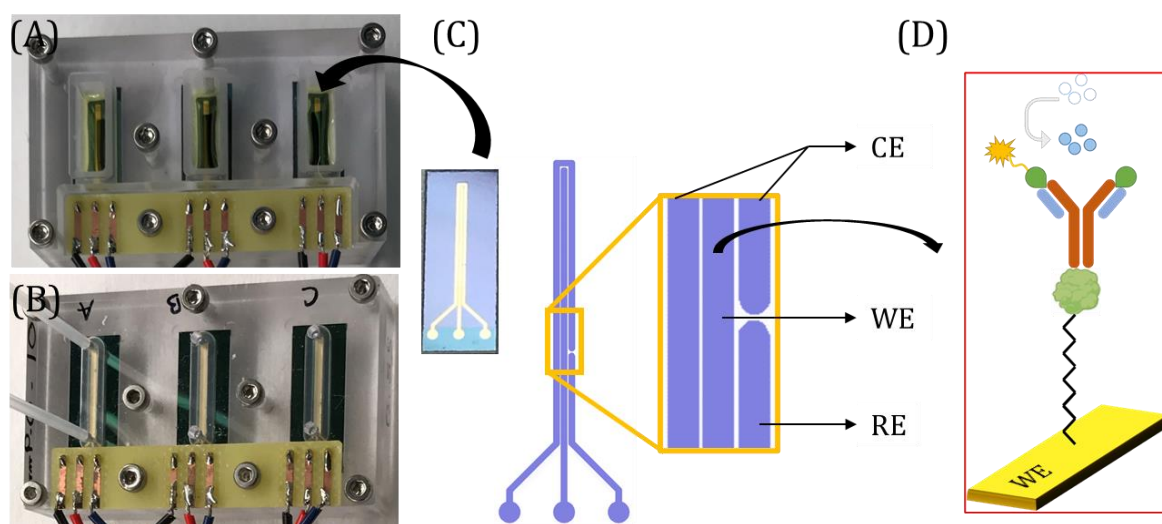


Figure 6.23 - Three parallel linear electrode chips in a batch setup (A) and in a fluidic thin-film electrochemical cell (B). (C) Electrode configuration fabricated on a Si wafer and the design showing CE, WE and RE. (D) The surface modification of the WE electrode.

Antibodies against cortisol were immobilised on the gold electrode surface using the procedure described above except for the use of MUA instead of MPA. The impedance spectra after each modification step is shown in Figure 6.24A. The electrodes were housed in the batch setup in Figure 6.23A for the regeneration study and the thin layer electrochemical flow setup in Figure 6.23B during amperometry. The binding efficiency was examined by injecting an HRP tracer (65IC08), then the TMB/H<sub>2</sub>O<sub>2</sub> substrate and subsequent detection of the enzymatic product. The oxidised product was collected from the batch setup and measured in a spectrophotometer at 630 nm (Figure 6.24B). Soon, various problems started to emerge. Although the reaction of the TMB with HRP was fast, a repeatable signal could not be obtained. Some plausible reasons could be instability of the immobilised antibody in the presence of the substrate and/or regeneration buffer or disruption of the antibody-antigen binding due to the flow (Figure 6.24).

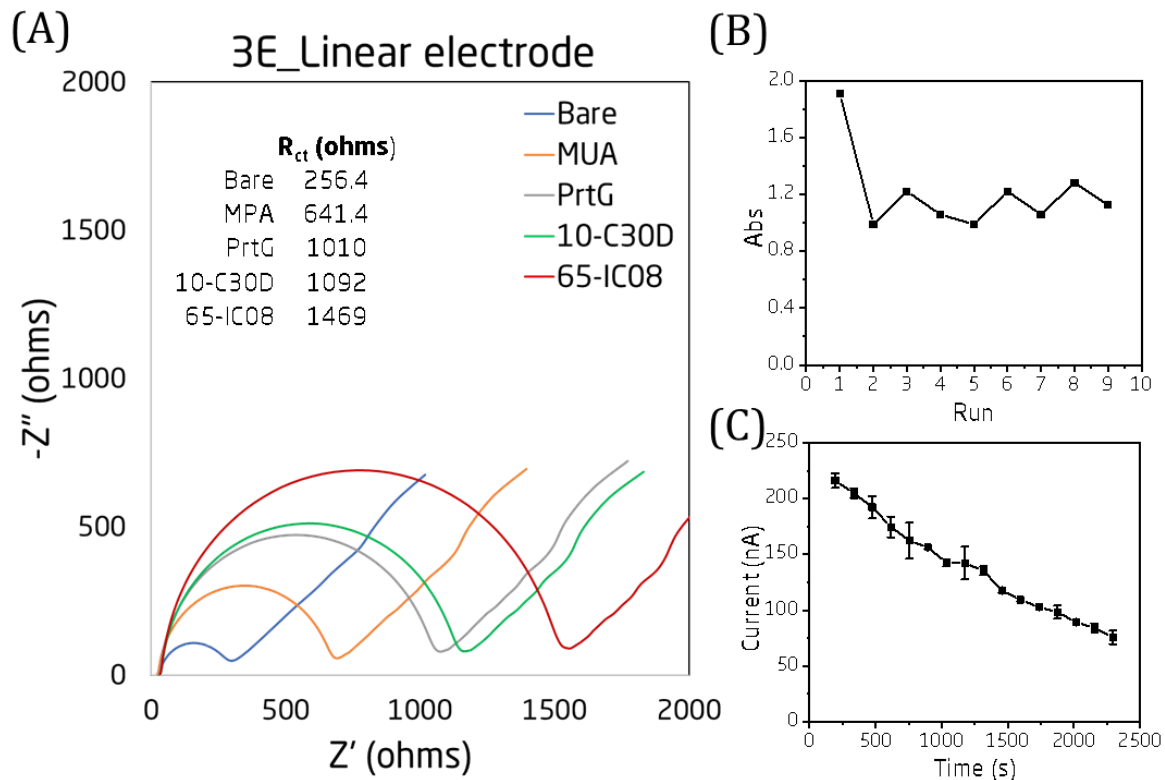


Figure 6.24 - (A) Impedance spectra after each modification (B) Multiple regeneration runs showing poor inter-assay stability (C) Electrode instability over repeated injections of the substrate .



Several investigations, such as varying the concentration of the MUA, antibody and tracer, cleaning the silicone gasket to prevent nonspecific binding, were performed to try and solve the problem, but without any success. The substrate was injected multiple times, and the product was amperometrically measured. Here, the signal decreased with each successive run, indicating that the HRP tracer was removed (Figure 6.24 C). This experiment gave evidence of the substrate disrupting the antibody-antigen binding.

As a result, it was decided to separate the immunoreaction part from the enzyme product detection part. A separate immunoreaction chamber (IRC), housing the immobilised antibody, was developed that was connected downstream to an electrochemical flow cell, which from now on is referred to as the detector electrode used for detection of the enzymatic product. The following sections describe the fabrication of different detector electrodes.

Although the previously developed linear electrode could function as the detector electrode, it could not be configured in a wall jet format where the inflow impinges directly on the working electrode and disperses symmetrically. Due to the elongated design, it is not possible to have a symmetrical dispersion. Hence, the next detector electrode design was inspired by the commercially available SPE electrodes used in section 6.2.1.2, but the same fabrication protocol described for linear electrode was used. Three different electrode designs with the same layout were tried out. A small ( $\varnothing = 960 \mu\text{m}$ ), medium ( $\varnothing = 1440 \mu\text{m}$ ) and large ( $\varnothing = 1920 \mu\text{m}$ ) sized WEs were tested. As expected, the largest WE gave the highest current during testing and was selected for all further studies.

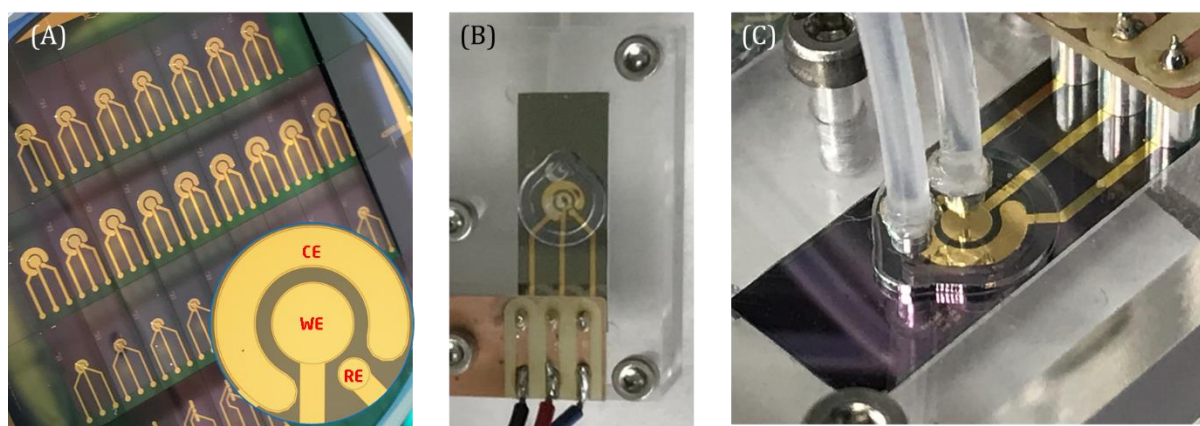


Figure 6.25 - (A) Different electrode designs fabricated on a silicon substrate with varying working electrode areas. (B) Test setup for the electrodes (C) Flow set up where the fluid impinges on the working electrode.

Figure 6.25 shows the fabricated and diced electrode chips ready for testing. It was observed that the dicing saw (DISCO dicing saw, an old tool from the mid-1990s), used to cut the wafer, left a thin, uneven edge when the chips were broken off. This **uneven edge had to be carefully 'sandpapered' to snug fit in the test setup smoothly.** Otherwise, there was a risk that the chips would break.

As the detector electrode should be part of a continuous flow system, it was repeatedly tested for three weeks in a FIA set-up to ensure its stability. The stability was characterised by checking the amperometric peak current for injections of 10 mM ferricyanide showing a stable system, the detailed results being reported in Paper I.

#### 6.2.2.2 Detector electrodes on polymer substrates

The reason to move towards a polymer substrate was to make it easy for industrial adaptation of the entire FIA system. It was envisioned that if all the components were made of polymer, they could be injection moulded and bonded together to form a cartridge system.

Once the electrode size and shape had been decided, the next step was to fabricate the same electrodes as above but on a polymer substrate. Commercially available PMMA and COC plates were tested as potential substrates. Although PMMA is readily available, unlike COC, the high chemical resistance of COC is an advantage when used with ethanol or acetone. The PMMA plates (10 cm x 10 cm) were 5 mm thick and manufactured by extrusion, whereas the COC discs ( $\varnothing = 85\text{mm}$ ) were 1.5 mm thick and injection moulded. The PMMA plates were micromilled to form a 100 mm diameter disc, and positioning holes were drilled before processing them in the cleanroom.

The cleanroom process was different from that previously described for silicon wafers. Here, the UV photolithography step was eliminated. Instead, metal deposition **was performed using a 'shadow mask'**. Depending on the needed feature size, the shadow mask can either be made from a metal (100  $\mu\text{m}$  thick) or a polymer (500  $\mu\text{m}$  thick) sheet that acts as a stencil. Only the places where the deposition is to happen are exposed; hence, the name shadow mask. The minimum feature size practically feasible for the micromilling machine is 50  $\mu\text{m}$ , and for the laser micromachining tool, 25  $\mu\text{m}$ . Polymer shadow masks are fabricated by micromilling, and metal masks are fabricated using laser ablation. Other than the feature size, the time to prepare a metal shadow mask using laser ablation is ten times less than micromilling a polymer shadow mask. However, when it comes to the alignment of the shadow mask on the substrate, since the feature size was large, the transparent polymer shadow mask could be aligned visually, but the opaque metal shadow mask required alignment pins to be placed.

After **cleaning the polymer substrate by sonication in 1 % Triton™ X-100** followed by distilled water, the substrate was dried. After that, 50 nm titanium as adhesion layer and then 200 nm gold were deposited on top using e-beam evaporation through the shadow masks. There was no lift-off step involved since there was no photoresist to be removed. Hence, it is a fast and relatively easy method, but the mask fabrication method limits the feature size. The trade-off in a faster process using a shadow mask

instead of photolithography is compromised by the minimum achievable feature sizes. However, with shadow masks, during their fabrication, problems such as material redeposition during LASER ablation and burr formation during micromilling, need to be addressed before using them inside the cleanroom.

After fabrication, the electrodes were electrochemically tested in the batch setup (Figure 6.26A). The CVs were acquired using the on-chip gold reference electrode (Figure 6.26B) at a scan rate of 50 mV/s, and the results are presented in Table 6.4.

Table 6.4 - Cyclic voltammetry results.

Polymer	$I_{\text{peak-peak}}$ ( $\mu\text{A}$ )	$I_{\text{ox}}$ ( $\mu\text{A}$ )	$I_{\text{red}}$ ( $\mu\text{A}$ )	Peak ratio ( $I_{\text{ox}}/I_{\text{red}}$ )	Peak separation (mV)
PMMA	$223.3 \pm 2.1$	$113.7 \pm 1.5$	$109.7 \pm 0.6$	1.04	$96.7 \pm 5.8$
COC	$227.3 \pm 1.2$	$115.3 \pm 1.2$	$112.0 \pm 0$	1.03	$96.7 \pm 5.8$

The electrodes worked very well and gave repeatable results even at different scan rates.

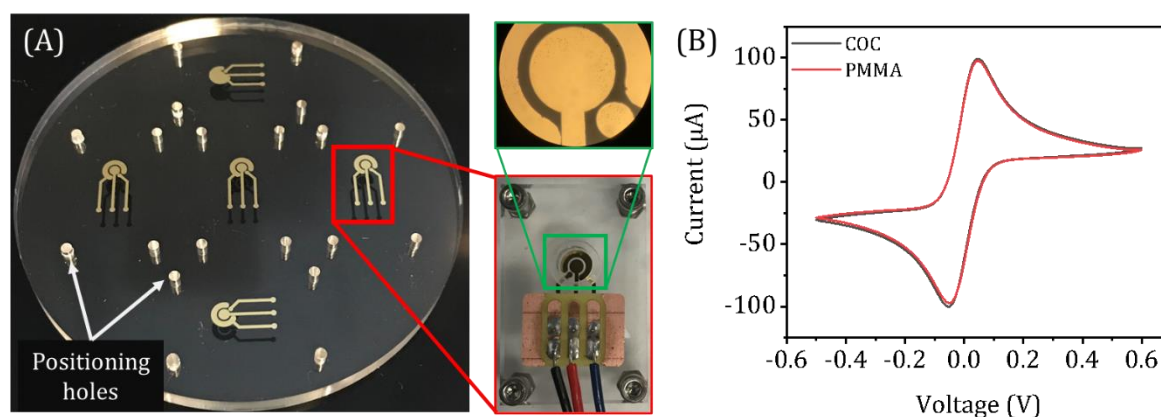


Figure 6.26 - (A) Electrodes fabricated on a PMMA substrate (COC substrate not shown). Insets: electrode test setup and microscopic image. (B) CVs acquired in 10 mM ferri/ferrocyanide for electrodes on both PMMA and COC polymer substrates.

To test the limits of cleanroom fabrication of gold electrodes on injection moulded COC substrates, IDEs with 10  $\mu\text{m}$  digits were fabricated using a unique process (detailed process flow in Appendix A.3).

The COC substrates from the in-house injection moulded batch ID-3 as described in section 6.1.4 were further used to fabricate the IDEs in Figure 6.27B. In brief, the **COC discs were cleaned by sonication in 1% Triton™ X-100** followed by distilled water, dried and spin-coated with a photoresist layer. An automated spin coater (Gamma 4M from Süss MicroTec) was reprogrammed to pick the COC substrate manually and perform the photoresist coating. After that, a photomask or a maskless aligner was used to perform UV exposure of the photoresist followed by photoresist development and deposition of titanium and gold. The final step was to remove the underlying photoresist by stripping (called lift-off) in a solvent bath, leaving only the required gold pattern on the substrate (Figure 6.29B).

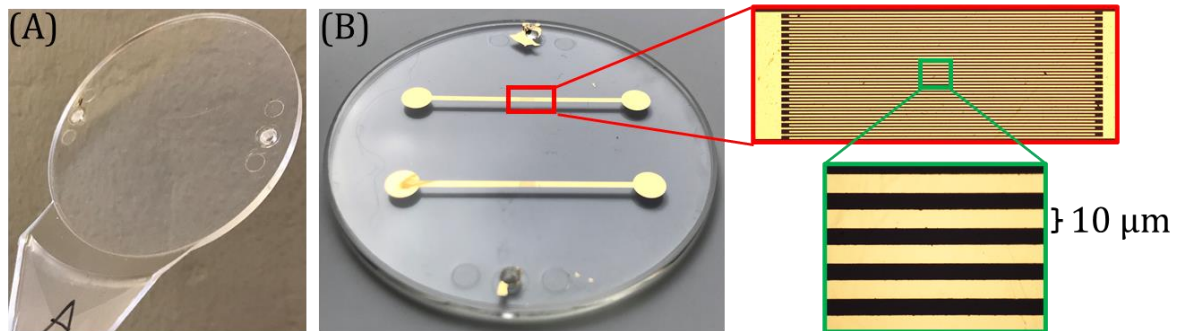


Figure 6.27- (A) An injection moulded 50 mm disc. (B) Micromilled disc to remove burred edges with fabricated IDE (Inset shows the microscopic images of the digits).

There are many parameters to be optimised to precisely realise microstructures on the polymer surface. One crucial parameter is the UV dose or the time the photoresist is exposed to the UV for curing. A particular image reversal photoresist (AZ5214E) was used in the process. Underexposure causes under-curing of the photoresist, leaving the gold still sticking to the surface, and over-curing causes structural variations (Figure 6.28).

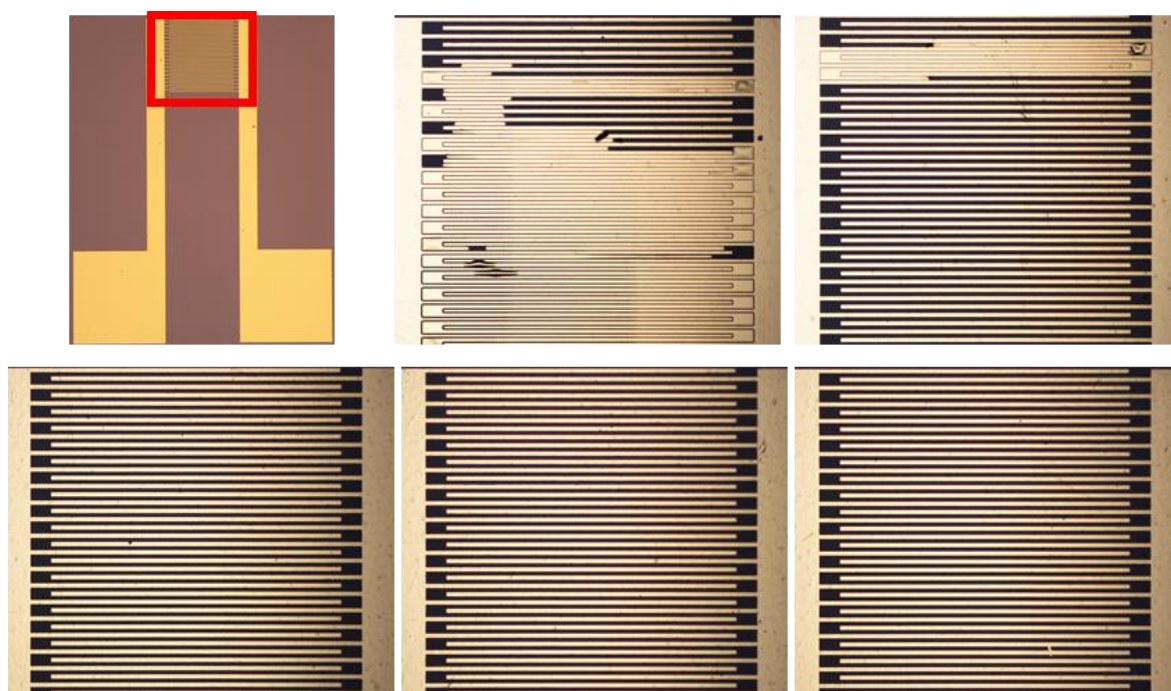


Figure 6.28 - UV exposure dose testing from  $75 \text{ mJ/cm}^2$  to  $95 \text{ mJ/cm}^2$  to ensure that the gold 'lift off' was functioning properly

To test the IDEs after fabrication, a makeshift setup was created to acquire a CV (Figure 6.29C) using an Ag|AgCl pseudo-RE.

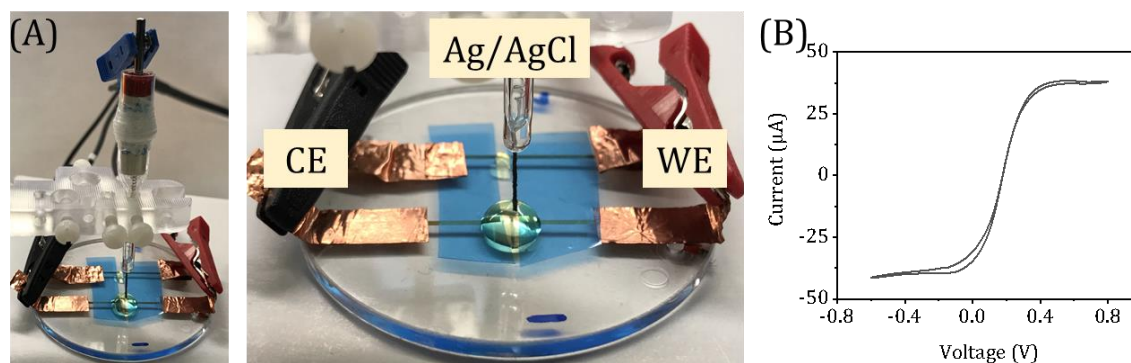


Figure 6.29 - (A) Testing of the electrode using Ag/AgCl as a pseudo-RE. (B) Cyclic voltammograms for polymer substrate-based IDE with 10 mM ferri/ferrocyanide.

Figure 6.29B shows the typical electrochemical behaviour of the fabricated IDEs with a sigmoidal CV having practically no capacitive hysteresis. This result demonstrates



that it is possible to successfully fabricate electrodes with such small features on injection moulded polymer substrates, and as far as I know the first time it has been realised.

Another issue observed during the fabrication of the planar three-electrode systems was caused by cracks and bubbles formed on the gold surface (Figure 6.30). The gold deposition process involves e-beam evaporation, which can heat the substrate. The thermal expansion may cause cracks, and the bubbles are probably due to gas evolution from the polymer substrate. A solution for mitigating the cracks and bubbles was to increase the deposition rate, thereby reducing the substrate's exposure to heat. The deposition rate was initially kept low for the formation of fine grains during the deposition of the gold layer. However, a trade-off had to be made to solve these problems. Hence, increasing the deposition rate from 2 Å/s to 10 Å/s might be a solution.

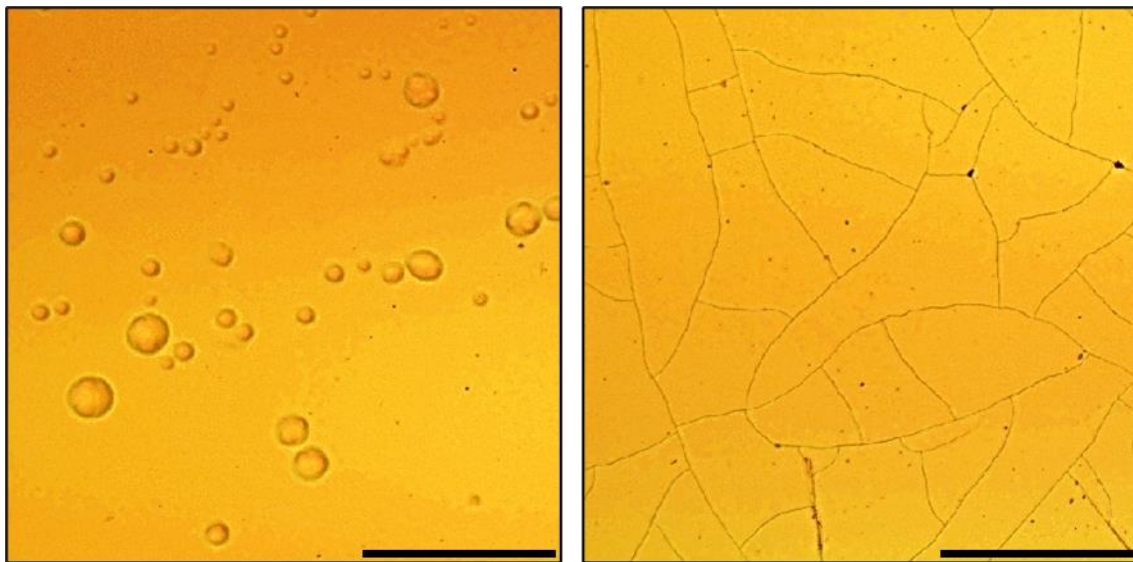


Figure 6.30- Gold surface on COC showing bubbles and cracks on the surface. The scale bar is 50  $\mu\text{m}$ .

Figure 6.31 shows a summary of electrodes fabricated on polymer and silicon substrates.



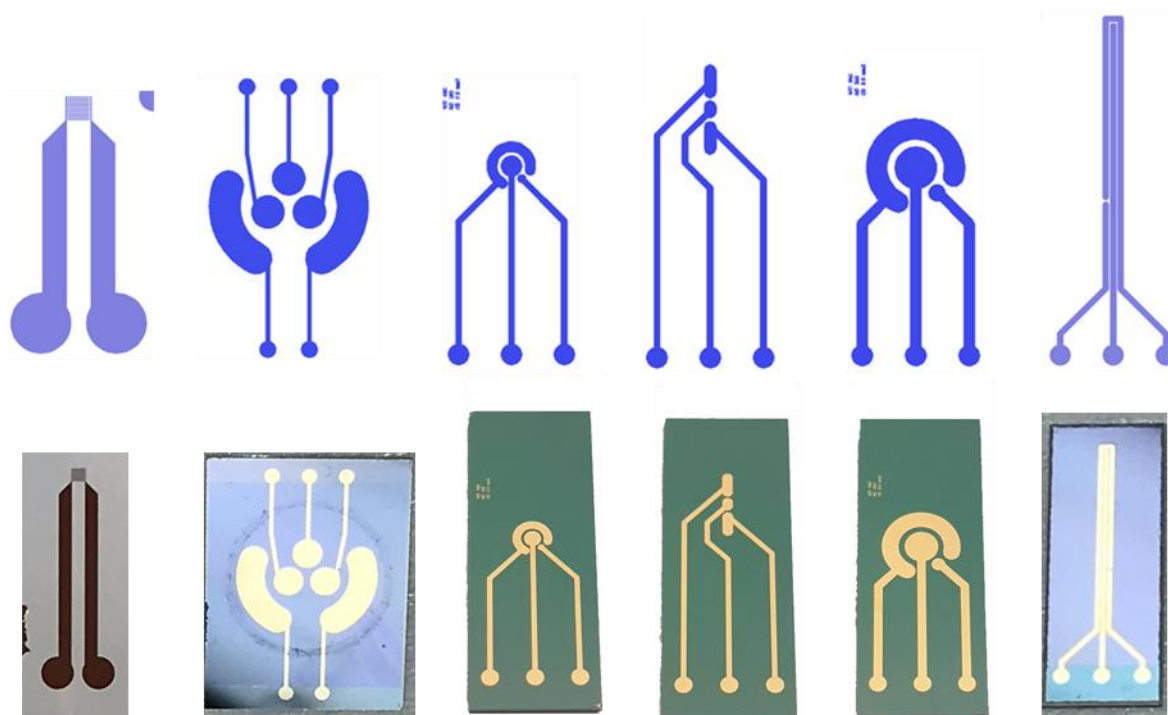


Figure 6.31 – Except for the first design, an IDE on a polymer substrate, the rest are all three-electrode configurations on a silicon substrate. (The contact pads are 1 mm in diameter).

## Chapter 7 Immunoassay development

As mentioned in the previous chapters, the final immunoassay format chosen for this thesis was a competitive heterogenous assay with an enzyme tracer and electrochemical detection. However, initially, a competitive immunoassay with a labelled Ab was tested. In some of the initial experiments, when optimising the Fc binding protein, Irgarol, was used as the analyte to test the assay. The choice of such a **'test' analyte was mainly attributed to the ready availability of all the necessary reagents from the lab in Spain (external research stay)**. Unless otherwise specified, all other assays have been performed using cortisol antibody and cortisol-HRP tracer.

### 7.1 Competitive cortisol assay using labelled Ab

For performing this assay, cortisol conjugated with bovine serum albumin (BSA) was prepared in house. Cortisol was conjugated to BSA to facilitate immobilisation on the surface. Cortisol was derivatised to provide a reactive carboxylic group that could interact with the amine groups of BSA. Hydrocortisone 21-hemisuccinate sodium salt (MW 484.5 Da) was selected as the hapten. An active ester method was used to conjugate the cortisol hapten (CH) to BSA (Figure 7.1). The detailed protocol is given in Appendix A.4. Since BSA has around 35 amine groups, the number of CH per BSA varied depending on the CH:NHS:DCC ratio used. The four different ratios tested are marked from A to D.

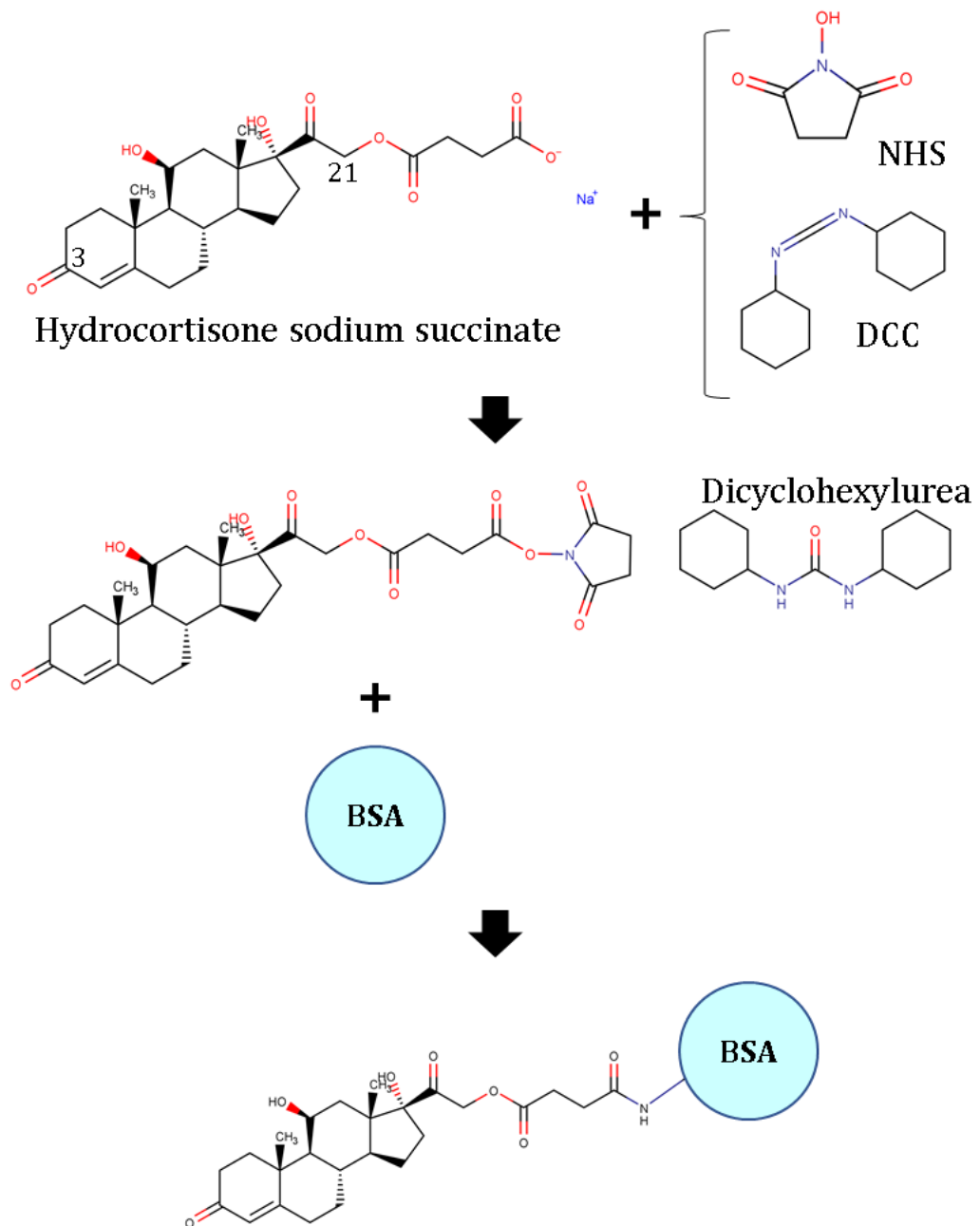


Figure 7.1 – Active Ester method for the conjugation of cortisol to BSA.

The results from Matrix-assisted laser desorption ionization-time of flight mass spectrometry (MALDI - TOF MS) are shown in Figure 7.2, and further calculations shown in Table 7.1 reveal the number of CH attached per BSA. The molecular weight of BSA was estimated from the result as 66478.9 Da.

Table 7.1 - Number of hapten per BSA molecule obtained from MALDI TOF MS analysis

	[CH] in 0.5% BSA soln	CH:NHS:DCC	MALDI TOF MS (Intensity a.u)	CH per BSA
A	12.5 $\mu$ M	1:2.5:5	75810.1	19
B	6.25 $\mu$ M	1:2.5:5	70408.8	8
C	6.25 $\mu$ M	1:1.5:1.5	68387.2	4
D	3.125 $\mu$ M	1:1.5:1.5	67474.8	2

The Cortisol hapten-BSA (CH-BSA) conjugates were purified by dialysis. CH2-BSA indicates a loading of 2 cortisol haptens per BSA and, accordingly, CH4-BSA, CH8-BSA, and CH19-BSA indicate 4, 8 and 19 cortisol haptens per BSA. A standard ELISA was run on a 96-well plate to check the different cortisol BSA conjugates. A 1D assay was performed with the different cortisol conjugates immobilised on the ELISA plate. The primary antibody was a mouse monoclonal cortisol antibody (ab1949 from Abcam, Cambridge, USA) at 1  $\mu$ g/mL, and the secondary antibody was a goat anti-mouse peroxidase (A4416 from Sigma-Aldrich Corporation, St. Louis, USA) at 1/6000 dilution. The detailed protocol is found in Appendix A.6. Figure 7.3A depicts 1D indirect assay results to determine the optimal coating antigen concentration to be used for the competitive assay.

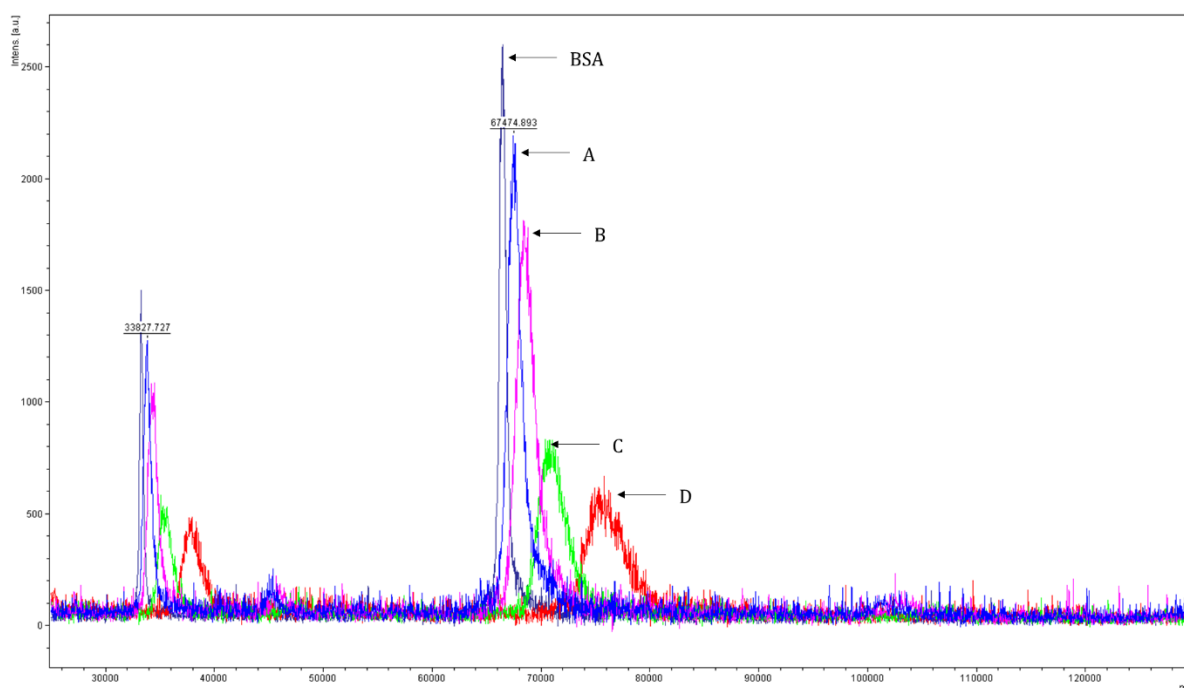


Figure 7.2- Results from MALDI TOF MS for BSA and cortisol conjugated with BSA indicating (A) CH19-BSA (B) CH8-BSA (C) CH4-BSA and (D) CH2-BSA.

Based on the results shown in Figure 7.3A, CH8-BSA at a 6.25  $\mu\text{g}/\text{mL}$  concentration was considered the best candidate for further studies. CH2-BSA and CH4-BSA gave poor signals even at the maximum concentration of 50  $\mu\text{g}/\text{mL}$ , and CH19-BSA was not considered for the study due to its high loading of cortisol haptens. Figure 7.3B shows the result obtained from the competitive assay with CH8-BSA at 6.25  $\mu\text{g}/\text{mL}$ . However, the obtained  $\text{IC}_{50}$  value was 26.9 nM, which was unsatisfactory considering the already high concentration of coating antigen.

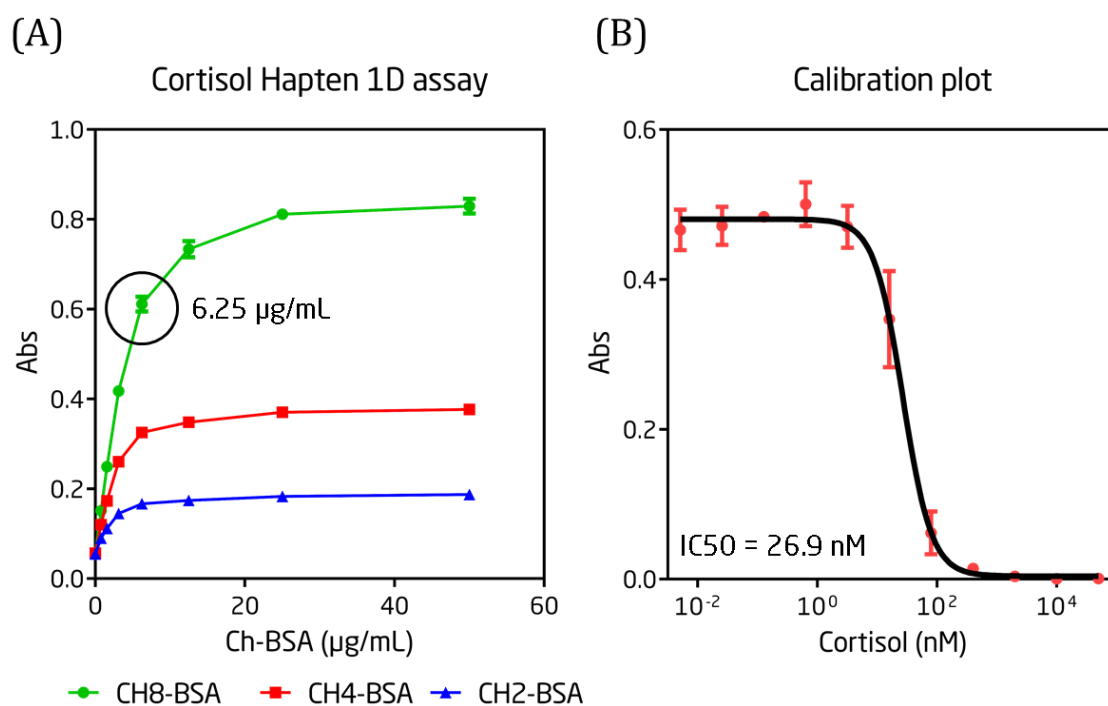


Figure 7.3 - ELISA results (A) 1D assay - indirect format. (B) Competitive assay with CH8-BSA

A major drawback of the synthesised CH-BSA conjugates was the choice of the BSA conjugation position (C21) (Figure 7.1), which could lead to cross reactivity given the structural similarities of other compounds, as can be seen from Figure 7.4.

Therefore, it was decided that the assay format and reagents should be reconsidered. A competitive assay format using a labelled hapten with a commercially available matched antibody and tracer pair were chosen for further experiments. An important consideration was the position of conjugation, and the antibody-tracer pair was selected to make the essential epitope accessible.

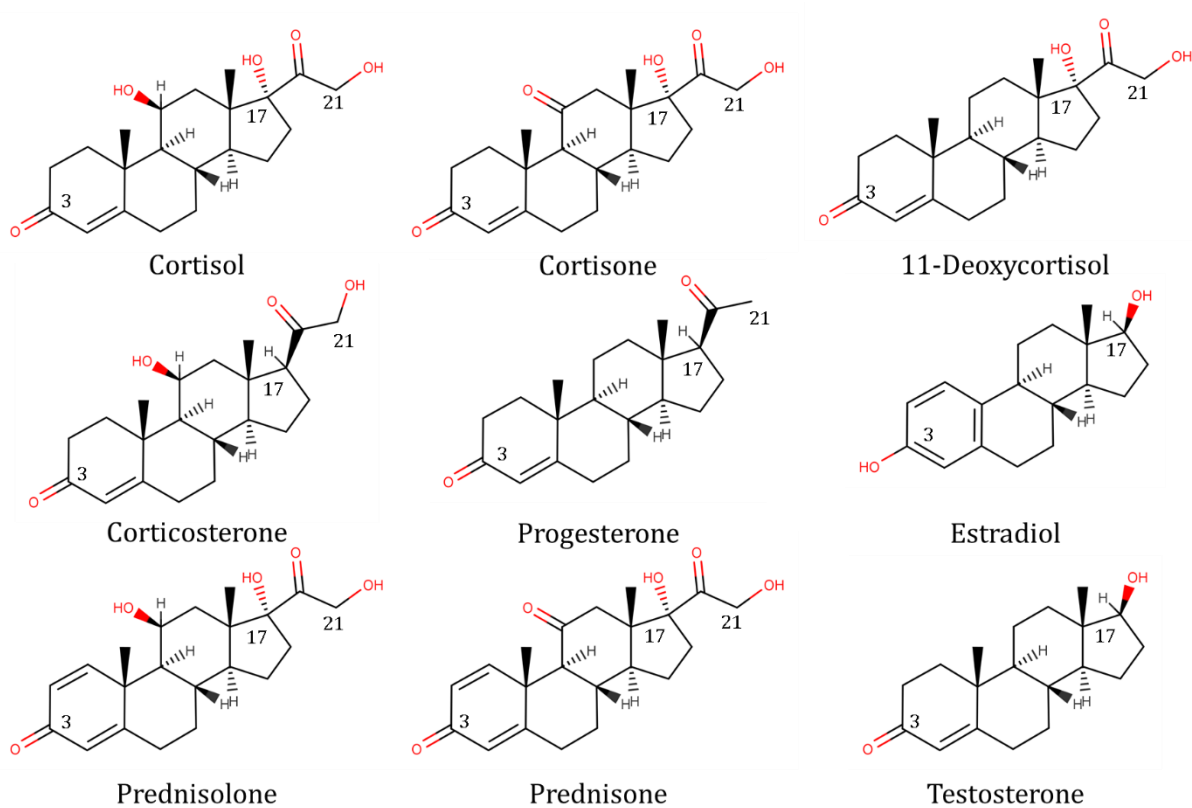


Figure 7.4- Structural homology of cortisol and various steroid molecules.

## 7.2 Competitive cortisol assay using labelled antigen

Another commercial cortisol antibody - tracer pair was selected from Fitzgerald Industries International, USA. A monoclonal antibody (10-C30D), produced from the clone obtained from immunising a mouse using Hydrocortisone-3-carboxymethyloxime (CMO)-BSA hapten and the corresponding cortisol 3 CMO-HRP tracer (65-IC08) were used for all further experiments. The cortisol 3 CMO-HRP conjugate was selected so that the epitope around C21 on cortisol, which differ from the other cross-reacting steroids, are well exposed. Therefore, the antibody was reported to have very low cross-reactivity (11-Deoxycortisol 0.9%; Prednisolone 5.6%; Corticosterone 0.6%; 11-Deoxycorticosterone <0.1%; Progesterone <0.1%; 17-

---

Hydroxyprogesterone <0.1%; Testosterone/Estradiol/Estriol <0.1%; Danazol <0.01%) and high specificity ( $K_a = 1.7 \times 10^9 \text{ M}^{-1}$ ) for the tracer.

The cortisol antibody-tracer pair was similarly as above first evaluated using ELISA. This provides a rough idea regarding the antibody and tracer concentration to be used and behaviour of the antibody with different immobilisation strategies, e.g., the presence of an Fc binding protein-like Protein-G. The detailed results are given in Paper I, and the experimental protocols are found in the Appendix A.7.

As discussed in chapter 4, an essential requirement in a heterogenous assay format is to immobilise either the antibody or antigen on a solid support, which is commonly a gold or polymer surface. Different immobilisation strategies were introduced in section 4.2.1 and can be used independently or in combination. In this thesis, a polymer substrate was used for conventional ELISA. As described in Chapter 4, Protein-G has been reported to improve certain aspects of immunoassays by ensuring that the paratopes of the antibodies are standing upright. Here, either the antibody or Protein-G was physisorbed in the 96-well plate through overnight incubation at 4°C in carbonate buffer (pH 9.6). For the particular well plate used (Nunc Maxisorp®), the pH of the coating buffer was critical as it was tested and shown that a normal pH of 7.4 was unable to facilitate protein adsorption to the surface.

All other immobilisation steps were performed on a gold surface or on superparamagnetic beads inside the IRC, as will be described in section 7.2.5.

### 7.2.1 Optimisation of Protein G immobilisation

Standard ELISA experiments were performed to determine whether adding an Fc binding protein, like Protein-G, would improve the ELISA results. The results were in accordance with the literature and indicated an improvement in the assay performance, especially in terms of the required antibody concentration (results shown in Paper I). When Protein-G was present, it enabled a lower antibody concentration to be used when immobilised on the surface. The experiment was also



used to determine the suitable Protein-G concentration required to run further assays. The manufacturer's recommendation was to use 10  $\mu\text{g}/\text{mL}$ . A 96-well plate ELISA was run in the direct format with the Protein-G coating as the first layer. Protein-G concentration was varied from 50  $\mu\text{g}/\text{mL}$  to 0.05  $\mu\text{g}/\text{mL}$ . In this case, a polyclonal Irgarol antibody (Ac87) with its corresponding HRP tracer (4d-HRP) was used at 2  $\mu\text{g}/\text{mL}$  and 0.2  $\mu\text{g}/\text{mL}$ , respectively. The results from the experiments showed that the signal intensity was not lost even at 1  $\mu\text{g}/\text{mL}$  of Protein-G (Figure 7.5A). The following experiment was to test higher antibody concentration to investigate the signal stability with Protein-G concentration varied from 50  $\mu\text{g}/\text{mL}$  to 3.125  $\mu\text{g}/\text{mL}$ . The Irgarol antibody was tested at 20  $\mu\text{g}/\text{mL}$ , 10  $\mu\text{g}/\text{mL}$  and 5  $\mu\text{g}/\text{mL}$  with the same tracer concentration of 2  $\mu\text{g}/\text{mL}$  (Figure 7.5B). The result showed very stable absorbance over the entire tested range, and hence, a Protein-G concentration of 3.125  $\mu\text{g}/\text{mL}$  was used in further assays.

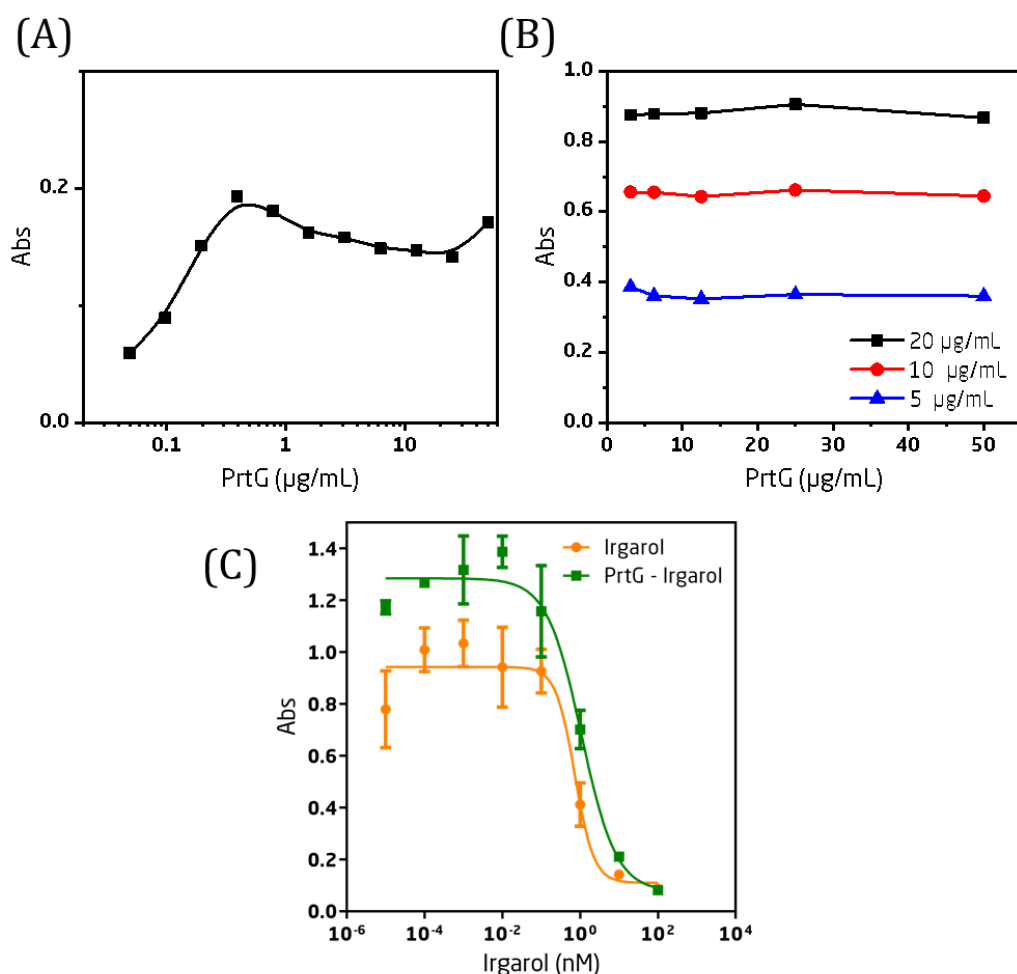


Figure 7.5 - Absorbance measurements for (A) varying Protein G concentrations while maintaining a fixed antibody and tracer concentration; and (B) varying Protein-G concentrations at three different antibody concentrations and fixed tracer concentration at 2  $\mu\text{g/L}$  (C) A competitive assay performed with and without Protein-G with 2.5  $\mu\text{g/mL}$  of Irgarol antibody As87 and 2  $\mu\text{g/mL}$  of tracer 4d-HRP.

Another aspect of using Fc binding protein-like Protein G or Protein A was to create a system where the immobilised antibody for one particular analyte could be removed by regenerating the Protein-G surface and introduce a different antibody for another analyte. Such a system would improve the versatility by enabling multi-analyte detection. Commonly, chromatographic columns are used for affinity purification of antibodies where antibodies are captured by Protein-A or Protein-G from a complex matrix. All other unwanted molecules are washed away, and the captured antibodies are eluted using a regeneration buffer. However, it was observed that the

recombinant Protein-G and the cortisol monoclonal mouse antibody IgG<sub>2a</sub> could not be separated under the regeneration conditions established in the experiments. Several different regeneration strategies were tested, but none of them led to the removal of cortisol antibody. Hence, Protein-G was used simply to improve the orientation of the immobilised antibody.

### 7.2.2 Regeneration of the antibody surface

Unlike ELISA, which is generally a single-use assay, a flow-based immunosensor needs to be used multiple times. There is thus a need to regenerate the antibody surface to prepare it for the subsequent measurement. In the case of a competitive assay, the antigen and the tracer bound to the antibody needs to be detached. The regeneration capability is especially crucial for an automated online monitoring system. Although an essential part of immuno sensor development, most reported papers do not mention the regeneration part.

A good review paper by Jack Goode *et al.* describes the theory and various methods used to regenerate biosensors [156]. The fundamental physics behind regeneration is to overcome the attractive forces between the antibody and antigen. It is estimated that the binding force between antibody to antigen is 35 to 165 pN [157]. The interaction between the antibody and antigen (Figure 7.6A) is due to weak bonds such as Van der Waals (1-20 kJ/mol), Hydrogen (5-40 kJ/mol), Hydrophobic <40 kJ/mol, and Ion-dipole (10-50 kJ/mol) bonds [158,159]. Hence, the solvent environment, like pH, can significantly influence the binding capacity. One standard method used is to alter the pH to disrupt the bonds. High or low pH buffers are used along with solvents like dimethylsulfoxide (DMSO), non-ionic detergents like TWEEN® 20, glycine and urea. Glycine has the advantage of binding to the surface of the antibody and antigen during regeneration and has a mild screening effect of preventing further re-binding [156].

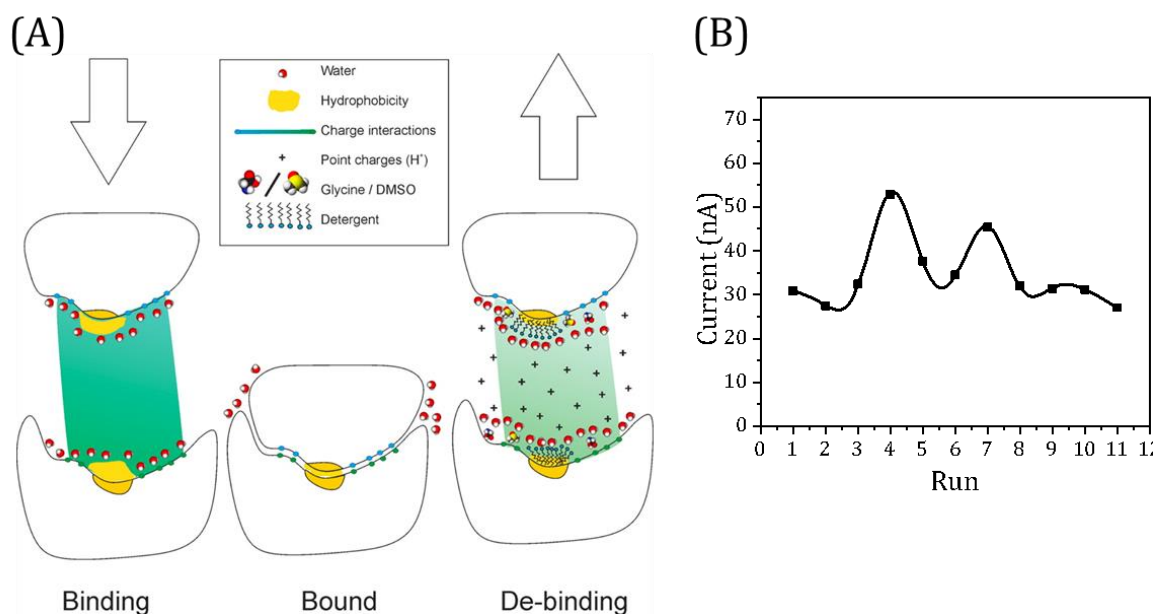


Figure 7.6 - (A) Schematic of biosensor regeneration showing relevant forces in binding and de-binding. Adapted from [156] (B) Improper regeneration leads to erratic signals in each complete run.

Glycine buffer at a pH of ~2 has been widely reported to be used as a regeneration buffer [160-163]. However, in my work, the output signal was inconsistent when the glycine buffer was used to regenerate cortisol tracer 65-IC08 from the immobilised antibody 10-C30D (Figure 7.6B). The assay was run with a tracer concentration of 1  $\mu\text{g}/\text{mL}$ , TMB/ $\text{H}_2\text{O}_2$  as substrate and incubation time of 400s. Each point in the graph corresponds to the reduction peak value from amperometric detection of the substrate product at the end of the incubation time.

The initial doubt was on the flow rate since shear forces inside the chamber could also remove the bound antibodies. However, it was found that, since cortisol is a highly hydrophobic molecule ( $\log K_{ow} = 1.61$ ), for complete removal, it required some polar aprotic solvent as DMSO added in the aqueous glycine buffer [164]. 1 % DMSO was added to the glycine buffer, and it started efficiently removing all the bound cortisol. Later it was also established that the flow rate and the choice of the substrate also had a role in the stability of the system. Finally, the system was

optimised to give very stable signal. The final result, with all the issues addressed and corrected, is given in paper-I.

### 7.2.3 Electrochemical substrate for the HRP enzyme

As mentioned in section 4.2.2, HRP was chosen as the enzyme label. HRP catalyses reduction of  $H_2O_2$  into water and oxygen. However, the specificity for the second  $H_2O_2$  molecule is low, allowing the substitution of many other electron donors. There are many chromogenic compounds for HRP like 4-chloro-1-naphthol (4-CN), o-phenylenediamine, 3-amino-g-ethyl carbazole, 2,2'-azino-bis(3-ethylbenzthiazolone), Hanker-Yates reagent (HYR), 3-methyl-2-benzothiazolinone hydrazone hydrochloride (MBTH) + 3dimethylaminobenzoic acid, 4-aminoantipyrene and a phenol, 3,3'-diaminobenzidine (DAB) and its derivatives, such as 3,3',5,5'-tetramethylbenzidine (TMB), o-dianisidine, and dicarboxidine [165].

TMB has proven to be the best among the substrates [166,167], and the oxidised product of TMB is electroactive. In this thesis, TMB/ $H_2O_2$  was chosen as the substrate for HRP. The substrate solution was prepared in citrate buffer (pH 5.5) at 0.4 mM of TMB (6 % stock prepared in DMSO) with 1.2 mM of  $H_2O_2$  [168]. The highest peroxidase activity is achieved at an  $H_2O_2$  concentration of 1 to 3 mM at a pH value in the range of 3.8-4.4 [169]. The TMB/  $H_2O_2$  substrate is light sensitive and had to be prepared fresh. Hence, a one-component commercial TMB/  $H_2O_2$  substrate (TMB Plus 2 from Kem-En-Tec Nordic A/S, Denmark) was tested and proved superior to the in-house prepared substrate. The commercial substrate was stable at room temperature for days and it is claimed by the manufacturer to have a shelf life of over a year if stored at 4 °C. The final automated FIA system demanded a stable substrate and moreover the commercial substrate had faster kinetics and a higher signal for the same incubation time than the substrate made in-house. The background signal observed, during amperometry, for the commercial substrate was comparable to the in-house substrate below 4% (~30-60 nA) of the maximum signal (~1500 nA).

A simple experiment was performed to check the substrate stability at concentration of HRP at 1  $\mu\text{g}/\text{mL}$ . 3.125  $\mu\text{g}/\text{mL}$  of Protein-G was on a coated ELISA plate (kept at 4  $^{\circ}\text{C}$  overnight and washed), followed by the addition of 1  $\mu\text{g}/\text{mL}$  of cortisol antibody (10-C30D) (30 min at RT and washed), 2  $\mu\text{g}/\text{mL}$  of HRP tracer (65-IC08) (30 min at RT and washed) and then the substrates were added for a 30 min incubation in the dark. The results are shown in Figure 7.7

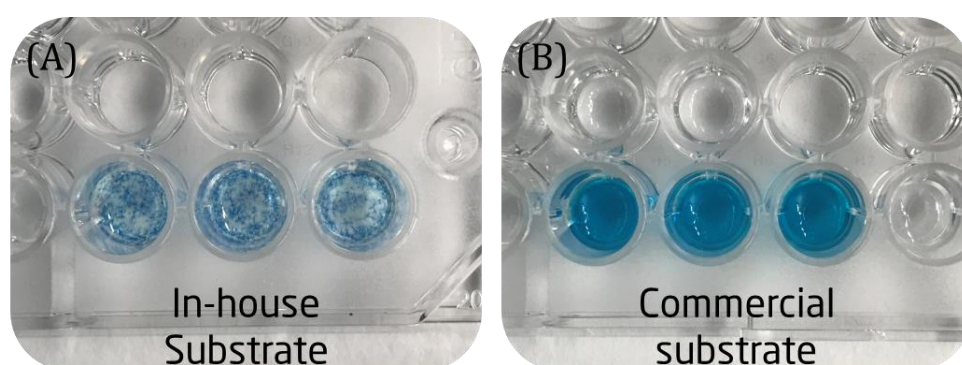


Figure 7.7 - Comparison of substrate stability at HRP concentration of 1  $\mu\text{g}/\text{mL}$ . (A) The in-house substrate precipitated (B) The commercial substrate proved to be stable.

The precipitation of the in-house substrate (Figure 7.7A) could be due to the pH. The commercial substrate has a more acidic pH ( $\sim 3.8$ ) than the in-house substrate ( $\sim 5.5$ ), and hence it could be due to the higher solubility of the oxidised substrate product formed. The commercial substrate also includes some undisclosed proprietary stabilisers, which may be providing stability (Figure 7.7B). Inter-assay stability between the in-house substrate and commercial substrate is given in Paper I, and it shows that the commercial substrate has less inter-assay variation. Hence the commercial substrate has been used in all experiments unless otherwise specified.

#### 7.2.4 Optimisation of Protein G based ELISA

An ELISA was run to determine the apt concentration of cortisol antibody and HRP tracer. 3.125  $\mu\text{g}/\text{mL}$  of Protein-G in carbonate buffer (pH 9.6) was added to the 96-well plate and incubated overnight at 4  $^{\circ}\text{C}$ . The concentration of cortisol antibody

(10-C30D) was varied from 12  $\mu\text{g/mL}$  to  $\sim 0.02 \mu\text{g/mL}$ , and three different HRP tracer (65-IC08) dilutions, 1/3000, 1/6000 and 1/12000, were tested with results shown Figure 7.8A. Based on this experiment, an antibody concentration of 0.38  $\mu\text{g/mL}$  was chosen for further experiment. Competitive ELISAs were performed for a cortisol concentration ranging from 100 nM to 0.1 pM with the same three tracer concentrations (Figure 7.6B). The result shows that an HRP tracer concentration of 1/3000 gave the required absorbance value of around 1 for the lowest cortisol concentration.

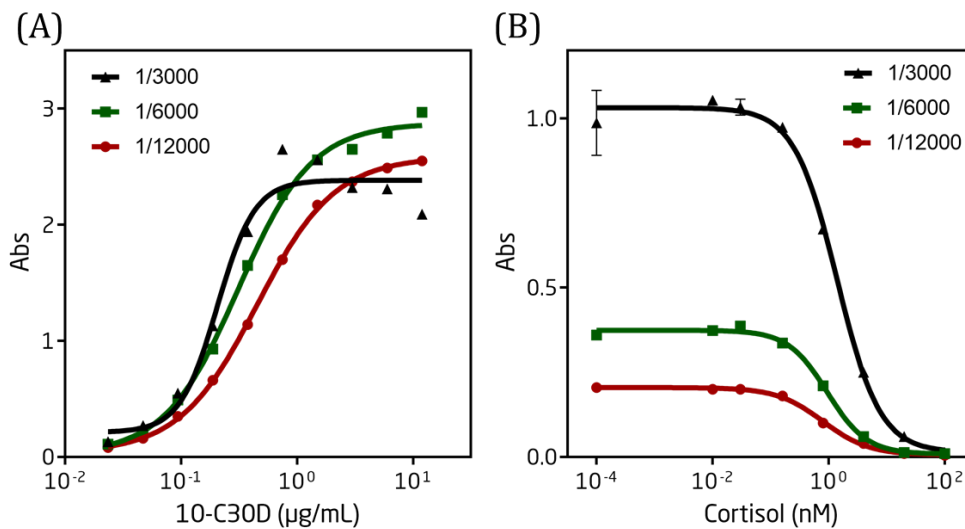


Figure 7.8 - ELISA results for assays at three different HRP tracer dilutions: (A) Absorbance at varying concentrations of cortisol antibody and (B) calibration curves for cortisol.

As a thumb rule, during the subsequent experiments involving IRCs, the cortisol antibody and HRP tracer concentration were chosen to be at least thrice the one used in the ELISA tests. Hence, a concentration of 1  $\mu\text{g/mL}$  was chosen for both the antibody and HRP tracer in the actual assays using IRCs.

### 7.2.5 Immobilisation of Protein G in IRC

The IRC designs are shown in Chapter 6, Figure 6.9 had channels with and without a gold layer. Therefore, three different immobilization strategies were tested:

Strategy 1: The antibody was immobilised directly on the gold surface using thiol chemistry (Figure 7.9A)

Strategy 2: The antibody was bound to Protein-G, which in turn was immobilised on the surface using thiol chemistry (Figure 7.9B)

Strategy 3: The antibody was bound to Protein-G, which was covalently immobilised to superparamagnetic beads (held in place using a permanent magnet) (Figure 7.9C).

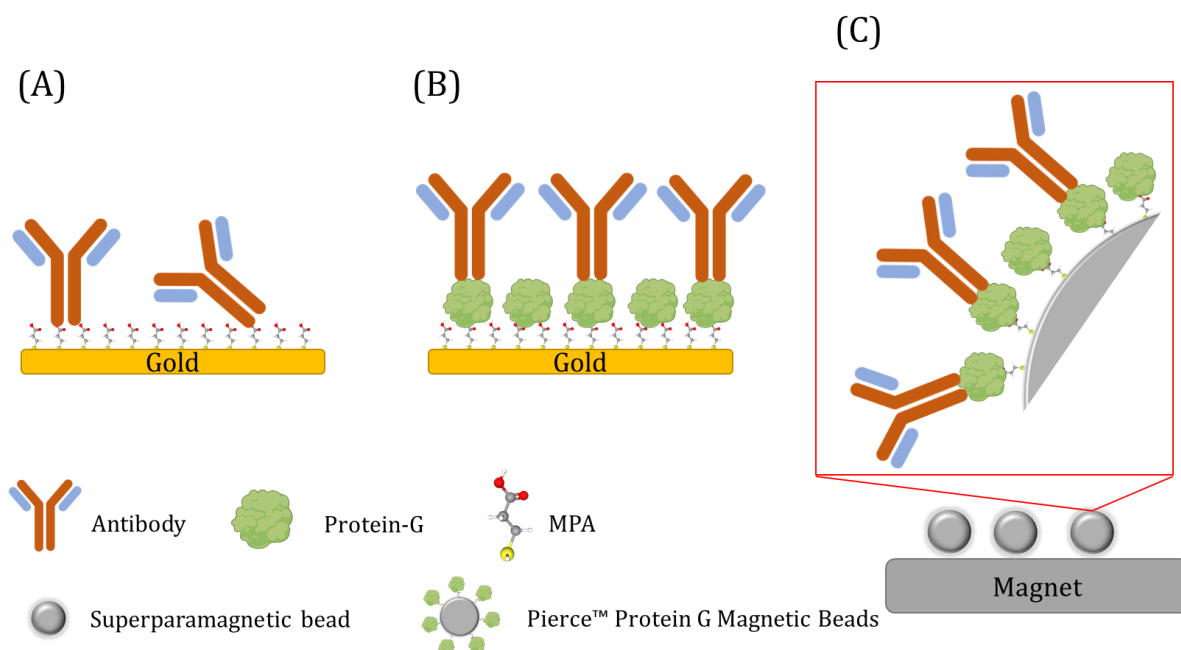


Figure 7.9 - Immobilisation strategies: (A) An MPA SAM on the gold surface with antibodies immobilised after intermediate activation of the carboxylic groups; (B) an MPA SAM with covalently immobilised Protein-G and antibodies bound to the Protein-G; (C) Superparamagnetic beads with covalently immobilised Protein-G and bound antibodies (zoom-in of the details in the inset).

The 1<sup>st</sup> and 2<sup>nd</sup> strategies use self-assembled monolayers of a carboxylate terminated thiol compound on the gold surface [170]. Carboxylated terminals form amide bonds with the amino groups present on the protein using zero-length crosslinkers, as depicted in Figure 7.10. Protein-G or any antibody can be immobilised through this technique.



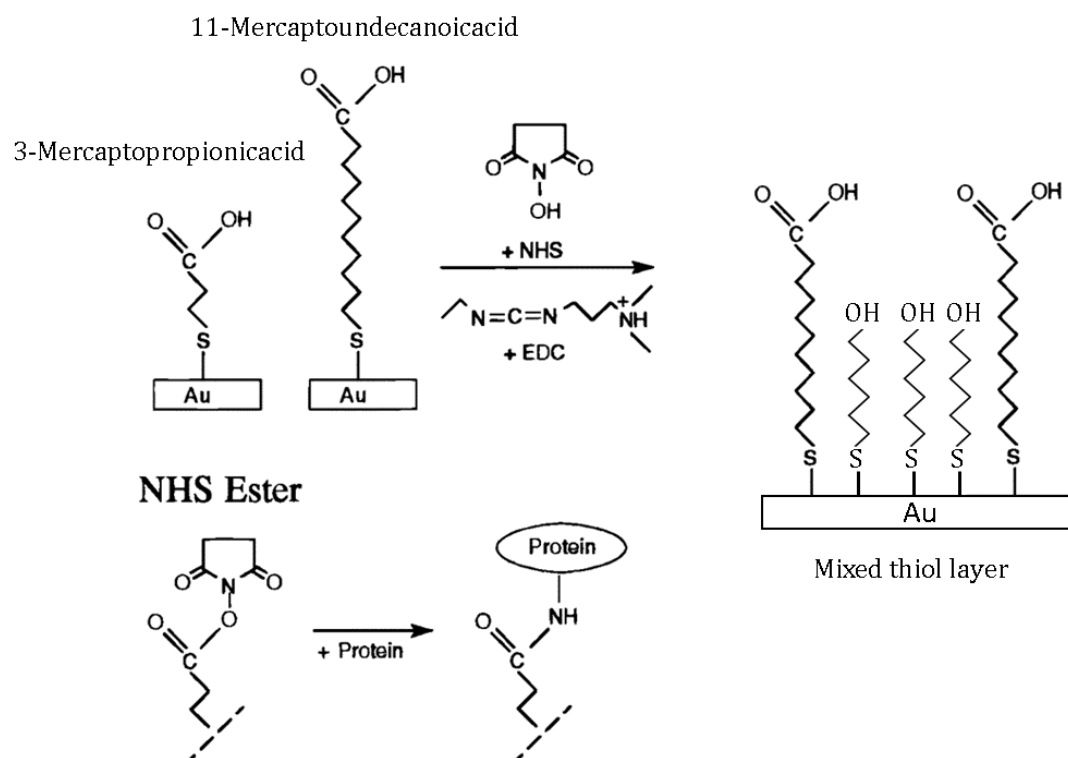


Figure 7.10 - Protein immobilisation strategies where a SAM of 3-Mercaptopropionic acid and 11-Mercaptoundecanoic acid is used in combination with zero-length crosslinkers to bind the protein. Adapted with permission from [170] Copyright 1997 American Chemical Society.

The self-assembled monolayer (SAM) can be a long chain molecule like MUA or a short-chain compound like MPA, where both have carboxylated terminals. Sometimes a mixture of MUA and a shorter molecule like 6-Mercaptohexanol (MH) create a **'mixed' thiol SAM, which is used to reduce steric hindrance** by separating out the MUA with the non-reactive functional group of MH.

In this thesis, both the 1<sup>st</sup> and 2<sup>nd</sup> strategies used MPA to form the SAM inside the gold coated channel of IRC (Figure 6.9B). MPA was chosen since it can be deposited from an aqueous solution whereas MUA needs ethanol as the solvent. As mentioned before, ethanol cannot be used with PMMA based parts.

In the 1<sup>st</sup> strategy, 100 mM of MPA in MilliQ water was added to the gold layer and kept for 2 h. After that, 200 mM EDC and 50 mM NHS in MES buffer was added and kept for 25 min, washed, and immediately 1 µg/mL of cortisol monoclonal antibody (10C30D) was added and kept at room temperature for 30 min. In the 2<sup>nd</sup> strategy, 3.125 µg/mL of Protein-G was added after the EDC/NHS step and kept at room temperature for 1 h before adding the cortisol antibody. The final results of these two competitive assays are presented in Paper I.

The 3<sup>rd</sup> strategy used commercially available Protein-G coated superparamagnetic beads. However, the crosslinkers used to attach the Protein-G to the beads are not disclosed by the manufacturer. The Protein-G beads are supposed to have a binding capacity of 60 µg IgG/ mg of beads. In order to ensure maximum binding, 10 µL of 1.2 mg/mL cortisol antibody (10-C30D) was added to 20 µL of 10 mg/mL Protein-G, and 70 µL of PBS was added to make it to a final volume of 100 µl. 10 µL of this solution was added to the IRC and washed after placing a permanent magnet in the magnet slot. The result of the magnetic bead assay is also presented in Paper I.

In summary, the IC<sub>50</sub> and LOD of the three assays are summarised in Table 7.2, concluding that the best performing assay was SAM-Protein G-Ab. However, the magnetic bead-based assay has advantages due to its versatility in changing the antibody when required. Moreover, these results indicated that the sensitivity of the assays was not good enough to detect cortisol in the water of a fish tank (2 -30 ng/mL)<sup>6</sup> and thus, the ISLM clean-up and pre-concentration step was included. Preliminary experiments using ISLM showed that extraction of cortisol and its preconcentration was possible (Paper I).

Table 7.2 - Performance of the IRC based assay using the three different immobilization strategies

Immobilization	IC <sub>50</sub>	LOD
SAM-Protein G-Ab	0.91 nM	0.6 pM
Magnetic beads-Protein-Ab	7.8 nM	1.3 pM

<sup>6</sup> For a tank containing Rainbow trout. The stress response of fish is dependent on species.



## Chapter 8 Automation of the FIA system

*“Suffering arises from trying to control what is uncontrollable, or from neglecting what is within our power.”*

*— Epictetus*

*But we can always make a control system*

*— Claudy*

---

Modern aquafarms like RAS employ automated control systems to optimise efficiency by reducing manual intervention, utility costs and improving overall performance. The fundamental principle is to control the environmental parameters for maximal growth output. As mentioned in the literature, the control system could be a simple feedback control system that **compares a predetermined ‘setpoint’ to the measured value and** adjusts the process parameters, or an advanced distributed control system (DCS) employing a network of several discreet programmable logic controllers (PLC) or SCADA [19]. Such process control systems have only been utilised to control parameters that would optimise fish production but not fish welfare. It has been described in Chapter 3 how the welfare of fish and cortisol measurement can benefit the farmer. However, the unavailability of such a stress sensor for commercial application in a fish farm has only been addressed recently [171,172]. This thesis has focussed on two main aspects of addressing the problem as mentioned above; to create a non-invasive online measurement system and to automate the same so that it can be integrated into the control system in the aquafarm. This chapter describes how the automation of the cortisol measurement system was achieved.

In the mid-90s, there have been reports of numerous LabVIEW or PC based control units designed for FIA systems [173-177]. However, none of the systems described

the actual development of the FIA system or the interfacing circuitry required to control various components and relied on a semi-automated FIA system. The existing commercial FIA systems either come in pre-configured setups or provide limited flexibility. These limitations led to the development of a versatile open-ended system where any number of devices can be controlled and configured to perform most of the experiments. It was an additional challenge that an immunoassay also had to be automatically performed in addition to the development of a FIA system.

The FIA system is all about controlling some pumps and turning some valves. Figure 6.1 depicts the schematic for the control system. The design is similar to a PLC, where multiple relays are used to build a controller capable of carrying out repetitive sequential type control operations. The FIA system comprises three pumps, a multiposition valve (MPV) and a two-position valve (2PV). All the components can be controlled using a simple relay, but the MPV required a binary coded digital (BCD) to decide the position. The controller thus had to switch the pumps on and off selectively, switch the two-position valve between 'inject' and 'fill' modes, and move the MPV to the required position.

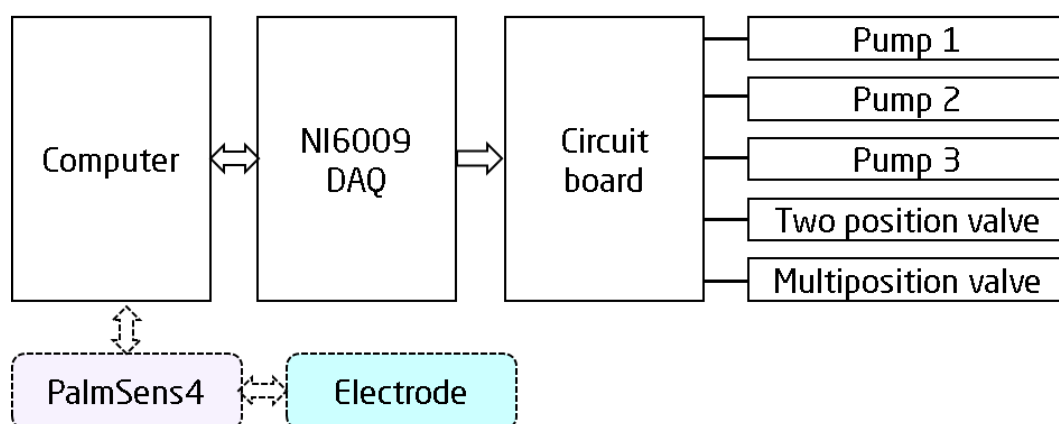


Figure 8.1- Control system block diagram

Figure 8.1 depicts a simplified block diagram of the system. A laptop or a computer running LabVIEW forms the processor for the control system, a data acquisition board (DAQ) model NI6009 from National Instruments forms the input/output device, and a

custom-designed circuit board encompasses the relay system and connectors for all the actuators.

Figure 8.2 depicts the various components in the automation system. 1, 2 and 3 are peristaltic pumps, 4 is the MPV, 5 is the 2PV, 6 is a NI6009 DAQ, 7 is the custom-made circuit board, 8 is the laptop and 9 represents the PalSsens4 potentiostat.

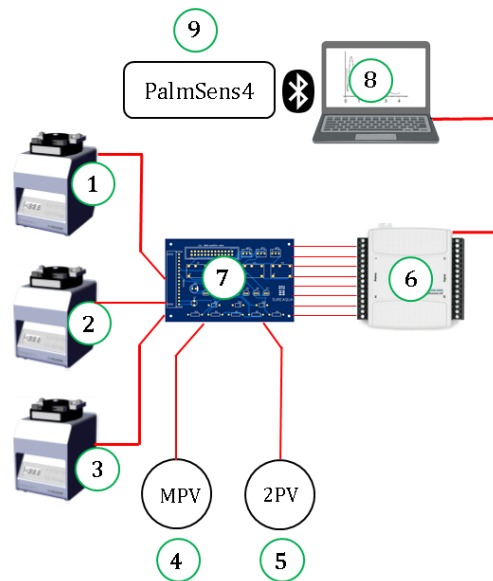


Figure 8.2- Schematic of the automation system.

## 8.1 The 'brain' of the system

The computer forms the system's brain, where commands to the external circuit can be programmed, stored, and processed through the LabVIEW program. The software LabVIEW acronym for 'Laboratory Virtual Instrument Engineering Workbench' is a graphical modular programming language built to cater for instrumentation and control engineers. It has visual depictions or 'tasks' of general process control components that can be assembled to form a complete control system, hence the name 'graphical language'. These tasks are subroutines written in C or C++, thereby saving the programmer time by having ready-made subroutines for most processes in a control system. Figure 8.3 depicts a sample program that shows two tasks in a

'loop' (the outer box depicts a loop function). The first task is a simple delay routine, and the second task sends a command signal to the outside input/output unit NI6009 to give out specific values on its ports.

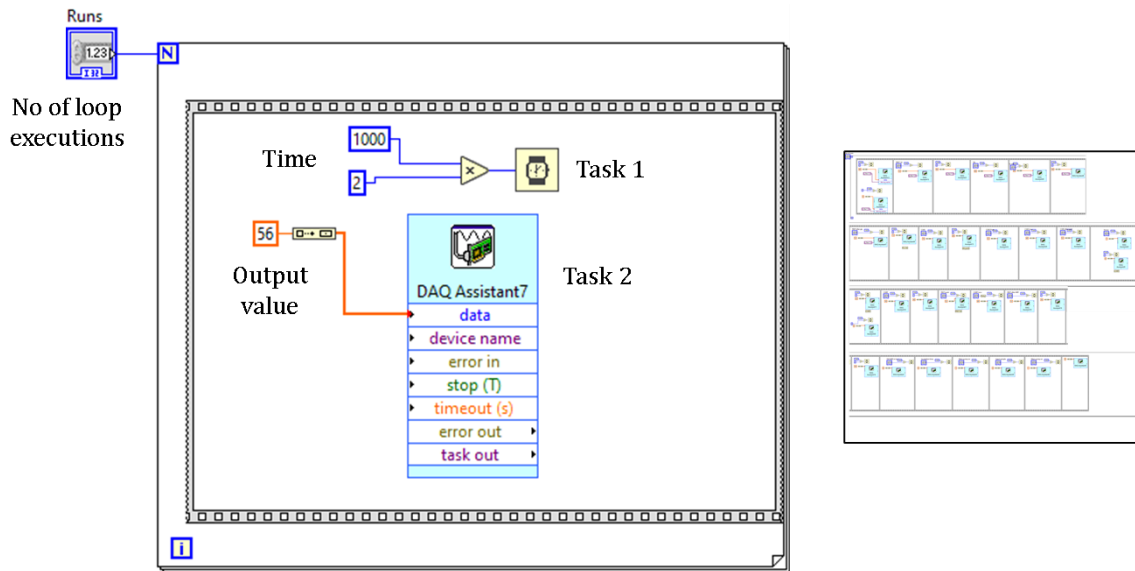


Figure 8.3 - A sample graphical program written in LabVIEW, and the entire program with almost 30 of such sequences is shown on the right.

Using a sequence of such simple building blocks, we can control the entire FIA system. During the testing phase, the flow rate and sequence of operation of the pump and valves were decided. After that, the assay was optimised by keeping time as the only variable. Once the assay functioned correctly, the program could be converted to a single executable file. The front panel of the LabVIEW program with provision to change the assay timing is shown in Figure 8.4.

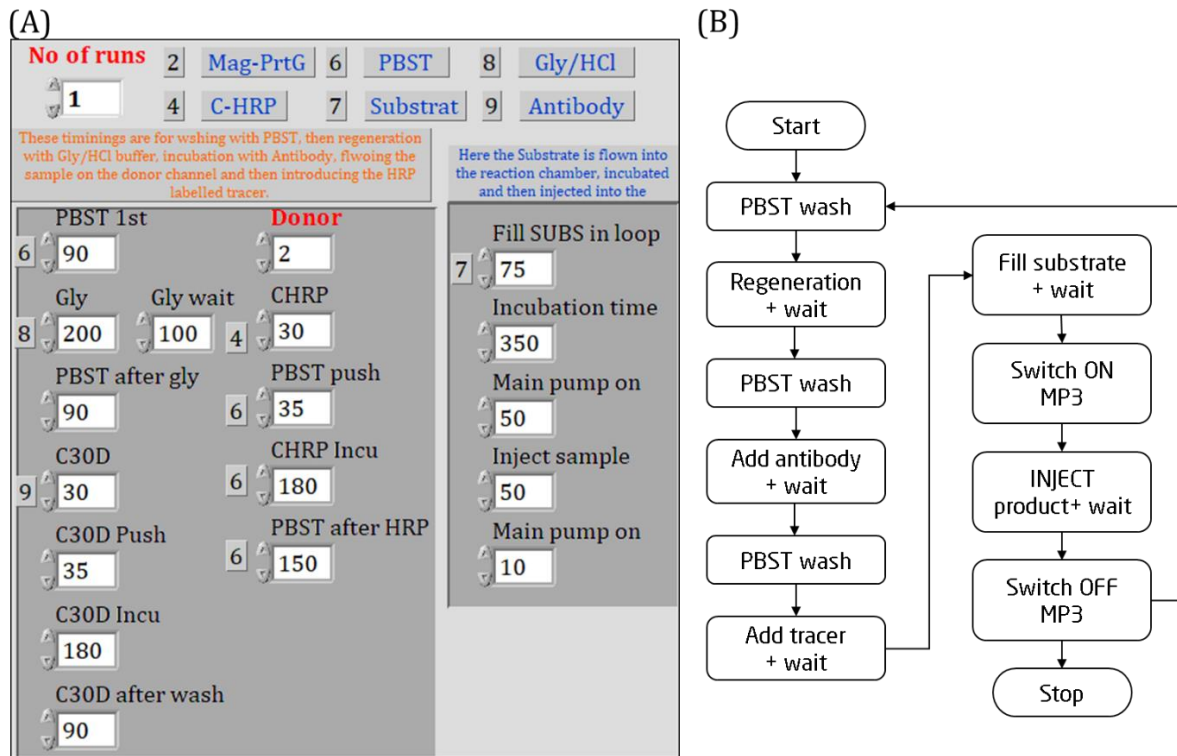


Figure 8.4- (A) Front panel of the LabVIEW program (B) Flowchart to run the assay.

Once the program was coded, the output is sent out as 8-bit digital signals through the USB and accessed via the NI6009.

### 8.1.1 Interface to the outside world - NI6009

The NI6009 is a small device connected to the computer's USB port and powered through the same port. It serves as a 'converter' for the serial data from the USB port to more accessible 12-bit digital output/input, eight analogue input (14-bit, 48 kS/s), two analogue output (150 Hz) and a 32-bit counter. As described in the next part, it can acquire electrical signals from sensors or instruments and send out signals used to control various actuators.



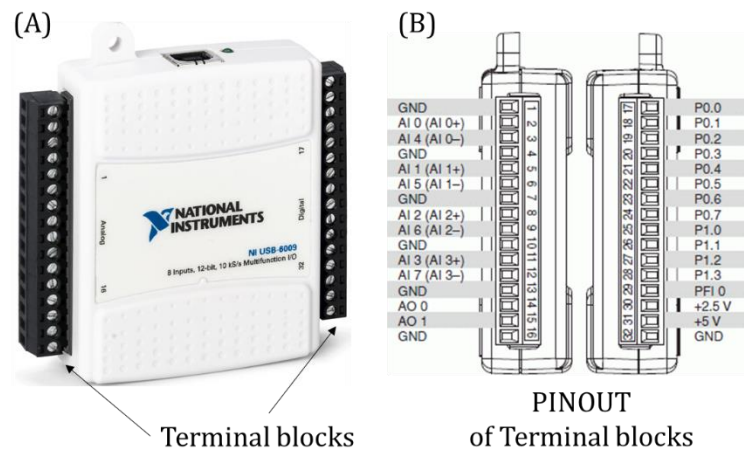


Figure 8.5 - (A) The USB NI6009 DAQ unit from National instruments and (B) the corresponding pinout diagram

As briefly mentioned before, the three pumps can be operated using relays. However, the 2PV and the MPV have stepper motors as actuators and inbuilt control circuits. The 2PV could, nevertheless, be controlled using relays but the MPV required BCD signal (a code the computer understands which uses binary numbers). NI6009 has **two digital output ports with port no. '0' and port no. '1'**. Port0 has 8 bits (p0.0 to p0.7), whereas port1 has 4 bits (p1.0 to p1.3). The relay could be turned on and off using a single bit binary output from the NI6009 except for MPV, which required four-bit binary output. Two pumps (MP2 - Miniplus2, MP3 - Miniplus 3), 2PV and MPV, uses port0, and the third pump (A/L- Alitea or Longer), used for flowing the water sample through the donor phase of the ISLM, was controlled using port1. Table 8.1 indicates the exact ports used to control each component. Note how all the ten positions of the MPV can be accessed using four bits, namely p0.3, p0.4, p0.5, p0.6, which represents 1, 2, 4 and 8 of BCD (A combination of 1, 2, 4 and 8 can be used to make all decimal numbers from 0 to 15).

Table 8.1 - Logic for the digital output from Ni6009 and the corresponding decimal code used in the program.

NI6009 port No		p0.6	p0.5	p0.4	p0.3	p0.2	p0.1	p0.0	p1.0	Binary (port0)	Decimal	
Reagents	Pos.	8	4	2	1	MP2	2PV	MP3	A/L		Switch	MP2 ON
Mag-PrtG	No2	0	0	1	0	0	0	0	0	0010000	16	20
Air	No3	0	0	1	1	0	0	0	0	0011000	24	28
C-HRP	No4	0	1	0	0	0	0	0	0	0100000	32	36
Air	No5	0	1	0	1	0	0	0	0	0101000	40	44
PBST	No6	0	1	1	0	0	0	0	0	0110000	48	52
SUB	No7	0	1	1	1	0	0	0	0	0111000	56	60
Gly/HCl	No8	1	0	0	0	0	0	0	0	1000000	64	68
Antibody	No9	1	0	0	1	0	0	0	0	1001000	72	76

For MP2, MP3, and A/L, '0' denotes OFF state, and '1' denotes ON state; for the 2PV '0' denotes 'FILL' as in fill the IRC and '1' denotes 'INJECT' the product formed in IRC to the detector electrode. In the LabVIEW program, the decimal equivalent of the required output is used to control the pumps and valves.

### 8.2 Circuit board for the actuators

The signal from the NI6009 is a digital output, which can be either low (0) or high (1), and the absolute maximum voltage range is from -0.5 V to 5.8 V with reference to GND. Since the USB powers it, the maximum current is limited to ~0.1A per port. Hence, the NI6009 cannot operate a relay to control the pumps and valves; however, it can directly control the MPV via transistors using only the digital output.

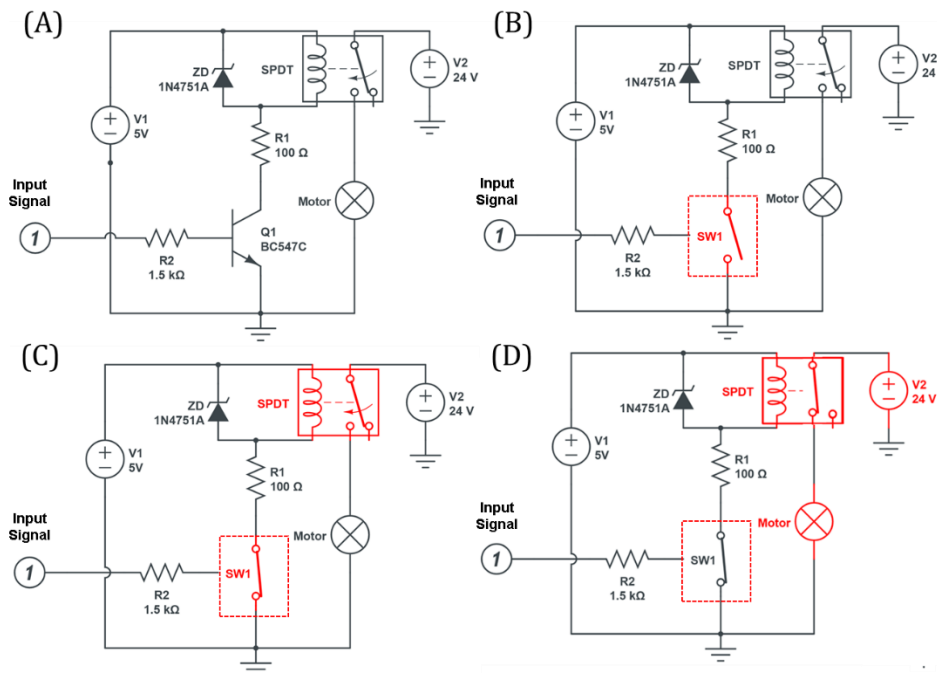


Figure 8.6- The working of a transistor configured as a switch (A) Circuit for NPN transistor along with a relay and motor (B) NPN transistor depicted as a switch. (C) The closed switch powers the relay (SPDT) (D). The closed relay switches the motor ON.

To operate the relay and thereby control the pump, a transistor was used. A transistor is a semiconductor device used to amplify an AC signal or function similar to a switch. If the

transistor is configured in the way depicted in Figure 8.6A and C, we can make the transistor function as a simple switch.

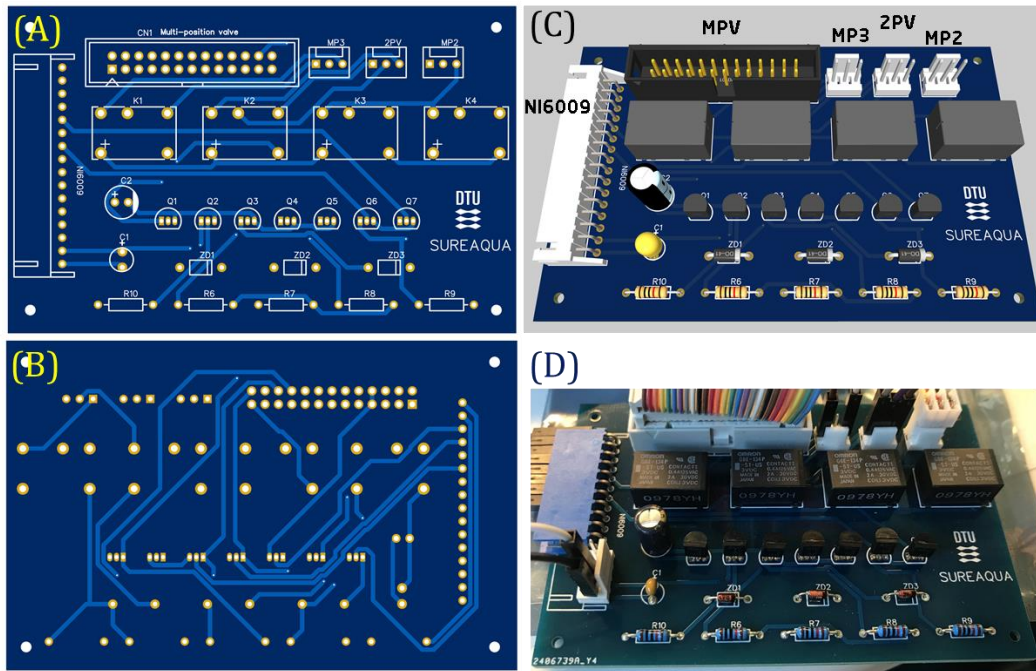


Figure 8.7- (A) Layer1 (top) of the PCB (B) Layer0 (bottom) of the PCB (C) 3D rendering of the final circuit with components and (D) The actual circuit being used in the control system.

When a high digital signal is given, the transistor ‘closes’, allowing current from the 5V supply to flow through the single pole double throw (SPDT) relay. The relay is an electromagnetically actuated switch, and once the relay is powered, it attracts the built-in lever to the ‘CLOSE’ position. When the relay is closed, the current from the 24 V supply can reach the motor, turning it ON. When the digital signal goes low, the transistor ‘opens’ and cuts off the power to the relay, thus turning the motor OFF. Therefore, a single bit of high or low signal, like the digital output signal from NI6009, can turn a motor ON or OFF. The same method can be used to control the 2PV. The transistor-relay pair forms the fundamental component that can be repeated to address as many devices as possible limited only by the digital output capability of the NI6009 being used.

A circuit board has been built to interface all the pumps and valves. The design of the circuit board is given in Figure 8.7, and the actual circuit diagram is given in Figure 8.8.

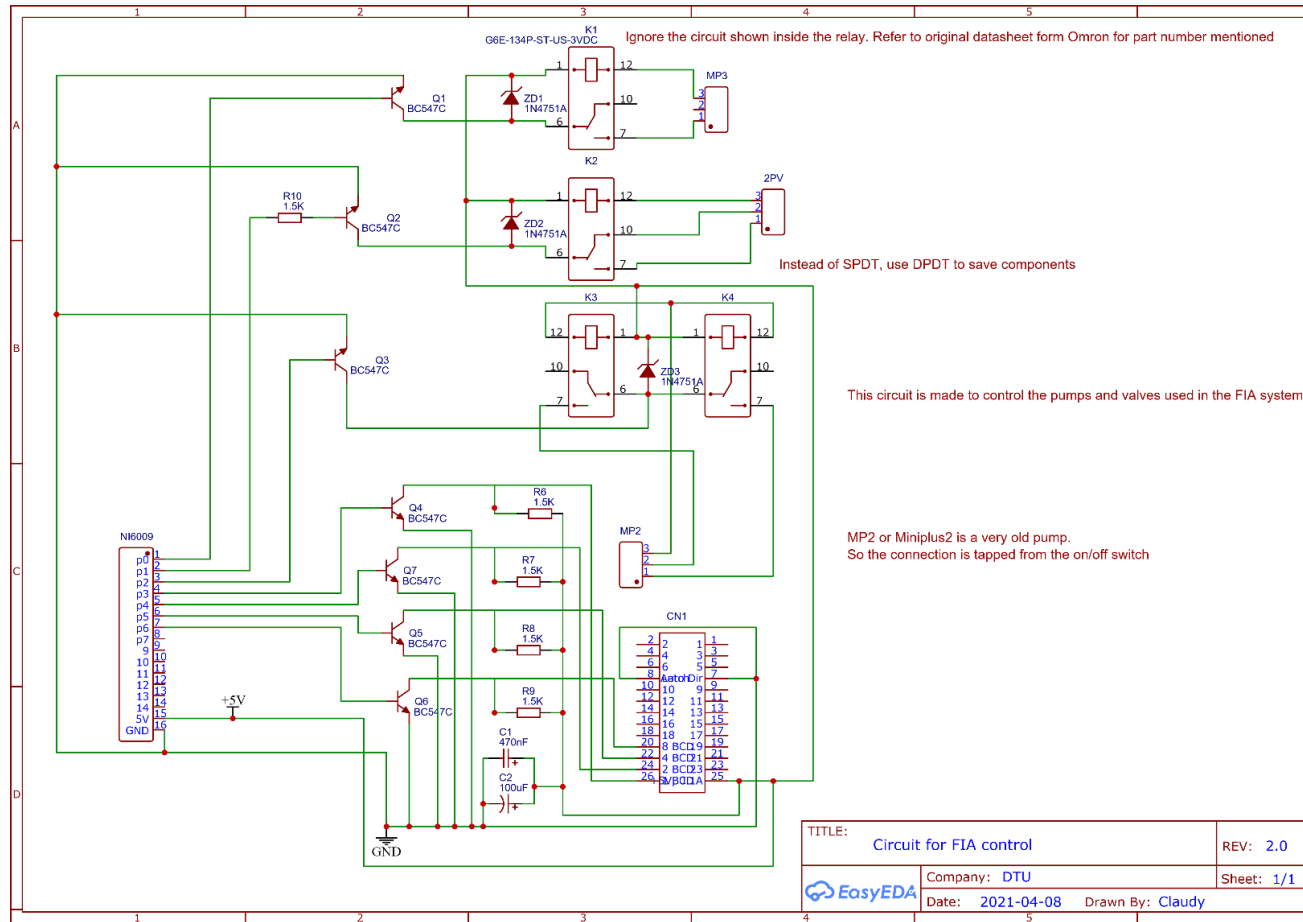


Figure 8.8- Circuit diagram for the control board.

The presented control system only controls the FIA system and not the electrochemical detection. Therefore, the control system and potentiostat had to be synchronised. The easiest way was to determine the time for one entire assay and write a small script in the potentiostat software PStace 5.8 to initialise the measurement at the specified time as shown in Figure 8.9.

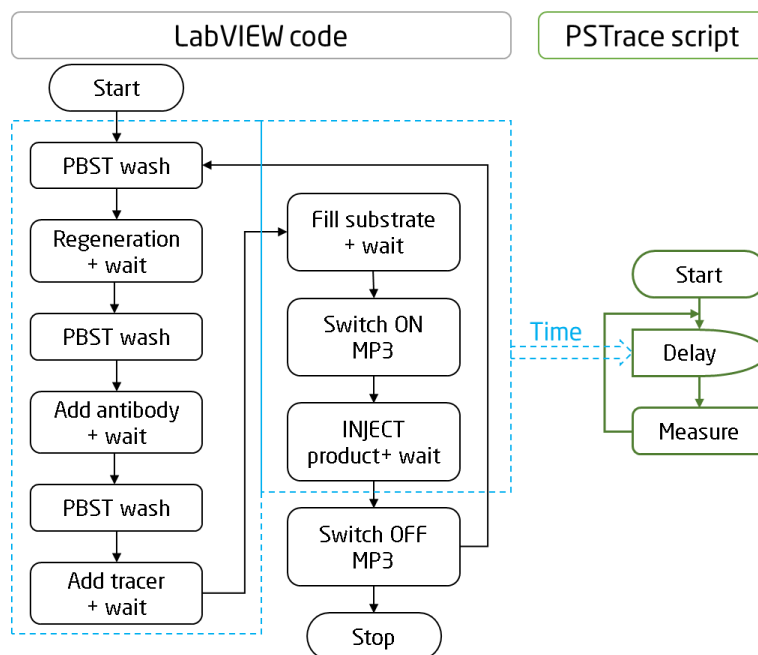


Figure 8.9- Flowchart for the entire assay and the potentiostat measurement. The time required for one assay is fed into the PStace script.

However, the PalmSens4 potentiostat provides an auxiliary port (DB15) with voltage, current and four digital output lines. Through this auxiliary port, the output of PalmSens4 can be connected with the NI6009, thus enabling measurement synchronisation and data acquisition from the potentiostat. The data from the potentiostat can, therefore, be accessed via the auxiliary port and fed into the primary process control system. Moreover, the LabVIEW software can function as the process controller, making the integration of the cortisol measurement signal easier.

Figure 8.10 shows the actual automated FIA system.

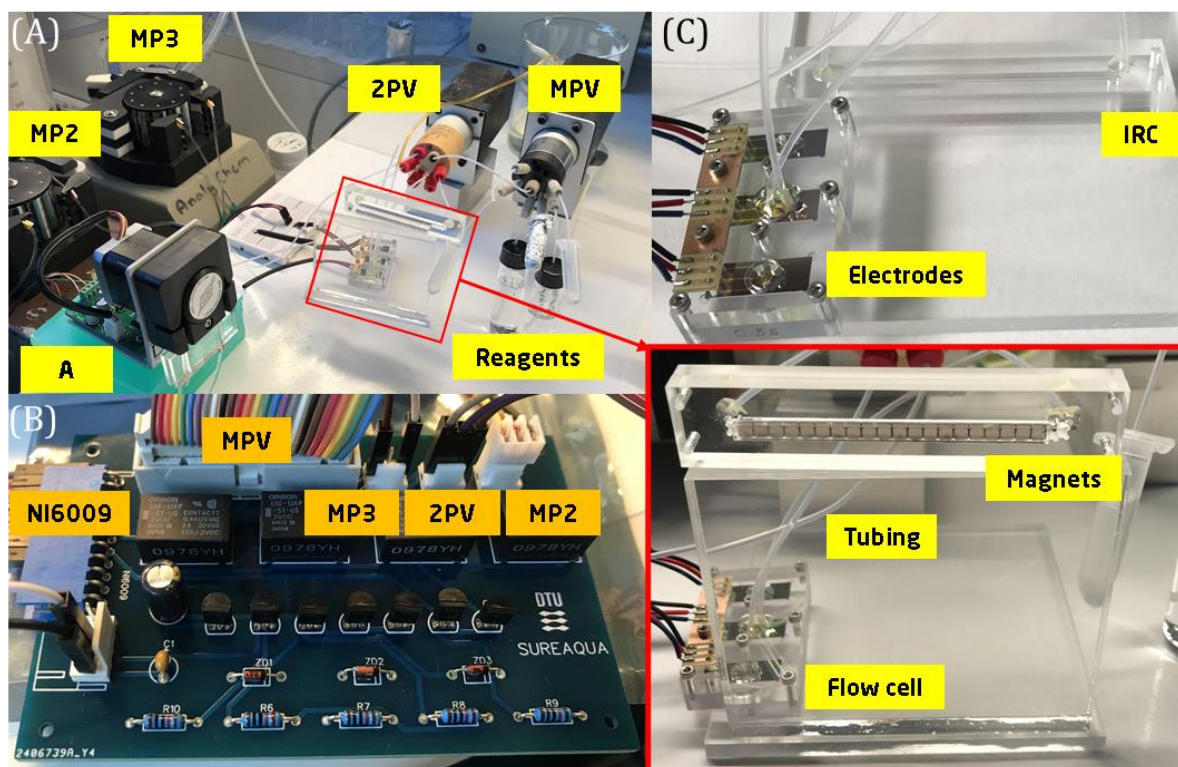


Figure 8.10- Photographs of the actual setup. (A) Shows the various pumps and valves used. (B) The circuit board with all the connections made (C) Close up of the IRC and detector electrode inside the flow cell

### 8.3 Process flow algorithm

The algorithm followed to operate the FIA is given below. Figure 6.1 to be referred for the numbering of components.

1. Set the time in PalmSens4 script and LabVIEW to synchronise the product injection with amperometric detection. Set the number of repetitions.
2. Set MPV (10) to No-6 for PBST, Switch on pump MP2 (2), Run for 90 s [WASH STEP]
3. Set MPV (10) to No-8 for Gly/HCl regeneration buffer, Switch on pump MP2 (2), Run for 200 s

4. Switch off pump MP2 (2), Wait for 100 s
5. [WASH STEP]
6. Set MPV (10) to No-9 for Antibody, Switch on pump MP2 (2), Run for 30 s
7. Set MPV (10) to No-6 for PBST, Switch on pump MP2 (2), Run for 35 s [This pushes a plug of antibody into the IRC chamber, thereby reducing the amount of antibody used]
8. Switch off pump MP2 (2), Wait for 180 s
9. [WASH STEP]
10. Set MPV (10) to No-4 for HRP tracer, Switch on pump MP2 (2), Run for 30 s
11. Set MPV (10) to No-6 for PBST, Switch on pump MP2 (2), Run for 35 s [This pushes a plug of tracer into the IRC chamber, thereby reducing the amount of tracer used].
12. Switch off pump MP2 (2), Wait for 180 s
13. [WASH STEP]
14. Set MPV (10) to No-7 for Substrate, Switch on pump MP2 (2), Run for 75 s
15. Switch off pump MP2 (2), Wait for 350 s
16. Switch on pump MP3 (1), Wait for 50 s [\*The PalmSens4 starts amperometry]
17. Switch 2PV (9) to INJECT position. (substrate gets injected and amperometry recorded).
18. Switch off pump MP2 (2), Switch 2PV to FILL position.
19. Wait for 10s
20. Switch off MP3 (1)



21. Repeat if set.

During the calibration run, the sample with the spiked analyte is mixed with HRP-tracer and introduced at Step.10. In ISLM extraction, before Step 10, a third pump (3) is switched on for a predetermined time to allow the analyte to cross the membrane.

The most critical parameter to be optimised was the flow rate of MP2 and MP3. MP2 carried out the entire assay, whereas MP3 was pumping the carrier buffer during the amperometry stage. The flow rate for MP2 was initially set to 600  $\mu\text{L}/\text{min}$ , which disrupted the immobilised layer inside the IRC. The flow rate was later reduced to 150. The flow rate of MP3 was set at 600  $\mu\text{L}/\text{min}$ . Although a high flow rate for IRC, it is subjected to this flow only for 50 s (Step 16). A stable one compound commercial substrate and the addition of 1% DMSO into the regeneration buffer significantly improved the overall performance of the assay.

Observe that the magnetic beads must be manually loaded and washed before the assay starts. In brief, MPV No-2 port is used to load 10  $\mu\text{l}$  of Protein-G magnetic beads mixed with cortisol antibody into the IRC. The magnet is introduced once the plug fills the IRC completely.

In conclusion, I have in my thesis developed a control system that can be used to control a FIA system and be easily reconfigured. The system can be scaled up by adding extra relay circuit boards limited only by the available digital output ports (12 in our case).

The plan is to publish the work developed in Chapter 8 as a paper in Sensors and Actuators B: Chemical.

## Chapter 9 Conclusion and prospects

*Made weak by time and fate, but strong in will*

*To strive, to seek, to find, and not to yield.*

*- Ulysses. Lord Alfred Tennyson*

---

### 9.1 Conclusion

The hypothesis was that developing a system capable of non-intrusive continuous **monitoring of cortisol by sampling water from the fish tank instead of sampling fish's blood** can provide data for a better aquafarm control system, thereby improving the **fish's welfare, farm productivity**, and overall sustainability.

Cortisol, an indicator of stress, was chosen as the apt analyte to assess the welfare situation of the fish. Since fish release cortisol into the water via the gills during a stressful encounter, water from the fish tank had to be discreetly sampled to detect cortisol non-invasively. The large body of water diluted the cortisol released, so the cortisol levels to be detected were in the pM range. The developed system also had to be fully automated to be incorporated into the existing control system of an aquafarm. All the components were also to be fabricated using industrial manufacturing techniques. To accomplish all this, the project was divided into the following tasks.

1. Development and testing of an apt immuno-sensing format to measure cortisol at pM levels
2. Design and fabricate electrodes for electrochemical detection of the formed substrate product from the immunoassay.

3. Fabrication of polymer parts for handling fluid, provide mechanical support for the immunoassay and testing of electrodes and implement industrial manufacturing techniques for ways of scaling up the production of the said polymer parts.
4. Implementation of a FIA system for automation of the entire assay.

The 1<sup>st</sup> task was straightforward and required the selection of a suitable format from the various immunoassay methods discussed in Chapter 4. The competitive format using a labelled antigen and immobilised antibody was chosen after testing other formats like label-free assay with impedance spectroscopy and competitive assay with a labelled antibody and a cortisol hapten BSA conjugate as the immobilised layer. The assays were performed on ELISA plates and on gold layers and magnetic particles inside an IRC.

The 2<sup>nd</sup> task involved the fabrication of various electrodes to perform the experiments as decided in the 1<sup>st</sup> task. Many different electrode configurations were tested and finally a three-electrode configuration was chosen, having a circular gold WE. Electrodes were tested in batch, thin-film, and wall-jet electrochemical cells, finally choosing the wall-jet format for downstream amperometric detection. Half of Chapter 6 covers these aspects.

The 3<sup>rd</sup> task was to fabricate all the test setups, flow cells, and IRCs to cater to the described 1<sup>st</sup> and 2<sup>nd</sup> tasks. The subtask was to ensure that the fabrication techniques were scalable and easily adaptable for industrial manufacturing. Hence, cleanroom fabrication, injection moulding, and thermal bonding techniques were used.

The 4<sup>th</sup> task dealt with the development of the complete FIA system along with the immunoassay. The subtask was to automate the entire process.

Although not mentioned as a task, testing actual samples, and using the system in **'real world'** forms an essential part of the assay development.

The tasks mentioned were not performed in series but rather a very complex parallel processing was involved. The electrode fabrication and immunoassay development had to go hand in hand. The actual sample collection had to be planned according to the availability of the required model RAS setup at DTU Aqua, situated 500 km away from our department. So, there was no way the system could be checked at the different developmental stages. When it came to building the automated system, there was the need to maintain a semi-automated system to run day to day experiments for the assay development and at the same time develop the components for complete automation. Dummy test setups and light emitting diodes (LEDs) were used for the initial test runs of the automation unit. There were times when it was impossible to determine the source of assay instability as both the assay and the FIA were being developed together. An example was the negative trend observed when the assay was being performed in the flow system. The reasons for the observed drift ranges from antigen-antibody instability, poor regeneration buffer performance, flow rate, nonspecific adsorption, effect from the unstable substrate, improper immobilisation of protein-G, degradation of the gold layer in the IRC, external lighting condition, improper range selection of the potentiostat, circuit error and so on. However, it was finally zeroed in on the flow velocity and substrate stability. There were numerous such challenges which were all systematically solved<sup>7</sup>.

All four tasks were completed successfully, and actual samples were tested. Promising results indicate proper system development. For the first time a system that can provide information on the welfare state of the fish or indicate the presence of a stressor in the environment non-invasively and automatically has been materialised.

---

<sup>7</sup> As Jenny puts it, one parameter at a time.

## 9.2 Challenges addressed

The biggest challenge was to build a system capable of detecting pM levels of cortisol non-invasively from a fish tank. Building a robust IRC, executing a stable immunoassay, acquiring repeatable measurements, and automating the system ensured that the challenge were resolved.

To build a robust IRC, the fabrication process was optimised such that there were no leaks or loose fittings, and UV assisted thermal bonding gave further ruggedness to the IRC. To achieve stability for the immunoassay, various immunoassay formats and reagent combinations were tried out. The electrode design, antigen-antibody pair, the substrate, and the immobilisations strategies were all carefully designed and chosen to ensure maximum stability. The entire fluidic system was made robust to ensure repeatable measurements, and the assay integrity was ensured by separating the IRC and opting for downstream detector instead of *in situ* detection. The fluidic circuit was kept as short as practically possible to ensure minimum dispersion. Automation of the FIA system was inevitable, considering the final application at an aquafarm. Moreover, the automation was executed so that the system could be configured differently, and provisions are included for scalability in case more components needs to be added. The choice of an electrochemical sensor that gave a direct electrical signal as output simplifies further signal manipulation.

## 9.3 Challenges not addressed

Two challenges were left unaddressed. The 1<sup>st</sup> was the inability to injection mould larger and thicker polymer substrate due to the prohibitive cost involved in making a new mould design. A larger injection moulded substrate would mean that, the electrode and IRC could be realised on the same substrate. Although there were attempts to establish a collaboration, it was not fruitful. Time, as usual was another factor that limited in investing more time into the injection moulding process.

The 2<sup>nd</sup> challenge that was left unaddressed was the miniaturisation of the FIA system into a portable unit whilst preserving all the essential properties like the robust valves and connectors. Smaller stepper motor-controlled pumps were procured but it could not be integrated into the system on time. Here, the LabVIEW script could be replaced by a more dedicated microcontroller like PIC or Atmel Atmega and operated via battery supply.

## 9.4 Recommendations for Future Work

The possibilities are limitless, however, what I consider as the most important aspects are discussed below.

The priority would be to field test the system. The system will have to be made more compact for this purpose. Testing an instrument in the field is crucial to gather all the uncertainties that would emerge only at the field setting, especially the variation in temperature and humidity.

The next step in automation would be to incorporate a potentiostat circuit into the automation unit such that the external PalmSens4 potentiostat could be removed. Since amperometry is performed and the biasing voltage is known, a circuit dedicated solely for amperometric detection would suffice. Thereby LabVIEW itself could be used to procure, analyses, store, display and transmit the signal. Also, the NI6009 interface can address up to 12 bits translating to a maximum 9 components, since MPV take up 4 bits and the rest one bit each. So additional pumps and valves could be incorporated and kept ready for future use. Going further, if a different DAQ unit is used, it can provide even more digital and analogue input/out ports and contain built in timer and counter. Such a system also opens the possibility of incorporating more sensors like temperature, pressure, pH, salinity, dissolved oxygen, and turbidity sensor.

Another improvement would be to add an electromagnet to control the assay with magnetic beads. So that the beads can be loaded and removed automatically.

Priority needs to be given for extensive collaboration to bring in expertise from all the relevant fields to avoid reinventing the wheel.

For the benefit of all stakeholders involved, data from existing farms needs to be analysed for identifying problematic trends and employ machine learning to predict a possible stress event so that the control system can avert it by taking necessary corrective action. Eliminating the stressor before it occurs, a sort of early warning system for the aquafarm.

## References

- [1] FAO, The State of World Fisheries and Aquaculture 2018 - Meeting the sustainable development goals, Rome, 2018.
- [2] FAO, The State of World Fisheries and Aquaculture 2020. Sustainability in action., Rome, 2020. <https://doi.org/https://doi.org/10.4060/ca9229en>.
- [3] R.L. Naylor, R.J. Goldburg, J. Clay, M. Troell, H. Mooney, J.H. Primavera, C. Folke, M.C.M. Beveridge, N. Kautsky, J. Lubchenco, Effect of aquaculture on world fish supplies, *Nature*. 405 (2002) 1017-1024.
- [4] D. Pauly, V. Christensen, S. Gu enette, T.J. Pitcher, U.R. Sumaila, C.J. Walters, R. Watson, D. Zeller, Towards sustainability in world fisheries, *Nature*. 418 (2002) 689-695. <https://doi.org/10.1038/nature01017>.
- [5] J.H. Tidwell, *Aquaculture Production Systems*, Wiley-Blackwell, Oxford, UK, 2012. <https://doi.org/10.1002/9781118250105>.
- [6] A. Saeki, Studies on Fish Culture in the Aquarium of Closed-circhlating System. Its fundamental theory and standard plan, *Nippon Suisan Gakkaishi*. 23 (1958) 684-695. <https://doi.org/10.2331/suisan.23.684>.
- [7] K. Hirayama, Water control by filtration in closed culture systems, *Aquaculture*. 4 (1974) 369-385. [https://doi.org/10.1016/0044-8486\(74\)90066-0](https://doi.org/10.1016/0044-8486(74)90066-0).
- [8] P.B. Liao, R.D. Mayo, Salmonid hatchery water reuse systems, *Aquaculture*. 1 (1972) 317-335. [https://doi.org/10.1016/0044-8486\(72\)90033-6](https://doi.org/10.1016/0044-8486(72)90033-6).
- [9] H. Rosenthal, Recirculation systems in western Europe, in: *World Symp. Aquac.*



- Heated Effluents Recirc. Syst. Stavanger, Inst. Für Kuesten-Und Binnefischerei, Bundesforschungsanstalt Hamburg, BRD, 1980.
- [10] M. Badiola, D. Mendiola, J. Bostock, Recirculating Aquaculture Systems (RAS) analysis: Main issues on management and future challenges, *Aquac. Eng.* 51 (2012) 26-35. <https://doi.org/10.1016/j.aquaeng.2012.07.004>.
- [11] V.C. Mota, P. Limbu, C.I.M. Martins, E.H. Eding, J.A.J. Verreth, The effect of nearly closed RAS on the feed intake and growth of Nile tilapia (*Oreochromis niloticus*), African catfish (*Clarias gariepinus*) and European eel (*Anguilla anguilla*), *Aquac. Eng.* 68 (2015) 1-5. <https://doi.org/10.1016/j.aquaeng.2015.06.002>.
- [12] A.J.T. Dalsgaard, Book of Abstracts Workshop on Recirculating Aquaculture Systems Helsinki , October 5-6 , 2011, Helsinki, 2011.
- [13] C.I.M. Martins, E.H. Eding, M.C.J. Verdegem, L.T.N. Heinsbroek, O. Schneider, J.P. **Blancheton, E.R. d'Orbcastel, J.A.J. Verreth, New developments in recirculating aquaculture systems in Europe: A perspective on environmental sustainability**, *Aquac. Eng.* 43 (2010) 83-93. <https://doi.org/10.1016/j.aquaeng.2010.09.002>.
- [14] M. Badiola, O.C. Basurko, R. Piedrahita, P. Hundley, D. Mendiola, Energy use in Recirculating Aquaculture Systems (RAS): A review, *Aquac. Eng.* 81 (2018) 57-70. <https://doi.org/10.1016/j.aquaeng.2018.03.003>.
- [15] T. Lasner, A. Brinker, R. Nielsen, F. Rad, Establishing a benchmarking for fish farming - Profitability, productivity and energy efficiency of German, Danish and Turkish rainbow trout grow-out systems, *Aquac. Res.* 48 (2017) 3134-3148. <https://doi.org/10.1111/are.13144>.
- [16] P.G. Lee, Process control and artificial intelligence software for aquaculture, *Aquac. Eng.* 23 (2000) 13-36. [https://doi.org/10.1016/S0144-8609\(00\)00044-3](https://doi.org/10.1016/S0144-8609(00)00044-3).

- 
- [17] J.B. Hoy, Temperature Control and Temperature Recording in an Receptacle, (1985) 105-109.
- [18] E. Hansen, Computer Aided Control and Monitoring of Aquaculture Plants, IFAC Proc. Vol. 20 (1987) 187-192. [https://doi.org/10.1016/s1474-6670\(17\)59177-6](https://doi.org/10.1016/s1474-6670(17)59177-6).
- [19] P.G. Lee, A review of automated control systems for aquaculture and design criteria for their implementation, Aquac. Eng. 14 (1995) 205-227. [https://doi.org/10.1016/0144-8609\(94\)00002-I](https://doi.org/10.1016/0144-8609(94)00002-I).
- [20] **B.G. Liptak, Instrument engineers' handbook, volume two: Process control and optimization**, CRC press, 2018.
- [21] J. Bentham, reprint 1982 An Introduction to the Principles of Morals and Legislation, (1789). <http://www.earlymoderntexts.com/assets/pdfs/bentham1780.pdf>.
- [22] E.J. Branson, Fish Welfare, 2008. <https://doi.org/10.1002/9780470697610>.
- [23] K. Buchanan, B. de Perera, C. T, C. C, H. T, H. A, J. R, M. D, P. N, P. T, S. F, S. L, T. C, Guidelines for the treatment of animals in behavioural research and teaching, Anim. Behav. 83 (2012) 301-309. <https://doi.org/10.1016/j.anbehav.2011.10.031>.
- [24] FAWC, The five freedoms, London, 1992. <http://webarchive.nationalarchives.gov.uk/20121010012427/http://www.fawc.org.uk/freedoms.htm>.
- [25] F.A. Huntingford, C. Adams, V.A. Braithwaite, S. Kadri, T.G. Pottinger, P. Sandøe, J.F. Turnbull, Current issues in fish welfare, J. Fish Biol. 68 (2006) 332-372. <https://doi.org/10.1111/j.0022-1112.2006.001046.x>.
- [26] J.M. Weiss, Psychological factors in stress and disease, Sci. Am. 226 (1972) 104-

- 113.
- [27] S. Calabrese, T.O. Nilsen, J. Kolarevic, L.O.E. Ebbesson, C. Pedrosa, S. Fivelstad, C. Hosfeld, S.O. Stefansson, B.F. Terjesen, H. Takle, C.I.M. Martins, H. Sveier, F. Mathisen, A.K. Imsland, S.O. Handeland, Stocking density limits for post-smolt Atlantic salmon (*Salmo salar* L.) emphasis on production performance and welfare, *Aquaculture*. 468 (2017) 363-370. <https://doi.org/10.1016/j.aquaculture.2016.10.041>.
- [28] J.D. Rose, The Neurobehavioral Nature of Fishes and the Question of Awareness and Pain, *Rev. Fish. Sci.* 10 (2002) 1-38. <https://doi.org/10.1080/20026491051668>.
- [29] H. Selye, Stress and the General Adaptation Syndrome, *BMJ*. 1 (1950) 1383-1392. <https://doi.org/10.1136/bmj.1.4667.1383>.
- [30] A.D. Pickering, *Stress and fish*, Academic Press, London/New York, 1981.
- [31] F. Huntingford, M. Jobling, S. Kadri, *Aquaculture and behavior*, John Wiley & Sons, 2011.
- [32] A. Munck, P.M. Guyre, N.J. Holbrook, Physiological Functions of Glucocorticoids in Stress and Their Relation to Pharmacological Actions\*, *Endocr. Rev.* 5 (1984) 25-44. <https://doi.org/10.1210/edrv-5-1-25>.
- [33] J.W. Mason, A re-evaluation of the concept of 'non-specificity' in stress theory, *J. Psychiatr. Res.* 8 (1971) 323-333. [https://doi.org/10.1016/0022-3956\(71\)90028-8](https://doi.org/10.1016/0022-3956(71)90028-8).
- [34] D.H. Evans, J.B. Claiborne, *The Physiology of Fishes*, 3rd ed., CRC Press, Boca Raton, 2006.
- [35] P.K. Bondy, G.V. Upton, G.E. Pickford, Demonstration of cortisol in fish blood, *Nature*. 179 (1957) 1354-1355. <https://doi.org/10.1038/1791354a0>.

- 
- [36] A.D. Pickering, T.G. Pottinger, Stress responses and disease resistance in salmonid fish : Effects of chronic elevation of plasma cortisol, *Fish Physiol. Biochem.* 7 (1989) 253-258. <https://doi.org/10.1007/BF00004714>.
- [37] K.A. Lockridge, *Fish Stress and Health in Aquaculture*, Cambridge University Press, 1981.
- [38] T. Ellis, B. North, A.P. Scott, N.R. Bromage, M. Porter, D. Gadd, The relationships between stocking density and welfare in farmed rainbow trout, *J. Fish Biol.* 61 (2002) 493-531. <https://doi.org/10.1006/jfbi.2002.2057>.
- [39] B. Barton, C. Schreck, L. Barton, Effects of chronic Cortisol administration and daily acute stress on growth, physiological conditions, and stress responses in juvenile rainbow trout, *Dis. Aquat. Organ.* 2 (1987) 173-185. <https://doi.org/10.3354/dao002173>.
- [40] P.J. Ashley, Fish welfare: Current issues in aquaculture, *Appl. Anim. Behav. Sci.* 104 (2007) 199-235. <https://doi.org/10.1016/j.applanim.2006.09.001>.
- [41] T.P. Mommsen, M.M. Vijayan, T.W. Moon, Cortisol in teleosts: dynamics, mechanisms of action, and metabolic regulation, *Rev. Fish Biol. Fish.* 9 (1999) 211-268.
- [42] L.M. Romero, J.M. Reed, Collecting baseline corticosterone samples in the field: is under 3 min good enough?, *Comp. Biochem. Physiol. Part A Mol. Integr. Physiol.* 140 (2005) 73-79.
- [43] **N.M. Sopinka, M.R. Donaldson, C.M. O'Connor, C.D. Suski, S.J. Cooke, Stress Indicators in Fish**, Elsevier Inc., 2016. <https://doi.org/10.1016/B978-0-12-802728-8.00011-4>.
- [44] L.J.G. Barcellos, L.C. Kreutz, G. Koakoski, T.A. Oliveira, J.G.S. da Rosa, M. Fagundes, Fish age, instead of weight and size, as a determining factor for time course differences in cortisol response to stress, *Physiol. Behav.* 107 (2012) 397-400.

- <https://doi.org/10.1016/j.physbeh.2012.09.008>.
- [45] A.D. Pickering, T. Pottinger, Seasonal and diel changes in plasma cortisol levels of the brown trout, *Salmo trutta* L, *Gen. Comp. Endocrinol.* 49 (1983) 232-239.
- [46] J.H. Van Weerd, J. Komen, The effects of chronic stress on growth in fish: A critical appraisal, *Comp. Biochem. Physiol. - A Mol. Integr. Physiol.* 120 (1998) 107-112. [https://doi.org/10.1016/S1095-6433\(98\)10017-X](https://doi.org/10.1016/S1095-6433(98)10017-X).
- [47] T.R. Gregory, C.M. Wood, The Effects of Chronic Plasma Cortisol Elevation on the Feeding Behaviour, Growth, Competitive Ability, and Swimming Performance of Juvenile Rainbow Trout, *Physiol. Biochem. Zool.* 72 (1999) 286-295. <https://doi.org/10.1086/316673>.
- [48] T. Ellis, H.Y. Yildiz, J. López-Olmeda, M.T. Spedicato, L. Tort, Ø. Øverli, C.I.M. Martins, Cortisol and finfish welfare, *Fish Physiol. Biochem.* 38 (2012) 163-188. <https://doi.org/10.1007/s10695-011-9568-y>.
- [49] N.J. Galt, S.D. McCormick, J.M. Froehlich, P.R. Biga, A comparative examination of cortisol effects on muscle myostatin and HSP90 gene expression in salmonids, *Gen. Comp. Endocrinol.* 237 (2016) 19-26. <https://doi.org/10.1016/j.ygcen.2016.07.019>.
- [50] G.B. Skomal, J.W. Mandelman, The physiological response to anthropogenic stressors in marine elasmobranch fishes: A review with a focus on the secondary response, *Comp. Biochem. Physiol. - A Mol. Integr. Physiol.* 162 (2012) 146-155. <https://doi.org/10.1016/j.cbpa.2011.10.002>.
- [51] A.D. Pickering, T.G. Pottinger, P. Christie, Recovery of the brown trout, *Salmo trutta* L., from acute handling stress: a time-course study, *J. Fish Biol.* 20 (1982) 229-244.
- [52] T. Ellis, J.D. James, C. Stewart, A.P. Scott, A non-invasive stress assay based upon measurement of free cortisol released into the water by rainbow trout, J.

- Fish Biol. 65 (2004) 1233-1252. <https://doi.org/10.1111/j.1095-8649.2004.00499.x>.
- [53] A.P. Scott, M. Pinillos, T. Ellis, Why measure steroids in fish plasma when you can measure them in water?, *Perspect. Comp. Endocrinol. Unity Divers. Proc. 14th Int. Congr. Comp. Endocrinol.* (2001) 1291-1295. <https://www.cefas.co.uk/publications/files/3402.pdf>.
- [54] T. Ellis, J.D. James, A.P. Scott, Branchial release of free cortisol and melatonin by rainbow trout, *J. Fish Biol.* 67 (2005) 535-540.
- [55] R. Earley, T. Ellis, K. Hirschenhauser, A. Scott, R. Oliveira, A. Canario, P. Hubbard, N. Bender, M. Huertas, M. Pavlidis, M. Sebire, Non-invasive measurement of steroids in fish-holding water: important considerations when applying the procedure to behaviour studies, *Behaviour.* 145 (2008) 1307-1328. <https://doi.org/10.1163/156853908785765854>.
- [56] T. Ellis, J.D. James, H. Sundh, F. Fridell, K. Sundell, A.P. Scott, Non-invasive measurement of cortisol and melatonin in tanks stocked with seawater Atlantic salmon, *Aquaculture.* 272 (2007) 698-706. <https://doi.org/10.1016/j.aquaculture.2007.07.219>.
- [57] T. Ellis, M.B. Sanders, A.P. Scott, Non-invasive monitoring of steroids in fishes, *Wien. Tierarztl. Monatsschr.* 100 (2013) 255-269. <https://doi.org/urn:nbn:nl:ui:11-dbi/52820484b78fe>.
- [58] B. Sadoul, B. Geffroy, Measuring cortisol, the major stress hormone in fishes, *J. Fish Biol.* 94 (2019) 540-555. <https://doi.org/10.1111/jfb.13904>.
- [59] O. Parlak, Portable and wearable real-time stress monitoring: A critical review, *Sensors and Actuators Reports.* 3 (2021) 100036. <https://doi.org/10.1016/j.snr.2021.100036>.
- [60] M. Zea, F.G. Bellagambi, H. Ben Halima, N. Zine, N. Jaffrezic-Renault, R. Villa, G.

- Gabriel, A. Errachid, Electrochemical sensors for cortisol detections: Almost there, *TrAC - Trends Anal. Chem.* 132 (2020) 116058.  
<https://doi.org/10.1016/j.trac.2020.116058>.
- [61] M. Sekar, R. Sriramprabha, P.K. Sekhar, S. Bhansali, N. Ponpandian, M. Pandiaraj, C. Viswanathan, Review—Towards Wearable Sensor Platforms for the Electrochemical Detection of Cortisol, *J. Electrochem. Soc.* 167 (2020) 067508.  
<https://doi.org/10.1149/1945-7111/ab7e24>.
- [62] A. Kaushik, A. Vasudev, S.K. Arya, S.K. Pasha, S. Bhansali, Recent advances in cortisol sensing technologies for point-of-care application, *Biosens. Bioelectron.* 53 (2014) 499-512. <https://doi.org/10.1016/j.bios.2013.09.060>.
- [63] A. Boolani, D. Channaveerappa, E.J. Dupree, M. Jayathirtha, R. Aslebagh, S. Grobe, T. Wilkinson, C.C. Darie, Trends in analysis of cortisol and its derivatives, *Adv. Exp. Med. Biol.* 1140 (2019) 649-664. [https://doi.org/10.1007/978-3-030-15950-4\\_39](https://doi.org/10.1007/978-3-030-15950-4_39).
- [64] B. Hock, Antibodies for immunosensors. A review, *Anal. Chim. Acta.* 347 (1997) 177-186. [https://doi.org/10.1016/S0003-2670\(97\)00167-0](https://doi.org/10.1016/S0003-2670(97)00167-0).
- [65] S.A. Berson, R.S. Yalow, A. Bauman, M.A. Rothschild, K. Newerly, Insulin-I 131 metabolism in human subjects: demonstration of insulin binding globulin in the circulation of insulin treated subjects, *J. Clin. Invest.* 35 (1956) 170-190.
- [66] R.S. Yalow, S.A. Berson, Assay of plasma insulin in human subjects by immunological methods, *Nature.* 184 (1959) 1648-1649.
- [67] R.S. Yalow, S.A. Berson, Immunoassay of endogenous plasma insulin in man, *J. Clin. Invest.* 39 (1960) 1157-1175.
- [68] G. Köhler, C. Milstein, Continuous cultures of fused cells secreting antibody of predefined specificity, *Nature.* 256 (1975) 495-497.

- 
- [69] J. Janata, Immuno-electrode, *J. Am. Chem. Soc.* 97 (1975) 2914-2916.
- [70] L.J. Harris, E. Skaletsky, A. McPherson, Crystallographic structure of an intact IgG1 monoclonal antibody, *J. Mol. Biol.* 275 (1998) 861-872.
- [71] E. Delavenay, IMMUNOLOGICAL SPECULATIONS I By, (1960).
- [72] J. Janata, Principles of chemical sensors, Springer Science & Business Media, 2010.
- [73] C.P. Price, D.J. Newman, Principles and practice of immunoassay, Springer, 1991.
- [74] J.P. Gosling, A decade of development in immunoassay methodology, *Clin. Chem.* 36 (1990) 1408-1427.
- [75] C. Nistor, J. Emneus, Immunoassay : potentials and limitations, in: G. L (Ed.), *Compr. Anal. Chem.* XLIV, 2005: pp. 375-427.
- [76] **W.G. Wood, "Matrix effects" in immunoassays, *Scand. J. Clin. Lab. Invest.* 51 (1991) 105-112.**
- [77] D.W. Chan, General principle of immunoassay, in: *Immunoass. a Pract. Guid.*, Academic Press Orlando, Fla, 1987: pp. 1-23.
- [78] A. Kausaite-Minkstimiene, A. Ramanaviciene, J. Kirlyte, A. Ramanavicius, Comparative study of random and oriented antibody immobilization techniques on the binding capacity of immunosensor, *Anal. Chem.* 82 (2010) 6401-6408. <https://doi.org/10.1021/ac100468k>.
- [79] I. Hafaiedh, H. Chammem, A. Abdelghani, E. Ait, L. Feldman, O. Meilhac, L. Mora, Supported protein G on gold electrode: Characterization and immunosensor application, *Talanta.* 116 (2013) 84-90. <https://doi.org/10.1016/j.talanta.2013.04.059>.
- [80] M. Tudorache, A. Tencaliec, C. Bala, Magnetic beads-based immunoassay as a sensitive alternative for atrazine analysis, *Talanta.* 77 (2008) 839-843.



- <https://doi.org/10.1016/j.talanta.2008.07.040>.
- [81] J. Quinn, P. Patel, B. Fitzpatrick, B. Manning, P. Dillon, S. Daly, R. O’Kennedy, M. Alcocer, H. Lee, M. Morgan, K. Lang, The use of regenerable, affinity ligand-based surfaces for immunosensor applications, *Biosens. Bioelectron.* 14 (1999) 587-595. [https://doi.org/10.1016/S0956-5663\(99\)00032-9](https://doi.org/10.1016/S0956-5663(99)00032-9).
- [82] S.K. Arya, P.R. Solanki, M. Datta, B.D. Malhotra, Recent advances in self-assembled monolayers based biomolecular electronic devices, *Biosens. Bioelectron.* 24 (2009) 2810-2817. <https://doi.org/10.1016/j.bios.2009.02.008>.
- [83] L.W. Bruch, Theory of physisorption interactions, *Surf. Sci.* 125 (1983) 194-217. [https://doi.org/10.1016/0039-6028\(83\)90453-3](https://doi.org/10.1016/0039-6028(83)90453-3).
- [84] K. Huse, H.J. Böhme, G.H. Scholz, Purification of antibodies by affinity chromatography, *J. Biochem. Biophys. Methods.* 51 (2002) 217-231. [https://doi.org/10.1016/S0165-022X\(02\)00017-9](https://doi.org/10.1016/S0165-022X(02)00017-9).
- [85] P. Nygren, M. Eliasson, L. Abrahamssén, M. Uhlén, E. Palmcrantz, Analysis and use of the serum albumin binding domains of streptococcal protein G, *J. Mol. Recognit.* 1 (1988) 69-74. <https://doi.org/10.1002/jmr.300010204>.
- [86] C.R. Goward, L.I. Irons, J.P. Murphy, T. Atkinson, The secondary structure of **Protein G’, a robust molecule**, *Biochem. J.* 274 (1991) 503-507. <https://doi.org/10.1042/bj2740503>.
- [87] J.N. Vranish, M.G. Ancona, E. Oh, K. Susumu, I.L. Medintz, Enhancing coupled enzymatic activity by conjugating one enzyme to a nanoparticle, *Nanoscale.* 9 (2017) 5172-5187. <https://doi.org/10.1039/c7nr00200a>.
- [88] E. Engvall, Enzyme-linked immunosorbent assay (ELISA) quantitative assay of immunoglobulin G, *Mol. Immunol.* 8 (1971) 871-874. [https://doi.org/10.1016/0161-5890\(71\)90063-0](https://doi.org/10.1016/0161-5890(71)90063-0).

- 
- [89] J. Castillo, S. Gáspár, S. Leth, M. Niculescu, A. Mortari, I. Bontidean, V. Soukharev, S.A. Dorneanu, A.D. Ryabov, E. Csöregi, Biosensors for life quality - Design, development and applications, *Sensors Actuators, B Chem.* 102 (2004) 179-194. <https://doi.org/10.1016/j.snb.2004.04.084>.
- [90] X.M. Li, X.Y. Yang, S.S. Zhang, Electrochemical enzyme immunoassay using model labels, *TrAC - Trends Anal. Chem.* 27 (2008) 543-553. <https://doi.org/10.1016/j.trac.2008.04.002>.
- [91] J. Seth, L.M. Brown, A simple radioimmunoassay for plasma cortisol, *Clin. Chim. Acta.* 86 (1978) 109-120. [https://doi.org/10.1016/0009-8981\(78\)90465-5](https://doi.org/10.1016/0009-8981(78)90465-5).
- [92] A. Vermeulen, M. Van Der Straeten, N. Eeckman, Determination of Plasma Cortisol by a Fluorometric Method, *J. Clin. Endocrinol. Metab.* 24 (1964) 1188-1194. <https://doi.org/10.1210/jcem-24-11-1188>.
- [93] T. Ito, N. Aoki, S. Kaneko, K. Suzuki, Highly sensitive and rapid sequential cortisol detection using twin sensor QCM, *Anal. Methods.* 6 (2014) 7469-7474. <https://doi.org/10.1039/c4ay01387e>.
- [94] R.C. Stevens, S.D. Soelberg, S. Near, C.E. Furlong, Detection of Cortisol in Saliva with a Flow-Filtered, Portable Surface Plasmon Resonance Biosensor System, *Anal. Chem.* 80 (2008) 6747-6751. <https://doi.org/10.1021/ac800892h>.
- [95] H. Arakawa, M. Maeda, A. Tsuji, Chemiluminescence enzyme immunoassay of cortisol using peroxidase as label, *Anal. Biochem.* 97 (1979) 248-254. [https://doi.org/10.1016/0003-2697\(79\)90352-X](https://doi.org/10.1016/0003-2697(79)90352-X).
- [96] Y. Velasco-Santamaría, Pablo Cruz-Casallas, Methodology for Determination of Plasma Cortisol in Fish Using Competitive Enzyme-Linked Immunosorbent Assay ( Elisa ), *Rev.MVZ Cordoba.* 12 (2007) 869-877. [http://www.scielo.org.co/scielo.php?script=sci\\_arttext&pid=S0122-02682007000100002&lng=en&nrm=iso](http://www.scielo.org.co/scielo.php?script=sci_arttext&pid=S0122-02682007000100002&lng=en&nrm=iso).

- 
- [97] C.A. Caldwell, J.M. Hinshaw, H.G. Kattesh, Validation of a solid-phase enzyme immunoassay technique for the measure of plasma cortisol in rainbow trout, *J. Aquat. Anim. Health.* 2 (1990) 228-230. [https://doi.org/10.1577/1548-8667\(1990\)002<0228:CVOASP>2.3.CO;2](https://doi.org/10.1577/1548-8667(1990)002<0228:CVOASP>2.3.CO;2).
- [98] B. Akerstrom, L. Bjorck, A physicochemical study of protein G, a molecule with unique immunoglobulin G-binding properties, *J. Biol. Chem.* 261 (1986) 10240-10247. [https://doi.org/10.1016/s0021-9258\(18\)67515-5](https://doi.org/10.1016/s0021-9258(18)67515-5).
- [99] L. Björck, G. Kronvall, Purification and some properties of streptococcal protein G, a novel IgG-binding reagent., *J. Immunol.* 133 (1984) 969-74. <http://www.ncbi.nlm.nih.gov/pubmed/6234364>.
- [100] M.B. Young, B.K. Oh, W. Lee, H.L. Won, J.W. Choi, Study on orientation of immunoglobulin G on protein G layer, *Biosens. Bioelectron.* 21 (2005) 103-110. <https://doi.org/10.1016/j.bios.2004.09.003>.
- [101] R.G. Hudson, Confusion in Scientific Terminology, *Science* (80-. ). 65 (1927) 500-501.
- [102] B. Liedberg, C. Nylander, I. Lunström, Surface plasmon resonance for gas detection and biosensing, *Sensors and Actuators.* 4 (1983) 299-304. [https://doi.org/10.1016/0250-6874\(83\)85036-7](https://doi.org/10.1016/0250-6874(83)85036-7).
- [103] P. Damborský, J. Švitel, J. Katrlík, **Optical biosensors**, *Essays Biochem.* 60 (2016) 91-100. <https://doi.org/10.1042/EBC20150010>.
- [104] R.B.M. Schasfoort, *Handbook of surface plasmon resonance*, Royal Society of Chemistry, 2017.
- [105] G.H. Yao, R.P. Liang, C.F. Huang, Y. Wang, J.D. Qiu, Surface plasmon resonance sensor based on magnetic molecularly imprinted polymers amplification for pesticide recognition, *Anal. Chem.* 85 (2013) 11944-11951. <https://doi.org/10.1021/ac402848x>.

- 
- [106] Q. Wang, R. Liu, X. Yang, K. Wang, J. Zhu, L. He, Q. Li, Surface plasmon resonance biosensor for enzyme-free amplified microRNA detection based on gold nanoparticles and DNA supersandwich, *Sensors Actuators, B Chem.* 223 (2016) 613-620. <https://doi.org/10.1016/j.snb.2015.09.152>.
- [107] R. Liu, Q. Wang, Q. Li, X. Yang, K. Wang, W. Nie, Surface plasmon resonance biosensor for sensitive detection of microRNA and cancer cell using multiple signal amplification strategy, *Biosens. Bioelectron.* 87 (2017) 433-438. <https://doi.org/10.1016/j.bios.2016.08.090>.
- [108] Y. Sun, D. Song, Y. Bai, L. Wang, Y. Tian, H. Zhang, Improvement of surface plasmon resonance biosensor with magnetic beads via assembled polyelectrolyte layers, *Anal. Chim. Acta.* 624 (2008) 294-300. <https://doi.org/10.1016/j.aca.2008.06.042>.
- [109] G. Sauerbrey, Verwendung von Schwingquarzen zur Wägung dünner Schichten und zur Mikrowägung, *Zeitschrift Für Phys.* 155 (1959) 206-222. <https://doi.org/10.1007/BF01337937>.
- [110] A. Shons, F. Dorman, J. Najarian, An immunospecific microbalance, *J. Biomed. Mater. Res.* 6 (1972) 565-570. <https://doi.org/10.1002/jbm.820060608>.
- [111] R.C. Ebersole, M.D. Ward, Amplified mass immunosorbent assay with a quartz crystal microbalance, *J. Am. Chem. Soc.* 110 (1988) 8623-8628. <https://doi.org/10.1021/ja00234a008>.
- [112] K. Icoz, M.C. Soylu, Z. Canikara, E. Unal, Quartz-crystal Microbalance Measurements of CD19 Antibody Immobilization on Gold Surface and Capturing B Lymphoblast Cells: Effect of Surface Functionalization, *Electroanalysis.* 30 (2018) 834-841. <https://doi.org/10.1002/elan.201700789>.
- [113] N. Ly, Surface Plasmon Resonance vs. Quartz Crystal Microbalance/ Biosensing instrument technical Note, 2010. <https://biosensingusa.com/technical->

notes/technical-note-103-surface-plasmon-resonance-v-quartz-crystal-microbalance/.

- [114] S.K. Arya, G. Chornokur, M. Venugopal, S. Bhansali, Antibody functionalized **interdigitated  $\mu$ -electrode (ID $\mu$ E) based impedimetric cortisol biosensor**, *Analyst*. 135 (2010) 1941. <https://doi.org/10.1039/c0an00242a>.
- [115] D. Kinnamon, R. Ghanta, K.C. Lin, S. Muthukumar, S. Prasad, Portable biosensor for monitoring cortisol in low-volume perspired human sweat, *Sci. Rep.* 7 (2017) 1-13. <https://doi.org/10.1038/s41598-017-13684-7>.
- [116] B.A. Cardinell, M.L. Spano, J.T. La Belle, Toward a label-free electrochemical impedance immunosensor design for quantifying cortisol in tears, *Crit. Rev. Biomed. Eng.* 47 (2019) 207-215. <https://doi.org/10.1615/CritRevBiomedEng.2019026109>.
- [117] A. Kaushik, A. Yndart, R.D. Jayant, V. Sagar, V. Atluri, S. Bhansali, M. Nair, Electrochemical sensing method for point-of-care cortisol detection in human immunodeficiency virus-infected patients, *Int. J. Nanomedicine*. 10 (2015) 677-685. <https://doi.org/10.2147/IJN.S75514>.
- [118] P. Manickam, S.K. Pasha, S.A. Snipes, S. Bhansali, A Reusable Electrochemical Biosensor for Monitoring of Small Molecules (Cortisol) Using Molecularly Imprinted Polymers, *J. Electrochem. Soc.* 164 (2017) B54-B59. <https://doi.org/10.1149/2.0781702jes>.
- [119] R.D. Munje, S. Muthukumar, S. Prasad, Interfacial tuning for detection of cortisol in sweat using ZnO thin films for wearable biosensing, in: 2016 IEEE Nanotechnol. Mater. Devices Conf., IEEE, 2016: pp. 1-2. <https://doi.org/10.1109/NMDC.2016.7777154>.
- [120] H. Wu, H. Ohnuki, H. Ren, H. Endo, Carbon-nanotube-enhanced label-free immunosensor for highly sensitive detection of plasma cortisol level in fish,

- 
- Sensors Mater. 27 (2015) 793-803. <https://doi.org/10.18494/SAM.2015.11116>.
- [121] T. Muramatsu, H. Ohnuki, H. Ushio, K. Hibi, M. Igarashi, T. Hayashi, H. Ren, H. Endo, Electrochemical flow injection immunoassay for cortisol using magnetic microbeads, *Int. J. Environ. Anal. Chem.* 91 (2011) 161-173.  
<https://doi.org/10.1080/03067319.2010.500725>.
- [122] M. Moreno-Guzmán, M. Eguílaz, S. Campuzano, A. González-Cortés, P. Yáñez-Sedeño, J.M. Pingarrón, Disposable immunosensor for cortisol using functionalized magnetic particles, *Analyst*. 135 (2010) 1926-1933.  
<https://doi.org/10.1039/c0an00206b>.
- [123] B.J. Sanghavi, J.A. Moore, J.L. Chávez, J.A. Hagen, N. Kelley-Loughnane, C.F. Chou, N.S. Swami, Aptamer-functionalized nanoparticles for surface immobilization-free electrochemical detection of cortisol in a microfluidic device, *Biosens. Bioelectron.* 78 (2016) 244-252. <https://doi.org/10.1016/j.bios.2015.11.044>.
- [124] G.G. Guilbault, M. Hjelm, Nomenclature for automated and mechanised analysis (Recommendations 1989), *Pure Appl. Chem.* 61 (1989) 1657-1664.  
<https://doi.org/doi:10.1351/pac198961091657>.
- [125] C.F. Poole, *Handbooks in Separation Science*, (2020) 45-89.  
<http://dx.doi.org/10.1016/B978-0-12-816911-7.00002-5>.
- [126] E. Carasek, J. Merib, Membrane-based microextraction techniques in analytical chemistry: A review, *Anal. Chim. Acta.* 880 (2015) 8-25.  
<https://doi.org/10.1016/j.aca.2015.02.049>.
- [127] M.E. Systems, L. Membrane, E. Techniques, T.L.M.T.L.M. Extraction, F. Devices, H. Devices, *Membrane Extraction : General Overview and Basic Techniques*, 2 (2012) 461-474. <https://doi.org/10.1016/B978-0-12-381373-2.10049-3>.
- [128] N. Ozbek, A. Baysal, S. Akman, M. Dogan, *Solid-Phase Extraction*, (2015) 1571-1594.

- 
- [129] L. Chimuka, L. Mathiasson, J.Å. Jönsson, Role of octanol-water partition coefficients in extraction of ionisable organic compounds in a supported liquid membrane with a stagnant acceptor, *Anal. Chim. Acta.* 416 (2000) 77-86. [https://doi.org/10.1016/S0003-2670\(00\)00853-9](https://doi.org/10.1016/S0003-2670(00)00853-9).
- [130] E. Thordarson, J.Å. Jönsson, J. Emnéus, Immunologic Trapping in Supported Liquid Membrane Extraction, *Anal. Chem.* 72 (2000) 5280-5284. <https://doi.org/10.1021/ac0005013>.
- [131] M. Tudorache, I.A. Zdrojewska, J. Emnéus, Evaluation of progesterone content in saliva using magnetic particle-based immuno supported liquid membrane assay (m-ISLMA), *Biosens. Bioelectron.* 22 (2006) 241-246. <https://doi.org/10.1016/j.bios.2006.01.002>.
- [132] M. Tudorache, C. Bala, Biosensors based on screen-printing technology, and their applications in environmental and food analysis, *Anal. Bioanal. Chem.* 388 (2007) 565-578. <https://doi.org/10.1007/s00216-007-1293-0>.
- [133] G. Bo, J. Gang, Study of interaction force between antigen and antibody using flow chamber method, *Annu. Int. Conf. IEEE Eng. Med. Biol. - Proc.* 7 VOLS (2005) 7584-7587. <https://doi.org/10.1109/iembs.2005.1616267>.
- [134] V. Cerdà, L. Ferrer, J. Avivar, A. Cerdà, Evolution and Description of the Principal Flow Techniques, in: *Flow Anal.*, Elsevier, 2014: pp. 1-42. <https://doi.org/10.1016/B978-0-444-59596-6.00001-2>.
- [135] M. Anne Tupta, Cyclic voltammetry, Tektronix. (2015). <https://www.tek.com/blog/performing-cyclic-voltammetry>.
- [136] K. Twomey, A. Truemper, K. Murphy, A portable sensing system for electronic tongue operations, *Sensors.* 6 (2006) 1679-1696.
- [137] D.S. Silvester, Electrochemical studies in room temperature ionic liquids, University of Oxford, 2008. <https://ora.ox.ac.uk/objects/uuid:be9e6269-f19a->

- 48de-96e3-41c0c7143d6a.
- [138] N.-T. Nguyen, S.T. Wereley, S.A.M. Shaegh, *Fundamentals and applications of microfluidics*, Artech house, 2019.
- [139] K. Gao, J. Liu, Y. Fan, Y. Zhang, Ultra-low-cost fabrication of polymer-based microfluidic devices with diode laser ablation, *Biomed. Microdevices*. 21 (2019) 83. <https://doi.org/10.1007/s10544-019-0433-6>.
- [140] I.G. Reichenbach, M. Bohley, F.J.P. Sousa, J.C. Aurich, Micromachining of PMMA—manufacturing of burr-free structures with single-edge ultra-small micro end mills, *Int. J. Adv. Manuf. Technol.* 96 (2018) 3665-3677. <https://doi.org/10.1007/s00170-018-1821-4>.
- [141] C.W. Tsao, D.L. DeVoe, Bonding of thermoplastic polymer microfluidics, *Microfluid. Nanofluidics*. 6 (2009) 1-16. <https://doi.org/10.1007/s10404-008-0361-x>.
- [142] R. Truckenmüller, P. Henzi, D. Herrmann, V. Saile, W.K. Schomburg, Bonding of polymer microstructures by UV irradiation and subsequent welding at low temperatures, *Microsyst. Technol.* 10 (2004) 372-374. <https://doi.org/10.1007/s00542-004-0422-3>.
- [143] J. Yan, Y. Zhao, X. Wang, S. Xia, Y. Zhang, Y. Han, J. Yu, B. Ding, Polymer Template Synthesis of Soft, Light, and Robust Oxide Ceramic Films, *IScience*. 15 (2019) 185-195. <https://doi.org/10.1016/j.isci.2019.04.028>.
- [144] G. Tosello, H.N. Hansen, *Micro-Injection Molding*, *Micromanufacturing Eng. Technol.* Amsterdam Elsevier. (2010) 90-113.
- [145] J.P. Greene, 14 - Injection Molding, in: J.P. Greene (Ed.), *Automot. Plast. Compos.*, William Andrew Publishing, 2021: pp. 241-254. <https://doi.org/https://doi.org/10.1016/B978-0-12-818008-2.00019-2>.



- 
- [146] T. Nguyen, A.C. Vinayaka, D.D. Bang, A. Wolff, A complete protocol for rapid and low-cost fabrication of polymer microfluidic chips containing three-dimensional microstructures used in point-of-care devices, *Micromachines*. 10 (2019). <https://doi.org/10.3390/mi10090624>.
- [147] M. Matteucci, A. Heiskanen, K. Zizler, J. Emnißus, R. Taboryski, Comparison of ultrasonic welding and thermal bonding for the integration of thin film metal electrodes in injection molded polymeric lab-on-chip systems for electrochemistry, *Sensors (Switzerland)*. 16 (2016). <https://doi.org/10.3390/s16111795>.
- [148] S. Tanzi, P.F. Ostergaard, M. Matteucci, T.L. Christiansen, J. Cech, R. Marie, R. Taboryski, Fabrication of combined-scale nano- and microfluidic polymer systems using a multilevel dry etching, electroplating and molding process, *J. Micromechanics Microengineering*. 22 (2012). <https://doi.org/10.1088/0960-1317/22/11/115008>.
- [149] M. Matteucci, S.T. Larsen, A. Garau, S. Tanzi, R. Taboryski, Polymer multilevel lab-on-chip systems for electrochemical sensing, *J. Vac. Sci. Technol. B, Nanotechnol. Microelectron. Mater. Process. Meas. Phenom.* 31 (2013) 06F904. <https://doi.org/10.1116/1.4832415>.
- [150] F. Blateyron, The Areal Field Parameters BT - Characterisation of Areal Surface Texture, in: R. Leach (Ed.), Springer Berlin Heidelberg, Berlin, Heidelberg, 2013: pp. 15-43. [https://doi.org/10.1007/978-3-642-36458-7\\_2](https://doi.org/10.1007/978-3-642-36458-7_2).
- [151] J. Ramón-Azcón, E. Valera, Á. Rodríguez, A. Barranco, B. Alfaro, F. Sanchez-Baeza, M.P. Marco, An impedimetric immunosensor based on interdigitated **microelectrodes (ID $\mu$ E) for the determination of atrazine residues** in food samples, *Biosens. Bioelectron.* 23 (2008) 1367-1373. <https://doi.org/10.1016/j.bios.2007.12.010>.
- [152] C. Berggren, B. Bjarnason, G. Johansson, Capacitive biosensors, *Electroanalysis*.

- 13 (2001) 173-180. [https://doi.org/10.1002/1521-4109\(200103\)13:3<173::AID-ELAN173>3.0.CO;2-B](https://doi.org/10.1002/1521-4109(200103)13:3<173::AID-ELAN173>3.0.CO;2-B).
- [153] J.P. Salvador, F. Sánchez-Baeza, M.P. Marco, Simultaneous immunochemical detection of stanozolol and the main human metabolite, 3'-hydroxy-stanozolol, in urine and serum samples, *Anal. Biochem.* 376 (2008) 221-228. <https://doi.org/10.1016/j.ab.2008.02.009>.
- [154] R. D'Aurelio, I. Chianella, J.A. Goode, I.E. Tothill, **Molecularly Imprinted Nanoparticles Based Sensor for Cocaine Detection**, *Biosensors.* 10 (2020) 22. <https://doi.org/10.3390/bios10030022>.
- [155] A. Mech-Dorosz, A. Heiskanen, S. Bäckström, M. Perry, H.B. Muhammad, C. Hélix-Nielsen, J. Emnéus, A reusable device for electrochemical applications of hydrogel supported black lipid membranes, *Biomed. Microdevices.* 17 (2015). <https://doi.org/10.1007/s10544-015-9936-y>.
- [156] J.A. Goode, J.V.H. Rushworth, P.A. Millner, *Biosensor Regeneration : A Review of Common Techniques and Outcomes*, (2015). <https://doi.org/10.1021/la503533g>.
- [157] U. Dammer, M. Hegner, D. Anselmetti, P. Wagner, M. Dreier, W. Huber, H.J. Güntherodt, Specific antigen/antibody interactions measured by force microscopy, *Biophys. J.* 70 (1996) 2437-2441. [https://doi.org/10.1016/S0006-3495\(96\)79814-4](https://doi.org/10.1016/S0006-3495(96)79814-4).
- [158] R. Reverberi, L. Reverberi, Factors affecting the antigen-antibody reaction, *Blood Transfus.* 5 (2007) 227-240. <https://doi.org/10.2450/2007.0047-07>.
- [159] C.J. Van Oss, Hydrophobic, hydrophilic and other interactions in epitope-paratope binding, *Mol. Immunol.* 32 (1995) 199-211. [https://doi.org/10.1016/0161-5890\(94\)00124-J](https://doi.org/10.1016/0161-5890(94)00124-J).
- [160] S. Fujishiro, H. Ohnuki, H. Wu, D. Tsuya, H. Endo, Regenerable myoglobin

- biosensor based on protein G immobilized on interdigitated electrodes, *Jpn. J. Appl. Phys.* 59 (2020). <https://doi.org/10.7567/1347-4065/ab48c6>.
- [161] J. Yakovleva, R. Davidsson, A. Lobanova, M. Bengtsson, S. Eremin, T. Laurell, J. Emnéus, Microfluidic enzyme immunoassay using silicon microchip with immobilized antibodies and chemiluminescence detection, *Anal. Chem.* 74 (2002) 2994-3004. <https://doi.org/10.1021/ac015645b>.
- [162] J. Yakovleva, R. Davidsson, M. Bengtsson, T. Laurell, J. Emnéus, Microfluidic enzyme immunosensors with immobilised protein A and G using chemiluminescence detection, *Biosens. Bioelectron.* 19 (2003) 21-34. [https://doi.org/10.1016/S0956-5663\(03\)00126-X](https://doi.org/10.1016/S0956-5663(03)00126-X).
- [163] J. Yakovleva, R. Davidsson, A. Lobanova, M. Bengtsson, S. Eremin, T. Laurell, J. Emnéus, Microfluidic Enzyme Immunoassay Using Silicon Microchip with Immobilized Antibodies and Chemiluminescence Detection, *Anal. Chem.* 74 (2002) 2994-3004. <https://doi.org/10.1021/ac015645b>.
- [164] V.B. Kandimalla, N.S. Neeta, N.G. Karanth, M.S. Thakur, K.R. Roshini, B.E.A. Rani, A. Pasha, N.G.K. Karanth, Regeneration of ethyl parathion antibodies for repeated use in immunosensor: A study on dissociation of antigens from antibodies, *Biosens. Bioelectron.* 20 (2004) 903-906. <https://doi.org/10.1016/j.bios.2004.03.027>.
- [165] S.M. Conyers, D.A. Kidwell, Chromogenic substrates for horseradish peroxidase, *Anal. Biochem.* 192 (1991) 207-211. [https://doi.org/10.1016/0003-2697\(91\)90208-B](https://doi.org/10.1016/0003-2697(91)90208-B).
- [166] H. Hosoda, W. Takasaki, T. OE, R. Tsukamoto, T. Nambara, A comparison of chromogenic substrates for horseradish peroxidase as a label in steroid enzyme immunoassay., *Chem. Pharm. Bull.* 34 (1986) 4177-4182. <https://doi.org/10.1248/cpb.34.4177>.

- 
- [167] X. Zhang, Q. Yang, Y. Lang, X. Jiang, P. Wu, Rationale of 3,3',5,5'-Tetramethylbenzidine as the Chromogenic Substrate in Colorimetric Analysis, *Anal. Chem.* 92 (2020) 12400-12406.  
<https://doi.org/10.1021/acs.analchem.0c02149>.
- [168] E.S. Bos, A.A. van der Doelen, N. van Rooy, A.H.W.M. Schuurs, 3,3',5,5'-Tetramethylbenzidine As An Ames Test Negative Chromogen For Horse-Radish Peroxidase In Enzyme-Immunoassay, *J. Immunoassay.* 2 (1981) 187-204.  
<https://doi.org/10.1080/15321818108056977>.
- [169] H. Gallati, H. Brodbeck, Peroxidase aus Meerrettich: Kinetische Studien und Optimierung der Aktivitätsbestimmung mit den Substraten H<sub>2</sub>O<sub>2</sub> und o-Phenylendiamin, *Clin. Chem. Lab. Med.* 20 (1982) 221-226.  
<https://doi.org/10.1515/cclm.1982.20.4.221>.
- [170] N. Patel, M.C. Davies, M. Hartshorne, R.J. Heaton, C.J. Roberts, S.J.B. Tendler, P.M. Williams, Immobilization of protein molecules onto homogeneous and mixed carboxylate-terminated self-assembled monolayers, *Langmuir.* 13 (1997) 6485-6490. <https://doi.org/10.1021/la970933h>.
- [171] H. Wu, H. Ohnuki, M. Murata, H. Endo, Flow immunosensor system with an electrode replacement unit for continuous cortisol monitoring for fish, *Sens. Bio-Sensing Res.* 13 (2017) 122-127.  
<https://doi.org/10.1016/j.sbsr.2017.01.002>.
- [172] J. Janting, R. Inglev, Towards an Online Polymer Optical Fiber Cortisol Sensor for Aquaculture, in: 27th Int. Conf. Opt. Fiber Sensors, Optical Society of America OSA, 2021.
- [173] A. Löhn, B. Hitzmann, A knowledge-based system for real-time validation of calibrations and measurements, *Chemom. Intell. Lab. Syst.* 46 (1999) 57-66.  
[https://doi.org/10.1016/S0169-7439\(98\)00146-4](https://doi.org/10.1016/S0169-7439(98)00146-4).

- 
- [174] C.W.K. Chow, D.E. Davey, D.E. Mulcahy, An intelligent sensor system for the determination of ammonia using flow injection analysis, *Lab. Autom. Inf. Manag.* 33 (1997) 17-27. [https://doi.org/10.1016/S1381-141X\(97\)00004-X](https://doi.org/10.1016/S1381-141X(97)00004-X).
- [175] M. Peris, V. Chirivella, S. Martínez, A. Bonastre, R. Ors, J. Serrano, Rule nets: application to the advanced automation of a flow-injection analysis system, *Chemom. Intell. Lab. Syst.* 26 (1994) 123-127. [https://doi.org/10.1016/0169-7439\(94\)90054-X](https://doi.org/10.1016/0169-7439(94)90054-X).
- [176] C. Wittmann, R.D. Schmid, Application of an automated quasi-continuous immuno flow injection system to the analysis of pesticide residues in environmental water samples, *Sensors Actuators B. Chem.* 15 (1993) 119-126. [https://doi.org/10.1016/0925-4005\(93\)85037-B](https://doi.org/10.1016/0925-4005(93)85037-B).
- [177] C.E. Lenehan, N.W. Barnett, S.W. Lewis, Design of LabVIEW®-based software for the control of sequential injection analysis instrumentation for the determination of morphine, *J. Autom. Methods Manag. Chem.* 24 (2002) 99-103. <https://doi.org/10.1080/14639240210136747>.

# Paper I

## **Flow injection immunoassay for continuous monitoring of cortisol**

Claudy D'Costa<sup>a</sup>, Arto Heiskanen<sup>a</sup>, Zoltán Guller<sup>a</sup>, Manuel Gestob<sup>b</sup>, J.-Pablo Salvador<sup>c</sup>, M.-Pilar Marco<sup>c</sup>, Anders Wolff<sup>a</sup>, and Jenny Emneus<sup>a,\*</sup>

<sup>a</sup> Department of Biotechnology and Biomedicine (DTU Bioengineering), Technical University of Denmark, Produktionstorvet, Building 423, 2800 Kgs. Lyngby, Denmark

<sup>b</sup> Institute of Aquatic Resources (DTU Aqua), Technical University of Denmark, Willemoesvej 2, 9850 Hirtshals, Denmark

<sup>c</sup> Department of Chemical and Biomolecular Nanotechnology, Institute for Advanced Chemistry of Catalonia (IQAC) of the Spanish Council for Scientific Research (CSIC), Jordi Girona 18-26, 08034, Barcelona, Spain

\* To whom correspondence may be addressed: [jemn@dtu.dk](mailto:jemn@dtu.dk); Tel.: +45 45256867

Keywords: cortisol, fish welfare, aquaculture, lab-on-a-chip, flow injection, immunoassay electrochemistry, TMB

## **Abstract**

The stress hormone cortisol has been shown to indicate non-optimal conditions in recirculating aquaculture systems (RAS). Non-invasive continuous detection of the low cortisol levels in water, released by fish through the gills, has not been possible. We present here an automated flow injection immunoassay system for on-line competitive immunoassay of cortisol. The system comprised multiple peristaltic pumps and injection valves control through a custom-made LabView operated automation circuit. We tested two different immunoreaction chamber (IRC) formats, where cortisol antibody was bound to Protein G on either a gold surface or superparamagnetic beads. They provided an IC<sub>50</sub> and LOD of 0.91 nM and 0.6 pM (gold), and 7.8 nM and 1.3 pM (beads), respectively. To test the performance with real water samples from a model RAS, the IRC with magnetic beads was modified to incorporate an immuno-supported liquid membrane (ISLM) unit for sample cleaning and enrichment. Despite the higher IC<sub>50</sub> and LOD, the loaded Protein G modified magnetic beads render the system highly versatile for use. The obtained results indicated that after 900 s of sample flow through the ISLM donor phase, the antibody binding sites in the acceptor phase were fully occupied by cortisol, showing that continuous detection of cortisol in water is feasible. Overall, aside from detection of low cortisol concentrations in water using magnetic beads and ISLM, this format renders the system useful for on-demand detection of any analyte by simply loading a new set of beads housing the desired antibody into the IRC.



## **1. Introduction**

By 2050, the global population is predicted to exceed 9 billion. Fisheries and aquaculture form a crucial part in ensuring food for all. Fish provided about 17 % of the animal protein consumed in 2017 [1]. Fish farming is not a new phenomenon, but an is ancient practice originating from China [2], and is based on the modifications of natural water bodies or wetlands to entrap young fish in enclosures. Today, this has evolved into more systematic, controlled, and scientific methods and techniques referred to as aquaculture systems. Aquafarming can be done through open sea cages, flow-through systems, raceways, ponds, or more advanced recirculating aquaculture system (RAS) [3]. Each of these has its advantages and disadvantages. As the name implies, a RAS involves a more closed system; instead of farming fish outdoors in open ponds and raceways, this system rears fish at high densities in indoor tanks with a "controlled" environment. In RAS, filtered and cleaned water is recycled back through fish culture tanks to achieve effective CO<sub>2</sub> recirculation leading to environmentally sustainable fish farming [4].

It was long considered that since fish do not have a well-developed pain perceiving system, there was no need to be concerned about fish welfare. However, according to the Guidelines for the treatment of animals in behavioural research and teaching [5], all animals, including fish, need to be treated in a way that involves minimum stress, pain, or discomfort. The release of stress hormones (e.g. cortisol) can be triggered when the fish perceives a stressor, which may be a larger fish in the surrounding [6], stocking density [7] or noise [8]. Acute stress may inhibit the fish from responding to immediate threats or changes in the environment [9,10] and make the fish more vulnerable to infection with the subsequent need for antibiotics treatment [11]. Studies have shown multiple disadvantages of elevated stress in terms of economic impact, causing a reduction in growth (low biomass) and deterioration of meat quality [12]. In addition, there is an increasing awareness of these issues in society, which has already led to well-informed consumers to avoid farmed fish. This reluctance can lead to a "Catch22" situation considering such aspects as economical return, sustainable production, and fish welfare. The present UN sustainability goals emphasise sustainable and resilient methods of production. Modern inland aquaculture employs multiple sensors to monitor the physical, chemical, and relevant biological parameters. Existing aquaculture systems

should thus adapt and be redesigned to include surveillance systems that also monitor stress indicators, such as cortisol, to understand better the impact of fish welfare.

Cortisol is a steroid hormone released in response to stress, and its presence in fish was established already in 1957 [13]. Since cortisol is a generic stress hormone, significant studies have focussed on determining cortisol level in human blood plasma, saliva, urine, and sweat. Studies showcased so far have reported a limit of detection of 27.6 pM for blood plasma [14], 2.8 pM in sweat [15], and 1 pM in saliva [16].

In aquaculture, routine plasma cortisol measurements are performed to evaluate the stress level of the fish. Cortisol can be measured from blood plasma, mucus, scales, urine, faeces, or its release via the gills by diffusion into the surrounding water. Plasma cortisol is measured by sampling blood from the tail portion of individual fish in a population. Invasive measurement of cortisol by taking a blood sample from the fish will by itself trigger a stress response [17]. Cortisol released into the water via the gills can, however, be measured non-invasively [18], and a direct correlation with plasma cortisol levels can be made [17]. Experimentally, baseline cortisol level as low as 2 pM has been detected in water samples using radioimmunoassay [19]. Measuring cortisol from a tank where water is recirculating is challenging since cortisol release and accumulation vary with time and depend on many factors [20]. Presently, there are no measurement systems to non-invasively and continuously monitor cortisol from the water of fish tanks. Moreover, all the reports so far are primarily for human samples. Continuous automated on-line monitoring of cortisol would be an excellent indicator of sub-optimal growth conditions and a measure of fish welfare.

We have developed an automated flow injection immunoassay (FIIA) system for continuous determination of low cortisol levels in water. The FIIA system had an immunoreaction chamber (IRC), housing immobilised anti-cortisol antibodies to capture the cortisol, which was detected in an on-line competitive immunoassay format, using an enzyme labelled hapten tracer to quantify the amount of bound cortisol. The IRC was in a final step integrated with a supported liquid membrane (SLM) extraction unit to facilitate sample clean-up and enrichment by immuno-supported liquid membrane (ISLM) extraction [21–24].

## 2. Experimental

### 2.1 Reagents and solutions

Anti-cortisol monoclonal antibody IgG2a (10-C30D) purified by ion-exchange chromatography and its matched horseradish peroxidase conjugate Cortisol-3-CMO Hapten (65-IC08) were purchased from Fitzgerald Industries International, Acton, MA, USA. Hydrocortisone (cortisol), glycine (Gly), hydrochloric acid 36.5-38.0%, sodium hydroxide, dimethyl sulfoxide (DMSO), potassium chloride, potassium hexacyanoferrate(III) ( $K_3[Fe(CN)_6]$ ), potassium hexacyanoferrate(II) trihydrate ( $K_4[Fe(CN)_6]$ ), TWEEN<sup>®</sup> 20, 30 % hydrogen peroxide, sodium carbonate, sodium bicarbonate, 3,3',5,5'-tetramethylbenzidine (TMB), sodium citrate tribasic dihydrate, acetic acid, 3-mercaptopropionic acid (MPA), N-(3-Dimethylaminopropyl)-N'-ethylcarbodiimide hydrochloride (EDC), N-Hydroxysulfosuccinimide sodium salt (NHS), Dulbecco's phosphate buffered saline (PBS, pH 7.2), 4-morpholineethanesulfonic acid (MES), and dihexyl ether were all bought from Sigma-Aldrich Corporation, St. Louis, MO, USA (subsidiary of Merck KGaA), and were of the highest purity available. *TMB Plus2* was acquired from Kementec Solutions A/S (Taastrup, Denmark). Pierce<sup>™</sup> Protein G Magnetic Beads (10 mg/mL) (88847) and Pierce<sup>™</sup> recombinant Protein G (21193) were purchased from Thermo Fisher Scientific, Waltham, MA, USA. Ultrapure water (resistivity 18.2 M $\Omega$ .cm) was obtained from a Milli-Q<sup>®</sup> water purification system (Merck Millipore, Billerica, MA, USA).

The following buffers were used in the experiments: PBS with 0.05 % TWEEN<sup>®</sup> 20 (PBST), carrier buffer - 0.2 M citrate buffer containing 0.1 M KCl (pH 5.5 adjusted with acetic acid), regeneration buffer - 0.4 M Gly containing 1 % DMSO (pH 2.2 adjusted with HCl), coating buffer - 0.05 M carbonate buffer (pH 9.6) prepared using sodium carbonate and sodium bicarbonate in ultrapure water and pH adjusted with NaOH. All the buffers were stored at 4 °C for up to a month, except carrier buffer that was freshly prepared.

Anti-cortisol antibody (1.2 mg/mL) aliquots were stored at -20 °C and dilutions were freshly prepared in PBS. Cortisol-HRP hapten (1 mg/mL) was kept at 4 °C and dilutions were freshly prepared in PBST. 10 mM cortisol stock solution was prepared in DMSO and stored at 4 °C until use; further dilutions were prepared in PBS. HRP substrate solution, prepared in citrate buffer (pH 5.5; prepared as described above but without added KCl)

according to a previously published protocol [25], contained 0.4 mM TMB and 1.2 mM H<sub>2</sub>O<sub>2</sub>.

## **2.2 Device Fabrication**

### *2.2.1 Fabrication of IRCs*

Three different IRC configurations were fabricated (Figure 1): a) A single-channel unit with a deposited 200 nm gold layer (electron beam (e-beam) evaporation through a micromilled 500 µm thick shadow mask), b) a single-channel unit (no gold layer) with a slot for the permanent magnets (3 mm N45 nickel-plated cube-shaped rare earth magnets from Webcraft GmbH, Gottmadingen, Germany) underneath, and c) a two-channel unit (donor: upper channel; acceptor: lower channel) with a supported liquid membrane (SLM) sandwiched between the channels and a slot for permanent magnets underneath.

The IRC were fabricated from two 5 mm thick 90 mm x 20 mm PMMA plates. The PMMA plates, channels (depth: 0.4 mm; width: 0.5 mm; length: 68 mm), and slot for magnets (depth: 3 mm; width: 3 mm; length: 66 mm) were designed in AutoCAD 2021 and micro-milled using a CNC Mini-Mill/3 Pro tool from Minitex Machinery Corp (Georgia, USA) based on G-code generated by EZ-Cam 17 Express. Liquid-tight reaction chambers were formed by UV assisted thermal bonding of the PMMA plates. First, the PMMA surfaces to be bonded were exposed to deep-UV for 45 - 50 s followed by thermal bonding at 85 °C and 6 MPa. The deep-UV system consisted of a mercury UV lamp from Dymax Corporation (Torrington, CT, USA), and the bonding press was PW 10H from Paul-Otto Weber GmbH (Remshalden, Germany), comprising a plate heating/cooling unit HKP300-Ø165 and a temperature control unit TRG2. Fluidic connections to the PMMA plates were made directly into the inlet/outlet slots using 1/16" PTFE tubes (I.D. 0.5 mm). The tubing interfaces were made liquid-tight by applying silicone paste.

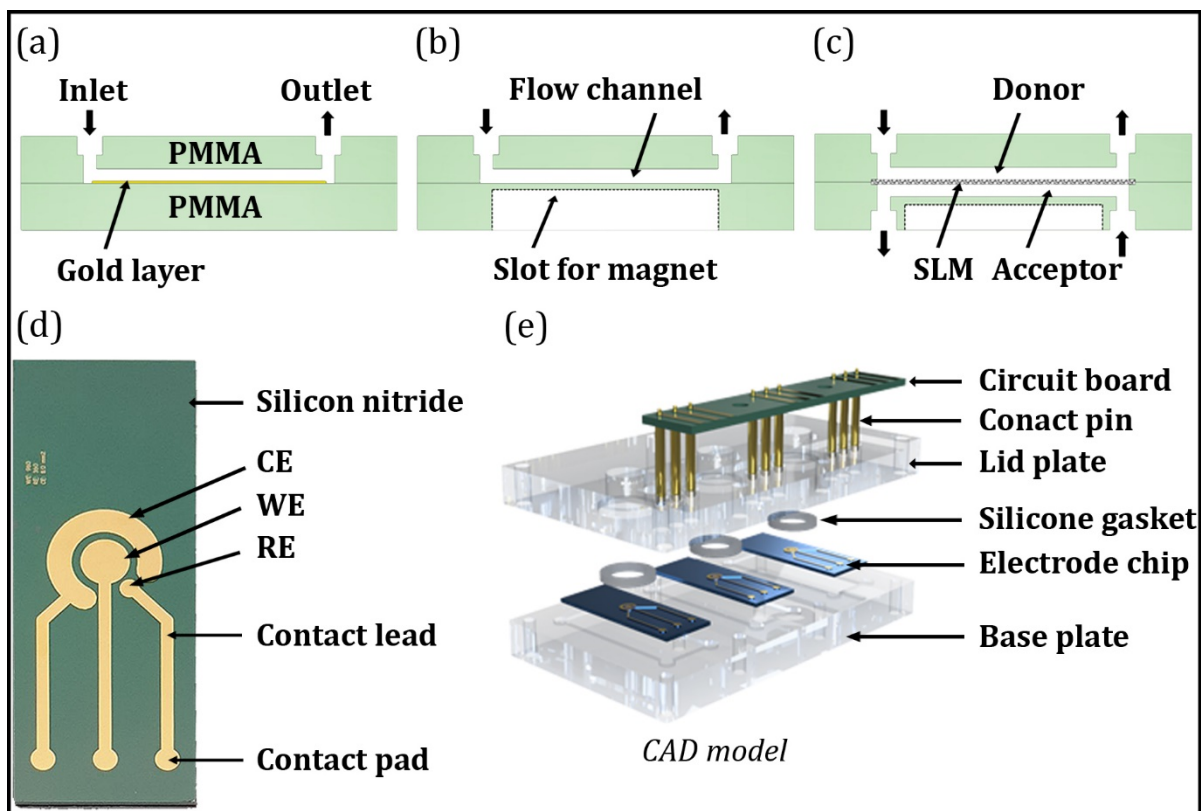


**Figure 1.** Schematic of three IRC, electrode chip, and detection chamber: A chamber with a) a gold layer and a channel above it, b) a slot below for placing permanent magnets to trap magnetic beads at the bottom of the chamber, c) A chamber with an SLM sandwiched between the donor and acceptor channel. The slot for placing permanent magnets is located under the acceptor channel. d) A photo of the electrode chip in a 3-electrode configuration (WE, CE, RE), contact leads and pads, and silicon nitride passivation layer on the wafer surface. e) A schematic of the detection chamber for three electrode chips, showing the lid plate with the electrochemical wall-jet cells, base plate with position for the electrode chips, circuit board and spring-loaded pins for electric connections, and silicone gaskets for fluid-tight connections for the electrochemical cells. The lid and base plate were assembled using 2 mm screws.

### 2.2.2 Fabrication of electrode chips and detection chamber

The chips with a 3-electrode system (Figure 1d), comprising a working electrode (WE), 1920  $\mu\text{m}$  in diameter, a counter electrode (CE), and a reference electrode (RE), were fabricated at the DTU Nanolab cleanroom (Technical University of Denmark) according to a previously published photolithography process [26]. In brief, a 500  $\mu\text{m}$  thick 4-inch silicon wafer was wet-oxidised in a furnace at 1050  $^{\circ}\text{C}$  to form 1  $\mu\text{m}$  thick  $\text{SiO}_2$  insulation layer. The oxidised wafers underwent an HDMS priming to enhance the adhesion of photoresist followed by spin coating of 1.5  $\mu\text{m}$  of the positive image reversal photoresist,

AZ 5214E (Merck Performance Materials GmbH, Wiesbaden, Germany), specially made for the lift-off process. After UV lithographic patterning, i.e. exposure of the photoresist (100 mJ/cm<sup>2</sup> through the photolithographic mask (designed using CleWin 5 software) and 250 mJ/cm<sup>2</sup> as flood exposure) and development in AZ 726MIF developer (Merck Performance Materials GmbH), of the areas, where the electrodes, leads, and contact pads were to be located, 50 nm of titanium and 200 nm of gold were deposited using e-beam evaporation. The unwanted deposited photoresist and metals were removed through a lift-off process using Microposit™ Remover 1165 having N-methyl pyrrolidone as the main component (Shipley Company, Marlborough, MA, USA). The exposed electrode areas and contact pads were defined using a 500 nm thick silicon nitride passivation layer. To obtain the individual electrode chips, the wafers were diced using a DAD 321 dicing saw (DISCO Hi-tec Europe GmbH, Munich, Germany).

The detection chamber (Figure 1e) was a wall-jet electrochemical cell (height: 800 µm; diameter: 6 mm). The lid and base plate were micromilled using 5 mm thick PMMA and assembled using 2 mm screws. The inlet was positioned toward the centre of the WE and the outlet was radially directed from the periphery of the chamber. The fluid-tight sealing of the electrochemical cell was done using a silicone gasket laser-cut from 1 mm thick silicone sheet (Reichelt Chemietechnik GmbH + Co., Heidelberg, Germany). Electric connections to electrodes were achieved using a custom-made circuit board with soldered spring-loaded contact pins. Figure 1c shows a schematic view of a setup having three parallel detection chambers.

## **2.3 Development of IRC and immunoassays**

### *2.3.1 Immobilisation of antibody in IRC*

In the first strategy (Figure 2a), the IRC with a gold layer was first modified using an aqueous solution of MPA (100 mM) for 1 h followed by activation of the carboxylic groups by EDC (200 mM) and NHS (50 mM) in 100 mM MES buffer (pH 6) for 25 min [27]. Usage of reagents that can be dissolved in water was preferable since PMMA can be dissolved in ethanol or other organic solvents. Protein G was then covalently attached to the gold surface from a 3 µg/ml solution in PBS for 1 h at room temperature. Protein G has a good affinity towards the Fab region of antibodies, which provides a better orientation for the

immobilised antibodies. In the final step, 10  $\mu\text{g/ml}$  cortisol antibody solution (diluted in PBS) was introduced into the IRC to allow binding to Protein G. The unbound antibody was washed off with PBST under a nominal flow rate of 150  $\mu\text{l/min}$ .

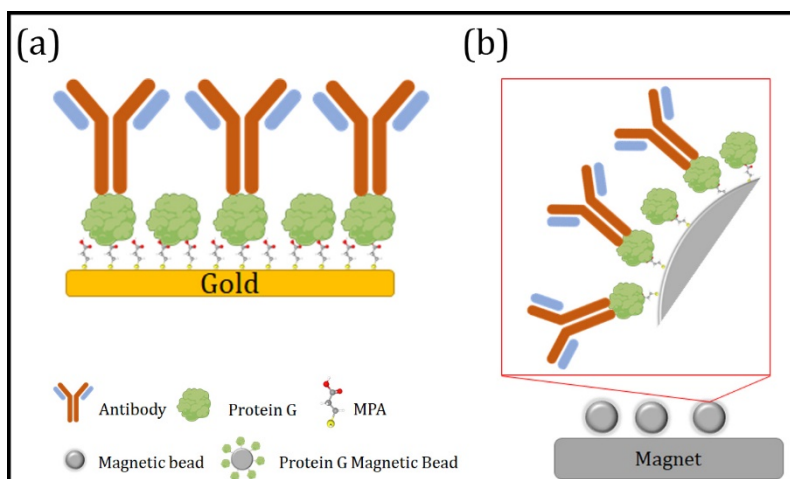


**Figure 2.** Different antibody immobilisation strategies. a) MPA SAM on the gold surface in the reaction chamber followed by carboxylic acid activation with EDC/NHS and immobilization of Protein G. The antibody solution was injected on-line into the IRC. b) Protein G loaded magnetic beads with bound antibody were injected into the reaction chamber and kept in position by magnets placed under the chamber.

The second strategy used superparamagnetic beads of 1  $\mu\text{m}$  mean diameter with covalently immobilized recombinant Protein G. According to the manufacturer's specifications, the protein G has two binding sites for IgG attachment and a binding capacity of  $\geq 60 \mu\text{g}$  rabbit IgG/mg of beads. 10  $\mu\text{L}$  of 1.2 mg/ml cortisol antibody was added to 20  $\mu\text{L}$  of 10 mg/ml suspension of Protein G functionalised magnetic beads and diluted to 100  $\mu\text{L}$  using PBS. After that, the beads with antibodies were gently mixed and kept at 4  $^{\circ}\text{C}$  overnight for binding. The solution was intermittently mixed since the magnetic beads tended to sediment. 10  $\mu\text{L}$  of this solution was gently introduced into the reaction chamber and held there by magnetic force during each experiment. Washing off of excess antibody or loose beads was carried out with PBST under a nominal flow rate of 150  $\mu\text{l/min}$ .

### *2.3.2 Operations of the automated flow injection immunoassay*

To establish an automated FIIA for detection of cortisol, the IRC (total volume of 13.6  $\mu\text{l}$ ) was incorporated as the injection loop in the system, as schematically shown in Figure 3. It comprised the following units and operations: Each of the reagents (PBST, HRP substrate, regeneration solution (Gly), antibody and tracer working dilutions) was dosed from a dedicated vial (1) using a Cheminert® C5-1340D 10-port multi-position valve (2) from VICI AG International (Schenkon, Switzerland) and fed through a Miniplus 2 peristaltic pump (3) from Gilson (Villiers-le-Bel, France) into a Cheminert® 11Y-0178L 2-position valve (4) (VICI AG International), which housed the IRC (5) as the injection loop. The excess of the solutions was collected into a waste container (6). A Miniplus 3 peristaltic pump (7) (Gilson) was used to feed carrier buffer (8) through the 2-position valve into the detection chamber (9) to record the baseline current. The excess of the buffer was collected into a waste container (10). Amperometric measurements were performed using a PalmSens4 potentiostat (11) from PalmSens BV (Houten, Netherlands). The potentiostat was entirely battery operated to reduce 50 Hz line noise, and the data was sent to a computer (12) over Bluetooth connection. The potential of the WE was poised at -0.15 V vs. the on-chip RE and the current sampling rate of the potentiostat was set to 100 ms. Computerised operation of the automated FIIA system (peristaltic pumps and injection valves) was achieved by using a custom-made digitally controlled relay circuit (13) and a NI-6009 multifunction I/O (14) interfacing unit (National Instruments Corp., Austin, TX, USA), addressed by a LabVIEW 2020 (National Instruments Corp.) script. Once all the reagents and buffers were loaded, the system was designed to perform the entire experiment automatically.



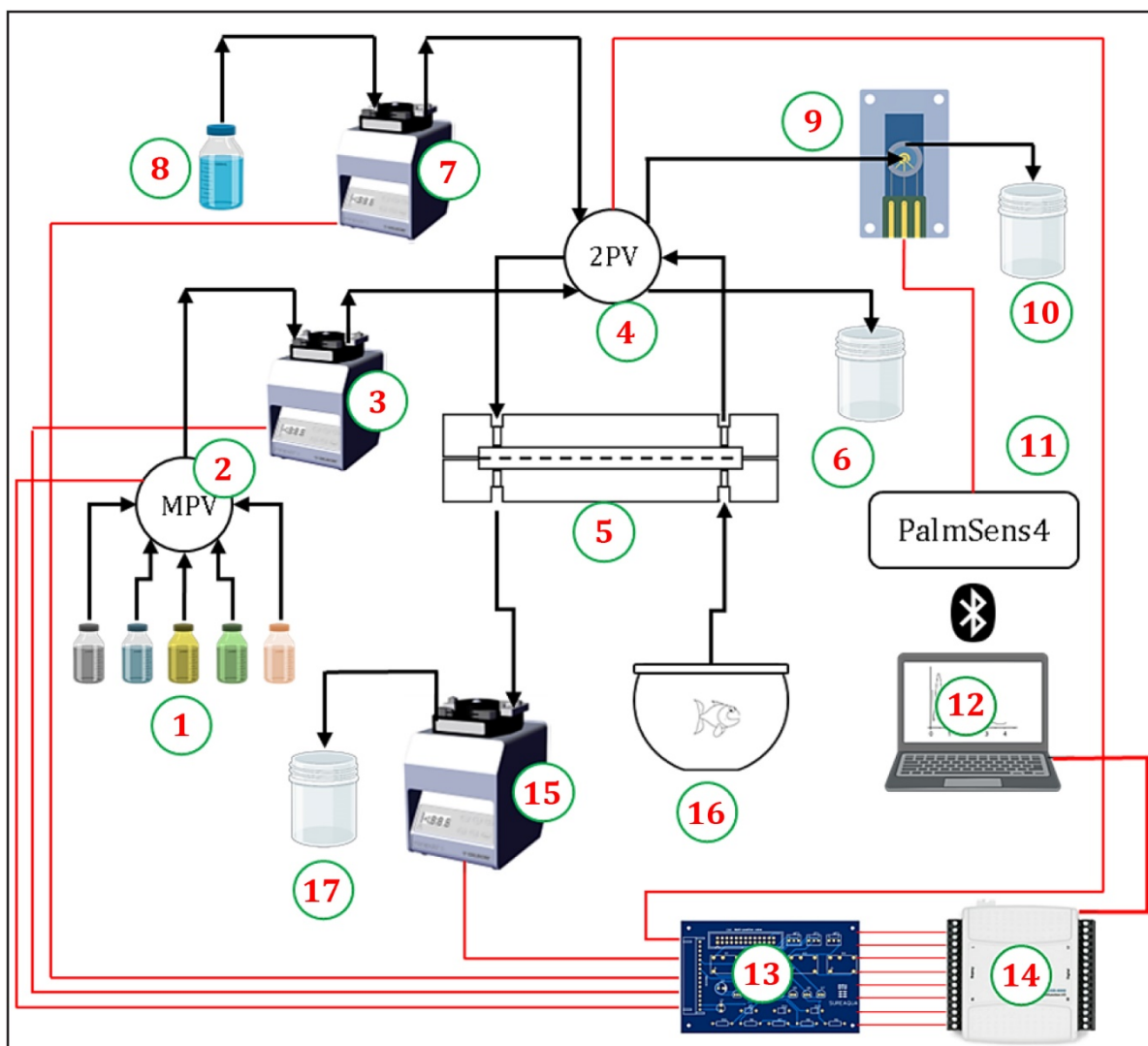


**Figure 3.** Schematic diagram of the automated FIIA system.

The entire FIIA was optimised in terms of the flow rate of the peristaltic pumps as well as duration of the washing with PBST, loading of the tracer/analyte and affinity reaction time, loading of the HRP substrate and reaction time, amperometric detection, and regeneration. The goal for optimisation of the individual parameters was to maximise reproducibility while maintaining the integrity of the IRC and minimising the overall duration of the assay.

When an IRC (based on either a gold surface or magnetic beads) with immobilised antibody was ready (described in section 2.3.1), the FIIA had the following sequence (assay steps: flow rate 150  $\mu\text{l}/\text{min}$ ; amperometric measurement step: flow rate 600  $\mu\text{l}/\text{min}$ ): All the buffer and reagent containers were loaded, and the fluidic circuit,

including the IRC and detection chamber, were primed to eliminate trapped air bubbles. After priming of the system, the IRC was rinsed with PBST for 90 s. A tracer plug was introduced by flowing the tracer solution (1 µg/ml) for 30 s followed by flow of PBST for 35 s to allow the plug to fill the IRC. The tracer was allowed to bind to the antibody under stopped-flow for 180 s followed by rinsing with PBST for 150 s. After that, the HRP substrate solution was allowed to flow for 75 s to fill the entire IRC. The flow was stopped for 400 s to allow the reaction to take place. 350 s after the start of the substrate reaction, the carrier buffer pump was switched on to record the amperometric baseline. After the completed reaction time, the 2-position injection valve was switched to inject the product (enzymatically oxidised substrate) into the detection chamber. During the amperometric measurement, the WE was poised at -0.15 V vs. the on-chip RE to reduce the product. The LabView script was used to repeat the assay after a fixed delay. When the assay continued after the completed detection step, the setup was rinsed with PBST for 90 s to remove non-specifically bound molecules and debris. Then, the regeneration buffer was allowed to flow for 200 s followed by stopped-flow for 100 s to remove any tracer or cortisol from the previous run. After the complete regeneration, the setup was rinsed again with PBST for 90 s. For a repeated run of FIHA, first 10 µg/ml anti-cortisol antibody solution was flown for 30 s to aspirate a plug, and then PBST was allowed to flow for 35 s to introduce the antibody solution plug into the reaction chamber. After that, stopped-flow was maintained for 180 s to allow the antibody to bind to Protein G followed by rinsing with PBST for 90 s. For calibration, the required cortisol concentration and tracer were mixed off-line and introduced into the IRC following the same procedure as described above for the tracer.

#### **2.4 Cortisol detection in water samples from RAS**

Water samples (pH 8.6) were collected from a fresh-water fish tank (volume ca. 1 m<sup>3</sup>) containing rainbow trout smolts (total biomass of 4.5 kg corresponding to 45 – 75 fish) before (control) and 45 min after introducing stressors. The fish were stressed by reducing the water level to 100 l, reducing the air supply by 40 %, tapping the sides of the tank to create noise, and mixing the water with a handheld net.

#### 2.4.1 Solid-phase extraction and ELISA

200 mL water samples were collected and extracted through a solid-phase extraction unit (Oasis HLB 1cc vacuum cartridges from Waters Corp.) according to the protocol of Reemeyers et al. [28]. The extracted cortisol was eluted with ethyl acetate and the concentration was determined using competitive ELISA on a standard ELISA kit from Cayman Chemical (Ann Arbor, MI, USA) according to the manufacturer's protocol. A 12-channel manual plate washer from CAPP (Norhausen, Germany) was used to make washing effective and reproducible. Absorbance of the HRP product was measured at 450 nm using an EL800 plate reader from BIO-TEK Instruments (Agilent Technologies, CA, USA) under control of Gen5 software.

#### 2.4.2 ISLM extraction

In the final step, the IRC was with integrated a supported liquid membrane (SLM) extraction unit to enable ISLM (Figure 1c). The SLM was composed of a polypropylene based microporous monolayer membrane (Celgard<sup>®</sup> 2500 from Celgard, LLC, Charlotte, NC, USA – a subsidiary of The Asahi Kasei Group) with thickness of 25 µm and average pore diameter of 64 nm impregnated with dihexyl ether. The same water samples were used as described above. Using a third peristaltic pump (15), VS2-10R-MIDI from Alitea (Stockholm, Sweden), the water samples (16) were fed at a flow rate of 100 µl/min through the donor channel of the IRC and further to a waste container (17). The samples were fed for different periods before adding 1 µg/mL of the tracer solution.

### 2.5 Data analysis

Prism 9.0.2 (GraphPad Software, San Diego, CA, USA) was used to analyse and plot the data recorded in experiments using ELISA and the developed FIAs. Data is presented ± standard deviation unless otherwise stated. The IC<sub>50</sub> values were calculated using the 4-parameter logistic equation (Eq. 1),

$$Y = Bottom + \frac{Top - Bottom}{1 + \left[ \frac{10^{\log(IC_{50})}}{10^{\log(C_{cortisol})}} \right]^{HillSlope}} \quad (1)$$

where Y is the measured value (absorbance or current) dependent on cortisol concentration, Bottom and Top represent the Y value at the bottom and top plateau of the sigmoidal curve, respectively,  $IC_{50}$  is the cortisol concentration corresponding to half maximal antibody binding site occupancy, and Hill slope represents the steepness of the central linear portion. The limit of detection (LOD) was estimated as 90 % of the maximal response.

### 3. Results and discussion

#### 3.1 Characterization of FIA system

The entire fluidic circuit developed for the automated FIIA system, comprising the peristaltic pumps, injection valves, as well as IRC (used as an injection loop) and electrochemical detection chamber (wall-jet electrochemical cell) is shown in Figure 3. The cross-sectional area of the reaction chamber (0.5 mm x 0.4 mm) as well as the inlet/outlet of the detection chamber were matched to the 0.5 mm diameter tubing used throughout the system. A uniform cross-section of the fluidic path was chosen to reduce the occurrence of uncontrolled vortices in the flow.

Aside from the fluidic circuit comprising all the components, the performance of an electrochemical FIIA system is dependent on the electrodes designed for detection. The fabricated electrode chips had three designs, each having a different diameter of the WE (960  $\mu\text{m}$ , 1440  $\mu\text{m}$ , and 1920  $\mu\text{m}$ ). Prior to performing fluidic characterization, the behaviour of the fabricated electrode chips was evaluated to choose the optimal WE dimension to be used in the detection chamber. Figure S-1a in the Supporting Information shows cyclic voltammograms acquired in 10 mM  $[\text{Fe}(\text{CN})_6]^{3-/4-}$  (prepared in PBS) at a scan rate of 100 mV/s using each of the electrode designs. Directly after fabrication, all of the WEs functioned well in terms of  $[\text{Fe}(\text{CN})_6]^{3-/4-}$  electrochemistry, which is indicated by the ratio of the anodic and cathodic peak current being close to one as well as the peak potential separation being slightly less than 100 mV. To provide effective and quantitative detection during FIIA experiments, the largest WE design was chosen for characterization of the FIIA system as well as for all of the subsequent experiments. For amperometric detection of the injected  $[\text{Fe}(\text{CN})_6]^{3-}$ , the WE was poised at -0.15 V to provide a sufficient driving force for reduction according to Figure S-1a in the Supporting Information.

The profile and reproducibility of the current peaks in an electrochemical FIA system are directly dependent on the length/diameter of the connecting tubing, the structure of the detection chamber, and flow rate. These factors determine the spreading of the plug of the injected electroactive species. The longer and wider the tubing connected to the detection chamber is, the wider the plug becomes during the time its passage takes at a specific flow rate. The structure of the detection chamber determines the degree of dispersion the plug undergoes from the moment it enters the chamber until it reaches the electrode surface. Pumps 1 and 2 (Figure 3) were calibrated to ensure the desired flow rate of PBS containing 10 mM of the electroactive species,  $[\text{Fe}(\text{CN})_6]^{3-}$ , and plain PBS to record the baseline, respectively. The injections were made using a fabricated reaction chamber (13.6  $\mu\text{l}$ ) as the injection loop. Figure 4a shows current peaks recorded at flow rates ranging from 67 to 1200  $\mu\text{l}/\text{min}$ . At the lower flow rates, the peaks appeared to be more widened due to spreading in the tubing and certain degree of dispersion in the detection chamber. At the flow rate of 67  $\mu\text{l}/\text{min}$ , the flux of  $[\text{Fe}(\text{CN})_6]^{3-}$  at the electrode surface was practically nonexistent. Figure 4b shows a zoom-in view of the current peak reaching only about 350 pA. Based on the profile of the recorded peaks, the two highest flow rates appeared to be the most optimal for amperometric detection. When the flow rate is sufficiently high, the spreading in the tubing and dispersion in the detection chamber are minimised. Figure 4c presents the relationship between the recorded current peaks and flow rate. The result indicates that the recorded current was linearly dependent on the increased flow rate only until 600  $\mu\text{l}/\text{min}$ . This further means that at 1200  $\mu\text{l}/\text{min}$  the flux was too high to facilitate quantitative detection of the reversible electroactive species. From the point of view of a competitive immunoassay relying on oxidised TMB ( $\text{TMB}_{\text{ox}}$ ) as the electroactive species, this flow rate would not be suitable due to the non-reversible nature of  $\text{TMB}_{\text{ox}}$ . Considering the most optimal behaviour of the recorded current peak at the flow rate of 600  $\mu\text{l}/\text{min}$ , this condition was used to evaluate the detection reproducibility. Figure 4d shows current peaks recorded during 17 consecutive injections. The calculated average peak height was  $623 \pm 12$  nA ( $\sim 2\%$  RSD), which indicates an excellent reproducibility. Using the same injection conditions as for the test depicted in Figure 4d, the dispersion coefficient ( $D_{\text{coeff}}$ ) was found to be 1.31 according to equation 2 [29],

$$D_{coeff} = \frac{I^0}{I} \quad (2)$$

where  $I^0$  is the current amplitude recorded during continuous injection of the total concentration of the electroactive species and  $I$  is the recorded peak current when the 13.6  $\mu\text{l}$  plug transiently passed the detection chamber, i.e. the current response for the concentration in the fluid volume of the detection chamber. The value of  $D_{coeff}$  indicates a minimal dispersion at the flow rate of 600  $\mu\text{l}/\text{min}$ , which means that when the injected plug, after having undergone a certain degree of spreading in the tubing, enters the detection chamber it is promptly impinged onto the electrode surface.

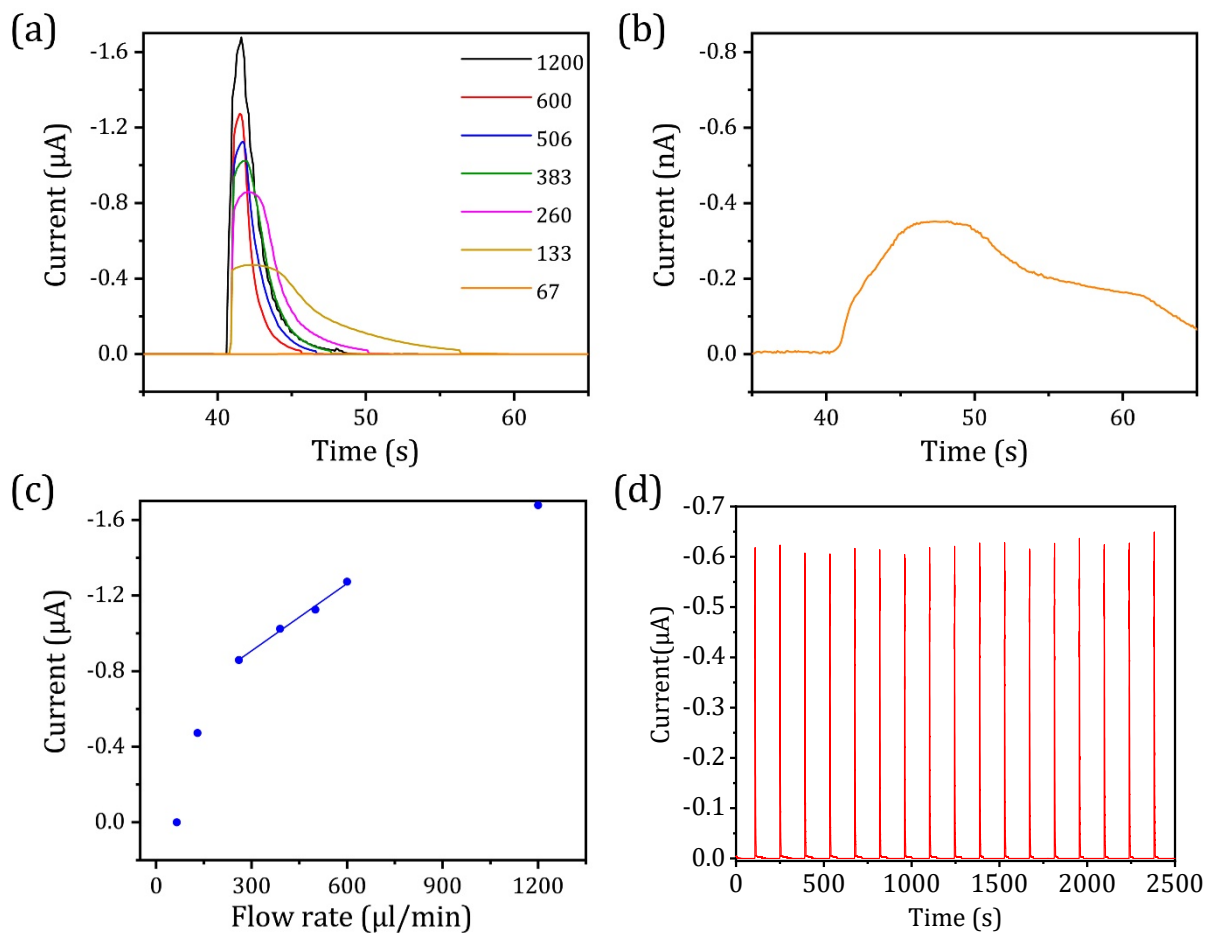


**Figure 4.** Amperometric detection of  $[\text{Fe}(\text{CN})_6]^{3-}$ . a) Current peaks recorded at different flow rates, b) zoom-in of the current peak recorded at 67  $\mu\text{l}/\text{min}$ , c) variation of peak currents with flow rate, and d) current peaks recorded during 17 injections at the flow rate of 600  $\mu\text{l}/\text{min}$ .

## 3.2 Development of competitive FIIA for cortisol

### 3.2.1 Antibody immobilisation

Development of a continuous competitive FIIA requires a suitable strategy for antibody immobilisation. The influence of antibody immobilisation on a substrate, which may be an electrode or a polymeric surface, has been explored in the literature [30–32]. The simplest approach, physisorption, has the inherent problem that the immobilised antibodies have a random orientation. This results in a considerable fraction of the antibodies being oriented in such a way that the antigen binding site may be close to or in direct contact with the immobilisation substrate, which causes steric hindrance for antigen binding, especially for an enzyme conjugated tracer [33]. Covalent immobilization of antibodies on chemically modified substrates is widely performed and provides robust, durable immunoreaction surfaces, which in the case of gold substrates can be achieved by first preparing a thiol-based self-assembled monolayer (SAM) using a carboxylic acid terminated thiol followed by carboxylic acid activation with EDC and NHS. Even in this case, the immobilised antibodies may be randomly oriented, since each antibody is immobilised via linkage to one of its surface bound amine groups, located in various positions. To alleviate the concomitant steric hindrance to antigen binding, which can influence covalently bound antibodies, immunoreaction surfaces on gold substrates are prepared using a mixed thiol SAM [34], e.g., a long-chain carboxylic acid terminated thiol, 11-mercaptoundecanoic acid, for antibody immobilisation, and a shorter spacer thiol, 6-mercapto-1-hexanol. A nature-inspired immobilisation approach is based on the application of Protein G, which has a strong affinity for the Fc domain of antibodies [33,35]. In comparison with the two other abovementioned approaches, Protein G-based immobilisation has proven to generate immunoreaction surfaces where the immobilised antibodies retain the maximal antigen binding capacity [32].

The effect of antibody immobilisation by physisorption and via Protein G linkage were compared using ELISA plates. Varying concentrations of antibody solution in PBS were used to coat the plates either directly (without Protein G) or after physisorption of Protein G on the plate surface. In all the tests, the tracer (HRP conjugated cortisol) concentration was 0.25  $\mu\text{g}/\text{ml}$  and the used substrate solution was a mixture of TMB and  $\text{H}_2\text{O}_2$  (described in section 2.1). Figure 5a shows that when antibody immobilisation (1  $\mu\text{g}/\text{ml}$ )

was done via Protein G linkage, higher absorbance values were obtained at low antibody concentration in comparison with physisorption of antibodies. Figure 5b shows calibration curves for cortisol assay on surfaces with and without Protein G. The distinct differences between the two calibration curves were the higher absorbance at low cortisol concentrations (maximal tracer binding) and lower Hill slope (increased linear range). Based on the performed ELISA tests, antibody immobilisation via Protein G linkage was chosen as the approach for further development of the continuous FIIA system.

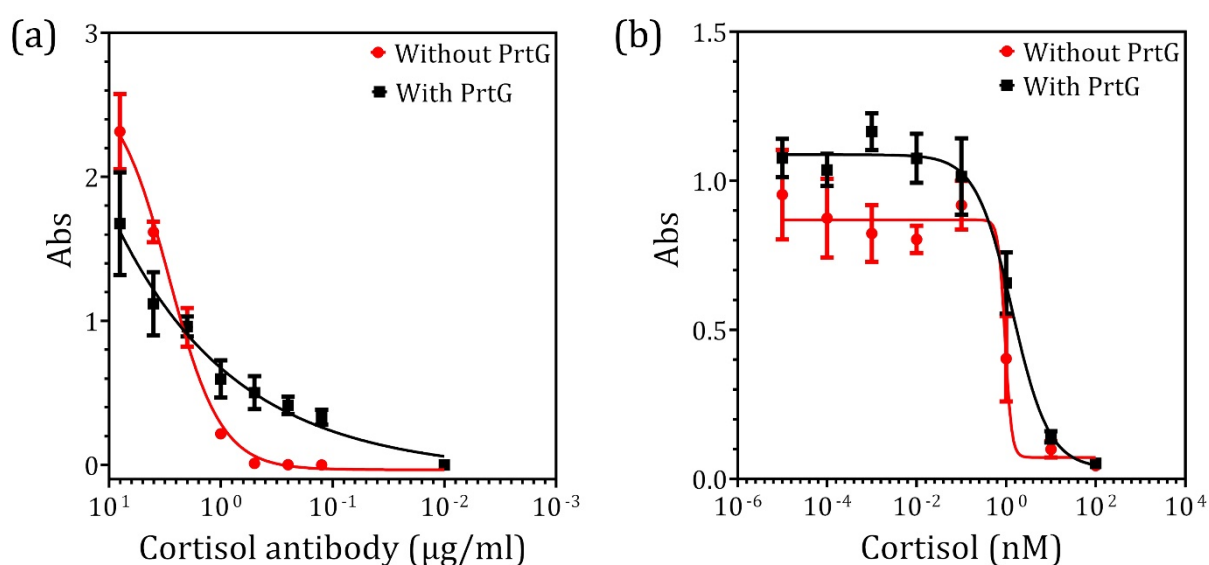


**Figure 5.** ELISA results showing a) the effect of different antibody concentrations and b) calibration curves for a competitive cortisol assay ( $1 \mu\text{g/ml}$  cortisol antibody) on ELISA plates with and without protein G. (tracer concentration  $0.25 \mu\text{g/ml}$ )

### 3.2.2 Optimisation of FIIA

When creating an on-line immunoassay system, the primary considerations are the stability of the IRC, i.e., functionality of the immobilised protein G, antibody and reagents, especially the enzyme substrate, and how effectively the IRC can be regenerated during repeated assays. The goal for developing a continuous FIIA is to optimise the duration of each step to maintain the optimal function. However, too high a flow rate may have one or several of the following consequences: (i) The antibody may be removed from the Protein



G, (ii) the tracer bound to the antibody may be dislodged, or (iii) the analyte bound to the antibody may be dislodged.

The overall function of the FIIA system was characterised and the optimal flow rate for amperometric detection was determined to be 600  $\mu\text{l}/\text{min}$  as presented in section 3.1. However, since the initial evaluation of the flow rates was performed using  $[\text{Fe}(\text{CN})_6]^{3-}$  as the electroactive species, only the fabricated reaction chamber was used without immobilised Protein G and antibody. Hence, the next step was to evaluate the effect of the flow on the integrity of a reaction chamber having a gold surface coated with immobilised Protein G and antibody. Each test comprised all necessary steps for the on-line assay, i.e., PBST rinsing, introduction of immunoreagents, and substrate, as well as feeding of the product from the reaction chamber into the detection chamber. Furthermore, each test was performed by recording the amperometric signal represented by complete tracer occupancy on the immobilised antibody, achieved using 1  $\mu\text{g}/\text{ml}$  tracer solution prepared as described in section 2.1. During the amperometric detection step, the WE was poised at -0.15 V to provide a sufficient driving force for reduction of  $\text{TMB}_{\text{ox}}$  according to Figure S-1b in the Supporting Information, and the used flow rate was 600  $\mu\text{l}/\text{min}$ . The flow rate during the other assay steps was varied between 75  $\mu\text{l}/\text{min}$  and 600  $\mu\text{l}/\text{min}$ .

The performed tests indicated that none of the flow rates below and until 150  $\mu\text{l}/\text{min}$  had a detrimental effect on the integrity of the Protein G-antibody complex or the tracer bound to the antibody during the assay steps (PBST rinsing, regeneration, and introduction of substrate). On the other hand, flow rates above 150  $\mu\text{l}/\text{min}$  clearly deteriorated the function of the reaction chamber either by disrupting the Protein G-antibody complex or by prematurely removing the bound tracer before the substrate reaction took place. Hence, to minimise the duration of one assay run to eliminate unequal reaction time caused by low flow rates during introduction of the substrate into the IRC, a flow rate of 150  $\mu\text{l}/\text{min}$  was chosen as optimal for the assay steps. Although the higher flow rate, 600  $\mu\text{l}/\text{min}$ , during amperometric detection only transiently passed the IRC, it could have a detrimental effect on the stability during repeated assay runs. Due to that, an additional step was included during further assay development to reinstate the condition of the Protein G-antibody complex.

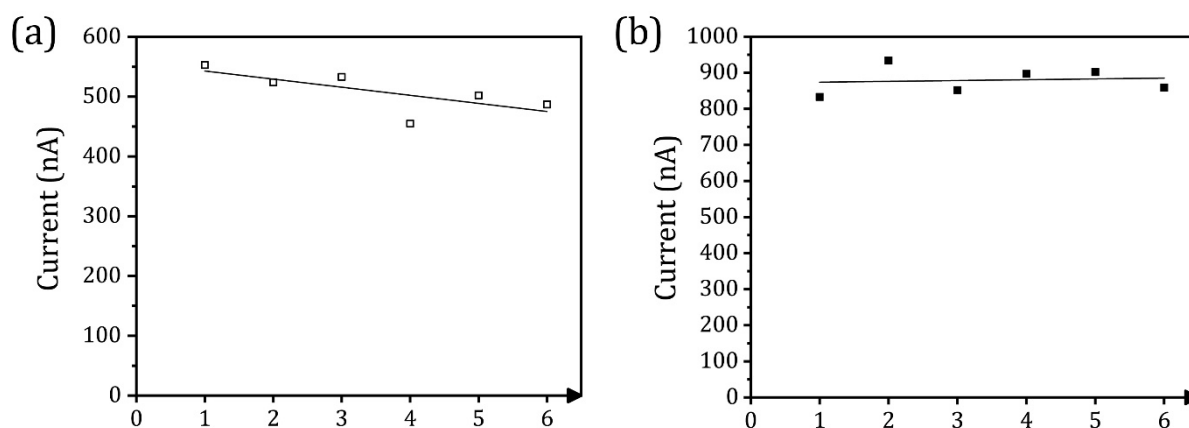


**Figure 6.** Test of HRP substrate stability and regeneration. Current vs. number of tests for a) home-made (0.4 mM TMB and 1.2 mM H<sub>2</sub>O<sub>2</sub> in citrate buffer, pH 5.5) and b) the commercial TMB Plus2 substrate. In both cases, a 1 µg/ml tracer solution was used.

During a continuous FIHA, the buffers, immunoreagents, regeneration and substrate solution are exposed to the ambient conditions for several hours. To assess the stability of the solutions, six tests were performed in the same way as described above for assessing the effect of flow rates, i.e., the IRC was regenerated after each test, which took approximately 4 h. Figure 6a shows that the obtained current signal decreased during continued testing. Individual tests, each time performed using a fresh substrate solution, proved that the buffers and immunoreagents were stable. Hence, the observed drift was clearly caused by instability of the substrate solution. In standard ELISA, the substrate is usually freshly prepared just before use and the ELISA plate is protected against light. One solution was to ensure that the substrate container, connecting tubes, and reaction chamber of the FIHA system were shielded from light. Such shielding was tested, and the result indicated that the substrate stability was improved. However, permanent shielding of the system to eliminate the drift caused by the light-sensitivity of TMB would make the overall assays cumbersome to perform. Another approach was to use a commercially available substrate, TMB Plus2, which has been tested in a previous immunoassay setup [36]. Based on the performed tests, this substrate proved to be stable throughout the test period and provided a higher current amplitude using the same reaction time (Figure 6b). Aside from the specific test described here, the stability of TMB Plus2 substrate was also evaluated by maintaining the substrate in a vial for several days and performing a test each day by injecting tracer to the IRC and recording the current signal due to complete antibody binding site occupancy.

The possibility to perform continuous FIIA in a reproducible manner depends on how well the immunoreaction surface can be regenerated [37]. One of the widely used approaches is based on an acidic glycine solution (pH ~ 2). The purpose of regeneration is usually to remove the antigen and tracer bound to the antibody while the immobilised antibody remains intact and ready for the next assay. When Protein G is used to immobilise the antibody, it is crucial that the used regeneration method does not harm Protein G, which could otherwise disrupt the Protein G-antibody complex. Here, the regeneration of the IRC was based on glycine solution at a pH of 2.2 with added 1 % DMSO. Based on preliminary tests, cortisol was not removed from the reaction chamber if regeneration was performed without added DMSO. Another factor that clearly influenced the outcome of regeneration was the dwelling time of the glycine solution in the reaction chamber. Too long a dwelling time affected the long-term stability of the IRC, whereas too short a time resulted in inadequate regeneration. Based on the result shown in Figure 6b, the reproducibility of six test runs under maximal tracer occupancy gave an RSD of 5.0 %, which indicates that the performed regeneration was effective and reliable. Moreover, an IRC remained stable in continuous assays for a few weeks before it had to be replaced.

### *3.2.3 Characteristics of the continuous FIIA – two formats*

Two different IRC (Figure 1a and b) were tested for the complete FIIA (Figure 7) (details in section 2.3.2): The antibody was immobilised on Protein G covalently bound on a gold surface (Figure 2a) and magnetic beads (Figure 2b). For acquiring the calibration curves (Figure 7), cortisol was spiked in PBS in the concentration range of 10 fM – 50  $\mu$ M (Figure 7a, gold) and 100 fM – 100  $\mu$ M (Figure 7b, magnetic beads). For the IRC with a modified gold surface, the calculated IC<sub>50</sub> and LOD were 0.91 nM and 0.6 pM (Figure 7a), respectively, whereas in the case of Protein G modified magnetic beads the corresponding values were 7.8 nM and 1.3 nM (Figure 7b), respectively. Aside from the difference in the IC<sub>50</sub> and LOD, the two IRC also had a significantly different linear region. For the modified gold surface, the linear region ranged from 10 pM to 100 nM. On the other hand, for the reaction chamber loaded with magnetic beads, the linear region was between 1 nM and 100 nM. Considering the superior performance of the IRC with modified gold surface, it would appear as the most optimal choice for continuous automated immunoassay

system. However, in the case of Protein G conjugated magnetic beads, the IRC was easier to construct and renew by simply loading a new batch of magnetic beads. As presented below, the actual concentration of cortisol in real water samples was so low that despite the significantly lower IC50 and LOD for the IRC with a gold surface, direct analysis of the water samples without preconcentration would not have been possible. Hence, the IRC with magnetic beads was chosen for further experiments to test sample clean-up and enrichment using ISLM. The additional advantage of using Protein G modified magnetic beads is that during water sampling through the donor phase the magnetic beads in the acceptor phase are suspended, which reduces the diffusion distance of the analyte compared to a gold surface that is at a fixed distance from the SLM.

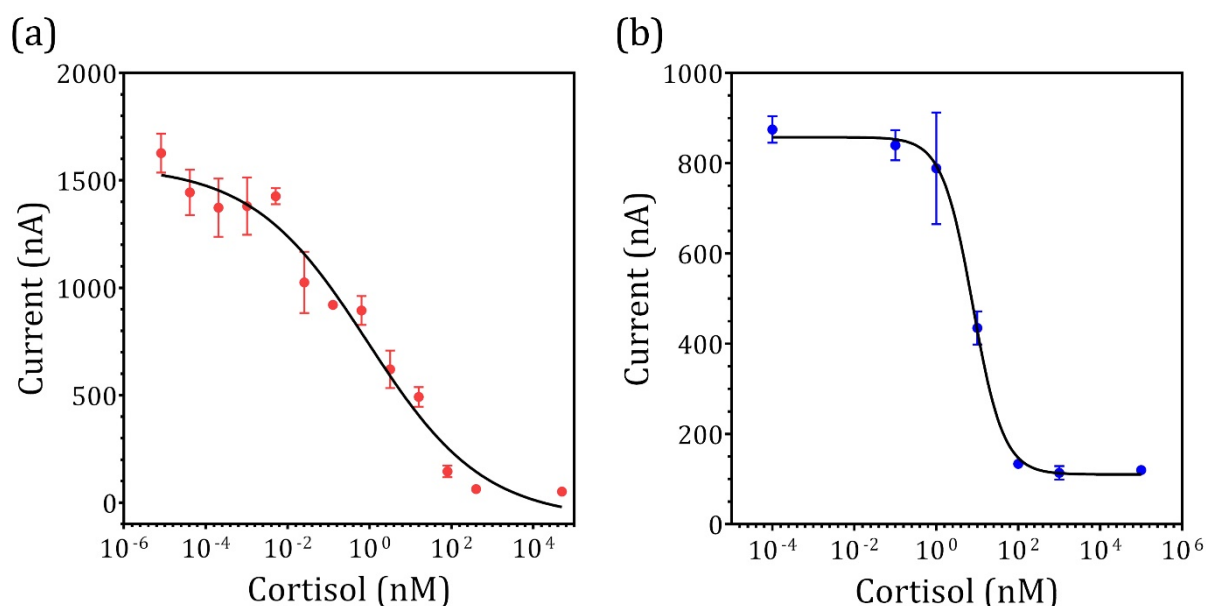


**Figure 7.** Calibration curves for continuous FIA using an IRC having Protein G immobilised on (a) a gold surface and (b) magnetic beads. (The error bars represent standard deviation,  $n = 3$ )

### 3.3 Quantitation of cortisol in water samples from RAS

#### 3.3.1 ELISA-based analysis

It has long been established that cortisol is released via diffusion from the gills fish into the surrounding water. The correlation between the cortisol released into the water and blood plasma cortisol level has also been established [38]. We sampled water from a

model RAS at DTU Aqua and determined the cortisol level using a commercial ELISA kit. Each of the collected water samples was 200 ml, and prior to ELISA the cortisol was preconcentrated using solid-phase extraction. The results (Supporting Information, Figure S-2) showed that in the control water samples (collected from the tank before the fish were stressed) the cortisol concentration was found to be  $6.1 \pm 0.3$  pM (standard deviation,  $n = 4$ ), whereas in the water samples collected 45 minutes after introduction of the stressors, the cortisol concentration was more than 10 times higher,  $68 \pm 4$  pM (standard deviation,  $n = 4$ ). Based on the performed ELISA, it was clear that the cortisol level in water sampled from a RAS could be determined, albeit not without preconcentration. Hence, to perform cortisol analysis using a continuous FIA system, a sample pre-treatment step had to be incorporated in the system.

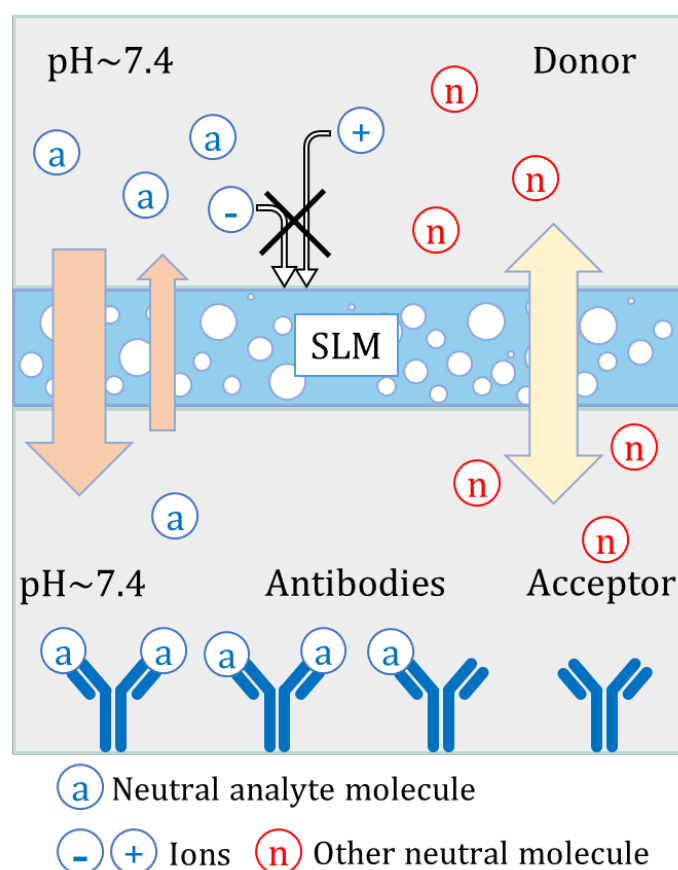


**Figure 8.** Functional principle of sample clean-up and enrichment using immuno-supported liquid membrane (ISLM).

### 3.3.2 FIIA with incorporated ISLM

The IRC with conjugated magnetic beads was easier to construct and renew. This was especially important in the case of the FIIA system with incorporated ISLM (Figure 1c). Figure 8 shows the functional principle of ISLM. In the generic SLM format, commonly used to clean up samples and specifically extract and enrich charged molecules (e.g. acids and bases), a shift in pH from donor to acceptor is used to create an analyte concentration gradient between donor and acceptor while excluding everything else [39]. Here, permanently neutral analyte molecules like cortisol can diffuse back and forth between donor and acceptor through the SLM but they cannot be trapped in the acceptor. In ISLM on the other hand, these molecules can be captured by analyte specific antibodies immobilised in the acceptor compartment [22–24]. This allows both sample clean-up and enrichment, i.e., other neutral molecules in the donor phase will diffuse back and forth through the SLM without enrichment, whereas ions and particulate matter in the donor phase, i.e., impurities in the sample matrix, cannot diffuse through the SLM.

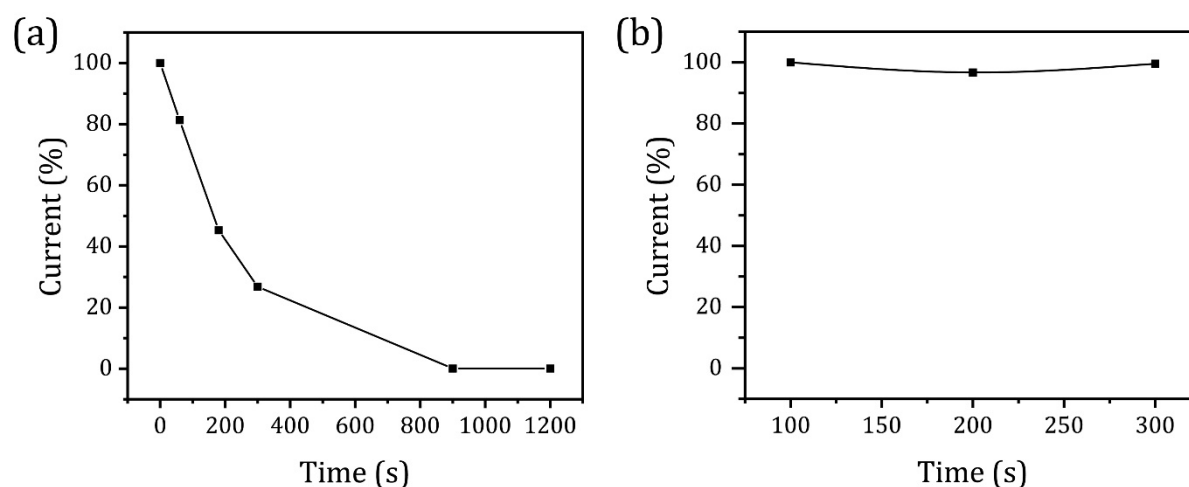


**Figure 9.** Relative current vs. flow time of water samples through the donor phase of the ISLM-based IRC (A) 45 min after and (B) before (control) inducing stress.

The purpose of the performed test using the ISLM format of the immunoreaction chamber was to assess the feasibility to detect cortisol in actual water samples and determine the required sampling time, i.e., how long a time the sample solution should be flown through the donor phase. The tested water samples were collected from the same RAS as

mentioned in section 3.3.1 before (control) and 45 min after introduction of stressors. Figure 9a shows that the relative current reached zero in approximately 15 min when using the water samples that had been collected 45 min after inducing stress. In practical terms, the result indicates that the amount of cortisol, which had been captured by the antibodies in the acceptor phase, was sufficient to saturate, i.e., fully occupy, the antigen binding sites of the immobilised antibody. In the case of the control sample, the relative current remained at about 100 %, indicating that during the 300-s test period the cortisol that reached the acceptor phase was below the limit of detection. Since according to the ELISA results, shown in Figure S-3, the control samples contained very low concentration of cortisol, detection using the ISLM-based extraction in the continuous FIIA system would require a significantly longer flow period than 300 s in the presented test.

#### **4. Conclusion**

We have developed an automated flow injection immunoassay (FIIA) system for continuous competitive immunoassays of cortisol in water to monitor cortisol level in recirculating aquaculture systems. The FIIA system comprised three peristaltic pumps and two injection valves, the operations of which were computer controlled using an interface based on a custom-made circuit and LabView script. Two types of immunoreaction chamber (IRC) were tested for immunoassay development: Cortisol antibody was bound to Protein G that had been covalently immobilised on (i) a gold surface through a combination of self-assembled monolayer of mercaptopropionic acid and carbodiimide activation of the carboxylic group (EDC/NHS), (ii) superparamagnetic beads. The IRC functioned as an injection loop of the FIIA system. The assay development, in terms of the fluidic operations and duration of the individual steps, addressed maximised reproducibility and long-term stability of the IRC, while striving for the shortest assay duration. The IRC with a gold surface provided the best performance in terms of the IC<sub>50</sub> and LOD. However, due to the versatility of the IRC loaded with Protein G modified magnetic beads, this format was considered as the optimal choice for testing the immuno-supported liquid membrane (ISLM) to clean up real water samples taken from a model recirculating aquaculture system and enrichment of cortisol. Ultimately, since any antibody bound to Protein G modified magnetic beads can easily be introduced

into the IRC, the entire developed FIIA system may be used on an on-demand basis for detecting different analytes of interest.

## **Acknowledgements**

This project was funded by NordForsk's Nordic Bioeconomy Programme under the Nordic Centre of Excellence (SUREAQUA), coordinated by the Norwegian Research Centre (NORCE). Dr. Van Ngoc Huynh (DTU Health Tech) and Dr. Suman Basak (DTU Chemistry) are acknowledged for help and discussions regarding polymer fabrication and water sample extraction, respectively.

## **References**

- [1] FAO, The State of World Fisheries and Aquaculture. Sustainability in Action, 2020.
- [2] A.G.J. Tacon, Fish farming, in: B. Caballero (Ed.), *Encycl. Food Sci. Nutr.*, Elsevier Science Ltd., 2003: pp. 2479–2486.
- [3] A. Saeki, Studies on Fish Culture in the Aquarium of Closed-Circhlating System. Its Fundamental Theory and Standard Plan, *Bull. Japanese Soc. Sci. Fish.* 23 (1958) 684–695.
- [4] C.I.M. Martins, E.H. Eding, M.C.J. Verdegem, L.T.N. Heinsbroek, O. Schneider, J.P. Blancheton, E.R. d'Orbcastel, J.A.J. Verreth, New developments in recirculating aquaculture systems in Europe: A perspective on environmental sustainability, *Aquac. Eng.* 43 (2010) 83–93. <https://doi.org/10.1016/j.aquaeng.2010.09.002>.
- [5] K. Buchanan, T.B. de Perera, C. Carere, T. Carter, A. Hailey, R. Hubrecht, D. Jennings, N. Metcalfe, T. Pitcher, F. Péron, L. Sneddon, C. Sherwin, J. Talling, R. Thomas, M. Thompson, Guidelines for the Use of Animals: Guidelines for the treatment of animals in behavioural research and teaching - Association for the Study of Animal Behaviour and Animal Behavior Society, *Anim. Behav.* 83 (2012) 301–309. [https://doi.org/10.1016/S0003-3472\(16\)30351-7](https://doi.org/10.1016/S0003-3472(16)30351-7).
- [6] P.J. Ashley, Fish welfare: Current issues in aquaculture, *Appl. Anim. Behav. Sci.* 104 (2007) 199–235. <https://doi.org/10.1016/j.applanim.2006.09.001>.



- [7] T. Ellis, B. North, A.P. Scott, N.R. Bromage, M. Porter, D. Gadd, The relationships between stocking density and welfare in farmed rainbow trout, *J. Fish Biol.* 61 (2002) 493–531. <https://doi.org/10.1006/jfbi.2002.2057>.
- [8] L.E. Wysocki, J.P. Dittami, F. Ladich, Ship noise and cortisol secretion in European freshwater fishes, *Biol. Conserv.* 128 (2006) 501–508.
- [9] A.D. Pickering, T.G. Pottinger, Stress responses and disease resistance in salmonid fish : Effects of chronic elevation of plasma cortisol, *Fish Physiol. Biochem.* 7 (1989) 253–258. <https://doi.org/10.1007/BF00004714>.
- [10] B. Barton, C. Schreck, L. Barton, Effects of chronic Cortisol administration and daily acute stress on growth, physiological conditions, and stress responses in juvenile rainbow trout, *Dis. Aquat. Organ.* 2 (1987) 173–185. <https://doi.org/10.3354/dao002173>.
- [11] A. Mustafa, D.J. Speare, J. Daley, G.A. Conboy, J.F. Burka, Enhanced susceptibility of seawater cultured rainbow trout, *Oncorhynchus mykiss* (Walbaum), to the microsporidian *Loma salmonae* during a primary infection with the sea louse, *Lepeophtheirus salmonis*, *J. Fish Dis.* 23 (2000) 337–341.
- [12] T.R. Gregory, C.M. Wood, The Effects of Chronic Plasma Cortisol Elevation on the Feeding Behaviour, Growth, Competitive Ability, and Swimming Performance of Juvenile Rainbow Trout, *Physiol. Biochem. Zool.* 72 (1999) 286–295. <https://doi.org/10.1086/316673>.
- [13] P.K. Bondy, G.V. Upton, G.E. Pickford, Demonstration of cortisol in fish blood, *Nature.* 179 (1957) 1354–1355. <https://doi.org/10.1038/1791354a0>.
- [14] A. Kaushik, A. Yndart, R.D. Jayant, V. Sagar, V. Atluri, S. Bhansali, M. Nair, Electrochemical sensing method for point-of-care cortisol detection in human immunodeficiency virus-infected patients, *Int. J. Nanomedicine.* 10 (2015) 677–685. <https://doi.org/10.2147/IJN.S75514>.
- [15] R.D. Munje, S. Muthukumar, A.P. Selvam, S. Prasad, Flexible nanoporous tunable electrical double layer biosensors for sweat diagnostics, *Sci. Rep.* 5 (2015) 14586.
- [16] S.K. Arya, G. Chornokur, M. Venugopal, S. Bhansali, Antibody functionalized

- interdigitated  $\mu$ -electrode (ID $\mu$ E) based impedimetric cortisol biosensor, *Analyst*. 135 (2010) 1941–1946. <https://doi.org/10.1039/c0an00242a>.
- [17] T. Ellis, J.D. James, C. Stewart, A.P. Scott, A non-invasive stress assay based upon measurement of free cortisol released into the water by rainbow trout, *J. Fish Biol.* 65 (2004) 1233–1252. <https://doi.org/10.1111/j.1095-8649.2004.00499.x>.
- [18] T. Ellis, M.B. Sanders, A.P. Scott, Non-invasive monitoring of steroids in fishes, *Wien. Tierarztl. Monatsschr.* 100 (2013) 255–269. <https://doi.org/urn:nbn:nl:ui:11-dbi/52820484b78fe>.
- [19] T. Ellis, J.D. James, H. Sundh, F. Fridell, K. Sundell, A.P. Scott, Non-invasive measurement of cortisol and melatonin in tanks stocked with seawater Atlantic salmon, *Aquaculture*. 272 (2007) 698–706. <https://doi.org/10.1016/j.aquaculture.2007.07.219>.
- [20] A.P. Scott, K. Hirschenhauser, N. Bender, R. Oliveira, R.L. Earley, M. Sebire, T. Ellis, M. Pavlidis, P.C. Hubbard, M. Huertas, A. Canario, Non-Invasive Measurement of Steroids in Fish-Holding Water : Important Considerations When Applying the Procedure to Behaviour Studies, *Behaviour*. 145 (2008) 1307–1328.
- [21] E. Thordarson, J.Å. Jönsson, J. Emnéus, Immunologic Trapping in Supported Liquid Membrane Extraction, *Anal. Chem.* 72 (2000) 5280–5284. <https://doi.org/10.1021/ac0005013>.
- [22] M. Tudorache, M. Co, H. Lifgren, J. Emnéus, Ultrasensitive magnetic particle-based immunosupported liquid membrane assay, *Anal. Chem.* 77 (2005) 7156–7162. <https://doi.org/10.1021/ac050978k>.
- [23] M. Tudorache, J. Emnéus, A micro-immuno supported liquid membrane assay ( $\mu$ -ISLMA), *Biosens. Bioelectron.* 21 (2006) 1513–1520. <https://doi.org/10.1016/j.bios.2005.07.002>.
- [24] M. Tudorache, I.A. Zdrojewska, J. Emnéus, Evaluation of progesterone content in saliva using magnetic particle-based immuno supported liquid membrane assay (m-ISLMA), *Biosens. Bioelectron.* 22 (2006) 241–246. <https://doi.org/10.1016/j.bios.2006.01.002>.

- [25] E.S. Bos, A. van der Doelen, N. van Rooy, A.H. Schuurs, 3,3',5,5' - Tetramethylbenzidine as an Ames test negative chromogen for horse-radish peroxidase in enzyme-immunoassay, *J. Immunoassay*. 2 (1981) 187–204.
- [26] A. Mech-Doros, A. Heiskanen, S. Bäckström, M. Perry, H.B. Muhammad, C. Hélix-Nielsen, J. Emnéus, A reusable device for electrochemical applications of hydrogel supported black lipid membranes, *Biomed. Microdevices*. 17 (2015) 21. <https://doi.org/10.1007/s10544-015-9936-y>.
- [27] E.C. Peláez, M.C. Estevez, A. Portela, J.P. Salvador, M.P. Marco, L.M. Lechuga, Nanoplasmonic biosensor device for the monitoring of acenocoumarol therapeutic drug in plasma, *Biosens. Bioelectron.* 119 (2018) 149–155. <https://doi.org/10.1016/j.bios.2018.08.011>.
- [28] J.E. Reemeyer, J.C. Harris, A.M. Hernandez, B.B. Rees, Effects of passive integrated transponder tagging on cortisol release, aerobic metabolism and growth of the Gulf killifish *Fundulus grandis*, *J. Fish Biol.* 94 (2019) 422–433. <https://doi.org/10.1111/jfb.13916>.
- [29] J. Růžička, E.H. Hansen, *Flow Injection Analysis*, 2nd. ed., John Wiley & Sons, Inc., Hoboken, NJ, USA, 1988.
- [30] A.A. Karyakin, G. V. Presnova, M.Y. Rubtsova, A.M. Egorov, Oriented immobilization of antibodies onto the gold surfaces via their native thiol groups, *Anal. Chem.* 72 (2000) 3805–3811. <https://doi.org/10.1021/ac9907890>.
- [31] T. Ibbi, M. Kaieda, S. Hatakeyama, H. Shiotsuka, H. Watanabe, M. Umetsu, I. Kumagai, T. Imamura, Direct immobilization of gold-binding antibody fragments for immunosensor applications, *Anal. Chem.* 82 (2010) 4229–4235. <https://doi.org/10.1021/ac100557k>.
- [32] A. Kausaite-Minkstiniene, A. Ramanaviciene, J. Kirlyte, A. Ramanavicius, Comparative Study of Random and Oriented Antibody Immobilization Techniques on the Binding Capacity of Immunosensor, *Anal. Chem.* 82 (2010) 6401–6408. <https://doi.org/10.1016/j.proeng.2012.09.277>.
- [33] F.J. Podlaski, A.S. Stern, Site-Specific Immobilization of Antibodies to Protein G-Derivatized Solid Supports, in: P. Bailon, G.K. Ehrlich, W.-J. Fung, W. Berthold (Eds.),

- Affin. Chromatogr., Humana Press Inc., Totowa, NJ, USA, 2003: pp. 41–48.  
<https://doi.org/10.1385/1-59259-041-1:41>.
- [34] N. Patel, M.C. Davies, M. Hartshorne, R.J. Heaton, C.J. Roberts, S.J.B. Tendler, P.M. Williams, Immobilization of protein molecules onto homogeneous and mixed carboxylate-terminated self-assembled monolayers, *Langmuir*. 13 (1997) 6485–6490. <https://doi.org/10.1021/la970933h>.
- [35] B. Akerstrom, L. Bjorck, A physicochemical study of protein G, a molecule with unique immunoglobulin G-binding properties, *J. Biol. Chem.* 261 (1986) 10240–10247. [https://doi.org/10.1016/s0021-9258\(18\)67515-5](https://doi.org/10.1016/s0021-9258(18)67515-5).
- [36] B. Uthuppu, A. Heiskanen, D. Kofoed, J. Aamand, C. Jørgensen, M. Dufva, M.H. Jakobsen, Micro-flow-injection analysis ( $\mu$ FIA) immunoassay of herbicide residue 2,6-dichlorobenzamide – towards automated at-line monitoring using modular microfluidics, *Analyst*. 140 (2015) 1616–1623. <https://doi.org/10.1039/C4AN01576B>.
- [37] J.A. Goode, J.V.H. Rushworth, P.A. Millner, Biosensor Regeneration: A Review of Common Techniques and Outcomes, *Langmuir*. 31 (2015) 6267–6276. <https://doi.org/10.1021/la503533g>.
- [38] A.P. Scott, M. Pinillos, T. Ellis, Why measure steroids in fish plasma when you can measure them in water?, *Perspect. Comp. Endocrinol. Unity Divers. Proc. 14th Int. Congr. Comp. Endocrinol.* (2001) 1291–1295.
- [39] S. Pálmarsdóttir, B. Lindegård, P. Deininger, L.E. Edholm, L. Mathiasson, J.A. Jönsson, Supported liquid membrane technique for selective sample workup of basic drugs in plasma prior to capillary zone electrophoresis, *J. Capillary Electrophor.* 2 (1995) 185–189.

## Supplementary Information

### Flow injection immunoassay for continuous monitoring of cortisol

Claudy D'Costa <sup>a</sup>, Arto Heiskanen <sup>a</sup>, Manuel Gesto<sup>b</sup>, J.-Pablo Salvador<sup>c</sup>, M.-Pilar Marco<sup>c</sup>, Anders Wolff <sup>a</sup>, and Jenny Emneus <sup>a,\*</sup>

<sup>a</sup> Department of Biotechnology and Biomedicine (DTU Bioengineering), Technical University of Denmark, Produktionstorvet, Building 423, 2800 Kgs. Lyngby, Denmark

<sup>b</sup> Institute of Aquatic Resources (DTU Aqua), Technical University of Denmark, Willemoesvej 2, 9850 Hirtshals, Denmark

<sup>c</sup> Department of Chemical and Biomolecular Nanotechnology, Institute for Advanced Chemistry of Catalonia (IQAC) of the Spanish Council for Scientific Research (CSIC), Jordi Girona 18-26, 08034, Barcelona, Spain

\* To whom correspondence may be addressed: [jemn@dtu.dk](mailto:jemn@dtu.dk); Tel.: +45 45256867

## S-1 Electrochemical characterisation

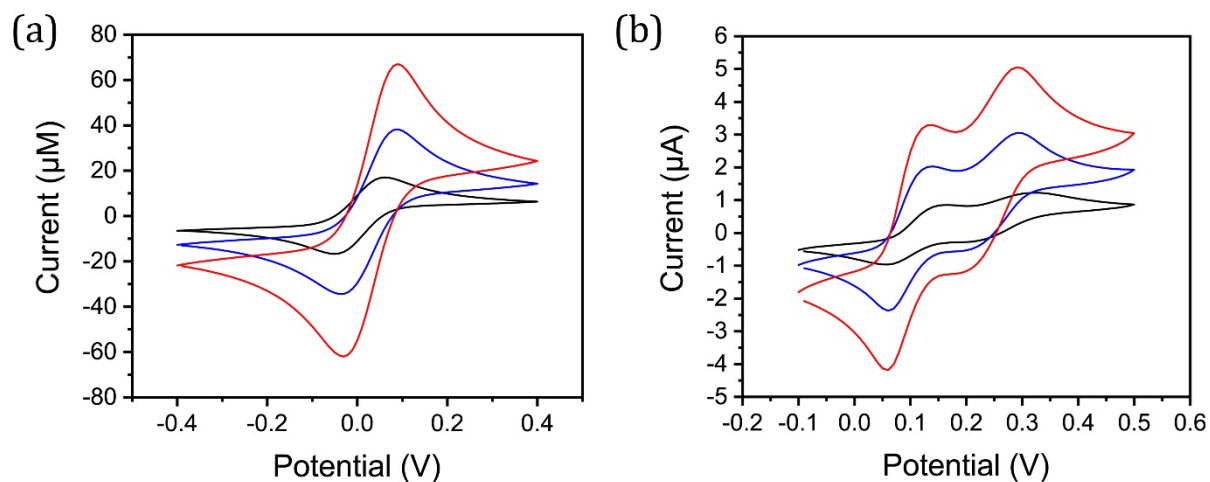


**Figure S-1.** Cyclic voltammograms acquired at WEs with varying area in (a) 10 mM [Fe(CN)<sub>6</sub>]<sup>3-/4-</sup> (prepared in PBS) and (b) TMB Plus2 substrate solution.

## S-2 ELISA-based analysis

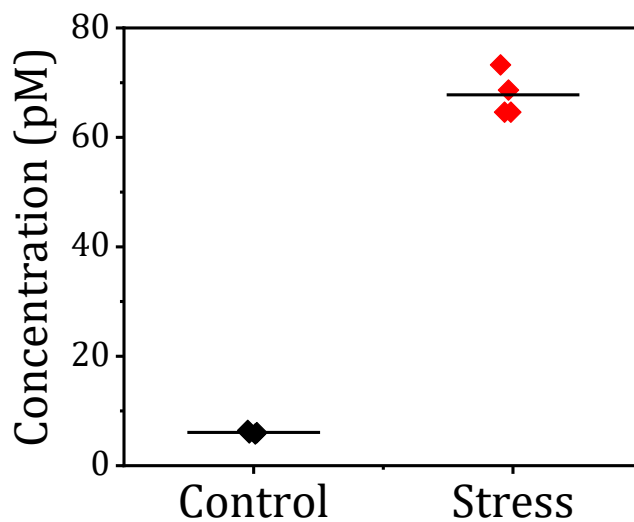


**Figure S-2.** ELISA of cortisol in water samples taken from a model RAS before (control) and after induction of stress (n = 4).

# Appendix A    Protocols

## A.1   DTU Aqua experiments

Aim: To measure cortisol released by fish into the water using solid-phase extraction and ELISA

Steps:

1. The first step is to collect the water sample (before and after stressing the fish)
2. The water sample collected is filtered as shown in Figure 1.



Fig. A.1 The water sample collected from the tanks were filtered using 0.45  $\mu\text{m}$  pore sized 47mm dia sterilized filter papers from Advantec. The setup is as shown in figure. All the glassware were washed thoroughly with ultra-pure water and ethanol.

3. The protocol is based on Reemeyer et al. 2019 and Ellis 2004.
4. 200 mL from the filtered samples was either spiked or used as is, depending on the experiment.
5. Oasis HLB 1cc vacuum cartridges were used, as shown in the setup in Figure 2. The vacuum pump was adjusted to perform the elution slowly.
6. The procedure for elution is as follows
  - a. 5 mL of methanol
  - b. 5 mL of Milli-Q ultrapure water
  - c. 200 mL sample to be eluted
  - d. 5 mL ethyl acetate for elution of cortisol (to be done very carefully and slowly)
  - e. The sample was left to evaporate overnight
  - f. Reconstitute the sample for ELISA

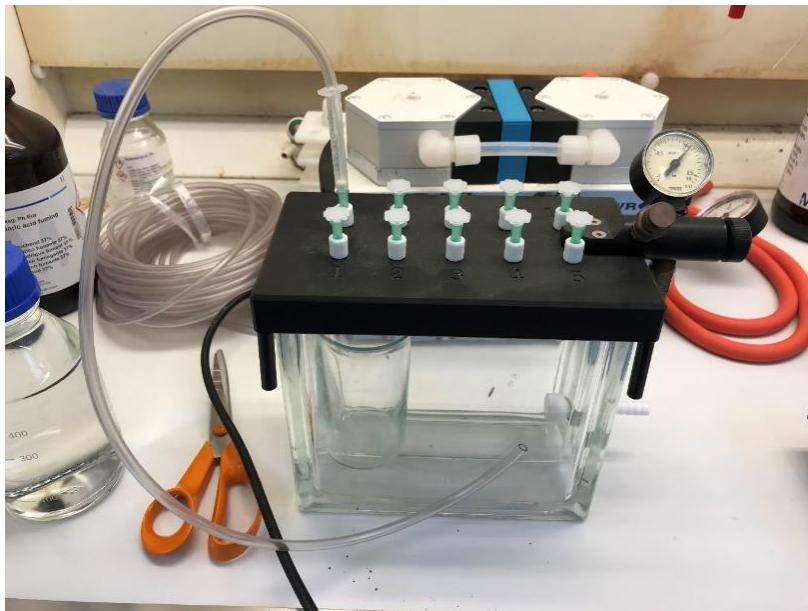


Fig. A.2 Oasis HLB 1cc vacuum cartridges (Waters Corp.) were used to elute the sample. 200 mL of samples took 23 minutes to pass. Though this is a higher flow rate than recommended in papers.



## A.2 Detector electrode on Si substrate

This process flow is to create gold electrodes which had different WE size based on **DRP design on a 4" Si wafer and then passivate with SU8 coating**

Step Heading	Equipment		Comments
Spin coat of AZ 5214E (Using premade SiO <sub>2</sub> wafers)			
Coat wafers	Spin Coater: Gamma UV	Resist: AZ 5214E (line 2) Spin: 30 s @ 3300 rpm (for 2.2µm) Softbake: 60 s @ 110 °C Sequence: (3420) DCH 100mm AZ nLOF2020 1.5um	Use (3421) for in-line HMDS priming.  Resist thickness can be measured on FilmTek
First Exposure			
Exposure	MLA03	Mask: 3E_SUAQ_DRP_20B20_v0.0 Layer: L0 Exposure dose: 43 mJ/cm <sup>2</sup> Defocus: 0 Exposure time: 14 mins	!!!INVERT the image!!!
Reversal Bake			
Reversal Bake	Developer: TMAH UV-lithography	Reversal Bake: 60 s @ 110 °C Sequences: 2002 DCH 100mm PEB120s@110C	Reversal bake
Flood Exposure			
Exposure	MA6-2	Mask: NONE Exposure mode: Flood E Exposure dose: 200 mJ/cm <sup>2</sup> Exposure time: MA6-2: 18s @ 11 mW/cm <sup>2</sup>	Information on exposure dose for other thickness or aligner: <a href="http://labadviser.danchip.dtu.dk/index.php/Specific_Process_Knowledge/Lithography/UVExposure_Dose">http://labadviser.danchip.dtu.dk/index.php/Specific_Process_Knowledge/Lithography/UVExposure_Dose</a>
Development, Rinse, and Dry			
Develop	Developer: TMAH UV-lithography	Development in TMAH: single puddle, 60s Sequences: 1002 DCH 100mm SP60s	Choose 60 s development for extra undercut (lift-off).
Gold deposition			
Deposit gold	E-Beam Evaporator (Temescal)	CrAu / TiAu Cr / Ti - 20nm @ 0.2 KÅ/s Au - 200nm @ 0.2 KÅ/s	Inbuilt recipe 'CrAu', 'TiAu'
Lift off			
Remove resist	Lift off	Remover 1165 Ultrasound power: 09 Time: 20mins*3	Make sure overheating does not happen

Passivation			
SU-8 spin coating	RCD8 spinner	2000rpm, 30s, 500rpm/s	"cladc_passivation_SU8 2005"
SU-8 pre-bake	Hotplate	15min @50°C, 2°C/min Cool down to 20 (3 hrs)	
Exposure	MLA03	Mask: 3E_SUAQ_DRP_20B20_v0.0 Layer: L1 Exposure dose: 2000 mJ/cm <sup>2</sup> Defocus: -10 Exposure time: 40 mins	!!!INVERT the image!!!  Check the intensity
SU-8 post-bake	Z3/ Hotplate	1.5 h, 50°C, 2°C/min	
SU-8 development	Z3/ Developer	1 min FIRST, 1 min FINAL	
Inspection			
Inspection	Optical microscope	Inspect pattern / alignment mark / process monitor	
Spin coat of AZ MiR 701 (Positive resist)			
Coat wafers	Spin Coater: Gamma UV or Spin Coater: Gamma e- beam & UV	Resist: AZ 5214E (line 1 or CO2 line 2) Spin: 30 s @ 4600 rpm (for 1.5µm) Softbake: 60 s @ 90 °C Sequence: (1410) DCH 100mm MiR 701 1.5um or (4210) DCH 100mm MiR 701 1.5um	Use (1411) or (4211) for in-line HMDS priming.  Resist thickness can be measured on FilmTek
UV Exposure			
Exposure	Aligner: Maskless 01 , Aligner: Maskless 02 or Aligner: Maskless 03	Design: your design file Exposure dose: 170+ mJ/cm <sup>2</sup> for MLA1 170-180 mJ/cm <sup>2</sup> for MLA2 (375nm) 180-200 mJ/cm <sup>2</sup> for MLA3 Defocus: 0 for MLA1 -6 for MLA2 (optical) 0 for MLA3	Information on exposure dose for other thickness or aligner: <a href="http://labadviser.danchip.dtu.dk/index.php/Specific_Process_Knowledge/Lithography/UVExposure_Dose">http://labadviser.danchip.dtu.dk/index.php/Specific_Process_Knowledge/Lithography/UVExposure_Dose</a>
Post Exposure Bake			
Post Exposure Bake	Developer: TMAH UV-lithography	Post Exposure Bake: 60 s @ 110 °C Sequence: (2001) DCH PEB 110C 60s or (3001) DCH 100mm PEB60s@110C+SP60s	PEB and development is typically done simultaneously
Development			
Development	Developer: TMAH UV-lithography	Development in TMAH (AZ 726 MIF): single puddle, 60 s Sequences: (1002) DCH 100mm SP 60s or (3001) DCH 100mm PEB60s@110C+SP60s	PEB and development is typically done simultaneously

Spin coat of AZ nLOF 2020			
Coat wafers	Spin Coater: Gamma UV	Resist: AZ nLOF 2020 (line 2) Spin: 30 s @ 3300 rpm (for 2 $\mu$ m) Softbake: 60 s @ 110 °C Sequence: (2420) DCH 100mm AZ5214E 1.5um	Use (2421) for in-line HMDS priming.  Resist thickness can be measured on FilmTek
UV Exposure			
Exposure	Aligner: Maskless 01 or Aligner: Maskless 02	Design: your design file Exposure dose: 220 mJ/cm <sup>2</sup> for MLA1 500 mJ/cm <sup>2</sup> for MLA2 (375nm) Defocus: 0 for MLA1 0 for MLA2 (optical)	Information on exposure dose for other thickness or aligner: <a href="http://labadviser.danchip.dtu.dk/index.php/Specific_Process_Knowledge/Lithography/UVExposure_Dose">http://labadviser.danchip.dtu.dk/index.php/Specific_Process_Knowledge/Lithography/UVExposure_Dose</a>
Post Exposure Bake			
Post Exposure Bake	Developer: TMAH UV-lithography	Post Exposure Bake: 60 s @ 110 °C Sequences: (2001) DCH PEB 110C 60s or (3005) DCH 100mm PEB60s@110C+SP30s (3001) DCH 100mm PEB60s@110C+SP60s	120 s PEB is better for Borofloat. May require lower exposure dose.  PEB and development is typically done simultaneously
Development, Rinse, and Dry			
Develop	Developer: TMAH UV-lithography	Development in TMAH (AZ 726 MIF): single puddle, 30 s or 60 s Sequences: (1001) DCH 100mm SP 30s (1002) DCH 100mm SP 60s or (3005) DCH 100mm PEB60s@110C+SP30s (3001) DCH 100mm PEB60s@110C+SP60s	Choose 60 s development for extra undercut (lift-off).  PEB and development is typically done simultaneously
Inspection			
Inspection	Optical microscope	Inspect pattern / alignment mark / process monitor	
Passivation layer - SiN			
Purpose: Add a passivation layer to protect wiring			
Instrument: STS PECVD3			
Layer thickness: 500nm			
Materials on wafer: Silicon, SiO <sub>2</sub> and TiAu			
Si <sub>3</sub> N <sub>4</sub> Deposition	STS PECVD3	Recipe name MFSiNLS2 Time: 12 mins SiH <sub>4</sub> flow [sccm] 30 NH <sub>3</sub> flow [sccm] 30 N <sub>2</sub> flow [sccm] 1470 Pressure [mTorr] 845 Power [W] 100HF 7.8s, 100LF 2.2s Deposition rate [nm/min] ~42.2	

Inspection	SEM	QBSD for residual particle detection		
Passivation layer Lithography				
Purpose: Coat a layer of resist for patterning passivation layer				
Instrument: Spin Coater: Gamma UV, MA6 - 2 Aligner				
Coating surface: Silicon Nitride				
Photoresist: AZ 5214E				
Mask: Layer 2				
Materials on wafer: Silicon, SiO <sub>2</sub> , TiAu and Si <sub>3</sub> N <sub>4</sub>				
Surface treatment	Oven: HMDS - 2	HMDS treatment for SiO <sub>2</sub> Recipe: 01	HMDS priming performed on Gamma spin coaters.	
Spin coat of AZ 5214E	Spin Coater: Gamma UV or Spin Coater: Gamma e-beam & UV	Resist: AZ 5214E (line 3 or CO2 line 1) Spin: 30 s @ 4500 rpm (for 1.5µm) Softbake: 60 s @ 90 °C Sequence: (3410) DCH 100mm AZ5214E 1.5um or (4111) DCH 100mm AZ5214E 1.5um	Use (3411) or (4111) for in-line HMDS priming.  Resist thickness can be measured on FilmTek	
Expose	Aligner: MA6 - 2	Mask: Layer 2 Exposure mode: Soft contact Exposure dose: 25 mJ/cm <sup>2</sup> for MA6 - 2 Exposure time: 1.9 s @ 13 mW/cm <sup>2</sup> for MA6 - 2		
Reversal Bake	Developer: TMAH UV-lithography	Reversal bake: 120 s @ 110 °C Sequence: DCH PEB 110C 120s		
Flood Exposure	Aligner: MA6 - 2	Mask: none Exposure mode: Flood exposure Exposure dose: 195 mJ/cm <sup>2</sup> for MA6 - 2 Exposure time: 15 s @ 13 mW/cm <sup>2</sup> for MA6 - 2		
Develop	Developer: TMAH UV-lithography	Development in TMAH: single puddle, 60 s Sequence: DCH 100mm SP 60s	Developer: TMAH UV-lithography	
Inspection	Optical microscope	Inspect pattern / alignment mark / process monitor		
Etching Si <sub>3</sub> N <sub>4</sub>				
Purpose: To open up electrode and contact pads				
Instrument: STS ICP Advanced Silicon Etcher				
Materials on wafer: Silicon, SiO <sub>2</sub> , AZ 5214E, TiAu and Si <sub>3</sub> N <sub>4</sub>				
Etch Si <sub>3</sub> N <sub>4</sub>	STS ICP Advanced Silicon Etcher	Recipe: Sin_RIE Chiller temperature: 20 °C Coil Power [W] 1300 Platen Power [W] 350	Platen temp [°C] 0 He flow [sccm] 174 CF4 flow [sccm] 40	

		Pressure [mTorr]
Cleaning process	Recipe: 1Clean20	4
20 minute O <sub>2</sub> clean on a dummy wafer		
Resist strip		
Purpose: To remove the photo resist		
Instrument: Wet etch		
Materials on wafer: Silicon, SiO <sub>2</sub> , AZ 5214E, TiAu and Si <sub>3</sub> N <sub>4</sub>		
Resist strip	Wet bench	Ultra sonication in acetone
Rinsing	Wet bench	Ethanol Deionized water N <sub>2</sub> drying
Inspection	Optical microscope or SEM Probe Station	Visual inspection Inlens or QBSD for residual particle detection Resistivity / Continuity

### A.3 Single TOPAS substrate processing

This document was created as part of the development of interdigitated gold electrodes on a polymer substrate (TOPAS COC 5013, 50mm disc with 1.5mm thickness).

Since normal recipe loaded in the Spin Coater: Gamma e-beam & UV cannot process a thick substrate (1,5mm), this special process was developed to partially control the system. Here manual inputs are incorporated into the normal functioning of a standard recipe.

**The process was developed by Thomas A and is to be used by Claudy D'Costa for the SUREAQUA project at DTU Nanotech.**

Date created : 28 Nov 18

Substrate : TOPAS COC 5013 injection molded disc 50mm dia and 1.5 mm thick

Recipe used : 2110-DCH 50mm AZ5214E 1,5um

1. Log in
2. Check the resist flow (if stuck, use acetone cleaning)
3. **Load 2" cassettes**
4. IO Door interlock active
5. Run the 2110-DCH 50mm AZ5214E 1,5um recipe (important to note that the selected recipe should be without HDMS treatment)
6. PAUSE the process
7. Request door access
8. **Place sample in the middle of the 'Stor1'**
9. IO Door interlock active
10. Close the door access request
11. **Load the substrate though 'Substr Create'**
12. **Pick the sample from 'Stor1' to 'C01'** - click YES when prompted
13. **Start the process by clicking 'C01' > 'View Recipe' > Start**
14. **Place sample in 'TempSlot13 Hot'** - click YES when prompted
15. **Start the process by clicking 'TempSlot13 Hot' > 'View Recipe' > Start**
16. **Place the sample back to 'Stor1'** - click YES when prompted
17. **Unload the substrate though 'Substr remove'**
18. Request door access
19. **Remove or replace sample in the middle of the 'Stor1'**
20. IO Door interlock active
21. Close the door access request
22. Continue through Step 11 - 21 OR Run 0200-DCH 50mm Coater1 clean

---

Lithography (Alignment Mark)

---

Purpose: Coat a layer of TOPAS COC with photoresist

---

Instrument: Labspin 02			
Coating surface: TOPAS COC			
Materials on wafer: TOPAS COC			
Wafer selection	Injection molder	TOPAS COC wafers are injection molded.	
Soap Sonic Cleaning	Wash bench at gowning area	01: Find holder 02: Close ultrasonic bath dump valve 03: Fill the ultrasonic bath with DI 04: Add of diluted Triton X-100 05: Close the bath lid 06: Start ultrasonic 07: Fill rinse bath with DI 08: Rinse samples 09: Blow dry the samples 10: Dump the Triton X-100 solution and rinse baths	50mm, 1.5 thick wafer  20 - 30 drops  10 mins
Spin coat of AZ 5214E	Labspin02 Manual spin coater	Resist: AZ 5214E Spin: 30 s @ 4500 rpm (for 1.5 $\mu$ m)	Resist thickness can be measured on FilmTek
Bake	Hot Plate / Oven	Hotplate: 60 s @ 90 °C Oven: 5 mins @ 90 °C	
Expose	Aligner: Maskless 01	Exposure dose: 75 Focus: -4	<i>job_2204</i>
Reversal Bake	Oven	Reversal bake: 120 s @ 110 °C	
Flood Exposure	Aligner: MA6 - 2	Mask: none Exposure mode: Flood exposure Exposure dose: 195 mJ/cm <sup>2</sup> for MA6 - 2 Exposure time: 15 s @ 13 mW/cm <sup>2</sup> for MA6 - 2	
Develop	Developer: TMAH Manual	Development in TMAH: single puddle, 60 s Sequence: DCH 100mm SP 60s	Developer: TMAH UV-lithography
Inspection	Optical microscope	Inspect pattern / alignment mark / process monitor	
Electrode Patterning			
Purpose: Deposit thin film of Cr-Au			
Instrument: Wordentec QCL 800			
Layer thickness: 10nm Titanium and 200nm Gold			
Materials on wafer: COC and AZ 5214E			
Thin film deposition	Wordentec QCL 800	Recipe: No 13 20nm Ti and 200nm Au Metal Rate (Å/s) Gold (Au) 10 Titanium(Ti) 5	Fill logbook before start
Inspection	SEM	Check cross sectional view in SEM in QBSD mode	Make a note of the profile
Lift Off			

Purpose: Pattern Ti-Au			
Instrument: Lift-off wet bench 07			
Resist Remover: NMP (Remover 1165)			
Materials on wafer: COC, AZ 5214E and CrAu			
Lift Off	Wet bench 07	Remover 1165 Ultrasonic agitation: Yes	Fill logbook before start
Rinse		Rinse in IPA	
Inspection	Optical microscope or SEM Probe Station	Inlens or QBSD for residual particle detection  Resistivity / Continuity	

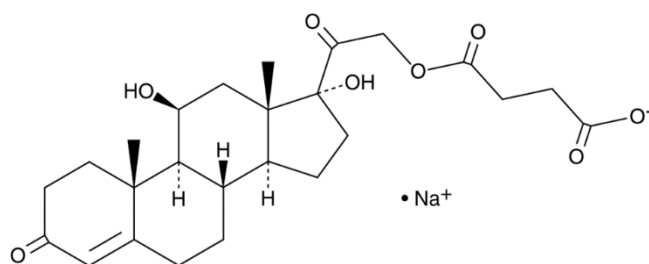
Alternate method to embed the gold electrode though etching of substrate.

Lithography			
Purpose: Coat a layer of TOPAS COC with photoresist			
Instrument: Labspin 02			
Coating surface: TOPAS COC			
Materials on wafer: TOPAS COC			
Wafer selection	Injection molder	TOPAS COC wafers are injection molded.	
Soap Sonic Cleaning	Wash bench at gowning area	01: Find holder 02: Close ultrasonic bath dump valve 03: Fill the ultrasonic bath with DI 04: Add of diluted Triton X-100 05: Close the bath lid 06: Start ultrasonic 07: Fill rinse bath with DI 08: Rinse samples 09: Blow dry the samples 10: Dump the Triton X-100 solution and rinse baths	50mm, 1.5 thick wafer  20 - 30 drops  10 mins
Spin coat of AZ 5214E	Labspin02 Manual spin coater	Resist: AZ 5214E Spin: 30 s @ 4500 rpm (for 1.5µm)	Resist thickness can be measured on FilmTek
Bake	Hot Plate / Oven	Hotplate: 60 s @ 90 °C Oven: 5 mins @ 90 °C	
Expose	Aligner: Maskless 01	Exposure dose: 75 Focus: -4	<i>job_2204 POSITIVE T2</i>
Expose	Aligner: Maskless 01	Exposure dose: 45 Focus: -4	<i>job_2275 NEGATIVE T3</i>
Reversal Bake	Oven	Reversal bake: 120 s @ 110 °C	
Flood Exposure	Aligner: MA6 - 2	Mask: none Exposure mode: Flood exposure	

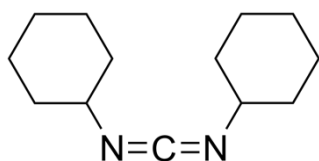


		Exposure dose: 195 mJ/cm <sup>2</sup> for MA6 - 2 Exposure time: 15 s @ 13 mW/cm <sup>2</sup> for MA6 - 2	
Develop	Developer: TMAH Manual	Development in TMAH: single puddle, 60 s Sequence: DCH 100mm SP 60s	Developer: TMAH UV-lithography
Inspection	Optical microscope	Inspect pattern / alignment mark / process monitor	
Etching TOPAS COC			
Purpose: To create an anisotropic etch on the TOPAS COC substrate Instrument: M/PLEX ICP - ASE (Advanced Silicon Etcher) Materials on wafer: COC and AZ 5214E			
Anisotropic etch	M/PLEX ICP - ASE	Slow TOPAS etch <i>O2 (sccm)</i> 50 <i>Pressure (mTorr)</i> 40 <i>Coil power (W)</i> 800 720 <i>Platen power (W)</i> 60 <i>Temperature (°C)</i> 20 TIME 35 s Etch rate (nm/min) ~350	To make the Au electrode flush with the substrate
Electrode Patterning			
Purpose: Deposit thin film of Cr-Au Instrument: Wordentec QCL 800 Layer thickness: 10nm Titanium and 200nm Gold Materials on wafer: COC and AZ 5214E			
Thin film deposition	Wordentec QCL 800	Recipe: No 13 20nm Ti and 200nm Au Metal Rate (Å/s) Gold (Au) 10 Titanium(Ti) 5	Fill logbook before start
Inspection	SEM	Check cross sectional view in SEM in QBSD mode	Make a note of the profile
Lift Off			
Purpose: Pattern Ti-Au Instrument: Lift-off wet bench 07 Resist Remover: NMP (Remover 1165) Materials on wafer: COC, AZ 5214E and CrAu			
Lift Off	Wet bench 07	Remover 1165 Ultrasonic agitation: Yes	Fill logbook before start
Rinse		Rinse in IPA	
Inspection	Optical microscope or SEM Probe Station	Inlens or QBSD for residual particle detection  Resistivity / Continuity	

## A.4 Creating the BSA-cortisol hapten

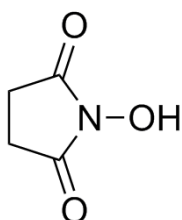


CAS no.: 125-04-2  
 Name: Hydrocortisone 21-hemisuccinate  
 sodium salt  
 Formula: C<sub>25</sub>H<sub>33</sub>NaO<sub>8</sub>  
 Molecular Weight: 484.57 g/mol



is an organic compound with the chemical formula (C<sub>6</sub>H<sub>11</sub>N)<sub>2</sub>C. It is a waxy white solid with a sweet odor. Its primary use is to couple amino acids during artificial peptide synthesis. The low melting point of this material allows it to be melted for easy handling. It is highly soluble in dichloromethane, tetrahydrofuran, acetonitrile and dimethylformamide,

CAS no.: 538-75-0  
 Name: Dicyclohexylcarbodiimide  
 (DCC)  
 Formula: C<sub>13</sub>H<sub>22</sub>N<sub>2</sub>  
 Molecular weight: 206,33 g/mol  
 Density: 1,06 g/cm<sup>3</sup>



is an organic compound with the formula (CH<sub>2</sub>CO)<sub>2</sub>NOH. It is a white solid that is used as a reagent for preparing active esters in peptide synthesis

CAS no.: 6066-82-6  
 Name: N-hydroxysuccinimide  
 (NHS)  
 Formula: C<sub>4</sub>H<sub>5</sub>NO<sub>3</sub>  
 Molecular weight: 115,09 g/mol  
 Density: 1,65 g/cm<sup>3</sup>

CAS no.: 68-12-2  
 Name: N,N-Dimethylformamide (DMF)  
 Formula: C<sub>3</sub>H<sub>7</sub>NO  
 Molecular weight: 73,11 g/mol  
 Density: 0,95 g/cm<sup>3</sup>

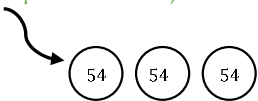


PART I - BSA Cortisol hapten			
1.	<p>We need anhydrous Dimethylformamide (DMF)</p> <ol style="list-style-type: none"> <li>Wear safety glasses and lab coat</li> <li>Start Vacuum pump (follow the instructions for the position of the valve)</li> <li>Turn on water flow valve on the right side of the fume hood. Check flow and adjust.</li> <li>Turn on the bottom lower red valve for initial circulation of evaporated ethanol</li> <li>Turn on heater, keep at DMF mark on dial</li> <li>Wait for it to boil and let it recirculate for a while.</li> <li>After the recirculation, close the red valve and wait for the DMF to get collected.</li> <li>Keep the following ready               <ol style="list-style-type: none"> <li>6ml glass vial</li> <li>1ml glass syringe</li> <li>Long metallic needle</li> </ol> </li> <li>Extract the anhydrous DMF through the inlet on top using the long needle and syringe, rinse the syringe a bit with DMF.</li> <li>AFTER EXPT               <ol style="list-style-type: none"> <li>Turn off the heater</li> <li>Clean up the hood</li> <li>Turn off water flow</li> <li>Turn off the Vacuum</li> </ol> </li> </ol>	Sensors lab DMF Laminar flow	
2.	<p>Prepare the following solutions Hapten:NHS:DCC -&gt; 1:2.5:5 Required: For 10mg BSA - 10<math>\mu</math>mol of hapten For 10mg HRP - 10<math>\mu</math>mol of hapten <b>!! Wait for the chemicals to come to room temperature before weighing!!</b> <b>20<math>\mu</math>mol</b> X 1 X 485.57g/mol = 9.6mg Cortisol hapten <b>20<math>\mu</math>mol</b> X 2.5 X 485.57g/mol = 5.7mg NHS <b>20<math>\mu</math>mol</b> X 5 X 485.57g/mol = 20.6mg DCC Mix 100<math>\mu</math>l of DMF with the chemicals except with Cortisol hapten (add 200 <math>\mu</math>l) The final volume is 400<math>\mu</math>l +, transfer it to a 1.5 ml eppendorf</p>	Cortisol Hapten Synthesis - 20° fridge, inside compartment 7  NHS and DCC inside Dry glass jar, Sensors lab fridge	DMF
3.	Keep the Eppendorf in a stand and on the magnetic stirrer at 100rpm for 3 hours.		
4.	<p>Centrifuge the solution at 10,000 RPM for 5 mins. Counter balance the weight with another 1.5 ml Eppendorf tube. Extract the supernatant to another 0.5 ml Eppendorf</p>	Synthesis lab Thermo Legend Micro 21	
5.	<p>Take a 6ml glass vial</p> <ol style="list-style-type: none"> <li>add 10mg of BSA and 1.8ml of Boric borax buffer 0.4M 8.7pH</li> <li>add 2mg of HRP and 1.8ml of Boric borax buffer 0.4M 8.7pH</li> </ol>	BSA in coupling proteins box HRP in Enzymes box Elisa fridge	Boric borax


PART II - Dialysis			
1.	<p>The following steps to be followed</p> <p>a) Keep the following ready</p> <ol style="list-style-type: none"> <li>Four plastic clips</li> <li>Plastic tweezers</li> <li>Scissors</li> <li>Aluminum foil</li> <li>Disposable glass pipettes</li> <li>Rubber bulb (to suck)</li> <li>5L plastic beaker</li> <li>50ml glass cylinder</li> </ol> <p>b) Cut approximately 10 cm of the cellulose membrane 12000Da</p> <p>c) Keep the membrane in warm water bath to wet the surface</p> <p>d) Prepare 5L of 0.5mM PBS in a plastic beaker. Put a magnetic stirrer.</p> $5l \times 0.5mM \frac{1}{100mM} = 25ml$ <p>e) Clip one end of the cellulose membrane, using the glass pipette, fill the membrane with HRP solution, careful not the introduce bubble. Seal the other end and cut off the extra membrane. Label the clips for identification.</p> <p>f) Repeat step e for BSA</p> <p>g) Put the sealed membranes in the beaker, keep it over stirrer and make sure they are vertical by adjusting the vortex.</p> <p>h) Change the solution every 2-3 hours for FOUR times and the final one with ONLY MQ</p>	<p>Elisa lab 4° incubator</p>	<p>MQ and PBS</p>

## A.5 Functionalization of glass surface using GTPMS - Electrode preparation

1. Wear safety glasses and lab coat
2. Open Air and Nitrogen main control valve above the entrance door
3. Open Nitrogen flow valve to the left of fume hood, check the flow in the bubbler above the distillation unit, adjust accordingly (low flow rate)
4. Turn on water flow valve on the right side of the fume hood. Check flow and adjust.
5. Turn on the bottom lower red valve for initial circulation of evaporated ethanol
6. Turn on heater, keep at 15% for ethanol
7. Wait for it to boil and let it recirculate for a while.
8. After the recirculation, close the red valve and wait for the ethanol to get collected.
9. Keep the following ready
10. Three long disposable needles
11. Two 10ml tubes with cap
12. 1ml plastic syringe
13. 15ml glass syringe
14. Long metallic needle
15. One balloon
16. Take out the GTPMS bottle, and keep ready
17. Extract the anhydrous ethanol through the rubber cap using the long needle and syringe, rinse the syringe a bit with ethanol. Collect some nitrogen gas along with the ethanol and transfer to the 10ml tube. Repeat for the other tube
18. Fill the balloon with nitrogen and insert it into the GTPMS bottle using needle
19. Insert another syringe into the bottle to create a flow
20. Extract 230-250ml of GTPMS and add into one of the 10ml tube containing ethanol.
21. AFTER EXPT
22. Turn off the heater
23. Dispose the used needles in the sharps container
24. Clean up the hood
25. Turn off water flow
26. Turn off the Nitrogen

Functionalization of glass surface using GTPMS - Electrode preparation			
2	1) Clean the electrodes a) Wash with MQ b) Wash with ethanol c) Repeat for three cycles d) Dry with nitrogen 2) UV/Ozone for 15 mins a) Load the chips, switch on ventilation, set the timer, switch on the machine and close the hood. 3) Characterize a) CV -0.6V - +0.8V at (a) 100mV/s and at (b) 50mV/s b) IMP 1MHz to 1 Hz at 100mV Wash with MQ, ethanol and dry with nitrogen 4) Insert it in 2ml Eppendorf tubes 5) ADD 0.5ml GTPMS	Sensors lab	
3	30 min @ Room temperature Wash with anhydrous ethanol and dry with nitrogen		
4a	Prepare coating antigen hBST-BSA Stock: 1mg/ml Required: 100µg/ml, 10µg/ml and 1µg/ml $\frac{60\mu\text{l} \times 100\mu\text{g/ml}}{1\text{mg/ml}} = 6\mu\text{l}$ ( 54ml PBS + 6µl hBST-BSA )  ADD 33ul of different dilution to each electrode	Antigen hBST-BSA 1.5ml vial Sensors fridge, inside Pablo box	PBS
5	2 hours 15 min @ Room temperature		
6	WASH with MQ		
7	Characterize a) CV -0.6V - +0.8V at (a) 100mV/s and at (b) 50mV/s b) IMP 1MHz to 1 Hz at 100mV		Ferri Ferro
8	WASH with MQ		
9	Primary antibody As147 (4) Stock: Serum (unknown conc) Required: 1/500 $1\text{ml} \times \frac{1}{500} = 2\mu\text{l}$ ( 0.998 ml PBST + 2µl As147 ) ADD As147 to electrode	Antiserum As147 0.5ml vial Sensors fridge, inside Pablo box	PBST
10	30 min @ Room temperature WASH 3 times PBST + 1 time PBS		
11	Prepare 10mM NaOH Add 33µl to the electrodes for regeneration		
12	WASH with PBS		
13	Characterize a) CV -0.6V - +0.8V at (a) 100mV/s and at (b) 50mV/s b) IMP 1MHz to 1 Hz at 100mV		Ferri Ferro
14	Repeat steps 8 - 11		

A.6 Competitive assay with new BSA Cortisol hapten

Ser no	Steps	Location	Solution
1	Coating antigen BSA-Cortisol hapten Stock: 1mg/ml Required: 6.25µg/ml 100µl / well (100x2x12 = 2.4ml)  $\frac{3ml \times 6.25\mu g/ml}{1mg/ml} = 18.75\mu l$ (3ml Coating buffer + 18.75µl BSA-Cortisol hapten )  Add to plate 100µl	Antigen hBST-BSA 1.5ml vial  Sensors fridge, inside Pablo box	Coating buffer
2	OVER NIGHT @ 4°C	ELISA lab	
	Next day (after 17 hours) First prepare and keep the antibody / ies ready		
3a	Competitive antigen Hydrocortisone Stock: 10mM (prepared in DMSO, freezes in fridge, need time to thaw) Required: 50µM 50µl / well (50x2x12 = 1.2ml)  $3ml \times 10mM \times 362.49g/mol = 10.87mg$  $1ml \times 50\mu M \times \frac{1}{10mM} = 5\mu l$ (0.995 ml PBST + 5µl Stanozolol)  ↓ Only till 10th tube we need 1/5 dilution   Serial dilution with 200ml till 7 <sup>th</sup> well	Substrate Hydrocortisone 1g bottle  Synthesis lab, -20 fridge 2 <sup>nd</sup> shelf	DMSO  PBST
3b	Primary antibody Ab 1949 Stock: 2mg/mL Required: 1ug/mL, 1/2000 Required: 4ug/mL, 1/500 50µl / well (50x2x8 = 0.8ml)  $2ml \times \frac{1\mu g/ml}{2mg/ml} = 1\mu l$ ( 1.999 ml PBST + 1µl Ab 1949)  $1ml \times \frac{4\mu g/ml}{2mg/ml} = 2\mu l$ (0.998 ml PBST + 2µl Ab 1949)  <b>ONLY ADD TILL THE 11th WELL!</b>	Antibody Ab 1949 0.5ml vials  Synthesis lab, -20 fridge 3 <sup>rd</sup> shelf inside bubble wrap	PBST
3c	a) Add the analyte 50µl b) Add the antibody 50µl		
4	30 min @ Room temperature and then WASH	ELISA lab	

5	<p>Label antibody GAR-PO (Goat anti rabbit - peroxidase) algG-HRP Stock: Required: 1/6000 100<math>\mu</math>l / well (100x3x8 = 2.4ml)</p> <p><b>12ml</b> <math>\times \frac{1}{6000} = 2\mu</math>l ((6ml <math>\times</math> 2) 12 ml PBST + 2<math>\mu</math>l GAR-PO)</p> <p>Add to plate 100<math>\mu</math>l</p>	<p>Antibody algG-HRP 0.5ml vial (marked as <b>prime ')</b></p> <p>ELISA fridge door</p>	PBST
6	30 min @ Room temperature and then WASH	ELISA lab	
7	<p>Substrate H<sub>2</sub>O<sub>2</sub>+TMB</p> <p>2x5.88 Citrate buffer + 48 <math>\mu</math>l H<sub>2</sub>O<sub>2</sub> 192 <math>\mu</math>l TMB</p> <p>Add to plate 100<math>\mu</math>l</p>	<p>H<sub>2</sub>O<sub>2</sub> - Sensors fridge door</p> <p>TMB - Armari 6</p>	Citrate buffer
8	<p>COVER WITH AL FOIL!! 30 min @ Room temperature and then WASH</p>	ELISA lab	
9	<p>STOP H<sub>2</sub>SO<sub>4</sub> 4N</p> <p>Add to plate 50<math>\mu</math>l</p>	Benchtop shelf	



A.7 ELISA for cortisol analyte

No	Steps	Location	Solution
1	<p><b>Coating Protein (Protein G)</b>                      Protein G (no. 19)                      Stock: 2mg/ml                      Required: 6.25 µg/ml or 1/160                      100µl / well (100x3x12= 3.6 ml)</p> <p><b>4 ml X 6.25µg/ml</b>  <math>\frac{2mg/ml}{2mg/ml} = 12.5\mu l</math>                      (3.987.5 ml Coating buffer + 12.5 µl Protein G)</p> <p>Add 100 µL of protein G mix in each well.</p>	Lab12 5 PrtG -20°C fridge  4°C fridge	Coat buf
	OVER NIGHT @ 4°C (after 17 hours)	L.125	-

1	<p><b>PREPARE BEFORE WASH</b>  <b>Antibody (1/3200)</b>                      Antibody 10-C30D                      Stock: 1mg/ml                      Required: 1/3200, working dilution 1/800                      100µl / well (100x3x11= 3.3 ml)</p> <p>1/800 - Sub stock.</p> <p><b>2 ml X 1.25 µg/ml</b>  <math>\frac{1mg/ml}{1mg/ml} = 2.5\mu l</math>                      (1.9975 ml PBST + 2.5 µl 10-C30D)</p> <p>1/3200</p> <p><b>4 ml X <math>\frac{1}{3200}</math></b>  <math>\frac{1}{800} = 1ml</math></p> <p>(3 ml PBST + 1 mL of sub stock)</p>		
---	---	--	--

**Analyte**

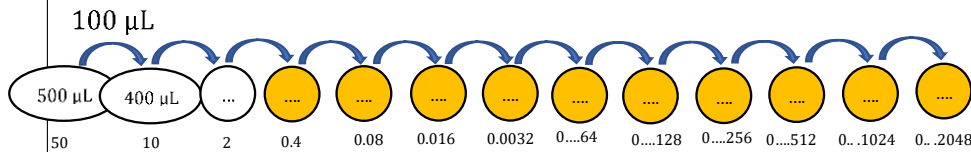
Analyte  
 Label Cortisol  
 Stock: 10 mM  
 Required: 50 μM (double up)  
 100μl/well (50x3 = 150 μL ~ 0.150 ml)

$$0.5 \text{ ml} \times \frac{100 \mu\text{M}}{10 \text{ mM}} = 5 \mu\text{L}$$

(495 μL of 1:5 diluted tomato juice + 5 μL of Cortisol stock.)  
 (Need to double (50 to 100 μM) since it gets diluted in 50 μL tracer.)

Diluted tomato juice = 400μLx12 + 500μL = 5.3 mL  
 (Mix 2 ml of raw tomato (TJ) and 8 mL of PBST to a total volume of 10 mL) x5

Dilutions: (400 μL 1:5 tomato juice in all tubes)  
 need to dilute 5 times each time.  
 Mark 0.4 as 1 and 0...2048 as 10. (yellow)



**Tracer**

Label HRP-Cortisol (C-HRP)  
 Stock: 1mg/ml  
 Required: 0.166μg/ml or 1/6000  
 100μl/well (50x3x12 = 1.8 ml)

Lab12  
 5  
 10-  
 C30D  
 -20°C  
 fridge  
 Lab12  
 5 4°C  
 Fridge

PB:  
 Al  
 10-C  
 0.5  
 vi:

2	<b>THROW OUT!</b> --- <b>WASH</b> 4 times with PBST 200 µL in each well, plate shake 2 mins 180 rpm and use suction	L005	-
	Add 100 µL antibody in every well expect for blank 30 min @ Room temperature		
	<b>THROW OUT!</b> --- <b>WASH</b> 4 times with PBST 200 µL in each well, plate shake 2 mins 180 rpm and use suction		
	Add 50µl to each well of the <b>analyte Cortisol</b> + Add 50 µL to <b>"zero"</b> and <b>"Blank"</b> of Tomato juice (x5) Add 50µl to each well of the <b>C-HRP tracer</b> 30 min @ Room temperature		
3a	<b>In the end of the 30 min prepare the substrate H<sub>2</sub>O<sub>2</sub>+TMB</b> Take a 15 ml tube and mix the reagents below together and cover it with an Al foil. 100µl/well (100x3x12 = 3.6 ml)  5.88 mL Citrate buffer + 24 µl H <sub>2</sub> O <sub>2</sub> + 96 µl TMB = 6 mL total SHAKE - Keep in pocket!! - NO LIGHT		
4	<b>THROW OUT!</b> ---- <b>WASH</b> 4 times in PBST 200 µL in each well, plate shake 2 mins 180 rpm and use suction	Lab00 5	PB:
5	Add 100 µL substrate in every well	Lab00	Dilut
6	<b>COVER WITH AL FOIL!!</b> 30 min @ Room temperature	Lab00 5	-
	STOP the reaction with H <sub>2</sub> SO <sub>4</sub> 4N -> Add 50µl to each well  Measure the absorbance at 450 nm		



